Xinya Song

Machine Learning assisted Digital Twin for event identification in electrical power system

Ilmenauer Beiträge zur elektrischen Energiesystem-, Geräte- und Anlagentechnik (IBEGA)

Herausgegeben von
Univ.-Prof. Dr.-Ing. Dirk Westermann
(Fachgebiet Elektrische Energieversorgung) und
Univ.-Prof. Dr.-Ing. Frank Berger
(Fachgebiet Elektrische Geräte und Anlagen)
an der Technischen Universität Ilmenau.

Band 34

Xinya Song

Machine Learning assisted Digital Twin for event identification in electrical power system

Universitätsverlag Ilmenau
2023

Impressum

Bibliografische Information der Deutschen Nationalbibliothek
Die Deutsche Nationalbibliothek verzeichnet diese Publikation in der Deutschen Nationalbibliografie; detaillierte bibliografische Angaben sind im Internet über http://dnb.d-nb.de abrufbar.

Diese Arbeit hat der Fakultät für Elektrotechnik und Informationstechnik der Technischen Universität Ilmenau als Dissertation vorgelegen.

Tag der Einreichung:	28. Februar 2022
1. Gutachter:	Prof. Dr.-Ing. Dirk Westermann (Technische Universität Ilmenau)
2. Gutachter:	Prof. Dr.-Ing. Christian Becker (Technische Universität Hamburg)
3. Gutachter:	Prof. Dr.-Ing. Przemyslaw Komarnicki (Fraunhofer-Institut für Fabrikbetrieb und -Automatisierung IFF)
Tag der Verteidigung:	21. Oktober 2022

Technische Universität Ilmenau/Universitätsbibliothek
Universitätsverlag Ilmenau
Postfach 10 05 65
98684 Ilmenau
https://www.tu-ilmenau.de/universitaetsverlag

ISSN 2194-2838
ISBN 978-3-86360-267-3 (Druckausgabe)
DOI 10.22032/dbt.55185
URN urn:nbn:de:gbv:ilm1-2022000438

Titelfotos:

Acknowledgment

With the achievement of a doctoral degree, it is the milestone that you have not only accomplished a scientific degree but also the personal career. During the period, I was accompanied by many people. I would like to express my thanks and acknowledgement to them for their support and professional comments.

Above all, I would like to thank my doctoral father, Mr. Univ.-Prof. Dr.-Ing. Dirk Westermann. During my studies, his contribution of time, patience, immense knowledge, encouragement, support and guidance made my doctor study enjoyable and productive. He opened up the door of my scientific exploration in the electrical power world, which I still enjoy it and will continue in the future.

Furthermore, I would like to thank Dr. Teng Jiang for his many ideas and advice for my study, work and research. At the same time, I would also give my appreciation to my friendly colleagues for their support in my working time.

Lastly, my thanks go to my parents, girlfriend and friends. Your supports make it possible for me to go this way.

Abstract

The challenges of stable operation in the electrical power system are increasing with the infrastructure shifting of the power grid from the centralized energy supply with fossil fuels towards sustainable energy generations. In Germany, the expansion of renewable energy sources (RES) to fulfil the climate policy goals for reducing CO_2 and moratorium on nuclear power plants is growing rapidly. This has resulted in significant change for all sectors of the electrical power system – generation, transmission and distribution as well as consumption. The predominantly RES plants, due to the non-linear electronic switch, have brought harmonic oscillations into the power grid, which not only increases the complexity of the power grid but also impacts the stability of the system. These changes lead to more difficulties for stable operation, reduction of outages and management of variations in electric power systems. The emergence of the Digital Twin in the power system brings the opportunity to overcome these challenges. Digital Twin is a digital information model that accurately represents the state of every asset in a physical system. It can be used not only to monitor the operation states with actionable insights of physical components to drive optimized operation but also to generate abundant data by simulation according to the guidance on design limits of physical systems.

With regard to this, the thesis firstly addresses the topic of the origin of the Digital Twin concept and how it can be utilized in the optimization of power grid operation. It specifies the aspects of dynamic state estimation, operation states monitoring, anomaly event identification, etc., in the power system with Digital Twin. The realization of these applications in the power system is based on the lifecycle management concept. The lifecycle flowchart of Digital Twin needs three main procedures from creation to its application: Digital Twin creation with parameter estimation, data generation with Digital Twin simulation, and training process with Digital Twin generated data for the application. This work emphasizes the investigation of the applicable parameter estimation algorithms for Digital Twin creation and the realization of event identification by Machine Learning based on the data generated with Digital Twin simulation. The investigation of different parameter estimation algorithms for Digital Twin creation is carried out on the basis of algebraic differential equations of electrical components in the power grid. The numerical case studies verify the accuracy of estimating the parameters and compare these algorithms' performance. After creating Digital Twin, it is used to simulate different events to generate the event-based data. Each event is fingerprinted with the generated data from the Digital Twin simulation. The Machine Learning algorithm training is conducted with the Digital Twin generated data. The event identification by Machine Learning is validated and evaluated with the case studies.

Kurzfassung

Die Herausforderungen für den zuverlässigen Betrieb des elektrischen Energiesystems werden mit der Umwandlung der Infrastruktur in Stromnetz von der zentralen Energieversorgung mit fossilen Brennstoffen hin zu der regenerativen Energieeinspeisung stetig zugenommen. Der Ausbau der erneuerbaren Energien im Zuge der klimapolitischen Zielsetzung zur CO_2-Reduzierung und des Ausstiegs aus der Kernenergie wird in Deutschland zügig vorangetrieben. Aufgrund der nichtlinearen elektronischen Schaltanlagen werden die aus EE-Anlagen hervorgegangenen Oberschwingungen in das Stromnetz eingebracht, was nicht nur die Komplexität des Stromnetzes erhöht, sondern auch die Stabilität des Systems beeinflusst. Diese Entwicklungen erschweren den stabilen Betrieb, die Verringerung der Ausfällen und das Management der Netzschwankung im elektrischen Energiesystem. Das Auftauchen von Digital Twin bringt die Gelegenheit zur Behebung dieser Herausforderung. Digital Twin ist ein digitales Informationsmodell, das den Zustand des physikalischen genau abbildet. Es kann nicht nur zur Überwachung der Betriebszustände mit nachvollziehbarem Einsichten über physischen Komponenten sondern auch zur Generierung der Daten durch Simulationen unter der Berücksichtigung der Auslegungsgrenze verwendet werden.

Diesbezüglich widmet sich die Arbeit zunächst der Fragstellung, woher das Digital Twin Konzept stammt und wie das Digital Twin für die Optimierung des Stromnetzes eingesetzt wird. Hierfür werden die Perspektiven über die dynamische Zustandsschätzung, die Überwachung des Betriebszustands, die Erkennung der Anomalien usw. im Stromnetz mit Digital Twin spezifiziert. Dementsprechend wird die Umsetzung dieser Applikationen auf dem Lebenszyklus-Management basiert. Im Rahmen des Lebenszyklusschemas von Digital Twin sind drei wesentliche Verfahren von der Modellierung des Digital Twins zur deren Applizierung erforderlich: Parametrierungsprozess für die Modellierung des Digital Twins, Datengenerierung mit Digital Twin Simulation und Anwendung mit Machine Learning Algorithmus für die Erkennung der Anomalie. Die Validierung der Zuverlässigkeit der Parametrierung für Digital Twin und der Eventserkennung erfolgt mittels numerischer Fallstudien. Dazu werden die Algorithmen für Online- und Offline zur Parametrierung des Digital Twins untersucht. Im Rahmen dieser Arbeit wird das auf CIGRÉ basierende Referenznetz zur Abbildung des Digital Twin hinsichtlich der Referenzmessdaten parametriert. So sind neben der Synchronmaschine und Umrichter basierende Einspeisung sowie Erreger und Turbine auch Regler von Umrichter für den Parametrierungsprozess berücksichtigt. Nach der Validierung des Digital Twins werden die zahlreichen Simulationen zur Datengenerierung durchgeführt. Jedes Event wird mittels der Daten von Digital Twin mit einem „Fingerprint“ erfasst. Das Training des Machine Learning Algorithmus wird dazu

mit den simulierten Daten von Digital Twin abgewickelt. Das Erkennungsergebnis wird durch die Fallstudien validiert und bewertet.

Table of contents

1 Introduction and motivation

The development of electrical power system for the purpose of providing a reliable, economical, and environmental friendly energy supply has become increasingly profound [1]. With the global climate shift, fossil resource dwindling, and the increasing concerns about nuclear energy, it drives to a shift in the thinking of a sustainable, secure, and economically viable power supply with renewable energy [2–4]. This trend is leading to the revolution of structure in the power supply system from a traditional central large power plant that feeds energy into high voltage level to the decentralized feed-in power with renewable generations (mainly solar and wind) in the distribution power grid [5, 6]. Thus, a significant increase in the use of renewable energy sources (RES) is taking place both at the European scale [7] and on the German scale [4].

According to the energy concept of the German government, 80 percent of the German gross electricity consumption should be supplied by renewable energy sources by 2050 [1, 4]. The development of the RES generations in the last 30 years is shown in Figure 1.1. With decreasing energy demand from 591.3 TWh in 2017 to 543.6 TWh in 2020 [8], which is even lower than in 1995 with 536.2 TWh [8] for the gross energy consumption, the RES takes a growing proportion of the total generation. In particular, the on- and offshore wind energy and the photovoltaic capacity have the highest growth rates, although their generations fluctuate due to weather conditions and are not demand-driven. Until 2020, the installed capacity of wind energy and solar energy has reached 131 TWh and 50.6 TWh, respectively, which have more than doubled since 2011 [4, 9].

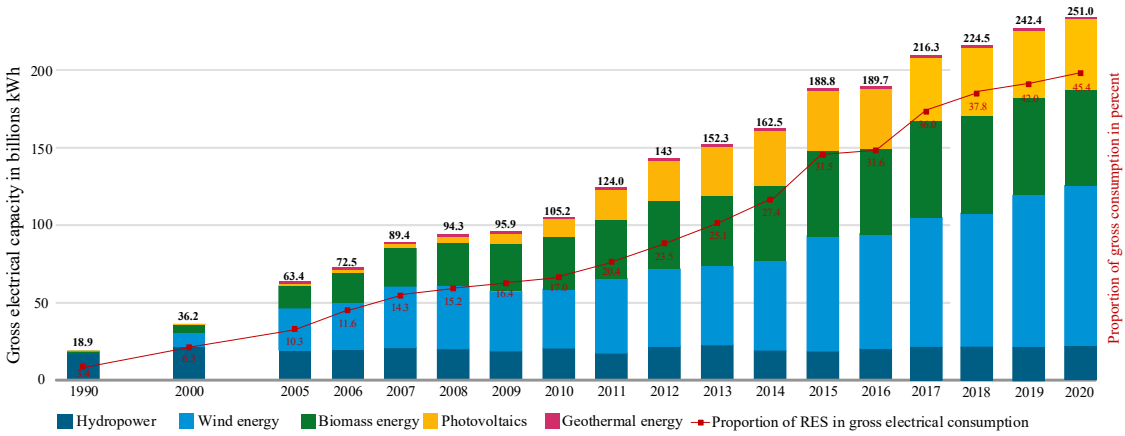

Figure 1.1: Development of electrical power generation from renewable energy and its percentage in Germany [4]

The expansion of RES and the developed demand for charging infrastructure for electric vehicles are facilitated by the application of inverter technologies [10]. The inverter is the

interface between the power grid and the supply or the load to transform the energy from direct current (DC) to alternating current (AC). However, because of the switching process in this transformation, the harmonic oscillations are brought into the power grid, posing potential stability issues [10, 11]. Not only the voltage and frequency stability are impacted by the oscillation, but also this instability phenomenon by the power electronic devices can feed into transmission grid to cause the rotor angle stability issues [11, 12]. Hence, it is essential to explore an accurate simulation model to investigate the mentioned stability issues.

The simulation technology provides a useful tool for the design and analysis of the power system [13]. The main idea of the simulation is to describe the phenomena of the real power system with a set of mathematical equations [13, 14]. The result of the simulation assists the engineer in making a reasonable decision for a reliable operation of the real power system. The studies with a simulation model can be used to identify and avoid possible deficiencies in the real system before it goes into operation [15]. During the operation, simulation studies help to locate the cause of the equipment failure and identify the operation mistakes. Besides, the corrective measures are developed with simulation studies to improve the system performance [13].

Since the first analogy-equivalent model for the representation of the power network was developed in 1929 [15], the simulation model of the power system is improved to assess the capability of the system to survive in the next event with considering the present state of the power system. Based on the development of the high-performance computing techniques, the new requirements of the simulation model in power system are proposed to build a highly accurate digital model for realistic portrayal of physical conditions and providing a highly reliable forecast of the future behaviour [16]. The emergence of Digital Twin (DT) coined in 2013 [17] provides the new horizon to realize the required simulation model for the power system in the next generation. DT is characterized by cyber-physical integration and is increasingly emphasized in both academic research field and industrial areas [18, 19]. Its central concept aims to integrate the physical agent and the virtual data throughout the lifecycle for monitoring the operation states of the physical agent and generating a huge volume of forecast data by advanced analytics to predictively maintain the agent and optimize the performance in the physical space [18–20].

In previous studies, the majority of them are concentrated on the future framework for the application with DT like dispatch optimization by DT [21], DT for state monitoring and prediction [22], etc. However, the creation of DT is an essential procedure before considering its application. In [23], the parameter estimation methods for creating the DT of inverter-based medium voltage power grid are investigated. Four parameter estimation methods are introduced for finding the “right” parameters for inverter DT according to the

measurement data from the real power grid. The results of this paper have presented that parameter estimation is the key procedure for DT creation to keep the adaptivity of DT with the physical system. An overview of the flowchart for DT from creation to the application is shown in Figure 1.2. After DT creation, it is utilized to simulate all the events that have already occurred and will potentially happen in the physical power grid to generate the training data for Machine Learning [24]. Machine Learning is famous for its efficiency to extract, classify and identify the feature pattern from the high-dimension dataset [25]. The trained algorithm in Machine Learning attempts to recognize feature patterns in big datasets automatically and rapidly [26, 27]. This ability enables an automatic and quick event detection for the power grid with it. The flowchart of event detection with Machine Learning and DT is outlined in Figure 1.3. In this framework, the process data from the power grid are gleaned and communicated with the remote terminal unit (RTU) and phasor measurement unit (PMU) [28]. The trained algorithm in Machine Learning detects the feature pattern from the gleaned data in the database. The identified event is assisted with operator guidance for the decision making.

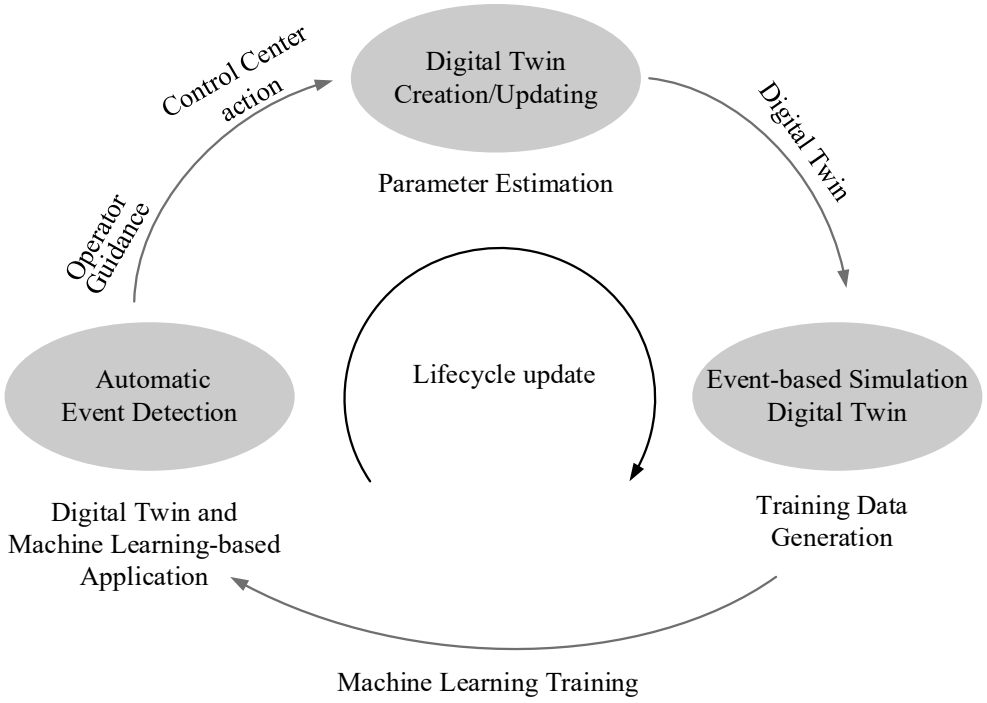

Figure 1.2: Flowchart of DT from creation to application in power system

In this work, the appropriate algorithms for realizing the procedures in the lifecycle of DT from creation to application with Machine Learning, according to Figure 1.2, are developed. First of all, the process of DT creation is focused on algebraic differential equation

modeling and parameter estimation of the power grid. The validation of the accuracy for DT in the second process aims to evaluate if DT can accurately rebuild and emulate the dynamic states of the physical system. Afterwards, the event-based simulation in DT is designed with all the potential scenarios to generate the data for training the algorithms in Machine Learning. These scenarios are then labelled from event 1 to event *k*, see Figure 1.3. The application of the Machine Learning in anomaly event detection is to identify the type of the occurred event from the labelled event list. The algorithm compares the anomaly event data with the labelled pattern. The output of Machine Learning algorithm declares the similarity degree between the labelled event and the anomaly event, which ranges from 0 to 100%. The identified anomaly with the highest similarity is confirmed as one of the known events from 1 to *k*.

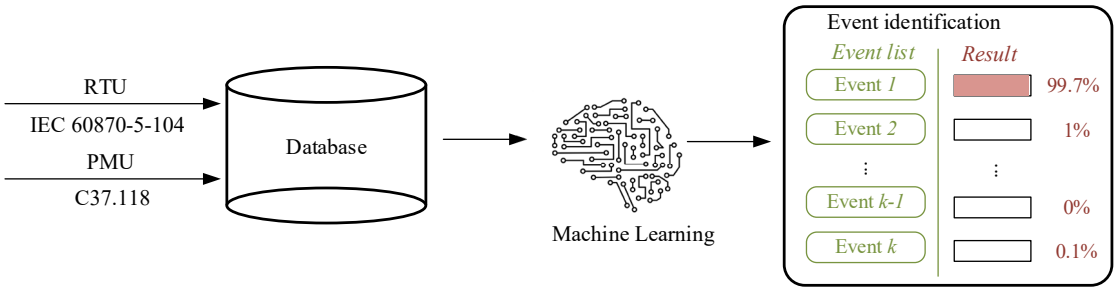

Figure 1.3: Event identification with Machine Learning [29]

1.1 Research questions and structure of work

The critical aspect to DT is the usage of the proper digital way to analyze and visualize the data to monitor and predict the operating assets over the lifecycle, which allows the operator to make a deeper understanding of the operations of the system and set up the preventive or corrective measures for unexpected failure [30]. The essential requirement in the application of DT is the modelling of DT. It needs the parameter estimation process, according to the measurements from the physical system, to calculate the real parameters for DT. By parameter estimation for building DT, it is not only referred to the accurate estimation of the parameters, but also it should have the real-time estimation ability, in that the estimated parameter can be updated into DT timely to keep the adaptivity with real system. In this context, three parameter estimation methods are investigated in this work for parameterizing DT. The procedure for parameterization is classified into three steps: First of all, the phase model-based simulation [31] emulates the dynamic states of the physical power grid. The generated data from the simulation is utilized in the parameter estimation process for the calculation of the right parameters according to the dynamic states from the physical power grid. Three parameter estimation methods are separately used and validated. After validation, DT with the estimated parameters that has the highest accuracy

in the rebuilding of the physical power grid is further applied for event-based simulation. The simulation in DT provides the data of the feature pattern for each event. Each pattern is labelled in the algorithm of Machine Learning as a fingerprint with the training process. Afterwards, the application of trained Machine Learning for anomaly identification is demonstrated in this work. The anomaly identification is one of the categories in event detection and classification, which is more specified in the detection and classification of the abnormal state [32, 33]. The traditional data anomaly detection is based on statistical methods like Gaussian, Regression, Fourier transformation etc. [34], which causes more difficulties with the increasing of data volume. Compared with the traditional methods, the learning problem of anomaly identification lacks marked supervised data in Machine Learning [32]. The participation of DT with event-based simulation enables the solution of it. Accordingly, the following research questions are addressed in this dissertation:

Q1 *Which parameter estimation method is suitable for Digital Twin creation?*

Q2 *How Digital Twin can be used for event identification?*

This thesis is dedicated to answering both research questions in six chapters. The first chapter provides an introduction of the topics and refers to the motivation and the background of the research relevance.

In chapter 2, an overview of the origin of DT and its state of art in power systems is initially introduced. Afterward, the parameterization with consideration of the current state of the art can be realized with three algorithms [35–37]:

- Non-linear least square
- Recursive least square
- Artificial neural network-based parameter identifier

In section 2.4, Machine Learning is reviewed with its current application in the power system field. Its powerful and efficient ability in data processing can be used for data classification and event identification. Several research projects related to DT and Machine Learning, from 2015 to 2021, are presented in the last section to assess their contributions to address the research questions considered in this work.

Chapter 3 is dedicated to answering the first research question to investigate the appropriate parameter estimation methods to calculate the proper parameters for the DT. Firstly, the modelling of DT is addressed with the consideration of two typical dynamic components in power grid: synchronous generator and the inverter-based generation. The integration of the proposed parameter estimation methods for parameterization of both dynamic components is explained in section 3.2. The acceleration of the parameter estimation process can be achieved with sensitivity analysis to reduce the dimension of the number of

estimated parameters. The calculation of the sensitivity indicator for selecting the key parameters is elaborated in section 3.3.

Chapter 4 first presents the fault types and the corresponding features utilized for Machine Learning for classification and identification. Before the classification and the identification of the anomaly event, the measured data usually includes a large amount of no-feature and noise data. These can lead to more extended calculations and inaccurate results in classification and identification. The methods depicted in section 4.2 can detect and extract the feature signal in high-dimensional measure data efficiently. With the labelled data, the algorithms based on Machine Learning theory are introduced to classify and identify anomaly events. Three approaches are applied in this work and then compared qualitatively for the accuracy of classification and identification.

The simulation and validation of the parameter estimation methods for DT creation and DT assisted with Machine Learning algorithms for event identification are carried out by numerical case studies in chapter 5. The research objective based on the CIGRÈ benchmark [38] is initially introduced in section 5.1 with the topology and the included dynamic components. To emulate the dynamics of the physical objective network, the reference model is simulated with real-time simulator [31] as the physical system. The application of the parameter estimation in tuning the parameters of synchronous generator and voltage source inverter with the measurement from the reference system as well as the case studies is illustrated in section 5.2. The validation of the accuracy in the representation of the reference system by DT after the parameter estimation is included in this section. The numerical case studies for DT assisted by Machine Learning for anomaly event identification is demonstrated in section 5.3.

Chapter 6 summarizes the results and evaluates them with respect to the formulated research questions. Finally, based on the findings, and an outlook is derived with regard to further research fields and recommendations for action.

1.2 Scientific contributions

The scientific contributions of this dissertation can be summarized as follows:

- As a key factor for the DT creation, three parameter estimation methods are compared for the offline and online parameterization of the inverter- and synchronous machine-based generation including the corresponding controllers according to the measurement from the reference power grid. [23, 39]
- Proposition of a lifecycle of DT in power system from creation to decision support for operator and then goes back to start point for DT updating with the parameter estimation. [29]

- Application of DT in dynamic state estimation to improve the system performance of the power system. [22]
- Proposition of DT application in surveillance of the operation state in electrical power system. [40]
- Realization of the hybrid simulation idea in the real-time simulator to improve the performance of the real-time ability. [41]

The scientific findings have resulted in book chapters, journal papers and conference publications.

Book chapters

- Jean-Nicolas Paquin ; Jean Bélanger; Sudipta Chakraborty ; Vahid Jalili-Marandi ; **Xinya Song**; Dirk Westermann; Marcelo Godoy Simões.,"Real-time simulation applications for future power systems and smart grids," in *Artificial Intelligence for Smarter Power Systems: Fuzzy logic and neural networks*, M. G. Simões, Ed.: Institution of Engineering and Technology, 2021, pp. 9–64. DOI: 10.1049/PBPO161E_ch

Journal papers

- **X. Song**, T. Jiang, S. Schlegel, D. Westermann, "Parameter tuning for dynamic digital twin in inverter-dominated distribution grid", *IET Renewable Power Generation*, vol. 14, n5, p. 811–821, abr. 2020, doi: 10.1049/iet-rpg.2019.0163.
- **X. Song**, H.Cai, T.Jiang, T. Sennewald, J.Kircheis, S.Schlegel, L.N. Martinetz, Y.Benzetta, D.Westermann, „Research on Performance of Real-Time Simulation based on Inverter-Dominated Power Grid", IEEE Access, S. 1, 2020, doi: 10.1109/ACCESS.2020.3016177.

Conference papers with peer review

- **X. Song**, T. Jiang, S. Schlegel, and D. Westermann, "Realization of Hybrid Model by different Inverter Model in Inverter-dominated Power Grid ," in IEEE Student Conference 2018, Magdeburg. (Best Paper Award)
- **X. Song**, YL.Zeng, T. Jiang, S. Schlegel and Dirk Westermann, "Digital Twin of Distribution Grid using Harmonic Measurement," in NEIS 2019: Conference on Sustainable Energy Supply and Energy Storage Systems, Hamburg, 19-20 September 2019.
- **X. Song**, T.Jiang, S. Schlegel, D. Westermann: "Parameter Tuning by Neural Network for Digital Twin of Inverter", in Proc. 2019 IEEE PES Innovative Smart Grid Technologies (ISGT). Bucharest, 2019

- **X. Song** et al., „Application of Digital Twin Assistant-System in State Estimation for Inverter Dominated Grid“ in 2020 55th International Universities Power Engineering Conference (UPEC), 2020, S. 1–6, doi: 10.1109/UPEC49904.2020.9209876.
- **X. Song**, H.Cai T. Jiang, S. Schlegel and Dirk Westermann, “Inventive Parameter Tuning Algorithm for Digital Twin of Inverter Model in Distribution Power,” in NEIS 2020: Conference on Sustainable Energy Supply and Energy Storage Systems, Hamburg, 19-20 September 2020.
- **X. Song**, H.Cai T. Jiang, S. Schlegel and Dirk Westermann, “Artificial Intelligent Method and Singular Value Decomposition based System Identification for Digital Twin of Inverter based Power Grid,” in Internationaler ETG Kongress 2021, Wuppertal, Germany.
- **X. Song**, H.Cai T. Jiang, S. Schlegel and Dirk Westermann, "Surveillance of Operation States for Distributed Renewable Generations by Digital Twin", CIGRE Symposium Ljubljana 2021.
- **X. Song**, H.Cai T. Jiang, S. Schlegel and Dirk Westermann, "Parameter Tuning for dynamic Digital Twin of Generation Unit in Power Grid", ISGT-Europe 2021
- T. Jiang, **X. Song**, S. Schlegel, and D. Westermann, “Hybrids-Simulation Using eMEGASIM and ePHASORSIM for Converter Dominated Distribution Grid,” in NEIS 2018; Conference on Sustainable Energy Supply and Energy Storage Systems, Hamburg, pp. 55–61.
- C. Brosinsky**, X. Song**, and D. Westermann, “Digital Twin - Concept of a Continuously Adaptive Power System Mirror,” in Internationaler ETG Kongress 2019, Esslingen, Germany.
- T.Jiang, **X. Song**, S.Schlegel and D. Westermann, “Aggregated Model to Investigate the Interaction in Inverter-dominated distribution grids,” in Proc. Internationaler ETG-Kongress, Esslingen am Neckar, 2019.
- J. Kircheis, **X. Song**, T. Jiang, S. Schlegel und D. Westermann, „Improving Distribution System Observability Using Neural Networks“ in 2020 55th International Universities Power Engineering Conference (UPEC), Torino, Italy, 9/1/2020 - 9/4/2020, S. 1–6, doi: 10.1109/UPEC49904.2020.9209778.
- H. Cai, **X. Song** et al., „Modeling Power-to-Gas in the Electrical Energy System in Real-Time Simulator“ in 2020 55th International Universities Power Engineering Conference (UPEC), 2020, S. 1–6, doi: 10.1109/UPEC49904.2020.9209793.
- H. Cai, Y. Zeng, **X. Song**, T. Jiang, S. Schlegel, and D. Westermann, “Investigations of real-time Performance Using OPAL-RT and acceleration methods based on different power converter models,” in VDE/IEEE Power and Energy Student Summit 2018

- H. Cai, **X. Song**, T. Jiang, S. Schlegel and D. Westermann, „Controller Optimization to Stabilize Inverter-dominated Distribution Grid“. Proc. VDE/IEEE Power and Energy Student Summit 2019, June 2019

2 State of art

The emergence of the Internet of Things (IoT) [42] is evolving the way of measuring data and exchanging information among different sources. The diffusion of technologies like embedded sensors and the actuators connected with the Internet through the Hardware-in-the-Loop-Simulation [43] concept allows the continuous and real-time data exchange [18] between the digital model and the physical system. With the integration of Machine Learning [44] for processing big data from IoT, it motivates one of the advanced technologies in the application of DT. DT is winning increasing attention due to its potential and powerful implications in application areas, including manufacturing, aerospace, healthcare, etc. The power system area is likewise attracted by its expected potentials.

On this basis, this chapter is intended to describe the current state of research and technology about the issues relevant to this work. After a short overview of the origin and development of DT, the following section 2.2 introduces the application standard of the DT concept in power systems, including the state estimation, monitoring, and identification of power grid operation by DT. In section 2.3, the discussion of DT creation by parameter estimation is supplemented with the state of art for estimation methods. Subsequently, section 2.4 specifies the application of Machine Learning in data processing and feature extraction for the usage in DT. The related research project in the German and European context is presented in the last section.

2.1 Origin of Digital Twin

The foundation of DT technology is the joint usage of the spreading information communication, embedded sensors collecting descriptive high dimensional data, artificial intelligence improvements in data processing, and the high-performance computing technology. It is the integrated solution of multi-technologies. Since the first official declaration of Artificial Intelligence (AI) in 1956 [45], several similar thoughts to the current DT concept have sprouted up. In the initially definition of AI concept, the descriptions like thinking machines, being human-like rather than becoming human, replica of the human mind, emulation of human reasoning, etc. were proposed for its broad sense. With its development, and also the advancement of computation technology, AI applications are providing their benefits in several fields. About 10 years later after the first declaration of AI, the first DT concept-based system, called mirror system was created to monitor unreachable physical spacecraft in emission process by NASA in 1970 [45, 46]. The engineer utilized the simulation environment to develop the operation of Apollo 13 during the emission. According to the simulation test, they found out that an improvised air purifier could be the possible solution to get the crew of Apollo 13 back to earth lives [45].

This successful example motivated the precursors of DT concept with consideration of the potential applications with the mirror system. The virtual and simulated models could be the role in bridging physical and digital spaces. However, these models lacked a seamless connection and real-time data exchange, which could not be the proper DT. The first milestone of DT concept was in 2002 [47]. The concept named Product Lifecycle Management (PLM) was informally introduced with title "Conceptual Ideal for PLM". In this concept, three primary elements were proposed:

(i). Physical space (also called real space in [47])

(ii). Virtual space

(iii). The link for data flow between physical space and virtual space

The link enables the data exchange and allows the convergence and synchronization of the virtual and physical systems. The simulation in virtual space can be applied to optimize the physical system. The connection between them would be linked throughout the entire lifecycle of the system, see Figure 2.1.

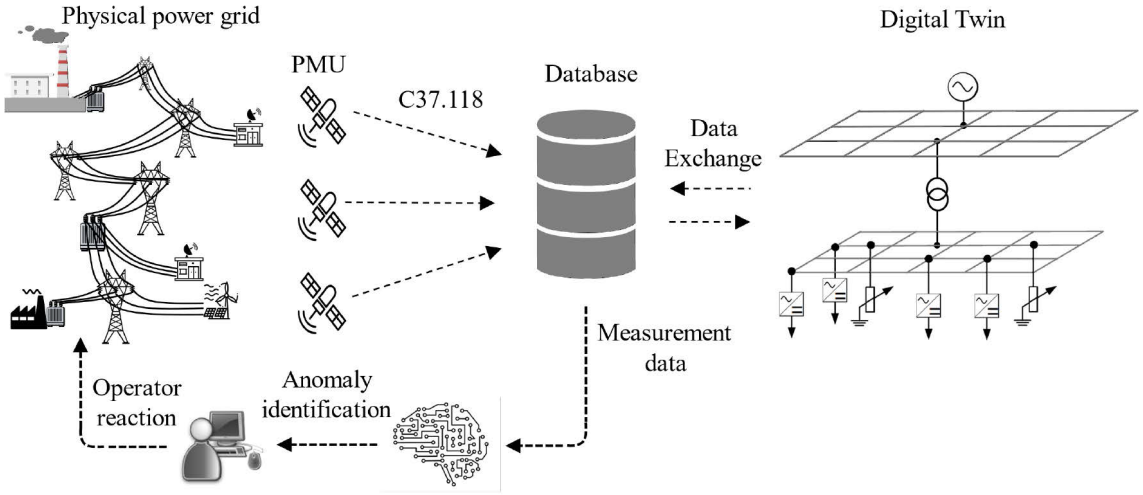

Figure 2.1: Schema of data exchange with DT concept in power system [29, 47]

The discussion of the proposed elements in PLM concept continued in the research report from Framling [48]. He exploited that the seamless connection provided by the spread of Internet technologies between the envisioned agent (DT in virtual space) and the physical counterpart should be synchronous. This proposal is based on the consideration that an effective PLM system enables a real-time view of the product status, from when it is planned and manufactured, through its time of use, and until the time of disposal [45]. Afterwards, the research about DT was considered on the will to increase the understanding about the mirror systems and the intension to reduce the costs and resources.

NASA started investigating and developing DTs in their roadmap [20] ten years after Grieves definition of PLM concept. The definition of the DT in aerospace was described as an integrated multi-physics, multi-scale, probabilistic simulation of system that uses the available physical models, sensor devices, fleet history, etc. to replica the life of its flying twin [49]. In the same year, the conceptual Airframe DT (ADT) model was proposed in [50] to investigate the applications like the predicting the life of aircraft structure and management of it over the entire lifecycle. This model is described as a computational model of individual aircraft. It was expected to be the potential way to improve the management effectiveness for U.S. Air Force. ADT could serve as a virtual health sensor and provide a forecast of future maintenance needs for an individual aircraft [45].

The DT concepts were mentioned in 2013 by U.S. Air Force [51], highlighting that they have a historical memory and the ability to exploit previous and current data to generate condition awareness and system prediction to ensure the agility and adaptivity for rapid development. The Digital Thread concept has been distinguished from DT concept in some research work [45]. Digital Thread refers to the communication framework that allows a connected data flow and integrated view of the asset's data throughout its lifecycle across traditionally siloed functional perspectives. Since the declaration by U.S. Air Force, DT concept is becoming more interest beyond aerospace and defence industry. The integration of digital manufacturing and cyber-physical system by DT concept is the key point of Industry 4.0 and smart manufacturing [52]. The development trajectory of DT mentioned above is summarized in the Figure 2.2:

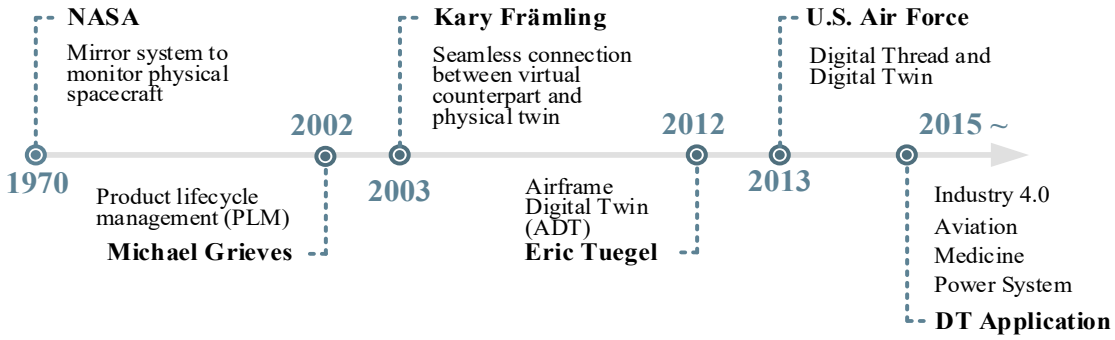

Figure 2.2: Development of DT [45, 47, 50]

The successful application of DT in aerospace has motivated research and implementation to some extent in manufacturing and industrial fields. In these areas, DT is defined as a computer-based digital model or set of digital models that can mirror its physical counterpart, receives information from the physical system, accumulates useful information and helps in decision-making and in the execution of processes [17, 19, 49–51, 53]. DT in the manufacturing area uses computer-based digital models to monitor the procedure in production process and with the assistance of AI algorithms, an autonomous and intelligent

manufacturing approach is executed with minimized human intervention [44]. It can respond to failures or unexpected contingency with automated decision-making among a set of alternative actions to prevent the damage on the whole process at the supervisory level. Also, the connectivity between DT and physical system allows the present and historical data analysis by human experts assisted by AI algorithms to derive solutions to improve operations [22, 45].

2.2 Digital Twins in power system

Regarding the merits of DT in aviation and industrial, the investigation of it in power system is being highly motivated to optimize stability, reduce unpredictable outages, manage variations in market conditions, fuel costs and weather patterns toward more profitability by application of DT concept. In this section, the application of DT are initially illustrated to give an overview about how to implement the concept in the future power system.

2.2.1 Definition of the Digital Twin

In [17, 45, 52], the definition of DT is defined as a set of virtual information for a full description of a potential or actual physical product from the micro atomic level to the macro geometrical level. At this optimal stage, any information that is obtained from the inspection of a physically manufactured product is available from its DT. With the development of simulation technology, this definition is developed as the DT are computer-based models that are simulating, emulating, mirroring the life of a physical entity, which is linked to its physical twin [53]. The integration of AI technology enables DT as a living, intelligent and evolving model, being the virtual counterpart of a physical entity [44]. It allows the lifecycle monitoring, predicting and optimizing of the physical entity. The continuous prediction of future states enables simulating and testing innovative configuration and concept for application of preventively maintenance. In power system, the definition of DT can be summarized by Figure 2.3.

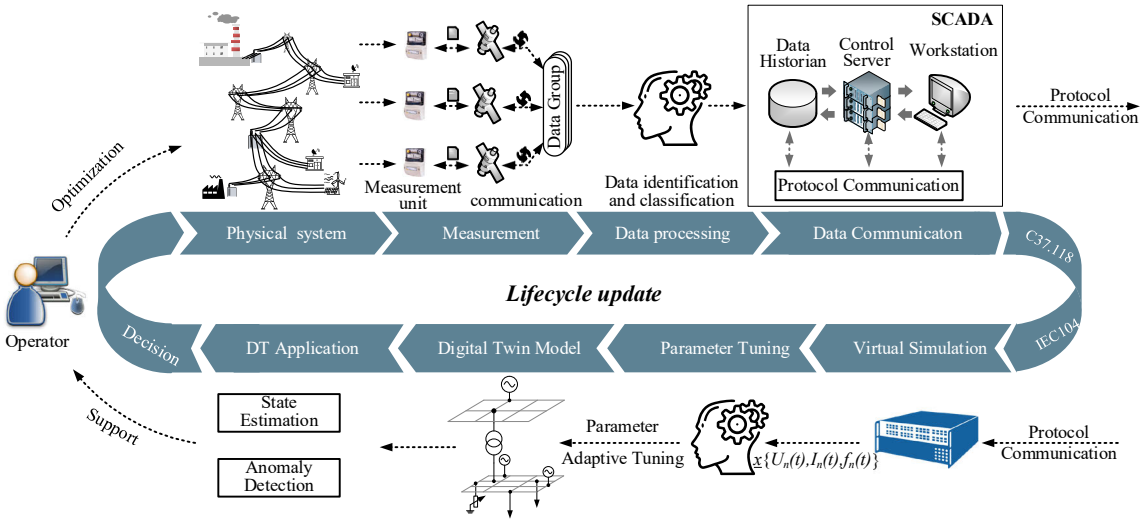

Figure 2.3: Concept of building DT as the precise simulation model for power system [29, 54]

According to the definition in [19, 55], DT in power system involves the measurement, data processing and communication between physical space and virtual environment, parameter estimation, modelling, and application. Figure 2.3 depicts the DT for power system in lifecycle. The states of the physical entity are measured and extracted initially to the data processing. The massive volume data from the measurement is reprocessed with data cleaning, data conversion, and data filtering [56]. Afterwards, the reprocessed data is exchanged to virtual space through the communication tunnel like C37.118. The digital model based on the modelling theory aims to build a virtual representation of the physical system, which needs the parameterization process with measurement from the physical system for adaptive updating the parameters in the virtual model for the purpose of evolving into DT. The DT of power system is a mirror reflection of the physical power grid, which depicts the same feature and behaviours in digital space [15, 57].

Within this dissertation, DT is specified as a dynamic digital model that not only accurately mirrors the phenomena of the physical power system to replicate the operation states for the monitoring, but also highly precisely predicts the dynamic behaviour of the power system to generate the training data for the identification of the type of the occurred event. With parameter estimation, DT is updated timely with the real parameters after status changes in physical system. It can be used as a lifecycle management to optimize and protect the electrical power system.

2.2.2 Applications with Digital Twin in power system

In the state of art, the DT in power system is developed as an assistant for operation optimization [23]. The state estimation is an essential issue for operation optimization in power

system [58]. It is mainly used to identify unknown values of state variates due to the measurements. This technique applies statistical criterion to estimate the actual status of the unknown variable. To provide a reliable and secure power supply, state estimation is used to monitor the operation status and to estimate the unknown values of power system state variables. Another vital function of it is to detect and identify the measurement error in power system, which may lead to the failure decision by operator. With the obtained imperfect measurements from SCADA and PMU, the state estimation is utilized to process the defective data, filter the noise measurements, detect error, and remove the corrupt measurements.

Dynamic State Estimation

The state estimation is a technical approach used to identify unknown values of state variates due to the measurements. This technique applies statistical criterion to estimate the actual status of the unknown variable. To provide a reliable and secure power supply, state estimation is used to monitor the operation status and to estimate the unknown values of power system state variables. Another vital function of it is to detect and identify the measurement error in power system, which may lead to the failure decision by operator. With the obtained imperfect measurements from SCADA and PMU, the state estimation is utilized to process the defective data, filter the noise measurements, detect error, and remove the corrupt measurements.

The static state of a power system is defined as the vector of the voltage magnitudes and angles from all the grid [59]. Correspondingly, the static state estimation is the processing of voltage data for converting redundant meter readings and other available information into an estimation of the static-vector [58]. However, the power system is a dynamic system including stochastic variations in demand and generation. The operation status of it is further aggravated by the large-scale integration of distributed feed-in generation, and complex loads and new demand-response technologies on the demand side, such as electric vehicles and internet of things devices. This kind of shift is leading to more uncertainties in the dynamic properties of the system. Accordingly, the static state estimation is unable to capture these dynamics in an operational environment. As a consequence, the static state estimation methods used in energy management system should be re-evaluated and supplemented by new surveillance techniques such as dynamic state estimation (DSE) [58–60]. DSE is capable of accurately monitoring the dynamics of system states and is expected to perform an essential function in the management and protection of energy system, especially in the increasing complexity resulting from the uncertainties of new technologies used on the generation and demand sides [60].

In [22, 29], DT is utilized as a tool for DSE. The DT -in-the-Loop simulation [43] opens the door for the use of DT in DSE, see Figure 2.4. As mentioned above, DT can mirror the

physical system or entity according to the measured data, which means that the states of physical system can be observed by DT and the dynamic uncertainties is accessible through estimation by dynamic simulation of DT. Accordingly, the meaning of DT in the context of loop simulation begins to be clearer.

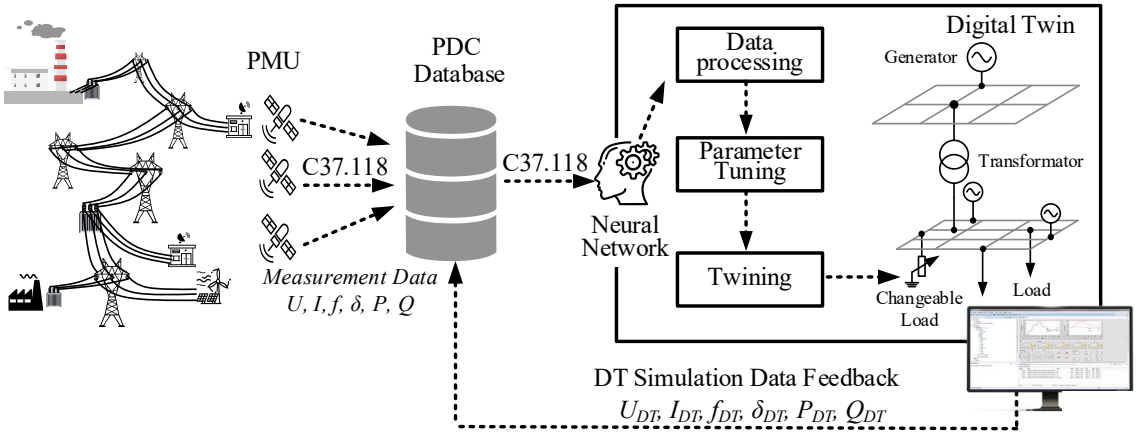

Figure 2.4: Digital Twin-in-the-Loop simulation for DSE [29]

But one necessary step, the twining process is still missing before the digital model evolves to DT. A simple understanding of the twinning process is to replicate the dynamic states from physical system in digital environment. This duplication process is adaptive and in real-time. Any slight changes can be detected and mirrored in the DT. Figure 2.4 allows us to understand he DT in-the-Loop simulation for DSE more clearly. The initial phase is the data measurement and data collection from physical power grid, which is stored in Phasor Data Concentrator (PDC) database. The measurement equipment like Phasor Measurement Unit (PMU) measure the operation states in power grid with phasor values, which includes the amplitude and angle (δ) of the voltage (U) and current (I). The operational frequency of physical power grid can also be measured by PMU. The active and reactive power (P and Q) can be calculated and then collected by the PDC database. These data are utilized later for parameter tuning for twining process. The physical power grid is not directly involved in the loop-simulation, but the measured data from the physical system, which is stored in the PDC database, participate in the loop simulation through the communication protocol. The real-time simulation receives the data through communication protocols and transfers it to the digital simulation environment. Before it takes part in parameter tuning process, the data needs firstly to be classified. The useless information like the measurement noise and white noise signal are removed in data processing. The mirroring process is completed by continuous adapting the parameters of virtual model that dynamically duplicate the operational state of physical power grid. The simulation results of DT are transferred through the back-loop link to PDC database, which can be used to monitor and predict the operating state of the physical system.

Predictive simulation and operator decision support

With Digital Twin, predictive simulation is possible to predict the operating status and possible critical events in the physical power grid. In the event of a fault event such as a short circuit in the nearby generator, the system can use the Digital Twin's predictive simulation to determine how this will affect the stability of the entire system. This approach is useful for evaluating and optimizing operation by informing the required maintenance in advance of the expected failures. Basically, this is a Digital Twin-based dynamic network security analysis (DSA). As shown in Figure 2.5, the operator can use the predictive simulation results to support the decision in the control room. Using AI algorithms such as machine learning, the data can be extracted with feature information to detect changes and identify key patterns and trends. The figure outlines how Digital Twin applications and DSA interact with the control room GUI to support the operator's decision. The SCADA database has access to the PDC database to receive the measured physical data from the PMU. The Remote Terminal Unit (RTU), a measurement and communication unit in a substation, provides the measurement data to the SCADA database via the IEC 60870-5-104 protocol [61]. These data are used in DSA, status estimation and power flow calculation in the digital control room to determine the operating status in the physical power network and make it available to the operator for evaluation. In the future, Digital Twin will provide additional predictive analyses to estimate future states and important changes in the power network to further support the operator in optimizing operation.

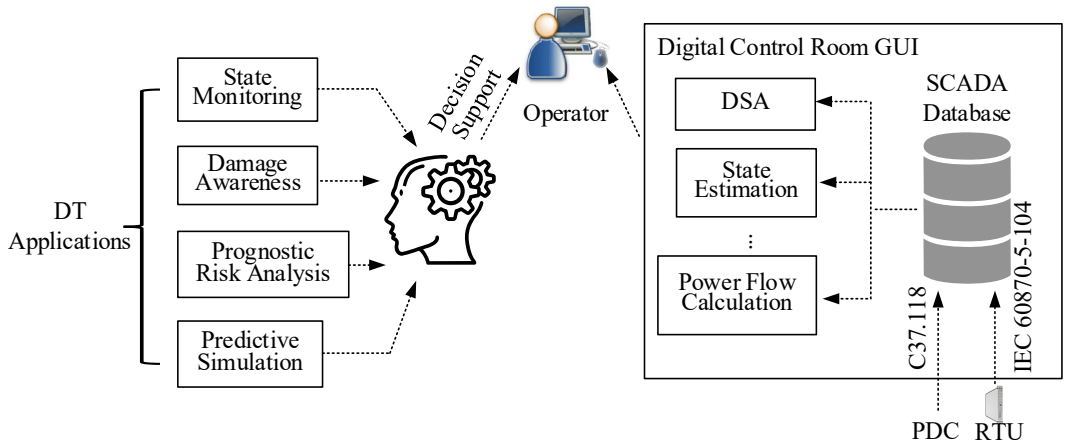

Figure 2.5: Decision support by Digital Twin applications [29]

Surveillance of operation states with Digital Twin

In [29, 40], the surveillance of operation sates by DT is introduced for the application in distribution grid. DT is characterized by its ability to monitor the physical system accurately and adaptively on different scales of time. Accordingly, the DT can be a part of the

cyber-physical system, which interacts with the physical entities, e.g. equipment, environment, and humans. The physical power grid communicates with virtual cyberspace through the closed-loop-simulation. Each component in physical power grid has its digital representation. Since the DT replicates the real world as closely as possible, the system can also be monitored on the basis of DT. Figure 2.6 outlines the interaction between the real network, the DT and the applications based on it. DT is thus the data supplier for applications such as stability considerations, forecasts and condition monitoring. In this sense, the DT takes on the current role of a SCADA database with subsequent state estimation.

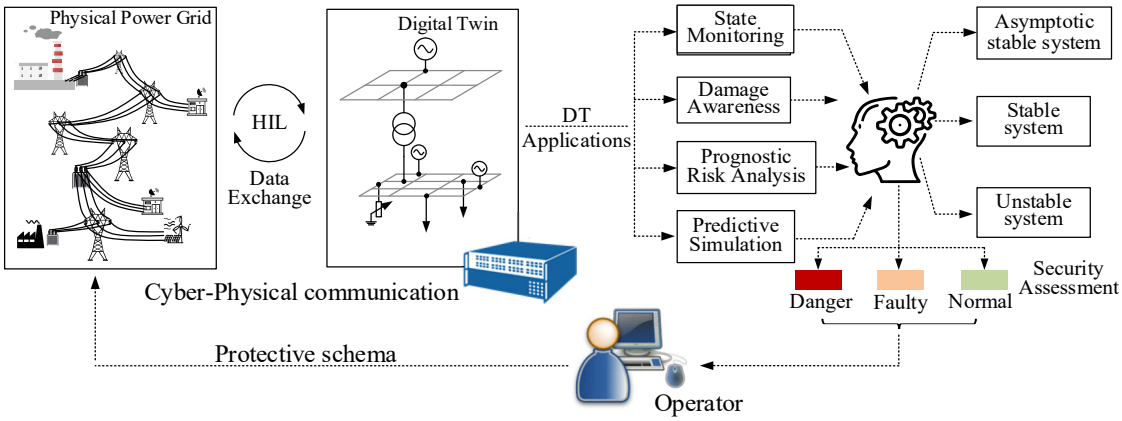

Figure 2.6: Surveillance of operation states by DT [29, 40]

This provides the operator with information about the system status and the development of the system state. The information base is much closer to the physical process than it could be with other processes. It is even foreseeable that in the future the operator will receive proposals for action for the network operation based on this information.

2.3 Digital Twin creation with parameter estimation

The parameter estimation is the essential step for DT creation [23]. In [23, 57], it shows that the DT creation without parameter estimation can lead to the low accuracy in emulating the dynamic behaviour of physical system. The parameter tuning can guarantee the adaptivity with updating proper parameters in the model for replica of the physical operation state [35]. Figure 2.7 outlines the complete process of parameter estimation and keeping the adaptivity of DT with physical power grid “alive”. The operation state in physical power grid is firstly measured by the measurement equipment e.g., PMU, which is transferred to the database by the data communication ways like the protocol communication mentioned above. Usually, the virtual model is not directly accessible to the database server for modelling DT. The DT simulation provides the link to connect the virtual simulation platform with the database server via power system communication protocols. The parameters of the component like the generator, transformer and the load are set up in the

digital model with a parameter set from the simulator (start set of parameters). The values of this start set of parameters typically differ slightly from the real, measured data due to climate conditions or changes in the operating behaviour of the components due to wear. The adaptive parameter tuning process aims to solve this problem. By updating of the physical operation data in tuning algorithm, the parameter is tuned correspondingly and updated in DT to keep the simulation as close to the real world as possible.

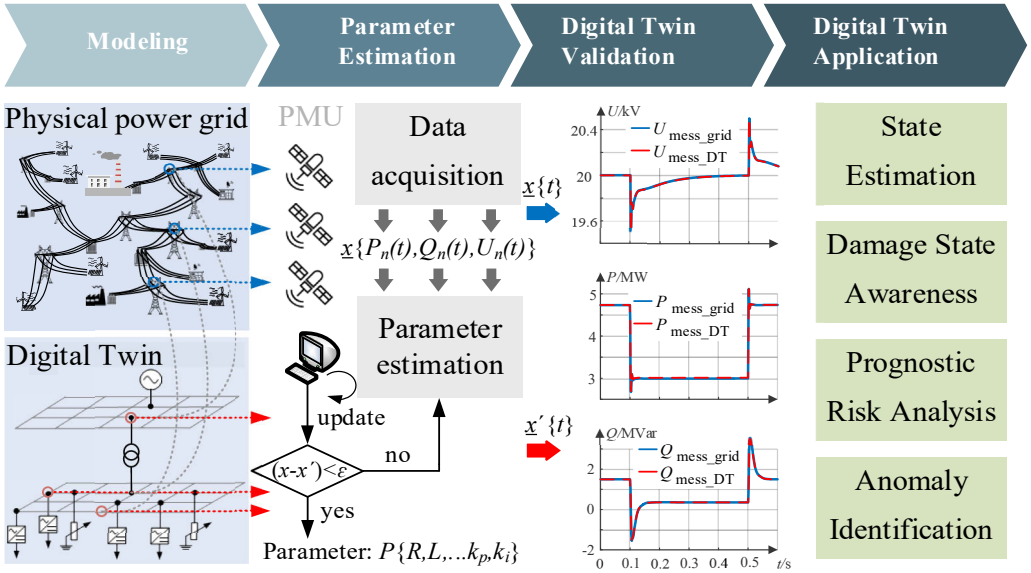

Figure 2.7: Schema of parameter estimation process for DT creation [39]

Parameter estimation problem is referred to be the subarea of system identification. In the context of DT creation, the DT that represents the dynamic feature usually contains inaccurate coefficients, which lead to a different dynamic reaction compared with the measured physical data. Accordingly, these coefficients need to be estimated by using numerical optimization to fit the DT to observed measurements [95]. Before applying the appropriate methods for parameter estimation, a prior knowledge and the physical insight of system are essential to select the correct methods for further numerical optimization. The DAE model can be distinguished in three types: white-box, grey-box and black-box as depicted in Figure 2.8.

In the white-box model, the DAEs that describe the relations between the states of physical system should be accurate and the parameters are totally known [62]. To accomplish this type of modelling, a prior knowledge about the structure, the parameters of the physical system and physical insight are required. These are usually unrealistic because of the lack of the explicit structure description of physical insight and the other uncontrollable conditions like weather change, temperature change that can lead to the change of parameters. In contrast to the white-box model, there is no a prior knowledge and no available physical

insight in black-box model. The available information is the input and output measurement. The identification of the model structure is the initial step to build the black-box model. According to the well-known types and the purpose of the identification task, the model structure is assumed for the further validation. The model can be assumed with the description in several structures which are not able to explicit reflect any internal physical relations inside the model. Grey-box model is between the above mentioned cases, which provide internal physical representation of system but several parameters are missing and need to be determined from measured data [62]. The typical modelling in power system is exactly from the grey-box modelling concept. A prior knowledge of power electrical components is utilized to set up the structure of the model and then the physical insight of these components can be manifested by DAEs.

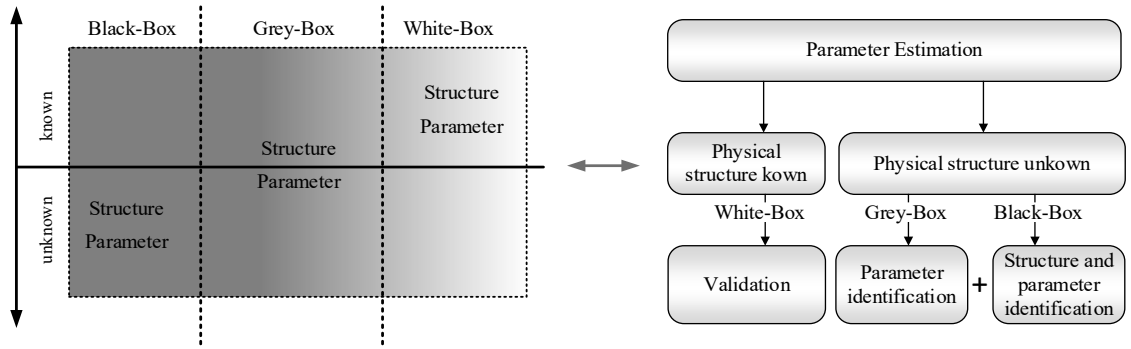

Figure 2.8: Classification of DAE model [62]

The idea of parameter estimation to calculate the coefficients in DAEs to fit the measurement vector. It is usually done by minimizing a scalar function called objective function that includes the difference or residuals $\boldsymbol{e}_i$ between input-output of the DT and the measured data [35, 63]:

$$\boldsymbol{e}_i = |\boldsymbol{\mathcal{X}}_i{}^m - \boldsymbol{\mathcal{X}}_i| \tag{2.1}$$

where $\boldsymbol{\mathcal{X}} = [\overline{\boldsymbol{y}}\ \boldsymbol{u}]^{\mathrm{T}}$ and $\boldsymbol{\mathcal{X}}^m$ is the measurement. $\overline{\boldsymbol{y}}$ is the calculated output using the estimated parameters. $\boldsymbol{u}$ denotes the vector of input data. Three methods based on this idea are used in this work for parameter estimation.

2.3.1 Least-square algorithm

In [39], the state of art for least-square (LSQ) based parameter estimation is introduced for creating DT of synchronous generator. The objective function of LSQ is the sum of squares of the errors [62]:

$$\varphi^{\mathrm{LSQ}} = \sum_{i=1}^{N} [(y_i{}^{\mathrm{m}} - y_i)^{\mathrm{T}} (y_i{}^{\mathrm{m}} - y_i)] \tag{2.2}$$

However, the use of pure residuals is not sufficient for the formulation of the parameter estimation problem. The following reasons are given [64]:

- The different state variables y represents different physical quantities, which ranges in different size.
- Some experimental data are not reliable. Therefore, it is useful to weigh these measured values less to reduce their influence on the results of the parameter estimation.

Another extended method based on least square form for a better estimation with conducting a series of runs is the weighted least square form. To take into account the above-mentioned aspects, the weighted least squares method is used by inserting the weighting matrix in objective function:

$$\varphi^{\mathrm{WLS}} = \sum_{i=1}^{N} \boldsymbol{e}_i{}^{\mathrm{T}} \cdot \boldsymbol{W}_i \cdot \boldsymbol{e}_i \tag{2.3}$$

where $\boldsymbol{e}_i$ is the residual vector and $\boldsymbol{W}_i$ is the weighting matrix. The elements selected in the matrix are used to indicate the degree of confidence that one can place in the individual measurement. Based on an initial parameter set, the model parameters φ are modified by a non-linear optimization procedure in a way that they initially assume a minimum with the mentioned objective function φ^{WLS}. The least square estimation (LSQ) and weighted least square (WLS) estimation enables the determination of the estimated parameters. But the parameter vector cannot provide the corresponding information on the accuracy of the estimated values. The solution to this problem is achieved by using the maximal likelihood (ML) estimation method. For linear system, this method can be demonstrated as a consistent, asymptotically efficient parameter estimation method, i.e., the accurate parameter can be obtained at the boundary condition with many disturbances in measurements. Under the assumption that the measurement errors are not correlated and normally distributed with the mean value, the probability function P can be calculated with the obtained measurements values $\boldsymbol{y}$ and the parameter set $\boldsymbol{p}$.

$$P(\boldsymbol{y}|\boldsymbol{p}) = (2\pi)^{-\frac{n \cdot N}{2}} \prod_{k=1}^{N} |\mathbf{C}_k|^{-\frac{1}{2}} \cdot e^{-\frac{1}{2}\sum_{k=1}^{N} [\mathbf{y}(p) - \mathbf{y}_{\mathrm{k}}{}^{m}]^T \boldsymbol{C}_{\mathrm{k}}{}^{-1} [\mathbf{y}(p) - \boldsymbol{y}_{\mathrm{k}}{}^{m}]} \tag{2.4}$$

where $\boldsymbol{C}_k$ is the covariance matrix of the measurement error at kth.

$$\boldsymbol{C}_k = E\{(\boldsymbol{y}_k - \boldsymbol{z}_k)(\boldsymbol{y}_k - \boldsymbol{z}_k)^{\mathrm{T}}\} \tag{2.5}$$

Here E is the expectation. $\boldsymbol{z}_{\mathrm{k}}$ is the reference value and $\boldsymbol{y}_{\mathrm{k}}$ is the measurement vector disturbed with the measurement error. The probability is exact by searching a maximum parameter $\boldsymbol{p} = \boldsymbol{p}^*$. With the optimization algorithm, the estimated parameter vector can be changed iteratively from the initial parameter set until the maximum is found. It is supposed that the correct model structure of the estimated model is recognized and therefore only the parameter set need to be calculated. The equation (2.4) can be simplified with the Logarithm:

$$\begin{aligned} \varphi &= -\ln P(\boldsymbol{y}|\boldsymbol{p}) \\ &= \frac{1}{2}\sum_{k=1}^{N} \ln(|\boldsymbol{C}_k|) + \frac{1}{2}\sum_{k=1}^{N} [y(p) - {y_{\mathrm{k}}}^m]^T {\boldsymbol{C}_{\mathrm{k}}}^{-1} [y(p) - {y_{\mathrm{k}}}^m] \end{aligned} \tag{2.6}$$

For further simplification, the constant parts in the equation (2.6)can be ignored, since they have no influence on the optimization result. Then the ML function takes the following form [65]:

$$\varphi^{\mathrm{ML}} = \sum_{i=1}^{N} {\boldsymbol{e}_i}^{\mathrm{T}} \cdot {\boldsymbol{C}_i}^{-1} \cdot \boldsymbol{e}_i \tag{2.7}$$

This simplified ML function is similar with the WLS. It is assumed that the inverse of the covariance matrix ${\boldsymbol{C}_i}^{-1}$ for weighted matrix $\boldsymbol{W}_i$.

2.3.2 Recursive least-square algorithm

The recursive LS (RLS) is referred in [40] for parameterizing DT of inverter-based feed-in generations to apply it for surveillance of physical operations in power system. In recursive process method, the parameter set in system are computed recursively over time [66]. The counterpart to online methods is the offline or batch methods (see the description in LS, WLS and ML), in which all the observations are used simultaneously to estimate the parameters in the model [35]. The mathematical process of RLS is considered with the Auto-Regressive Moving Average Exogenous (ARMAX) structure for parameter estimation. The normal ARMAX structure is [67]:

$$A(z)y(t) = B(z)u(t) + D(z)v(t) \tag{2.8}$$

where $u(t)$ and $y(t)$ are the system input and output, respectively, $v(t)$ is a stochastic white noise with zero mean and variance σ^2. $A(z)$, $B(z)$ and $C(z)$ are polynomials in z^{-1}, which are defined:

$$\begin{aligned} A(z) &= 1 + a_1 z^{-1} + a_2 z^{-2} \cdots + a_{n_\mathrm{a}} z^{-n_\mathrm{a}} \\ B(z) &= b_1 z^{-1} + b_2 z^{-2} \cdots + b_{n_\mathrm{b}} z^{-n_\mathrm{b}} \\ D(z) &= 1 + d_1 z^{-1} + d_2 z^{-2} \cdots + d_{n_\mathrm{d}} z^{-n_\mathrm{d}} \end{aligned} \tag{2.9}$$

The structure of the presented ARMAX model is shown in the Figure 2.9 with the assumption of the known n_a, n_b and n_c.

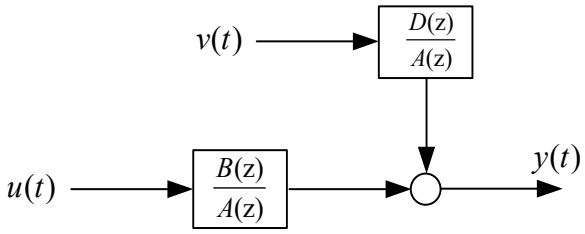

Figure 2.9: ARMAX model structure [40, 66, 68]

In case of a distributed system, the equation for describing the system in (2.8) can be rewritten for the observation with *N* measurements:

$$y(t) = \boldsymbol{\theta}^{\mathrm{T}} \boldsymbol{\varphi}(t) + \boldsymbol{e}(t) \tag{2.10}$$

where the notations are $\boldsymbol{\theta}^{\mathrm{T}} = \left[a_1, a_2, \cdots, a_{n_\mathrm{a}}, b_1, b_2, \cdots, b_{n_\mathrm{b}}, d_1, \cdots, d_{n_\mathrm{d}}\right]$ and $\boldsymbol{\varphi}^{\mathrm{T}}(t) = [-y(t-1), \cdots, -y(t-n_\mathrm{a}), \cdots u(t-n_\mathrm{b}), v(t-1) \cdots, v(t-n_\mathrm{d})]$. The $\boldsymbol{\theta}^{\mathrm{T}}$ is the vector of the estimated parameters and $\boldsymbol{\varphi}^{\mathrm{T}}(t)$ is the vector of the data including the system $\boldsymbol{\varphi}^{\mathrm{T}}{}_{\mathrm{s}}(t)$ and noise $\boldsymbol{\varphi}^{\mathrm{T}}{}_{\mathrm{n}}(t)$. $y(t)$ is the output of model and $v(t)$ is the noise signal in measurement data. The LS solution based on the observations $\boldsymbol{\varphi}_i$ is given as the solution to the normal equations [67]:

$$\left(\sum_{i=1}^{t} \boldsymbol{\varphi}_i \boldsymbol{\varphi}_i{}^{\mathrm{T}}\right) \widehat{\boldsymbol{\theta}}_{\mathrm{t}} = \left(\sum_{i=1}^{t} y_i \boldsymbol{\varphi}_i\right) \tag{2.11}$$

Under the assumption that the solution $\widehat{\boldsymbol{\theta}}_{\mathrm{t}}$ is unique, i.e., the matrix $\boldsymbol{M}_{\mathrm{t}} = \sum_{i=1}^{t} \boldsymbol{\varphi}_i \boldsymbol{\varphi}_i{}^{\mathrm{T}}$ is inversible. Since trivially matrix has

$$\boldsymbol{M}_{\mathrm{t}-1} = \boldsymbol{M}_{\mathrm{t}} - \boldsymbol{\varphi}_{\mathrm{t}} \boldsymbol{\varphi}_{\mathrm{t}}{}^{\mathrm{T}} \tag{2.12}$$

Then, the equation (2.11) is rewritten:

$$\widehat{\boldsymbol{\theta}}_{\mathrm{t}} = \boldsymbol{M}_{\mathrm{t}}{}^{-1}\left(\sum_{i=1}^{t-1} y_i\boldsymbol{\varphi}_i + y_{\mathrm{t}}\boldsymbol{\varphi}_{\mathrm{t}}\right) = \boldsymbol{M}_{\mathrm{t}}{}^{-1}\left(\boldsymbol{M}_{\mathrm{t}-1}\widehat{\boldsymbol{\theta}}_{\mathrm{t}-1} + y_{\mathrm{t}}\boldsymbol{\varphi}_{\mathrm{t}}\right) \tag{2.13}$$

With the integration of equation (2.12) into (2.13), we could get the recursive form of LS:

$$\begin{aligned}\widehat{\boldsymbol{\theta}}_{\mathrm{t}} &= \boldsymbol{M}_{\mathrm{t}}{}^{-1}\left((\boldsymbol{M}_{\mathrm{t}} - \boldsymbol{\varphi}_{\mathrm{t}}\boldsymbol{\varphi}_{\mathrm{t}}{}^{\mathrm{T}})\cdot\widehat{\boldsymbol{\theta}}_{\mathrm{t}-1} + y_{\mathrm{t}}\boldsymbol{\varphi}_{\mathrm{t}}\right)\\ &= \widehat{\boldsymbol{\theta}}_{\mathrm{t}-1} + \boldsymbol{M}_{\mathrm{t}}{}^{-1}\boldsymbol{\varphi}_{\mathrm{t}}\left(y_{\mathrm{t}} - \widehat{\boldsymbol{\theta}}_{\mathrm{t}-1}^{\mathrm{T}}\boldsymbol{\varphi}_{\mathrm{t}}\right)\end{aligned} \tag{2.14}$$

In summary of equation (2.14)

$$\begin{aligned}\varepsilon_{\mathrm{t}} &= y_{\mathrm{t}} - \widehat{\boldsymbol{\theta}}_{\mathrm{t}-1}^{\mathrm{T}}\boldsymbol{\varphi}_{\mathrm{t}}\\ \boldsymbol{K}_{\mathrm{t}} &= \boldsymbol{M}_{\mathrm{t}}{}^{-1}\boldsymbol{\varphi}_{\mathrm{t}}\\ \widehat{\boldsymbol{\theta}}_{\mathrm{t}} &= \widehat{\boldsymbol{\theta}}_{\mathrm{t}-1} + \boldsymbol{K}_{\mathrm{t}}\cdot\varepsilon_{\mathrm{t}}\end{aligned} \tag{2.15}$$

where the indicator ε_t is interpreted as the prediction error, which presents the difference between the observed sample y_t and the predicted value $\widehat{\boldsymbol{\theta}}_{\mathrm{t}-1}^{\mathrm{T}}\boldsymbol{\varphi}_{\mathrm{t}}$. If ε_{t} is small enough, the estimation $\widehat{\boldsymbol{\theta}}_{\mathrm{t}}$ is good and need not to be modified. The matrix $\boldsymbol{K}_{\mathrm{t}}$ is interpreted as the weighting matrix characterizing how much each element of the parameter vector $\widehat{\boldsymbol{\theta}}_{\mathrm{t}-1}$ should be modified with ε_{t}.

2.3.3 Artificial neural network

Except for passive parameter estimation mentioned above, the active parameter estimation based on artificial neural network (ANN) is the usually used method for a robust parameterization [69]. The state of the art concerning the estimation of the non-measurable states using ANN is presented in [23, 35] for adaptive estimating controller parameters to create the inverter DT. It is dedicated to parameter estimation in the continuous time domain for a large class of the unknown parameters. According to the state of art, the procedure with ANN for parameterization begins from a consideration of the class of nonlinear systems [70]:

$$\dot{\boldsymbol{x}} = f(\boldsymbol{x}, \boldsymbol{\theta}(t), \boldsymbol{u}) \tag{2.16}$$

where $\boldsymbol{x} \in \mathfrak{R}^{\mathrm{n}}$ is the vector of the states in system, $\boldsymbol{u} \in \mathfrak{R}^{\mathrm{m}}$ ($\mathrm{m} \leq \mathrm{n}$) is the measurable inputs, $\boldsymbol{\theta} \in \mathfrak{R}^{\mathrm{p}}$ is the vector of unknown parameters with $1 \leq \mathrm{p} \leq \mathrm{n}$. By Taylor formula, the nonlinear system can be rewritten as:

$$\dot{\boldsymbol{x}} = f(\boldsymbol{x}, \boldsymbol{\theta}_{\mathrm{n}}, \boldsymbol{u}) + \Delta f(\boldsymbol{x}, t, \boldsymbol{u}) \tag{2.17}$$

The term $f(\boldsymbol{x}, \boldsymbol{\theta}_{\mathrm{n}}, \boldsymbol{u})$ a continuous on a compact Ω. Therefore, it can be approximated by the ANN function [36]:

$$f(\boldsymbol{x}, \theta(t), \boldsymbol{u}) = \Psi(\boldsymbol{X}, \boldsymbol{w}) + e_f(\boldsymbol{x}) + \Delta f(\boldsymbol{x}, t, \boldsymbol{u}) \tag{2.18}$$

where Ψ is the neural observer. $\boldsymbol{X}$ is the measurable input of the ANN and $\boldsymbol{w}$ is the weight vector. $e_f(\boldsymbol{x})$ is the optimal approximation error tolerance, which is unknown and bounded $\forall \boldsymbol{x} \in \Omega$. The neural observer is written in details:

$$\dot{\hat{x}} = \Psi(\boldsymbol{X}, \hat{\boldsymbol{w}}) + \boldsymbol{b}(\boldsymbol{x}, \hat{\boldsymbol{x}}, t) = \sum_{i}^{N} \sum_{j}^{N} w_{ij} \Phi(\left\| X - C_j \right\|, v_j) + \sum_{i}^{N} b_i(x_i, \hat{x}_i) \tag{2.19}$$

where the terms bias *i.e.* $b_i(x_i, \hat{x}_i)$ are used to improve the convergence of the neural network, C_j and v_j are the central and the width of the jth hidden units. N is the number of hidden nodes. The radial basis functions Φ have the following from:

$$\Phi(Z, v) = \mathrm{e}^{\frac{-\|Z\|^2}{2v^2}} \tag{2.20}$$

The central C_j and the width parameter v_j of the jth hidden unit are chosen by the clustering methods [35]. To study the convergence of the neural observer, the observer error is considered $\boldsymbol{e} = \hat{\boldsymbol{x}} - \boldsymbol{x}$. The observer error dynamic can be computed as follows:

$$\dot{\boldsymbol{e}} = \Psi(\boldsymbol{X}, \hat{\boldsymbol{w}}) - \Psi(\boldsymbol{X}, \boldsymbol{w}^*) + \boldsymbol{b}(\boldsymbol{x}, \hat{\boldsymbol{x}}, t) - e_f(\boldsymbol{x}) - \Delta f(\boldsymbol{x}, t, \boldsymbol{u}) \tag{2.21}$$

To derive the bias $\boldsymbol{b}(\boldsymbol{x}, \hat{\boldsymbol{x}}, t)$ and the learning rule of the weight $\boldsymbol{w}$, the Lyapunov function is taken into account:

$$\mathrm{V} = \frac{1}{2} \boldsymbol{e}^{\mathrm{T}} \boldsymbol{e} + \frac{1}{2} \sum_{i=1}^{n} \sum_{j=1}^{N} (\hat{w}_{ij} - w_{ij}^*)^2 + \frac{1}{2} (\hat{\boldsymbol{\lambda}} - \boldsymbol{\lambda})^2 \tag{2.22}$$

The derivation of the Lyapunov function is [70]:

$$\dot{\mathrm{V}} = \sum_{i=1}^{n} e_i \dot{e}_i + \sum_{i=1}^{n} \sum_{j=1}^{N} \dot{\hat{w}}_{ij} (\hat{w}_{ij} - w_{ij}^*) + (\hat{\boldsymbol{\lambda}} - \boldsymbol{\lambda}) \dot{\hat{\boldsymbol{\lambda}}} \tag{2.23}$$

With integration of equation (2.21) into equation (2.23)

$$\dot{\mathrm{V}} = \boldsymbol{e}^{\mathrm{T}}\boldsymbol{b}(\boldsymbol{x},\hat{\boldsymbol{x}},t) + \sum_{i=1}^{n}\sum_{j=1}^{N}(\hat{w}_{ij} - w_{ij}^{*})(\dot{\hat{w}}_{ij} - e_i \frac{\partial \Psi_i}{\partial w_{ij}}\Big|_{w_{ij}=\hat{w}_{ij}}) - \boldsymbol{e}^{\mathrm{T}}(e_f(\boldsymbol{x}) + \Delta f(\boldsymbol{x},t,\boldsymbol{u})) + (\hat{\boldsymbol{\lambda}} - \boldsymbol{\lambda})\dot{\hat{\boldsymbol{\lambda}}} \tag{2.24}$$

The conditions to select the bias $\boldsymbol{b}(\boldsymbol{x},\hat{\boldsymbol{x}},t)$, the learning rule of the weight $\boldsymbol{w}$ and the unknown constant λ is to set the Lyapunov function to zero:

$$\begin{cases} b_i(x,\hat{x},t) = -\alpha e_i - \dfrac{\hat{\lambda}^2 e_i}{\left|\hat{\lambda} e_i\right| + \xi}, i = 1,\cdots,n \\ \dot{\hat{w}}_{ij} = e_i \dfrac{\partial \Psi_i}{\partial w_{ij}}\Big|_{w_{ij}=\hat{w}_{ij}}, i = 1,\cdots,n; j = 1,\cdots,N \\ \dot{\hat{\boldsymbol{\lambda}}} = \begin{cases} 0 \\ \sum\limits_{i=1}^{n}\left|e_i\right|, \text{when} \left\|e_i\right\| \geq \zeta \end{cases} \end{cases} \tag{2.25}$$

with $\alpha > 0$ and ξ is a small positive constant and the constant ζ satisfies the following property

$$\zeta > \sqrt{\frac{n\xi}{\alpha}} \tag{2.26}$$

It can be indicated that if $\|e\| > \sqrt{\frac{n\xi}{\alpha}}$, the above equation (2.24) satisfies the inequality condition of Lyapunov $\dot{\mathrm{V}} < 0$.

The above mentioned parameter estimation methods have been published in [23, 39, 40]. These methods are also utilized in this paper for creating DT of dynamic components in power system specialized for synchronous machine including its corresponding controllers and the inverter-based generations. The mathematical deduction with algebraic equations of these dynamic components in power system is detailed in chapter 3.

2.4 Digital Twin application for event identification

The DT is running in parallel with the operation to monitor the operating status of the real power grid. If there is a large deviation of the real measured data from the states of the DT, there is an indication of an anomaly in the real system. The operator can be warned immediately if the operating behaviour deviates from the expected predictive simulation (DT simulation).

The study for event identification in power systems have been investigated intensively for fault early detection and power system protection [32, 34, 71]. Generally, the efficient detection and identification help to protect equipment by the disconnection of fault lines before the significant damage [72]. The accurate location is applied to remove the persistent faults and locate areas where faults regularly occur to set up the protective measures for reducing the frequency of the outages [73]. Machine Learning algorithm for fault event diagnose in classification and location of different faults types optimizes the accuracy of the diagnose and reduce the response of the classification and identification [74]. Many issues have raised by development of an accurate event detection and identification system with Machine Learning [75]. Based on the created knowledge base, comprising the information of operation setpoints, Machine Learning algorithm can, according to the featured data, classify the safe or unsafe operation points using a post-disturbance variable criterion e.g. voltage at certain buses and frequency of the power system. In [76], a combined support vector classifier (SVC) is used to classify the operation performances for each critical contingency to support the assessment. It describes the process by dividing the original measured data into a subset of the data, which turns to solve a sub-problem of the original problem by each SVC solver. With SVC, a hyperplane is constructed as the decision surface, in such a way that the margin of separation between positive and negative examples is maximized [76]. An accurate identification of dynamic at different operating and contingency conditions can support the operator to rescheduled generator and shedding load to keep the stable operation of power system [77]. Through support vector machine (SVM) [77], coherent generator groups can be identified by the rotor angle values following a large disturbance. According to the identified swing state of generator, the operator decides the operation change at the load end or generator end to optimize the power system.

The training data from DT and measurement data from SCADA, PMU etc. are massive, high-dimensional, and sparse and spatial-temporally correlated data. The data contains nearly all the relevant information like the occurring events, operation states, etc. in the power system. With the massive and high-dimensional data, the power system operators often reach a cognitive barrier when information arrives too fast during the event [78, 79]. It is difficult for operators to properly classify and identify events for a correct diagnosis of the problem with such big data, leading to a wrong decision when the actions must be taken. AI provides the way to improve the EMS for an effective classification and identification of the occurring events to support the operator to make the proper decision [24]. Machine Learning, as one of the specifics from AI, refers to the practice of using algorithms to parse data, learn from it and then make determination or prediction [77]. With this feature, it can provide increasing levels of automation in the knowledge engineering process, replacing much time-consuming human activity with automatic techniques that improve accuracy and efficiency by discovering and exploiting regularities in training data

[80]. Accordingly, it has a huge potential to implement Machine Learning in big data analysis for evolving the smart grid.

In this work, Machine Learning is utilized to analyze the data from the DT and extract the feature data to detect and identify the anomaly in power system. With the applications of DT like state monitoring, state estimation, predict simulation, etc., these produce a big data. It is difficult for operators to make a fast decision with such high dimension information. Machine Learning have the ability to extract the attributes and identify the pattern of anomaly event in power system efficiently to support the decision for operator. The procedure for the application of Machine Learning in event identification is summarized with the Figure 2.10. Three steps are necessary before the application in event identification [81]: Data dimensionality reduction, algorithms training and evaluation.

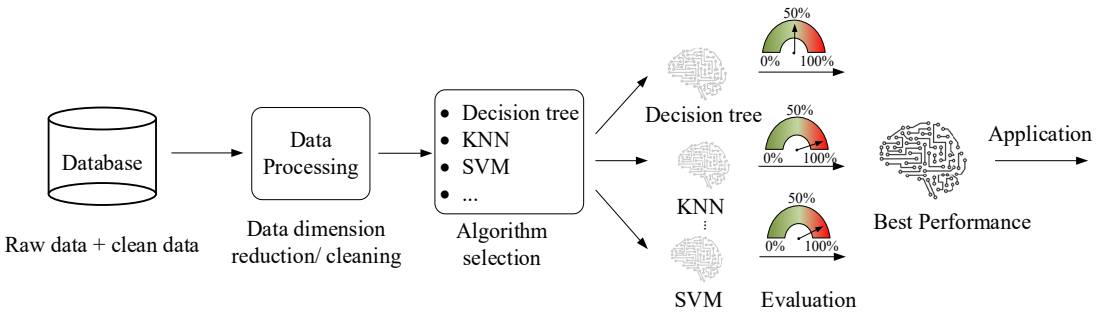

Figure 2.10: Procedure of Machine Learning from data processing to application [81]

2.4.1 **Data processing**

The framework of fault detection, classification and location is shown in Figure 2.11. The feature extraction enables a solution for extracting the signals with raw information. The feature extraction techniques dig out useful information purposefully and reduce the impact of variance within the system [73, 82]. The proper feature extraction method is useful to gain a better awareness of the character of the fault classification and location problems [83, 84]. Another advantage with feature extraction is to reduce the data dimensionality [83, 85, 86]. This procedure can boost the performance of the algorithms in the fault classifier and locators like increasing the accuracy, reducing the computation consumption and providing the robust results as fast as possible [87]. The feature extraction methods including dimension reduction are discussed in the subsequent section with applications [82].

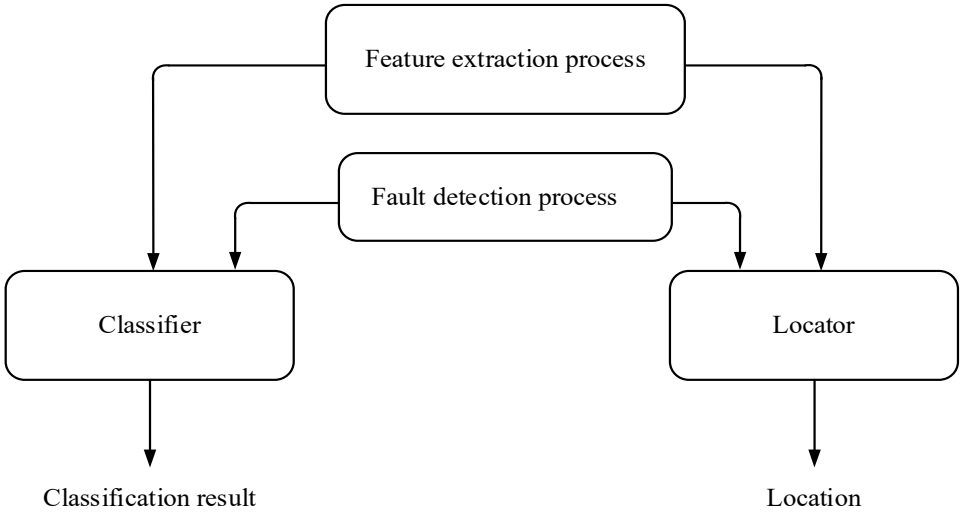

Figure 2.11: Framework for fault detection, classification and location [82]

a) Dimension reduction

The measured data from sensor technologies like PMU and the simulation data from DT can be high dimension, large scale and complex structure. The high dimension data can seriously hinder the efficiency of data classification and identification. Therefore, the data dimension reduction is the primary task for the data processing in Machine Learning before the feature data extraction. In state of art, the latest research progress of data processing algorithm for data dimensionality reduction in Machine Learning, including principal component analysis (PCA), singular value decomposition (SVD), kernel PCA, etc. are proposed in [25, 26, 88–90]. In this work, the PCA and SVD are utilized for data processing and introduced according to the state of art in following.

PCA is used to reduce the dimensionality of a data set including a large number of interrelated variables, meanwhile retaining the feature data as much as possible to keep the original character of the variable. This is achieved by converting the uncorrelated principal components (PCs), which are ordered so that the first few retain most of the variation present in all of the original data [91]. These PCs should meet the three criteria for further development [26]: Firstly, the PCs are linear combinations of the original variables. Then, these PCs are uncorrelated with each other namely orthogonal to each other. Thirdly, the PCs capture the maximum amount of variation in the data. With a relatively small group of PCs, the feature of the data can be captured and a high reduction on dimensionality with less noise data than original patterns. Depending on the application field, PCA is sometimes also referred as Karhunen-Loéve transformation [92]. Eigenvalues and eigenvectors are two important concepts in PCA. For an n × m matrix $\boldsymbol{M}$ and a nonzero vector $\boldsymbol{p}$, the values γ can satisfy the following equation:

$$\boldsymbol{M} \cdot \boldsymbol{q} = \gamma \cdot \boldsymbol{q} \tag{2.27}$$

where γ are called the eigenvalues of matrix $\boldsymbol{M}$, the vectors $\boldsymbol{p}$ satisfy the equation (2.27) are called eigenvectors. If M has n independent eigenvectors $\boldsymbol{p}_1, \cdots, \boldsymbol{p}_\mathrm{n}$, the matrix can be decomposed by a product of three matrices:

$$\boldsymbol{M}=\boldsymbol{Q}\boldsymbol{\Lambda}\boldsymbol{Q}^{-1} \tag{2.28}$$

whereby Λ is a diagonal matrix which consists the eigenvalues of the matrix in decreasing order $(\gamma_1, \cdots, \gamma_\mathrm{n})$, and $\boldsymbol{Q} = [\boldsymbol{p}_1, \cdots, \boldsymbol{p}_\mathrm{n}]$ contains the eigenvectors of the matrix. To evaluate the correlation of two attributes, the covariance is used as an indicator to show how strongly these attributes vary together. The covariance of two random variables $\boldsymbol{x}$ and $\boldsymbol{y}$ (with mean $\bar{x}$ and $\bar{y}$) can be calculated with the following equation:

$$\mathrm{Cov}(x, y) = \frac{1}{n-1}\sum_{i=1}^{n}(x_i - \bar{x})(y_i - \bar{y}) \tag{2.29}$$

The correlation coefficient can be calculated with the normalized deviations σ_x and σ_y:

$$\mathrm{Corr}(x, y) = \frac{\mathrm{Cov}(x, y)}{\sigma_x \sigma_y} \tag{2.30}$$

The principal components of matrix M are defined as [93]:

$$\boldsymbol{M}' = \boldsymbol{M} \cdot \boldsymbol{Q} \tag{2.31}$$

With $\boldsymbol{Q} = [\boldsymbol{p}_1, \cdots, \boldsymbol{p}_\mathrm{n}]$. Each column of $\boldsymbol{M}'$ is a linear combination of the original attributes. The columns of M' are the principal components. The variance of the i^{th} new attribute is γ_i, and the sum of the variances of all new attributes is equal to the sum of the variances of the original attributes.

The PCA is a fairly basic, non-parametric, generic method that can be utilized to find new, informative, uncorrelated features and also for reduction of dimensionality by filtering low variance features [77, 93]. Regarding orthogonal feature for each principal component, every principal component is uncorrelated with each other. The PCs are designed to account for the highest percentage of the variation among the variables with as few PCs as possible. A main drawback of PCA is, however, that it is limited to re-expressing the data as combinations of its basis vectors. Each PC is a linear combination of all original variables, thus leading to a potentially difficult interpretation of the PCs. Another negative feedback for using PCA is about its sensitivity with respect to the units of measurement [94].

If the units and variances of attributes vary a lot, variables with high variance tend to dominate the first few principal component, which lead to the prior normalization of data before PCA transformation. It leads to an expensive computational term. [26]

Another decomposition is the SVD [95, 96], which is a more general method to decompose any n × m matrix $\boldsymbol{A}$ of rank r into a product of three matrices:

$$\boldsymbol{A} = \boldsymbol{U}\Sigma\boldsymbol{V}^{T} \tag{2.32}$$

where $\boldsymbol{U}$ is m × m matrix, $\boldsymbol{\Sigma}$ is m × n matrix, and $\boldsymbol{V}$ is n × n matrix. In this equation, the matrices $\boldsymbol{U}$ and $\boldsymbol{V}$ are both orthonormal matrices with the feature $\boldsymbol{U}\boldsymbol{U}^{\mathrm{T}} = \boldsymbol{E}_{\mathrm{m}}$ and $\boldsymbol{V}\boldsymbol{V}^{\mathrm{T}} = \boldsymbol{E}_{\mathrm{n}}$. Σ is a diagonal m × n matrix, where the nonnegative and ordered elements along the diagonal of the left quadratic subblock are the singular values $\sigma_1 \geq \sigma_2 \geq \cdots \sigma_{\mathrm{r}} \geq 0$. The other elements in matrix Σ are equal to 0.

b) Feature extraction

According to the previous knowledge, it is known that the fault events lead to the change of current and voltage value. This change can be presented in frequency feature dramatically. In this work, two methods to analyze frequency feature of current and voltage signals are proposed for fault diagnosis. Fourier Transformation (FT) is one of the widely used methods for analysis of signals from time domain to frequency domain. Discrete Fourier Transformation (DFT) is utilized when both frequency and time domain coefficients are discrete, which can be computed by fast Fourier Transformation (FFT) [97]. The DFT and half cycle DFT are applied to decompose the DC and harmonic components to assess the phasor in [98]. Half cycle DFT is also used to analyze the fundamental and harmonic phasors for fault classification in [97]. The flaw of the FT is not efficient in decomposition of frequency changed signal. On account of it, the wavelet transformation (WT) is applied for various fault diagnosis system with more efficient in decomposing the signal in the frequency domain [99]. With the implementation of WT, the original measured signals like voltage and current can be decomposed into the signals with multiple frequency bands. Thus during the use of WT, it is essential to select the appropriate mother wavelet, which decides the properties of the decomposition, and find the proper level for decomposition before creating the features [85, 99]. In [100], a detailed comparison of various mother wavelets for fault detection and classification is illustrated and it recommends Bior3.9, Db10, Meyer, Sym8, and Coif5 mother wavelet for fault detection. Coefficients are selected in detail levels as a feature for fault classification in [101–103]. The Meyer wavelet is adopted with frequency bands of 1-2 kHz [103], while the Db2 wavelet is selected with frequency bands of 4-8 kHz [104–106]. The summation of absolute coefficients for detail level is used to extract feature in [101, 103]. The coefficients in 97-195 Hz or 99-199 Hz

frequency bands are assumed in [107, 108] and three Daubechies wavelets, namely Db1, Db4, and Db8 are selected.

Another method derived from WT and FT is the S-Transformation (ST), which is the combination of time-frequency method with frequency-dependent resolution based on a moving and scalable localizing Gaussian window [109]. By the two-dimensional time-frequency representation of ST, the local spectral feature can be used effectively for the detection of transient events [110]. The S-matrix calculated by ST can be plotted for a two-dimensional visualization. ST can overcome the flaw of WT like the too sensitivity to noise and unable to represent the feature of particular harmonics [111, 112]. In [113], ST is used to transform the standard deviation of the voltage signals for selection of faulty phase and section. The hyperbolic ST is implemented in [114] for computing the change of current and voltage signal for the further detection of the fault type.

c) Event detection

The detection of a fault event is done before the classification and location estimation. Based on the extracted feature, the self-governing method is utilized in fault detection and afterwards the classifier and locator are activated [115, 116]. One of the schemes for fault detection is to use an individual classifier to differentiate faulty and non-faulty states. Another idea is to set up a non-faulty threshold to categorize the output signals, and the fault is detected whenever the output is other than non-faulty states [117]. On account of the learning abilities of algorithms used in classification, there is no difference between both schemes when classifiers and locators are proficient to distinguish the faulty and non-faulty states. In [118], the negative sequence components for fault detection is used. To accurate detection of faulty states, a joint fault indicator is designed by convoluting the partial differential with considering time of negative sequence components with a triangular wave. This could increase the accuracy of detecting faults and shows robustness in case of frequency deviation and amplitude variation. A real-time fault detection in transmission line was proposed in [119] by using wavelet-based method. The wavelet coefficient was computed by the border effect of a sliding windows, which reduced the detection time. This method is not exaggerated by the choice of mother wavelet and has not shown the time delay for fault detection for both long and compact wavelets.

The detection of high impedance faults (HIF) have been conducted in [120–122] as conventional methods fail to detect HIF. The high-frequency data is extracted by WT with quadratic spline mother wavelet for HIF detection in [121]. The wavelet coefficient and converted scale coefficients calculated by WT to root-mean-square (RMS) value are used to detect HIF in [121]. PCA is applied to reduce the dimensionality of the values for WT coefficients at different frequency bands. The typical time consumption for fault detection is required in 2-10 ms, as compared to 30 ms for fault type classification. A comparison of

the fault detection methods is given in Table 2.1 considering the applied algorithm, complexity level, input signals, features, and results [123].

Table 2.1: Comparison of fault detection methods [124–128]

No.	Algorithm	Input	Feature	Result	Reference
1	Fuzzy-Neuro method	Voltage and current	• BP algorithm and fuzzy controller • High harmonic signal is removed by FFT	Fault detection within 10 ms	[124]
2	DWT and ANN	Voltage and current	• Normalized voltage and current from -1 to 1 • Consideration of the spectrum between 60 Hz to 1.2 kHz	100% accuracy in detection and 99.83% classification	[125, 127]
3	WT	Voltage and current	• Decomposition of signals with WT into three levels • 3960 cases are considered	99.2% accuracy in detection	[126]
4	Linear discriminant analysis (LDA) and WT	Current	• Decomposition of signals with WT into three levels	100% accuracy in both detection and classification	[128]

The flowchart in Figure 2.12 describes the procedures to extract feature data and detect event in transmission network. The first step with PCA and SVD for data dimension reduction has been mentioned in chapter 2. The decomposition methods like FT, WT etc. are used to decompose the signals into different frequency details [129]. The coefficients of the signals in different frequencies are transferred to event detection algorithms. The detection of HIF indicts the fault event occurrence in power system. The last step is to identify the types of the event with Machine Learning identifier. The implementation of the identifier algorithms is deducted in next section.

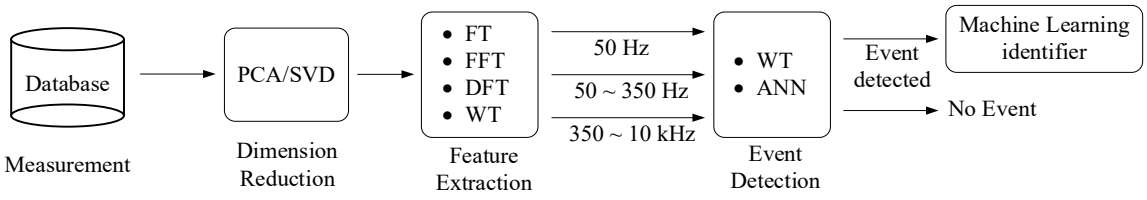

Figure 2.12: Schematic diagram of feature extraction and event detection [130]

2.4.2 Algorithms for event identification in Machine learning

After data processing, the next procedure is to select the algorithms in Machine Learning for the training process. This thesis aims at extracting the feature data of event to classify and automatically identify the anomaly event in the power system. The classification is a task of assigning a label to an input data while regression generates a continuous output. The algorithms used in Machine Learning are divided into three groups: supervised (predictive) ,unsupervised (descriptive) and reinforcement learning methods [24, 26, 89, 94, 131], see Figure 2.13. The supervised learning uses a set of labelled input and expected output examples, each with a feature vector and a class label [90]. With the given training data, the most training algorithm are computing an initial output, comparing with the expected output for producing a classifier model that maps an object to a class label. The unsupervised learning algorithms uses only input data. It aims at correlating the similarity among unlabelled data without class information. Due to its unsupervised feature, this learning algorithms cannot be directly used in classification. The application of supervised learning algorithms to classify and identify the anomaly events in power system is concentrated on this work.

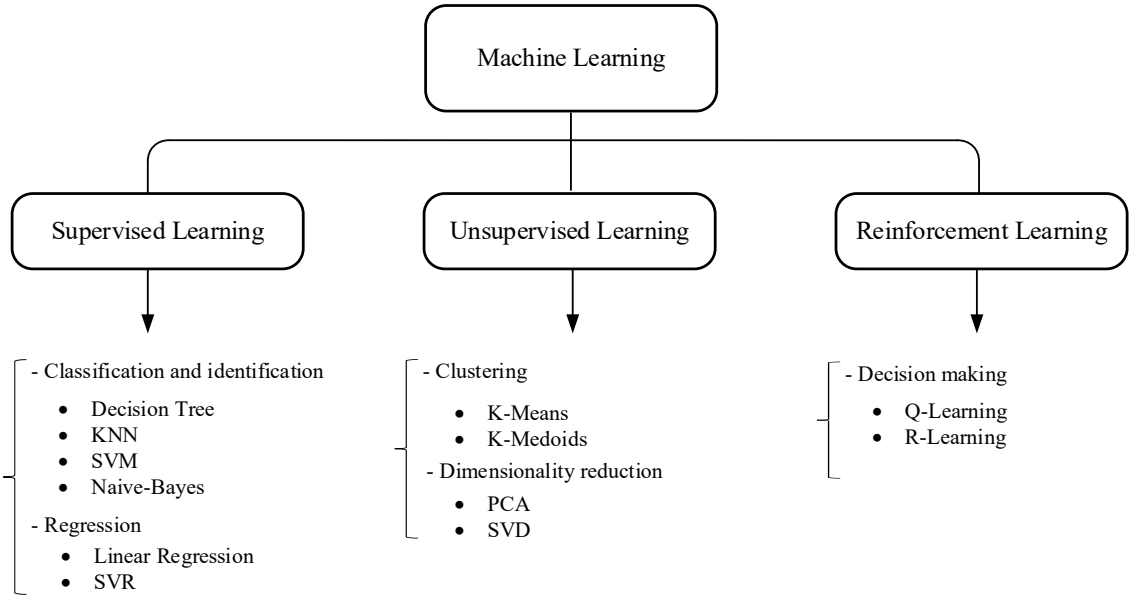

Figure 2.13: Types of Machine Learning algorithms [24, 26, 89, 94, 131]

Three algorithms are focused on in this work for event identification. The first algorithm is the k-nearest neighbor (kNN) [24, 88]. This is an intuitive algorithm in Machine Learning that belongs to the category of instance-based learners [26]. The kNN method has been widely used for anomaly detection [24]. This method is based on the principle that instances within a dataset generally exists in close proximity to other instances that have similar properties [81]. The similarity metric is utilized to measure the distance between

each anomalous window in a time series and the other windows, where a data window refers to a segment of data with the fixed length. Windows with similar sequences of data are called near neighbour [24]. Anomalous windows are those distinct from the underlying trend of the time series. k is a rather small odd positive number and the correct classification of the neighbor is known a prior. The distance of a window to its kth nearest neighbor, known as anomaly index, is the key of kNN to detect anomaly. The distance metric, also called similarity function is utilized to find the distance of an unclassified object, like the Euclidean distance (ED) [132, 133], the cosine similarity [134], and the dynamic time warp [135]. In these indicators, the ED is widely used with its simplicity and good geometrical interpretation. The definition is the 2-norm of the displacement vector between two points $\mathbf{m}$ and $\mathbf{n}$ in a N-dimensional space, which can be presented as follows:

$$\mathrm{D}(\boldsymbol{m},\boldsymbol{n}) \equiv \left\|\boldsymbol{m}^{\mathrm{T}} - \boldsymbol{n}^{\mathrm{T}}\right\|_2 = \sqrt{\sum_{j=1}^{N}(m_j - n_j)^2} \tag{2.33}$$

where $\boldsymbol{m}^{\mathrm{T}} = [m_1, m_2, \cdots, m_{\mathrm{N}}]$ and $\boldsymbol{n}^{\mathrm{T}} = [n_1, n_2, \cdots, n_{\mathrm{N}}]$ denote two data windows with N measurements in each one, $\mathrm{D}(\boldsymbol{m},\boldsymbol{n}) = 0$ indicates the maximum similarity, when two windows are equal in all N samples. (2.33) is used as the foundation for a window in a time series for anomalous index. It is calculated as the ED between this window and its kth nearest neighbor. The anomaly index for the anomalous data is significantly higher than other normal data, which is utilized to identify the anomaly in time series. However, the classification accuracy by kNN cannot reach the accuracy achieved with support vector machines or ensemble learners. Especially, kNN is intolerant to noise, because its similarity measures can easily be distorted by errors in the attribute values and is sensitive to irrelevant features.

Another algorithm in Machine Learning for data classification and identification is decision tree, also called classification trees or regression trees [90]. This method applies a divide- and conquer approach to the problem of learning from a set of independent instances. Through recursive partitioning of the data set, the data is classified by sorting them down the tree from the root node to some leaf node. It is a flowchart-like structure in which each internal node presents a test on an attribute. Each root node represents the outcome of the test, and each terminal node represents a class label. The route from root to leaf node represent classification rules, see Figure 2.14.

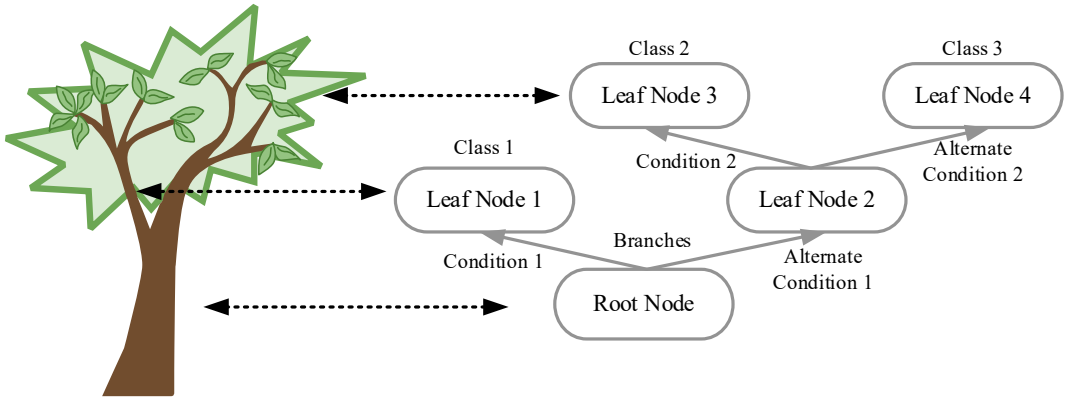

Figure 2.14: Decision tree architecture [26]

The problem of constructing an appropriate decision tree is an NP-complete problem [26], heuristic are used for constructing near-optimal trees. The critical step is to determine the feature to spilt on. The different evaluation rules are utilized for searching the best splitting feature. Some of these rules are derived from information theory , most of them being based on Shannon's entropy [136]. The principle of decision tree algorithm has the following procedure [26]: First of all, an attribute should be selected to place at the root node and create one branch for each possible value of this attribute. This splits up the training set into subsets, one for every value of the attribute. Afterwards, this procedure should be repeated recursively for each branch.

Three major groups of decision tree algorithms are used in Machine Learning for feature extraction. The most well-known algorithms are C4.5 and its successor C5.0 [137]. The both methods are the extensions of ID3 algorithm [138]. These trees algorithms utilize the information gain as splitting criterion and classify both categorical and numeric attributes. The C4.5 is able to deal with missing values, i.e., objects, where one or more attribute values are missing. The commercial successor C5.0 is faster and more memory efficient than C4.5. The classification and regression tree (CART) are a binary decision tree constructed by repeatedly splitting the parent node and subsequent nodes into two child nodes [139]. It begins with the root node which contains the whole learning sample. The CART algorithm use the Gini index is as the evaluation rule and the splitting gain is calculated with the following [139] :

$$\Delta G = \mathrm{Gini}(m) - [\frac{n_{1\mathrm{m}}}{n_{\mathrm{m}}}\mathrm{Gini}(m_{\mathrm{l}}) + \frac{n_{2\mathrm{m}}}{n_{\mathrm{m}}}\mathrm{Gini}(i_{\mathrm{m}})] \tag{2.34}$$

$\mathrm{Gini}(m)$ represents the uncertainty of the set m. ΔG represents the reduction of the Gini index after the decision tree node splits. The Gini index gain threshold ΔG_{p} and the number

of samples of the set m_p are set as the criterion for the split stop. When $\Delta G < \Delta G_\mathrm{p}$ or the number of node sample sets $m < m_\mathrm{p}$, the node stops splitting.

The CART algorithm has been used extensively in power system for different analysis. Because of its apparent robustness and efficiency, a security-dependability adaptive protection scheme separately using voltage angles and current magnitudes was developed in [27]. The voltage angles are used in decision tree processing for response-based discrete event control [140]. In [141], power system security assessment was done using decision trees built from voltage angles obtained from PMUs. A wide-area response-based control using phasor measurement and decision trees based on voltage angles was developed in [142]. CART is suitable for such applications, which requires a little data for its preparation, works well even if some of the assumptions made during generation are violated, and performs very well with large data in a comparatively short time [143]. Besides, the model is not difficult to understand and implement. The drawback for this method is that only univariate splits are allowed, i.e., each split in algorithm depends on the value of a single predictor variable. Accordingly, an optimum split cannot be performed with a single node when applied on data having too many attributes.

Support vector machine (SVM) is the third introduced algorithm in this work for event identification [144]. With SVM, an upper band on expected classification error can be minimized. It seeks the optimal separating hyperplane between two classed by maximizing the margin between the classes, which is accordingly referred as maximum margin classifiers.

Two possible decision boundaries are shown in Figure 2.15 with different margins between the classes. The decision boundaries with small margin (B_2) are susceptible to model overfitting and tend to do generalize poorly on previously unseen examples [145], which aims to find the decision boundary with the maximal margin (B_1 in Figure 2.15). Such a hyperplane, which maximizes the distance to closet points from each class is called maximum margin hyperplane. The closet points to the hyperplane are called support vectors. Only these points influence the position of the hyperplane.

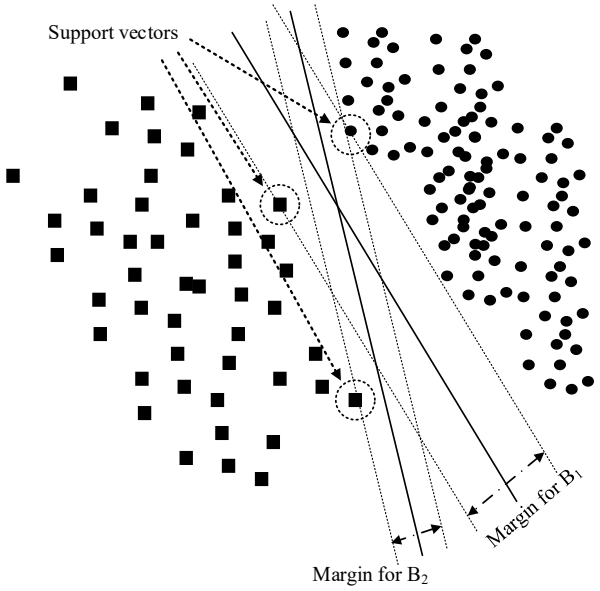

Figure 2.15: Maximum margin between groups

In power system, the event classification and identification involve many problems and the high dimensional data where no useful separating hyperplane can be found. Consequently, under this condition, the idea with SVM is taken into account to transform the involved data and map objects from their original coordinate space namely input space and into a new feature space, where the objects are linearly separable. This transformation is usually denoted as:

$$\phi : \mathbb{R}^{d_1} \rightarrow \mathbb{R}^{d_2}, \boldsymbol{x} \rightarrow \phi(\boldsymbol{x}), d_1 < d_2 \tag{2.35}$$

Figure 2.16 illustrates the transformation process. The data in its original (2-dimensional) input space is not linearly separable. The feature space is presented with $\phi(\boldsymbol{x})$. After mapping the data into the 3-dimensinal feature space, the data can be linearly separated. By a feature space with sufficiently high dimensionality, any consistent training set can be made linearly separable. This linear separation in the transformed feature space corresponds to a non-linear separation in the original input space [146].

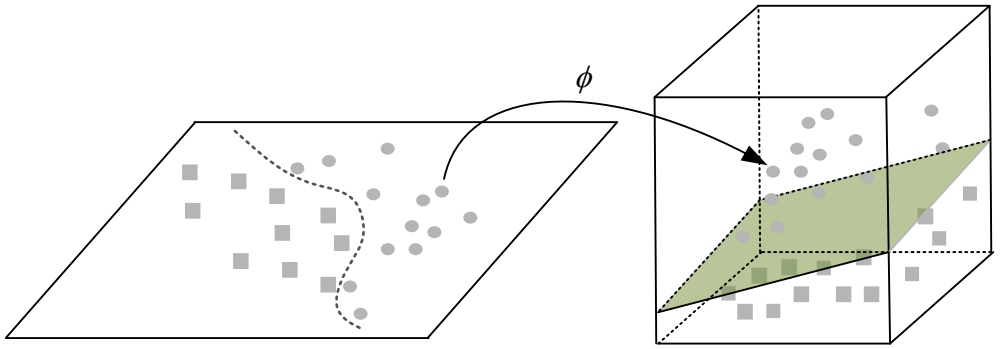

Figure 2.16: SVM for non-linear classification [146]

In linear SVM, each data can be denoted as a tuple (x_i, y_i) $(i = 1,2,\cdots,N)$, where $\mathbf{x}_i = (x_{i1}, x_{i2}, \cdots, x_{id})^{\mathrm{T}}$ corresponds to the attribute set for the i^{th} example, and $y_i \in \{-1, 1\}$ presents the class label. When the data set can be linearly separated, the boundary condition can be written as:

$$\boldsymbol{w} \cdot \boldsymbol{x} + b = 0 \tag{2.36}$$

where the weight vector $\boldsymbol{w}$ and the bias b are parameters of the model, and $\boldsymbol{x}$ is the set of attributes of the model. The decision rule is given by the active function:

$$\begin{aligned} f_{w,b}(x) &= \mathrm{sgn}(\boldsymbol{w} \cdot \boldsymbol{x} + b) \\ y_i &= \mathrm{sgn}(\boldsymbol{w}^{\mathrm{T}} \cdot \boldsymbol{x}_i + b) \end{aligned} \tag{2.37}$$

During the training phase, the parameters $\boldsymbol{w}$ and b fulfill the following conditions:

$$\begin{aligned} \boldsymbol{w} \cdot \boldsymbol{x} + b \geq 1, y_i = 1 \\ \boldsymbol{w} \cdot \boldsymbol{x} + b \leq 1, y_i = -1 \end{aligned} \tag{2.38}$$

The distance of the data point x_i from the hyperplane is:

$$d(x_i, w, b) = \frac{\left|\boldsymbol{w}^{\mathrm{T}} \cdot \boldsymbol{x}_i + b\right|}{\left\|\boldsymbol{w}\right\|^2} \tag{2.39}$$

According to the definition, the margin is $\frac{2}{\|\boldsymbol{w}\|}$. Hence, the optimization for a dataset with N training samples can then be written as:

$$\min_{\mathrm{w}} \frac{\|\mathbf{w}\|^2}{2} \text{ subject to } y_i(\boldsymbol{w} \cdot \boldsymbol{x} + b) \geq 1, i = 1,2,\cdots,N \tag{2.40}$$

Since this is a convex optimization problem, it can be solved using the standard Lagrange multiplier method. Accordingly, the optimization with Lagrange equation is described as the followed equation:

$$L_{\mathrm{p}} = \frac{1}{2}\|\boldsymbol{w}\|^2 - \sum_{i=1}^{N} \lambda_i (\mathrm{y}_i (\boldsymbol{w} \cdot \boldsymbol{x}_i + b) - 1) \tag{2.41}$$

which is known as the primary Lagrange for the optimization problem. The conditions to minimize the primary Lagrange are setting the derivative of L_{P} to zero:

$$\begin{cases} \dfrac{\partial L_{\mathrm{p}}}{\partial \boldsymbol{w}} = 0 \\ \dfrac{\partial L_{\mathrm{p}}}{\partial b} = 0 \end{cases} \Rightarrow L_{\mathrm{D}} = \sum_{i=1}^{N} \lambda_i - \frac{1}{2} \sum_{i,j} \lambda_i \lambda_j y_i y_j \boldsymbol{x}_i^{\mathrm{T}} \boldsymbol{x}_j \tag{2.42}$$

The extension of SVMs is the multi-class SVM [147], which is not only limited in application for binary, two class-tasks, but also can solve the problem with three or more classes. The multi-class SVM attempts to classify all classes by finding a decision boundary that is able to separate between more than two classes. There two possibilities to construct multi-class classifiers from combinations of several binary classifiers [26]. In one-against-all classification, one binary SVM for each class is built to separate elements of that class from elements of all others. In the pairwise classification, there is one binary SVM for each pair of classes to separate elements of one class from elements of the other class. The applications of SVM in power system are mainly focused on the classification and identification of fault events. An effective method of fault location identification was proposed in [148], which use the SVM and fundamental components of voltage and current in faulty phase for fault distance calculation. With the high frequency range characteristics of voltage and current, the fault location is able to be identified. An investigation using SVM for classification of fault type in transmission line was proposed in [149]. SVMs are trained with polynomial kernels and Gaussian kernels to obtain the optimized classifier. The method identifies the fault classification, ground detection, and section identification.

The comparison of the above mentioned algorithms is concluded in Table 2.2. *k*NN is characterized with its simplification for the implementation. It is able for the multi classification and identification, which requires no assumption for training data [150]. The first hyper parameter is need to be seriously considered but after that rest of the parameters are aligned to it. But in SVM, the hyper parameters are required to selected for different classification. Each hyper parameter will allow for sufficient generalization performance [147, 150]. SVM has high performance and accuracy in classification of high dimension data, but *k*NN is not that case. Decision tree or CART is the easiest algorithm in these three to

understand and implement it for the classification. The normalization of data is not required for data processing procedure. However, the classes in decision tree must be mutually exclusive, otherwise the accuracy is low [131, 150]. The training process with large dataset in decision tree is usually faster than the others [140, 150, 151].

Table 2.2: Comparison of typical supervised learning algorithm

Algorithm	Pros	Cons	Reference
*k*NN	+ Simple to understand and implement + Solvable for multi-class + No assumption for training data + One Hyper parameter	- Slow training process for large data sets - Sensitive to outliners - Not work well with large dimension dataset	[24, 88, 150]
Decision Tree	+ Easy to understand and implement + Normalization of data not needed + Automatic feature selection	- Prone to overfitting - Classes must be mutually exclusive - Low accuracy for multi-classes	[140, 150, 151]
SVM	+ High accuracy for classification + Non-linear boundaries + High performance in high dimension data + Durable to noise data	- Long training time - Poor performance with overlapped classes	[77, 145, 148, 150]

2.4.3 Event detection and identification with Machine Learning

An anomaly event is defined as the description of unexpectedly occurring incidents in operating process, which represent a deviation compared to the previous operating point [71, 152]. These include not only outages of operating equipment but also significant changes in load and generations or short circuits [152]. These events have an individual feature, which is composed in the available measurement data. The stage of this thesis aims at using the simulation results from DT assisted with Machine Learning to detect and identify the type of anomaly events for supporting operator decision. The identification of events and the underlaid dynamics can be summarized in three steps: detection of events, classification of events, and identification [74].

The detection process is defined as detecting an occurring event in the observed system [74]. Based on the measurement data, the anomalies can be determined by suitable methods, which indicates an occurrence of a fault event. This can be simplified by using defined threshold values [153]. The methods for the detection of event mentioned in the literature concentrate mainly on the monitoring the measurement data from PMU [78, 79, 154]. In [78, 79], two methods are presented for detection of events based on identification of the measured states with threshold values and a trained decision-making system. They have been developed and tested specifically for online use with PMU data. The method proposed in [78] utilizes the linear dynamic system to evaluate the system states by predefined rules based on PMU data and therefore detects events by fulfilling certain rules. The work in [154] uses the wavelet theory to detect events from PMU data. The other suitable methods for events detection are presented in [155]. The analysis methods include the Fast Fourier Transformation, Matric-Pencil Method, Yule-Walker spectral analysis, and the Min-Max method as well as the statistical method. The analysis is carried out centrally, resulting in an extremely high volume of data. Among the data, not all the analyzed data are relevant or useful, which depends on the size and the location of the event. The classification and identification of relevant data sets can optimize the detection process. The work in [78, 153] introduces an example with identification of particular prominent pilot nodes from the data stream and the rest of data are ignored. The use of this method for identification and clustering of relevant data belongs to the method for signal processing.

After the initial step namely the detection of occurring a critical event, the classification of the type and the investigation of the corresponding causes follows. In [156], the events data can be classified with measured voltage magnitude and phase into eight types: short-circuit, loss of a synchronous generator, connection/disconnection of a load, connection/disconnection of a capacity, switching off a synchronous motor, switching off a line. This is currently the objective of many studies, which are divided into data-related (data driven) [78, 157, 158]and model-related (physics driven) methods [78, 158].

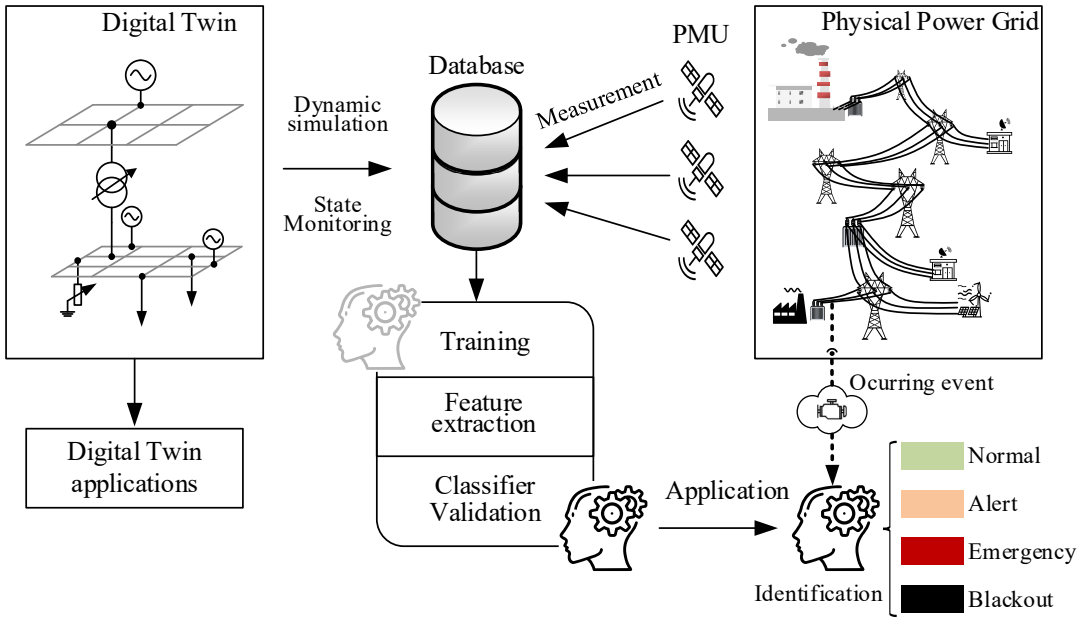

Figure 2.17: Classification and identification process of events by Machine Learning [29]

The data-related methods involve the comparison between current measurement data and an offline generated database containing data from existing events. These approaches typically consist pattern creation and classification. The comparison of the data is intended to identify the events occurred in operating system and the existed measured data within the database. Since the direct comparison of the time series data is not appropriate for finding the feature of event, especially in the high dimensional data, the feature extraction process is considered with using the trained classifier. This allows the classification of possible events based on the measured data or observed states from DT. The described procedure is shown in Figure 2.17. The used training data contains the historical measurements and the dynamic simulation from DT. In [156], several classification algorithms based on signal processing, statistical algorithm, and artificial intelligence like machine learning are presented. Like the process in Figure 2.17, the learning procedure begins from the training based on the recorded event data in database. In [159, 160], the SVM, *k*NN and Decision Tree are utilized for learning process.

Instead of using large amount of data, the model-related method focuses on replicating dynamics of physical system to derive the classification of events. An example of such a model-related approach is given by [161] using the so-called Energy Function. In the presented method, the state variables of synchronous machines like rotor angle and the selected components in Energy Function are identified by the centrally evaluated voltage angles. A follow-up sensitivity analysis of the components in Energy Function enables the detection and classification of events. This approach demonstrates initial positive results

in small systems, where the accurate digital models of the physical system are generated and under the observation to identify the occurring event.

The identification process involves a direct assignment of the measured anomalies and the related events. In the event of a transmission line failure, for example, it should be possible to identify the fault line within the system by suitable identification method. The identification is not necessarily based on the classification mentioned in the previous content but can be directly derived from a matching between database and measured data. Currently, there are no works in the literature dealing with the identification of events based on PMU data and other measured data from online operation. The work described in [162] is intended to detect cascaded failures based on identification of individual event. However, the SCADA-based and centralized approach for identification is not limited to the analysis of dynamic measurement data but is instead focused on the evaluation of stationary SCADA data, such as voltage amplitude, voltage angle and generator operation points. The database is based on results of a power flow calculation of the individual failure scenarios in the relevant offline simulation. To optimize the analysis of identification, the "big data" is decomposed and reduced by suitable methods in [160].

The monitoring of power system and the classification of occurring events provides active support of the safe operation. This is also called situation awareness which is referred as the cognition of the potential incidents that enables an effective reaction by operators during routine procedures and electrical disturbance. According to this, the following perspectives are indeed to be considered [163]:

1) Information about the current and future states for the corresponding system
2) Information about the states of related systems and their influence on its own system
3) Actions implemented to restore or main the system in a normal and secure state
4) Consideration of the maximum available time to implement the actions

If the system is able to ensure that even the complex and dynamic events can be captured and analyzed sufficiently and detailly, the power system can be operated in a safe and stable situation. Furthermore, the information gained through detection, classification and identification can also be used for other specific tasks in the operational management of complex power system. The supervisory protection concept is proposed in [161]. This concept can be understood as an extension of a fast signal processing, the event resulted in a circuit breaker tripping is checked and classified with the available data. The tripping of protection is thus verified, in case of a false trip (e.g. overload instead of a short circuit), the decision of the relay is revised, and the operator is informed. The decision support, which also includes operator action, can be extended to an automated execution of the

event-based measures. A unique identification of the event is thus required. This study presents and elaborates such a method based on artificial intelligence. The cyber security issue is also becoming increasingly important. In [164], it refers to the research of cyber security in power system field. One of the risks is that an external attack can cause switching actions to be executed that the operator cannot control and cancel the action [165]. The continuous monitoring and online evaluation of the measured data makes it possible to detect such anomalies during operation, and thus to recognize manipulations of the SCADA systems [78].

The above mentioned algorithms in data processing and event identification with Machine Learning are deduced with the variables of events in power system in chapter 4. These algorithms are evaluated and validated for the event identification with the numerical case studies in chapter 5.

2.5 Research project related to Digital Twin

The utilization of DT based framework for power system operation and optimization is being investigated within various projects and studies. For a better classification of the research questions addressed in this work, an overview of the state of art for the research projects is provided in this section.

e-TWINS

The project *e-TWINS*, funded by the German Federal Ministry for Economic Affairs and Energy, is addressed for a comprehensive application of DTs for the future energy system, taking into account of scalability, modularity, extensibility, and implementation on large-scale cross-regional systems through the design, implementation, application, and demonstration of a holistic software platform. With the revolution of power system from the centralized supply system to decentralized generation, the real-time condition monitoring, fault detection and operational optimization are taken more attention. The DT presents an innovative tool to fulfil these requirements and accelerate the revolutionary process. The ‘holistic twins for photovoltaic, battery and economics’ in the project aim to develop and test the DTs for the components in the power grid. All the DT components are integrated into a common high-level software framework as an overall system. It allows the whole power systems consisting of the above-mentioned components to be replicated as realistically as possible, and physical operation to be emulated and optimized on the basis of various scenarios. [166]

TwinERGY

The project *TwinERGY* is funded under the "Horizon 2020" program of the European Union. It proposes an novel DT framework to incorporates the intelligence required to optimize demand response at the local level without compromising consumers' well-being and their daily schedules and operations. The main idea behind the design of the *TwinERGY* project is the interest of the project partners to take advantage of the new business opportunities offered by the project implementation and to increase the relevance of optimization tools and strategies in the new generation of energy management systems. By coupling mature citizen engagement practices with service innovation through the lens of public value, *TwinERGY* will ensure that a broad range of interests, and particularly consumers/prosumers, are represented and supported in the energy marketplace.

In this context, *TwinERGY* will develop, configure and integrate an innovative suite of consumer tools, services and applications that enable an increase in awareness and knowledge of consumption patterns, energy behavior, generation/demand forecasting and an increase in local intelligence via properly set up DT-based consumer centric energy management and control decision support mechanisms that optimize demand side management locally. [167]

TwinPV

The project *TwinPV* is funded under the "Horizon 2020" program of the European Union. *TwinPV* intends to achieve an improvement in the field of photovoltaic and smart grid integration research at the University of Cyprus through effective linkages with the Austrian Institute of Technology and the Technical University of Denmark. The objectives directly related to the defined areas are to increase UCY's research and innovation (R&I) output, to strengthen its networking capacity, to improve the success of its research funding bids, to link academia and industry in Cyprus, to achieve sustainable synergies with AIT/DTU, to strengthen EU-Mediterranean research links and to contribute to the reversal of Cyprus' poor R&I indicators. This collaborative project aims to benefit AIT/DTU through access to new markets in sunbelt countries, the use of Cyprus as a test base for new smart grid technologies, and resource sharing. The methodology was set up as a systematic means to achieve set impact indicators through cross-fertilization of knowledge and skills. *TwinPV* is fully aligned with this work plan. The main idea is to bring UCY on par with the outstanding institutions in the field and to contribute to the elimination of the crowding-out effect in the European research field. It is expected that the Cypriot R&D and innovation system will also benefit, thus bringing Cypriot research institutions in line with leading international research entities and achieving smart, sustainable and inclusive growth as defined by the National Strategy for Smart Specialization. [168]

EPC4SES

The project *EPC4SES*, funded by the German Federal Ministry for Economic Affairs and Energy, focuses its activities in the project on developing a holistic concept for the planning of energy systems based on the existing knowledge regarding energy consumption analysis and energy project planning on building level. This concept should be applicable in a generalized way and will be made available to interested parties in the form of an open-source algorithm. For the use case in Germany on the outskirts of Berlin (Mahlow), the possible use of CHPs, thermal solar systems with de- and central storage(s) and heat pumps, or the optimization of the local heating network shall be considered in the modelling. The parameters influencing the energy consumption, such as thermal building inertia and user habits, are to be integrated into the model in order to optimize the final energy demand and power demand in the model and to enable load balancing. [169]

Digital-Twin-Solar

The project *Digital-Twin-Solar* is funded by the German Federal Ministry for Economic Affairs and Energy. The background of this project is in the context of the digitalization of power system. With the developed data communication and acquisition between the components in power grid, the Machine Learning is more in need for optimization. This project deals with solutions specifically tailored to solar energy utilization and electricity storage systems. It considers the entire chain from data collection in development, production and operation at the point of use in the PV system, through data transport, storage and processing, to model- and computer simulation-based and Machine Learning-based analysis and generation of useful, economically viable services based on this. The necessary conceptual, system-technical, technological and scientific foundations are being developed, and pilot systems suitable for use are being implemented and tested for the first selected attractive use cases. The focus of project is to exploit the potential of the latest Machine Learning methods for the design and use of essential components of DTs in the field of battery and PV system technology. This includes, among other things, exploring the potential of probabilistic prediction, transfer learning, active learning, explainable AI, generative adversarial networks, and autoencoders, as well as their further development or adaptation with respect to the goals of the project. [170]

DiMoWind-Inspect

The project *DiMoWind-Inspect*, which is funded by the German Federal Ministry for Economic Affairs and Energy, aims to provide the potential methods in terms of inspection, assessment approaches, data management and maintenance strategy with Digital-Twin based framework. The Jörss-Blunck-Ordemann (JBO), together with the partners of the DiMoWind network under coordination of the Federal Institute for Materials Research and Testing (BAM), has set the goal of standardizing the data accumulating during periodic inspections, in particular regarding damage, in terms of description and evaluation, to make

the prediction of remaining service life more precise, to archive it in a systematic and reconstructable manner, and to optimize it with consideration of inspections. The focus will be on damage caused by cracks in steel structures, for which fracture mechanics analysis methods will be made applicable to engineering practice. To place the results in a generally available environment, Building Information Modelling (BIM) was chosen as the working platform. This will make it possible to continue to use and update the digital representation of the wind turbine available from the planning and execution phase for operation. In this way, findings are clearly assigned to a location and the damage history remains visible throughout the service life. In addition, the model is used, for example, to automatically generate submodels for a re-evaluation of the structure. Structural changes to the real structure are accordingly transferred to the digital image. [171]

HyLITE

The project *HyLITE*, which is funded by the German Federal Ministry for Economic Affairs and Energy, addresses the current challenges of the energy transition and the digitalisation of supply infrastructures, both for current system situations and for future development. The aim of the HyLITE project is to implement a dynamic digital mirror using a DT-centric system and to realize the associated components and services. The focus in the development of the DT-centric system is on dynamic applications for energy supply systems. With the provision of the HyLITE system, it becomes possible to display a detailed image, including dynamic processes in the grid. Using a DT and the digital image of the system derived from it, states and system parameters are also calculated and usable that cannot be directly recorded in the real system via measured variables. The primary result of the project is the development of a reference system. This will be available both as a demonstrator and as a test platform for evaluating the functionalities of a DT-centric system and will allow the development of further applications and services for future functionalities. The results from the project will provide a future technology design for new generations of network control technology. These should enable system providers to develop new DT-centric solutions in the future and provide infrastructure operators with new tools for secure system operation. [172]

In summary, most research projects about DT are focused on the application concepts of DT in state monitoring, optimization of demand response under the background of increased decentralized generations etc. in power system. It lacks the “big picture” for DT in lifecycle development from creation to application. Except for it, there are still no studies and projects for the exploration of methods to parameterize the DT of power grid for the DT creation. Furthermore, the application of DT in detection and identification of anomaly event and fault event are not addressed. The “big picture” for integration of Machine Learning in anomaly identification with DT is also not addressed in the current research.

As a result, the research questions Q1 to Q2 addressed on the topic DT creation and DT application assisted with Machine Learning for anomaly event identification are answered with the next chapters in this thesis.

2.6 Conclusion

This chapter discusses the theoretical context related to the proposed research questions about DT. First of all, the origin of DT with considering its historical development, original definition, and the necessary elements are described. Subsequently, the DT in power system is defined within the framework of this dissertation. It is depicted as the lifecycle management tool to monitor and optimize the power system. Afterwards, its current applications in power systems are addressed with the current research outcome. As the necessary step in the lifecycle of DT, the parameter estimation process calculates correct parameters for DT according to the measured data from the physical system. Three methods based on minimizing the objective function that includes the difference between DT and the measured data are introduced for the parameter estimating procedure. Furthermore, the idea of applying DT in event identification assisted with Machine Learning is described. In this application, the DT is defined as the data producer to generate the simulation data of different scenarios. These data are used as the fingerprint for training Machine Learning. The process regarding Machine Learning for event identification includes data processing, training of algorithm, and application.

The current research projects regarding the topic of DT are concentrated on developing the application concepts in power system. However, the research questions about how to create DT and which methods are suitable for the creation of DT are not referred to. This work proposes the “big picture” of DT with lifecycle management from creation to application in the power system. The realization of this lifecycle requires three main procedures: DT creation, event-based simulation with DT, and application for event identification. The suitable parameter estimation algorithm for DT creation is proposed and implemented. In the next chapter, the integration of the parameterization methods in estimating the parameter of the synchronous machine and voltage source inverter-based generations are presented with the detailed mathematical deduction.

3 Modelling and parameter estimation of Digital Twin with proposed algorithm

The inherent of DT in power grid is a high-dimensional mathematical model [23]. The holistic mathematical model with the appropriate parameters can be utilized for process analysis, optimal process design, monitoring and control parameter testing etc [15]. It is essential to develop a rigorous dynamic DT in power system with a highly predictive quality to ensure a successful implementation of optimization and advanced control techniques since these applications depend heavily on the accuracy of the simulation results from it. Therefore, parameter estimation is a critical step in the creation and update of the DT to keep high accuracy. The DT to accurately emulate a dynamic process usually involves the nonlinear DAE system with many variables and parameters. Accordingly, a DT involved application like optimization and monitoring is referred to as complex DAE constrained optimization problems, which needs to be solved with parameter estimation [40]. Correlations among the parameters and untuned parameters in DT can lead to the deviation between the measured experimental data and the simulation results. Therefore, it is desirable to develop parameter estimation strategies and numerical algorithms which should be capable of solving such sophisticated estimation problems. The state of art for the existing parameter estimation methods for DT creation is introduced in chapter 2. The integration of the algorithms in estimating the parameters of the DT is based on the DAE of the component in power system. In section 3.1, it addresses the modelling of synchronous machine and VSI inverter based on DAEs. Afterwards, the proposed algorithms, i.e., LSQ, RLS and NN for the estimation of the parameters for 6^{th} order synchronous machine and inverter are addressed in chapter 3.2. The methods about sensitivity analysis are proposed in chapter 3.3 to reduce the computation duration.

3.1 Digital Twin modelling

The dynamic time series simulations used in this work are presented in electromechanical domain [173]. In Figure 3.1, it shows the typical classification of time domains in power system modelling as electromagnetic transient (EMT), electrotechnical transient, and quasi-stationary state [174, 175]. Based on the behavioural feature in the different time domains, the whole power system can be described as a periodic system with the coupling between electromagnetic and electromechanical systems [173]. For modelling of operation equipment like synchronous generator and inverter as well as the control procedures, the dynamic in this time domain is presented by the differential equations. The depth of model for description of the dynamic performance is mainly divided into three: detailed model, average value model, and phasor model [173, 174, 176].

A detailed model is available to simulate the dynamic response with high frequency till to MHz range, which can describe the behaviour in electromagnetic transient time domain. The average value model (AVM) neglects the dynamics in high frequency, which mainly considers the dynamic up to 150 Hz [177]. Compared to detailed model, not only the frequency but also the complexity of the AVM is reduced. The model is, however, sufficient for the comprehensive fundamental oscillation analysis and observation of the dynamic response in electromechanical time domain. The AVM is also widely applied for the modelling of power converters [177].

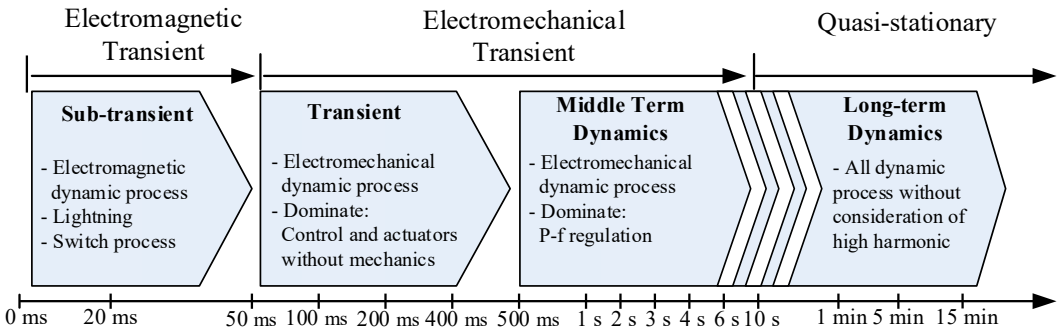

Figure 3.1: Classification of dynamic phenomena in power system modelling [177]

In the modelling procedure, three coordinate systems are related for description of the dynamic states in network and control loop: three-phase coordinate, αβ-coordinate, and dq-coordinate. The transformation between these coordinates is shown in Figure 3.2. By Clarke transformation [173], the three-phase sinuous variables are transferred to the rotated real- and imaginary part. The variable in αβ-coordinate is given by

$$\underline{x}(t) = x_{\alpha}(t) + j \cdot x_{\beta}(t) \tag{3.1}$$

where the variable x_{α} and x_{β} are the real- and imaginary part of state variable $\underline{x}(t)$. The general transformation matrix T_{M} is used for the transformation from three-phase to αβ-coordinate (vector coordinate).

$$\begin{bmatrix} x_0 \\ x_{\alpha} \\ x_{\beta} \end{bmatrix} = T_{\mathrm{M}} \cdot \begin{bmatrix} x_{\mathrm{a}} \\ x_{\mathrm{b}} \\ x_{\mathrm{c}} \end{bmatrix} = \frac{1}{3} \cdot \begin{bmatrix} 1 & 1 & 1 \\ 2 & -1 & -1 \\ 0 & \sqrt{3} & -\sqrt{3} \end{bmatrix} \cdot \begin{bmatrix} x_{\mathrm{a}} \\ x_{\mathrm{b}} \\ x_{\mathrm{c}} \end{bmatrix} \tag{3.2}$$

where the variable x_{α} and x_{β} are given by

$$x_\alpha = \frac{1}{3}\left(2 \cdot x_a - x_b - x_c\right)$$
$$x_\beta = \frac{1}{3}\left(\sqrt{3} \cdot x_b + \sqrt{3} \cdot x_c\right) \tag{3.3}$$

The variables x_a, x_b and x_c are the states in three-phase coordinate. Due to the symmetry of three-phase system, the dynamic rotating field states are reduced to two quantities as well as to represent the instantaneous value and the amplitude in a space vector. Thereby, the system under consideration is decomposed into components that are completely decoupled.

For designing the controller for the rotating field variables, it is practicable to transfer the stationary coordinate i.e. three-phase coordinate and αβ-coordinate into a rotating coordinate system with the angular speed of the rotor. The rotating coordinate system is related to the pole wheel or the rotor of the machine, see Figure 3.2. The dq-coordinate is aligned along the magnetization direction of the pole wheel. The merits of this coordinate system are, on the one hand, that it is easier to represent dynamic interrelationships in electrical system and, on the other hand, the sinusoidal alternating variables are transferred into steady-state variables, which allows the implementation of classical control method. The control performance is similar to the DC machine, which is characterized with its excellent controllability [178]. The transformation from αβ-coordinate to dq-coordinate is denoted by

$$\begin{bmatrix} x_d \\ x_q \end{bmatrix} = T_R \cdot \begin{bmatrix} x_\alpha \\ x_\beta \end{bmatrix} = \begin{bmatrix} \cos\varphi & \sin\varphi \\ -\sin\varphi & \cos\varphi \end{bmatrix} \cdot \begin{bmatrix} x_\alpha \\ x_\beta \end{bmatrix} \tag{3.4}$$

where $\varphi = \omega t$ is the angle of the difference between both coordinates. T_R is the transformation matrix for dq-coordinate.

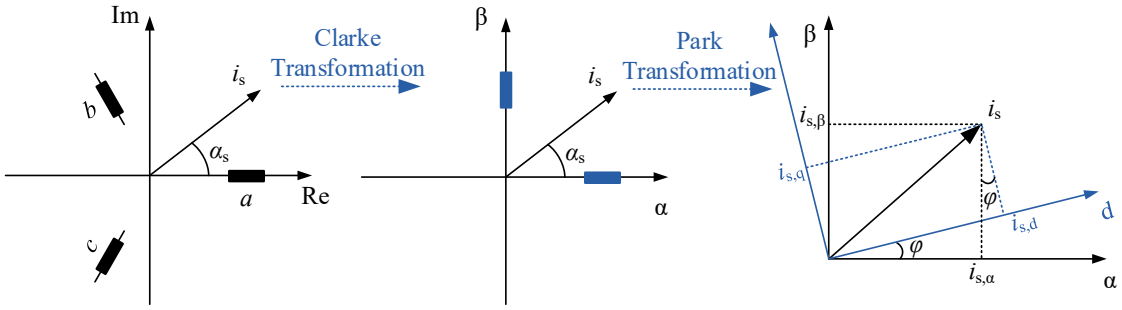

Figure 3.2: Transformation of three-phase coordinate, αβ-coordinate, and dq-coordinate[174]

3.1.1 Synchronous generator and its regulators

As one of the typical dynamic component in electrical power system, the alternate-current machine plays an essential role for the dynamic behaviour of power network. Accordingly, the correct parameter estimation of the synchronous machine in DT is the key factor to keep the adaptivity of DT with physical system. The sixth-order synchronous generator model (cf. [174]) is used in this work to build the synchronous machine. Except for the generator, the automatic voltage regulator (AVR) and turbine governor are responsible for the voltage regulation and rotor speed regulation. They also impact the dynamic feature of the power system. Figure 3.3 describes the coordination transformation between power grid and synchronous generator, and synoptic scheme of synchronous machine and its regulators.

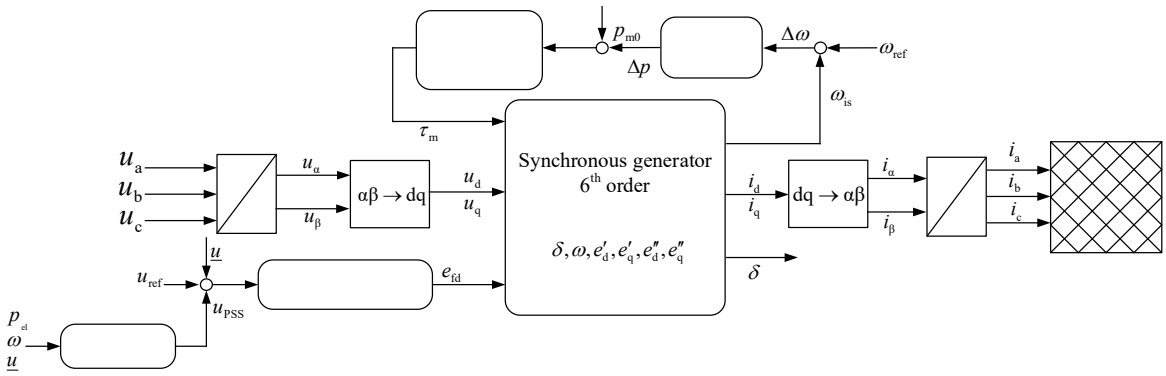

Figure 3.3: Synoptic scheme of synchronous machine and the regulators

In contrast to the higher-order model, the modelling of armature winding, and field winding considered on d- and q-axis in six-order synchronous generator are simplified. The states represented by the model include δ, ω, e'_d, e'_q, e''_d, e''_q, see. These are described by equations in (3.5).

$$
\begin{aligned}
\dot{\delta} &= \omega - \omega_0 \\
\dot{\omega} &= \frac{1}{2H}(T_m - T_e - D(\omega - \omega_0)) \\
\dot{e}'_q &= \frac{1}{T'_{d0}}\left(u^*_{fd} - e'_q - \left(x_d - x'_d - \frac{T''_{d0}}{T'_{d0}}\frac{x''_d}{x'_d}\left(x_d - x'_d\right)\right) i_d\right) \\
\dot{e}'_d &= \frac{1}{T'_{q0}}\left(-e'_d + \left(x_q - x'_q - \frac{T''_{q0}}{T'_{q0}}\frac{x''_q}{x'_q}\left(x_q - x'_q\right)\right) i_q\right) \\
\dot{e}''_q &= \frac{1}{T''_{d0}}\left(-e''_q + e'_q - \left(x'_d - x''_d + \frac{T''_{d0}}{T'_{d0}}\frac{x''_d}{x'_d}\left(x_d - x'_d\right)\right) i_d\right) \\
\dot{e}''_d &= \frac{1}{T''_{q0}}\left(-e''_d + e'_d + \left(x'_q - x''_q + \frac{T''_{q0}}{T'_{q0}}\frac{x''_q}{x'_q}\left(x_q - x'_q\right)\right) i_q\right)
\end{aligned}
\tag{3.5}
$$

where the electrical power, i.e., the electrical torque τ_e is given by

$$p_e = \left(u_q + r_a i_q\right) i_q + \left(u_d + r_a i_d\right) i_d \tag{3.6}$$

The field voltage includes a feedback of the rotor speed and the active power produced by the machine, which is denoted as

$$u_{fd}^* = u_{fd} + K_\omega(\omega - \omega_0) - K_P\left(P - P_0\right) \tag{3.7}$$

where P_0 is the initial electric power generated by the machine. In this equation, a simple oscillation stabilizer is implemented. The relationships between voltages and currents are described by the equations as follows.

$$\begin{aligned} 0 &= u_q + r_a i_q - e_q^{''} + (x_d^{''} - x_l) i_d \\ 0 &= u_d + r_a i_d - e_d^{''} - (x_q^{''} - x_l) i_q \end{aligned} \tag{3.8}$$

The typical used parameters and their value ranges is shown in Table 3.1. In this work, the parameters are applied according to [38] for the individual synchronous machine. The other related parameters are illustrated in Appendix. The block diagram of the synchronous generator with the above DAEs is shown in Figure 3.4.

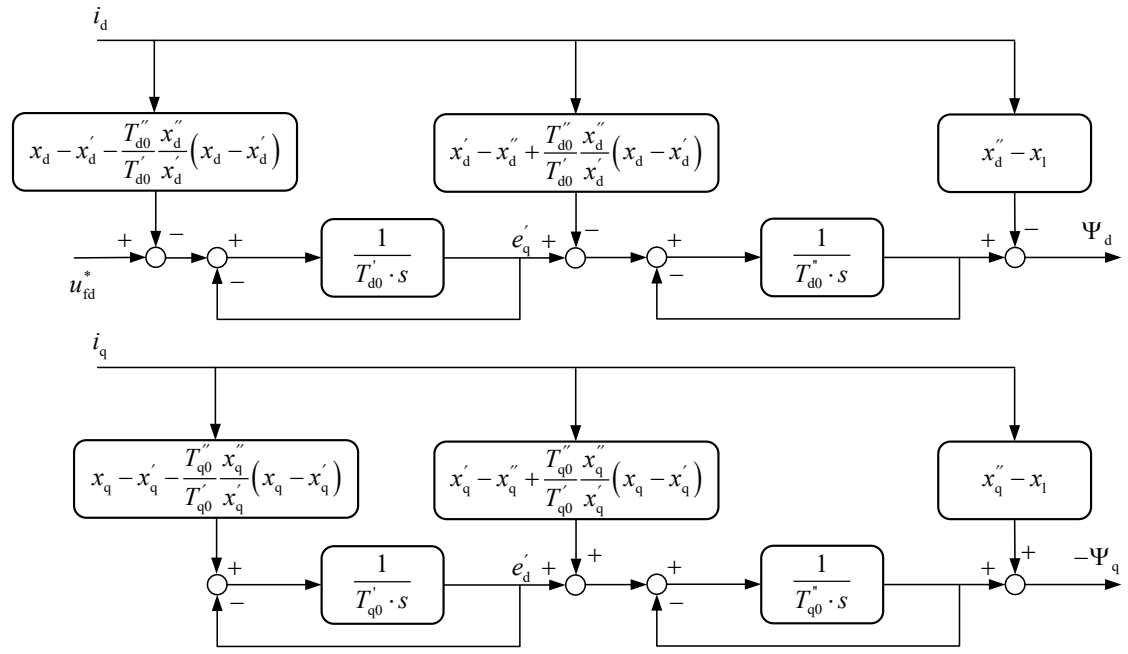

Figure 3.4: Block diagram of stator fluxes and rotor mechanism in 6th order synchronous generator

The turbine and governor define rotor speed control of synchronous machines, which is likewise an essential part for primary frequency control. Figure 3.5 shows the basic function of the primary control and the turbine governor model. To approximate the mechanical torque with the mechanical power, it is given by

$$\Delta p_{\mathrm{m}} = \frac{1}{R}(\omega_{\mathrm{ref}} - \omega) \tag{3.9}$$

Table 3.1: Typical parameters for modelling of synchronous generator [38, 174, 175]

Parameter	Description	Reference range	Used in reference model
H	Inertia constant	2.0 – 10.0 MWs/MVA	5.0 MWs/MVA
D	Damping coefficient	0 – 2.0	1.0
x_{d}	Synchronous reactance d-axis	1.0 – 2.3 pu	1.25 pu
x_{q}	Synchronous reactance q-axis	1.0 – 2.3 pu	1.0 pu
x'_{d}	Transient reactance d-axis	0.15 – 0.4 pu	0.333 pu
x'_{q}	Transient reactance q-axis	0.3 – 1.0 pu	0.3 pu
x''_{d}	Sub-transient reactance d-axis	0.12 – 0.3 pu	0.292 pu
x''_{q}	Sub-transient reactance q-axis	0.12 – 0.3 pu	0.292 pu
T'_{d0}	Transient time constant d-axis	3.0 – 10 s	5.0 s
T'_{q0}	Transient time constant q-axis	0.5 – 2.0 s	2.0 s
T''_{d0}	Sub-transient time constant d-axis	0.02 – 0.05 s	0.02 s
T''_{q0}	Sub-transient time constant q-axis	0.02 – 0.05 s	0.02 s
r_{a}	Armature resistance	0.0015- 0.005 pu	0.002 pu
x_{l}	Leakage reactance	0-0.02 pu	0.01 pu

where $R \in (0, \infty)$ so that the machine regulates the frequency proportionally to its related power. According to [175], the dynamics of the turbine and its control are represented by a speed governor, the servo motors and a reheat block. They are depicted by equations in (3.9). This structure ensures sufficient details for the investigation of transient process.

$$
\begin{aligned}
p_{\mathrm{in}} &= p_{\mathrm{m0}} + \frac{1}{R}(\omega_{\mathrm{ref}} - \omega) \\
\dot{x}_{\mathrm{g1}} &= \frac{1}{T_{\mathrm{s}}}(p_{\mathrm{in}} - x_{\mathrm{g1}}) \\
\dot{x}_{\mathrm{g2}} &= \frac{1}{T_{\mathrm{c}}}((1 - \frac{T_3}{T_{\mathrm{c}}})x_{\mathrm{g1}} - x_{\mathrm{g2}}) \\
\dot{x}_{\mathrm{g3}} &= \frac{1}{T_5}((1 - \frac{T_4}{T_5})(x_{\mathrm{g2}} + \frac{T_3}{T_{\mathrm{c}}}x_{\mathrm{g1}}) - x_{\mathrm{g3}}) \\
T_{\mathrm{m}} &= x_{\mathrm{g3}} + \frac{T_4}{T_5}(x_{\mathrm{g2}} + \frac{T_3}{T_{\mathrm{c}}}x_{\mathrm{g1}})
\end{aligned}
\tag{3.10}
$$

where R is the proportional of the primary frequency control. T_{s} is the time constant of governor. T_{c} and T_3 are the time constants of servo motor. T_4 and T_5 are the time constants of reheat block, see Figure 3.5. The typical values of the parameters for turbine governor are shown in Table 3.2.

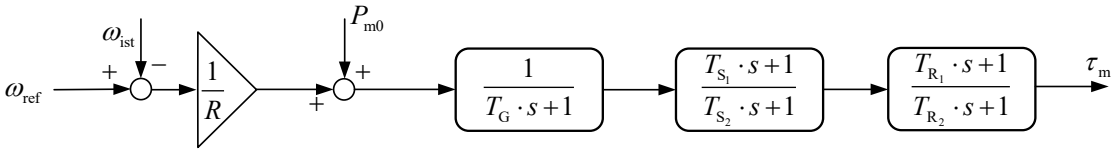

Figure 3.5: Scheme of turbine governor with primary frequency control [175]

The AVR defines the primary voltage regulation of synchronous machines. The AVR model takes the control of the excitation voltage E_{fd} or excitation current i_{fd} for excitation control into account. In [179], the review of typical AVR models with different levels of detail and complexity has been proposed. The simplified version of the classic IEEE standard DC1A is applied in this work for voltage control of synchronous generator [175, 180]. The block diagram of DC1A is shown in Figure 3.6. The reference range for selecting the values of the AVR , and the utilized parameters in this work are illustrated in Table 3.2. The function S_{E} defines the saturation characters of an excitation control system, which is used to determine the amount of field current beyond the air-gap line that is needed to provide a specified generator or exciter output voltage [180].

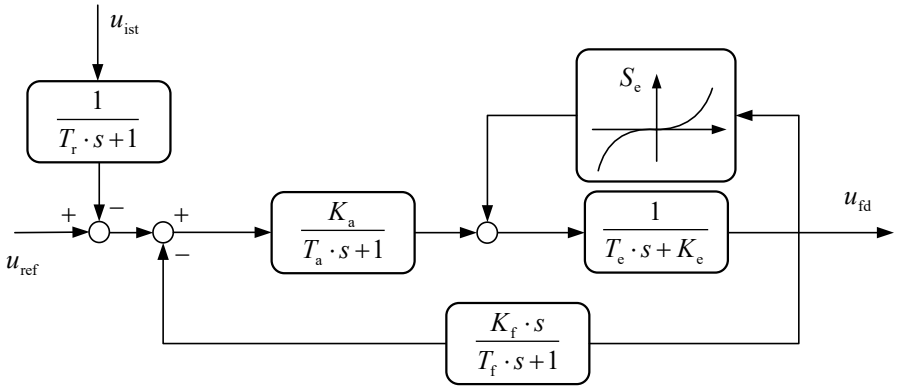

Figure 3.6: Block diagram of AVR with IEEE DC1A [180]

For damping the power system oscillations, the PSS is considered in this work. The basic function of PSS is to extend stability limits by modulating generator excitation to provide damping to the oscillations of synchronous machine rotors relative to one another [181]. These oscillations usually occur the frequency fluctuation with approximate range between 0.2 to 2.5 Hz, which may limit the ability to transmit the power in the system. To provide the appropriate damping by PSS, the stabilizer is necessary to bring about an electrical torque synchronized with the speed variations or the power changes in the system [182]. Commonly, the used inputs for PSS are rotor speed deviation, terminal frequency, and the active power [180, 181]. In [180], different types of PSS is reviewed. In this work, a simplified version of PSS is used, and Figure 3.7 shows its block diagram. The parameters in these blocks are illustrated in Table 3.2.

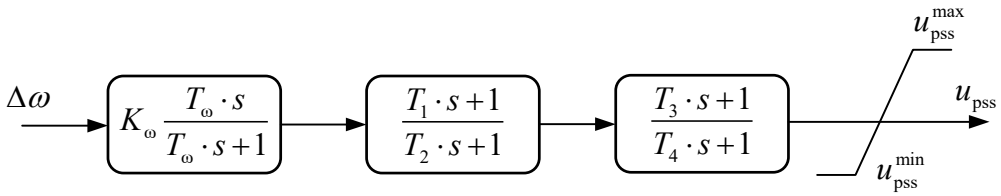

Figure 3.7: Block diagram of simplified PSS [180]

All parameters required for the regulators (Turbine Governor, Exciter and PSS) are presented in Table 3.2. Most of these parameters can be taken from the IEEE Recommended Practice for modelling synchronous machines and their controllers [174, 180]

Table 3.2: Typical parameters and the used values for regulators [38, 174, 175, 180]

Parameter	Description	Value used in reference model
T_G	Governor time constant	0.1 s
T_{S1}	Servo motor time constant	0 s

T_{S2}	Servo motor time constant	0.45 s
T_{R1}	Reheat block time constant	0 s
T_{R2}	Reheat block time constant	50 s
R	Proportional of primary frequency regulation	0.5 pu
T_r	Measure delay constant	0.02 s
T_C	Lead time constant	0.001 s
T_D	Lag time constant	0.01 s
K_a	Exciter field proportional constant	46 pu
T_a	Exciter field time constant	0.06 s
K_f	Rate feedback gain	0.05 pu
T_f	Rate feedback time constant	1 s
E_1	Exciter output voltage for saturation factor $S_E(E_1)$	3.1 pu
S_{E1}	Exciter saturation factor at exciter output voltage E_1	0.33
E_2	Exciter output voltage for saturation factor $S_E(E_2)$	2.3
S_{E2}	Exciter saturation factor at exciter output voltage E_2	0.1
K_{PSS}	PSS gain	3.15 pu
T_w	PSS washout time constant	10 s
T_1	PSS lead compensating time constant	0.05 s
T_2	PSS lag compensating time constant	0.02 s
T_3	PSS lead compensating time constant	3 s
T_4	PSS lag compensating time constant	5.4 s
u_{PSSmax}	Maximum PSS output	0.09 pu
u_{PSSmin}	Minimum PSS output	-0.09 pu

3.1.2 Voltage source inverter and its controller loop

The increasing inverter-based renewable generation connected with power grid is changing the infrastructure of power system [22]. This trend impacts the dynamic character of power system. According to this, the estimation of the correct parameters in inverter model and its controllers is another key factor for the accuracy of DT [23]. The focus of this section is to address the modelling of inverter and its controllers including their parameter design. Therefore, the ideal switch based inverter model in Figure 3.8 describes the topology of the inverter circuit.

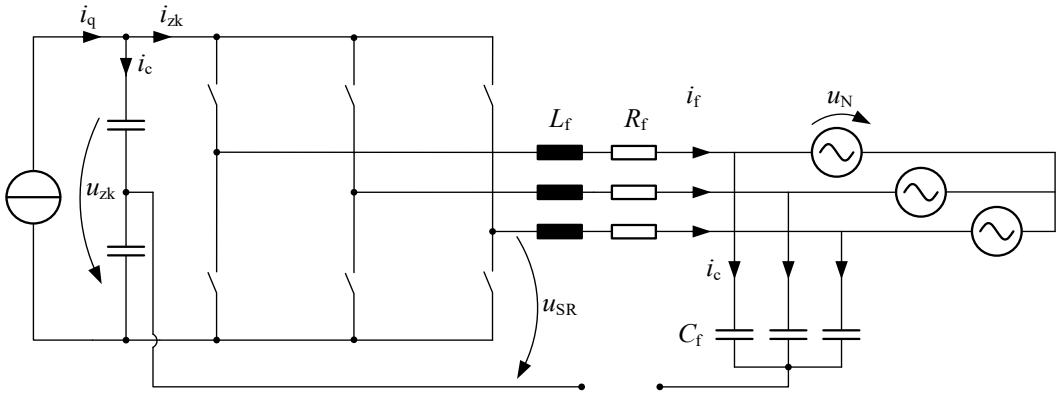

Figure 3.8: The model of the inverter with ideal switch

The circuit is shown in natural coordinates and includes a three-phase inverter with intermediate voltage circuit, a filter inductor and a capacitor. To model the dynamic process by DAEs, the system behaviour is first transformed into vector coordinates. As shown in the following figure, the model can be divided into DC side and AC side. As shown in Figure 3.9, the differential equations of state of the AC and DC sides are written in the space vector coordinates as follows. In AC side:

$$\begin{cases} \vec{\boldsymbol{u}}_{\mathrm{SR}} = R_{\mathrm{f}} \cdot \vec{\boldsymbol{i}}_{\mathrm{f}} + L_{\mathrm{f}} \cdot \dot{\vec{\boldsymbol{i}}}_{\mathrm{f}} + \vec{\boldsymbol{u}}_{\mathrm{C_f}} \\ \vec{\boldsymbol{u}}_{\mathrm{C_f}} = R_{\mathrm{N}} \cdot \vec{\boldsymbol{i}}_{\mathrm{N}} + L_{\mathrm{N}} \cdot \dot{\vec{\boldsymbol{i}}}_{\mathrm{N}} + \vec{\boldsymbol{u}}_{\mathrm{N}} \\ \vec{\boldsymbol{i}}_{\mathrm{f}} = \vec{\boldsymbol{i}}_{\mathrm{N}} + \vec{\boldsymbol{i}}_{\mathrm{C_f}} \end{cases} \tag{3.11}$$

In DC side, the DAE is depicted as:

$$i_{\mathrm{q}} = i_{\mathrm{c}} + i_{\mathrm{zk}} = i_{\mathrm{zk}} + C \cdot \dot{u}_{\mathrm{zk}} \tag{3.12}$$

where I_{q}, I_{c} and I_{zk} are respectively the source current, capacitor current and the current feeds into network.

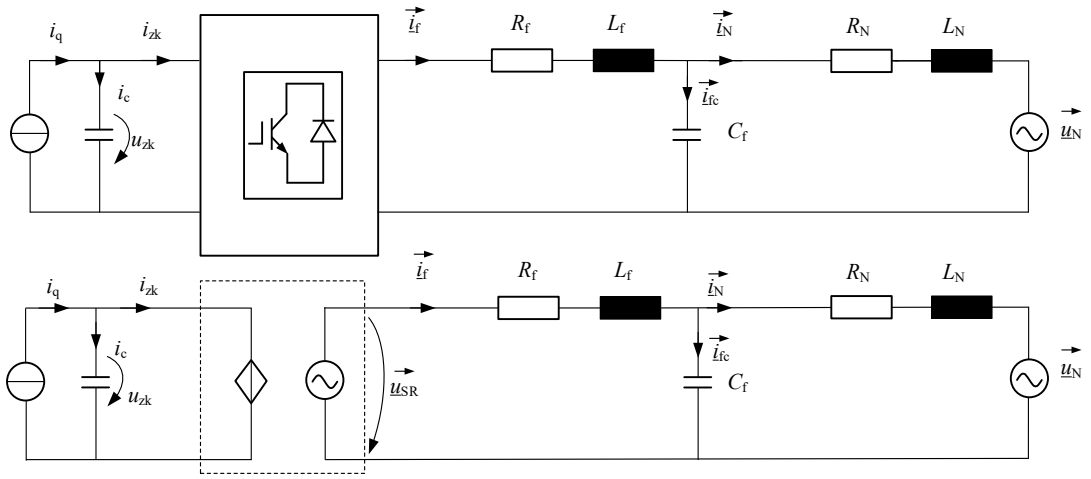

Figure 3.9: Equivalent circuit diagram of the inverter in vector coordinate

To link the AC and DC sides, the power correlation from both sides is used here:

$$p_{ac} = p_{dc} \Rightarrow \frac{3}{2} \cdot \vec{\boldsymbol{i}}_f \cdot \vec{\boldsymbol{u}}_{SR} = i_{zk} \cdot u_{zk} \tag{3.13}$$

where the inverter voltage $\vec{\boldsymbol{u}}_{SR} = \vec{\boldsymbol{v}} \cdot \frac{u_{zk}}{2}$. The $\vec{\boldsymbol{v}}$ is the control signal of switch in inverter to convert the DC power to AC power. Based on this relation, the equation (3.13) is rewritten as:

$$i_{zk} = \frac{3}{4}(v_\alpha i_{f\alpha} + v_\beta i_{f\beta}) \tag{3.14}$$

Since the state variables rotate in vector coordinates with the power frequency at the angular velocity ω , and these are not suitable for design the parameters in control loop, they are supposed to be transformed by a rotary vector into coordinates synchronized with the power frequency. Then the AC-side state variables can be transformed into dq coordinates by the following equations.

$$\begin{aligned} \vec{\boldsymbol{u}}_{SRdq} &= \vec{\boldsymbol{u}}_{SR} \cdot e^{-j\omega t} = u_{SRd} + j \cdot u_{SRq} \\ \vec{\boldsymbol{i}}_{fdq} &= \vec{\boldsymbol{i}}_f \cdot e^{-j\omega t} = i_{fd} + j \cdot i_{fq} \end{aligned} \tag{3.15}$$

With the DAEs mentioned above, the voltage and current relations in inverter is concluded on dq coordinates as follows:

$$
\begin{aligned}
\frac{\mathrm{d}i_{\mathrm{fd}}}{\mathrm{d}t} &= \frac{1}{L_{\mathrm{f}}} \cdot (-R_{\mathrm{f}} \cdot i_{\mathrm{fd}} + \omega L_{\mathrm{f}} \cdot i_{\mathrm{fq}} + u_{\mathrm{SRd}} - u_{\mathrm{C_f d}}) \\
\frac{\mathrm{d}i_{\mathrm{fq}}}{\mathrm{d}t} &= \frac{1}{L_{\mathrm{f}}} \cdot (-R_{\mathrm{f}} \cdot i_{\mathrm{fq}} - \omega L_{\mathrm{f}} \cdot i_{\mathrm{fd}} + u_{\mathrm{SRq}} - u_{\mathrm{C_f q}}) \\
\frac{\mathrm{d}i_{\mathrm{Nd}}}{\mathrm{d}t} &= \frac{1}{L_{\mathrm{N}}} \cdot (-R_{\mathrm{N}} \cdot i_{\mathrm{Nd}} + \omega L_{\mathrm{N}} \cdot i_{\mathrm{Nq}} + u_{\mathrm{C_f d}} - u_{\mathrm{Nd}}) \\
\frac{\mathrm{d}i_{\mathrm{Nq}}}{\mathrm{d}t} &= \frac{1}{L_{\mathrm{N}}} \cdot (-R_{\mathrm{N}} \cdot i_{\mathrm{Nq}} - \omega L_{\mathrm{N}} \cdot i_{\mathrm{Nd}} + u_{\mathrm{C_f q}} - u_{\mathrm{Nq}}) \\
\frac{\mathrm{d}u_{\mathrm{C_f d}}}{\mathrm{d}t} &= \frac{1}{C_{\mathrm{f}}} \cdot (-\omega C_{\mathrm{f}} \cdot u_{\mathrm{C_f q}} + i_{\mathrm{fd}} - i_{\mathrm{Nd}}) \\
\frac{\mathrm{d}u_{\mathrm{C_f q}}}{\mathrm{d}t} &= \frac{1}{C_{\mathrm{f}}} \cdot (\omega C_{\mathrm{f}} \cdot u_{\mathrm{C_f d}} + i_{\mathrm{fq}} - i_{\mathrm{Nq}})
\end{aligned}
\tag{3.16}
$$

The block diagram of the inverter model with the above DAEs is shown in Figure 3.10:

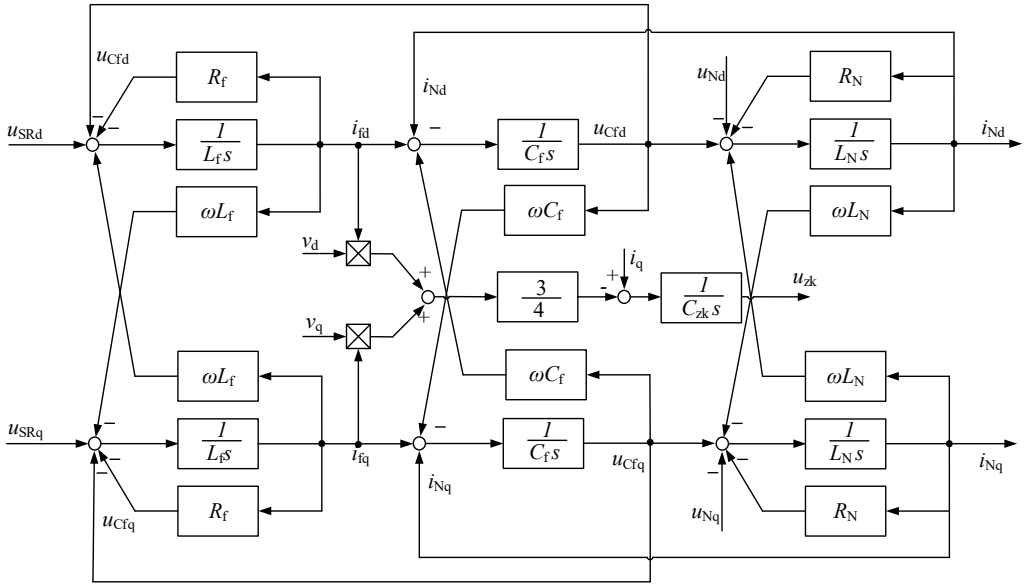

Figure 3.10: Block diagram of modelling inverter

To maintain the current and voltage at the desired value, the controller is designed to eliminate the disturbance that counteracts the operation of the inverter. The control schema of inverter is presented in Figure 3.11. The task of the overlaid voltage regulator is to keep the measured DC link voltage U_{zkist} at $U_{\mathrm{zksoll}}$by specifying the setpoint for the filter current. The current controller regulates the deviation between I_{fsoll} and I_{fist} on d and q axis to keep the operation states of the current loop. To regulate the filter current, the power is exchanged between the DC link source and the grid-connected current controller. Its task is

to ensure that the actual current value I_{fist} consisted of the active current component $I_{\mathrm{fd}}$and the reactive current component I_{fq} is regulated to the setpoint I_{fsoll}. The setpoint of the active current component I_{fd} is determined by the DC link voltage control. The setting of the reactive current setpoint I_{fqsoll} is normally denoted to zero. In the context of this work, the reactive current setpoint is determined by the reactive power regulator.

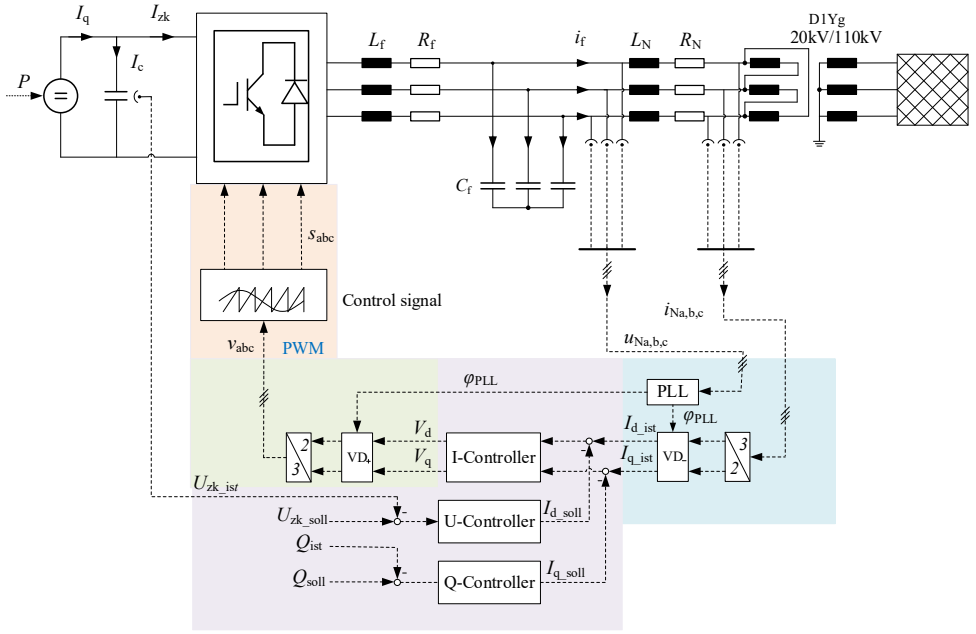

Figure 3.11: Schema of voltage and current controller for VSI [23, 41]

Figure 3.12 shows the block diagram of the current control loop and the decoupling blocks. The series decoupling method is used to eliminate the coupling between d- and q-axis in inverter [183]. In feedback loop, the PT_1 block is applied as a low pass filter to simulate the measurement delay. Two PI-controllers are used on d- and q-axis respectively to regulate the currents. The used parameters in current control loop are illustrated in Table 3.3. The setpoint value of I_{fd} is obtained by dynamically keeping the DC link voltage equal to the specified DC voltage setpoint. As a result, the DC link voltage and the voltage of the inverter from AC network are interconnected by the switching function, which is referred to the V_{d} and V_{q} in Figure 3.12.

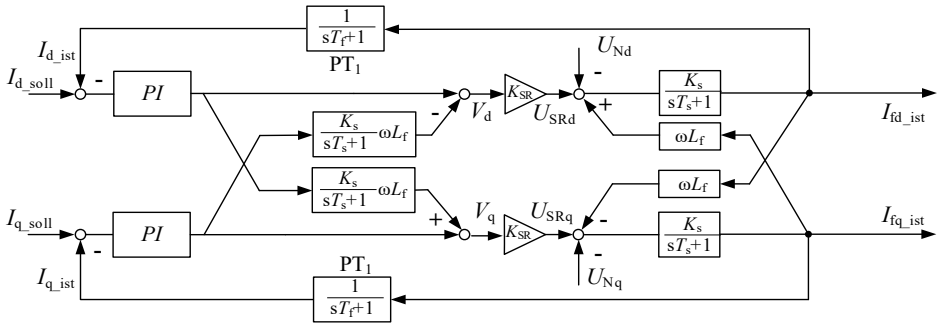

Figure 3.12: Block diagram of controller and controlled system

In this work, the inverter is installed in medium voltage network. The setpoint of DC link voltage for inverter is specified to 40 kV, which connected with the medium-voltage level is 20 kV. The block diagram of the voltage control is shown in Figure 3.13. The current loop including its PI-controllers are reduced as a transfer function $\frac{G_0(s)}{G_0(s)+1}$.

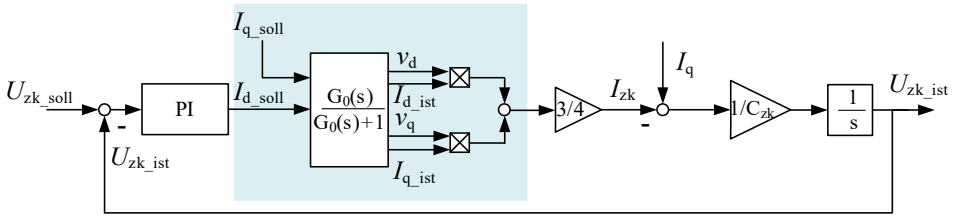

Figure 3.13: Block diagram of voltage control

The phase-locked-loop (PLL) is used for the phase control to transform three-phase variables into the dq coordinate [177]. This allows the active and reactive components of the current to be specified independently. The phase control focuses on the detection of the phase angle and the frequency of the network voltage. In the simulation, the network voltage is required to determine the angle φ_{U_N}. From Figure 3.14, the PLL consists of a phase comparator, a PT_1-filter, a PI controller and an integrator. The phase angle of the network is obtained by Kart-Pole transformation [184]. The PT_1-filter eliminates the oscillation in the angle. The controlled angle φ_{PLL} is used for coordinate transformation.

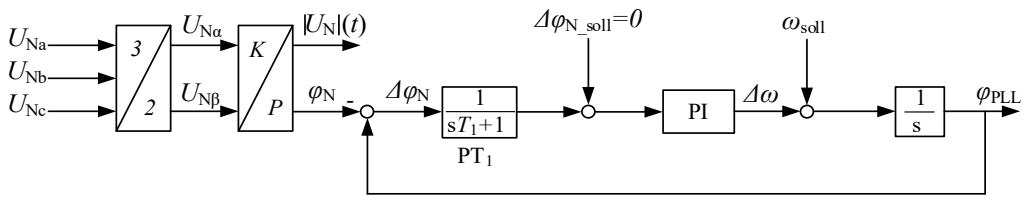

Figure 3.14: Block diagram of PLL

The design of the controller parameters in voltage loop and current loop is achieved according to the optimalization theory for controller in [185–187]. The optimized form of transfer function for open loop is given by:

$$G_{\mathrm{opt}}(\mathrm{s}) = G_{\mathrm{R}}(\mathrm{s}) \cdot G_{\mathrm{S}}(\mathrm{s}) = \frac{1}{2 \cdot \mathrm{s} \cdot T_{\mathrm{k}} (1 + \mathrm{s} \cdot T_{\mathrm{k}})} \tag{3.17}$$

where $G(\mathrm{s})_{\mathrm{R}}$ and $G(\mathrm{s})_{\mathrm{S}}$ are the transfer function of regulator and controlled system. T_{k} is the time constant in optimal form of transfer function for open loop of inverter. To fulfill the open loop formula in (3.17), the parameters of overlaid voltage controller and underlaid current controller are determined by eliminating the T_{k} and the coefficient. Firstly, the PI current controller has the typical transfer function:

$$G_{\mathrm{R}_{\mathrm{current}}}(\mathrm{s}) = k_{\mathrm{P_C}} + \frac{1}{T_{\mathrm{I_C}} \cdot \mathrm{s}} = \frac{1 + k_{\mathrm{P_C}} \cdot T_{\mathrm{I_C}} \cdot \mathrm{s}}{T_{\mathrm{I_C}} \cdot \mathrm{s}} \tag{3.18}$$

where $k_{\mathrm{P_c}}$ is the proportional parameter, and $T_{\mathrm{I_c}}$ is the time constant in integral block of current PI controller. The transfer function of current system is depicted in Figure 3.12, and is denoted by:

$$G_{\mathrm{S}}(\mathrm{s}) = \frac{K_{\mathrm{s}}}{1 + T_{\mathrm{s}} \cdot \mathrm{s}} \tag{3.19}$$

where K_{S} and T_{S} are the gain factor and the time constant for current loop system respectively. To remove the harmonic, a low-pass filter $PT1$ is placed in the feedback loop. The transfer function of the filter is given by

$$G_{\mathrm{f}}(\mathrm{s}) = \frac{1}{1 + T_{\mathrm{f}} \cdot \mathrm{s}} \tag{3.20}$$

With (3.18)-(3.20), the current open loop is denoted as

$$G_{\mathrm{c_{open}}}(\mathrm{s}) = \frac{1 + k_{\mathrm{P_C}} \cdot T_{\mathrm{I_C}} \cdot \mathrm{s}}{T_{\mathrm{I_C}} \cdot \mathrm{s}} \cdot \frac{K_{\mathrm{s}}}{1 + T_{\mathrm{s}} \cdot \mathrm{s}} \cdot \frac{1}{1 + T_{\mathrm{f}} \cdot \mathrm{s}} \cdot K_{\mathrm{SR}} \tag{3.21}$$

To satisfy the form in (3.17), the following conditions are required.

$$\left.\begin{aligned} T_{\mathrm{s}} &= k_{\mathrm{P_C}} \cdot T_{\mathrm{I_C}} \\ T_{\mathrm{I_C}} &= 2 \cdot T_{\mathrm{f}} \cdot K_{\mathrm{SR}} \cdot K_{\mathrm{s}} \end{aligned}\right\} \Rightarrow k_{\mathrm{P_C}} = \frac{T_{\mathrm{s}}}{2 \cdot T_{\mathrm{f}} \cdot K_{\mathrm{SR}} \cdot K_{\mathrm{s}}} \tag{3.22}$$

After implementation of the conditions (3.22) into (3.21), the function of current loop is optimized as:

$$G_{O_C}(s) = \frac{K_s \cdot K_{SR}}{T_{I_C} \cdot s \cdot (1 + T_f \cdot s)} = \frac{1}{2T_f \cdot s \cdot (1 + T_f \cdot s)} \tag{3.23}$$

The damping ratio in (3.23) is $\vartheta = \frac{1}{\sqrt{2}}$.. Due to the relatively large damping ratio in the function $G_{O_C}(s)$, the simplification is permitted according to [188, 189] for replacement of (3.23) with a $PT1$ to simplify the further calculation. Thus, the transfer function of voltage loop according to Figure 3.13 is simplified as:

$$G_{O_U}(s) = (K_{P_U} + \frac{1}{s \cdot T_{I_U}}) \cdot \frac{1}{T_f \cdot s + 1} \cdot \frac{K_f}{s \cdot C_{zk}} \tag{3.24}$$

where K_{P_U} and T_{I_U} are parameters of voltage PI controller. $\frac{1}{1+sT_f}$ is the simplified block for (3.23). C_{zk} presents the capacitor in DC link. The gain factor K_f determines the relation of current variables between DC and AC side, which is given by

$$I_{zk} \cdot U_{zk} = \frac{3}{2} \cdot |U_{SR}| \cdot i_{fdist} \Rightarrow K_f = \frac{i_{zk}}{i_{fdist}} = \frac{3}{2} \cdot \frac{|U_{SR}|}{U_{zk}} \tag{3.25}$$

The parameters of voltage PI controller are optimized according to [186, 187]. The overlaid voltage loop needs to be the symmetrical optimum form as follows:

$$\frac{1 + 4 \cdot s \cdot T_f}{(s \cdot T_f + 1) \cdot 4^2 \cdot T_f^2 \cdot s^2} = \frac{(K_{P_U} \cdot T_{I_U} \cdot s + 1) \cdot K_f}{T_{I_U} \cdot C_{zk} \cdot s^2 (T_f \cdot s + 1)} \Rightarrow \begin{cases} \frac{K_f}{T_{I_U} \cdot C_{zk}} = \frac{1}{4^2 \cdot T_f^2} \\ K_{P_U} \cdot T_{I_U} = 4 \cdot T_f \end{cases} \tag{3.26}$$

By (3.26), the voltage PI parameters are denoted by

$$\begin{aligned} T_{I_U} &= \frac{K_f \cdot 4^2 \cdot T_f^2}{C_{zk}} \\ K_{P_U} &= \frac{4 \cdot T_f}{T_{I_U}} = \frac{C_{zk}}{4 \cdot K_f \cdot T_f} \end{aligned} \tag{3.27}$$

The parameters of controller are designed based on the values of the filter and capacitor of DC side. The typical values of the LC-filter and capacitor are shown in Table 3.3 according to [23].

Table 3.3: Parameters and the used values for VSI

Parameter	Description	Value used in reference model
L_{f}	Induction of filter	13 mH
R_{f}	Resistance of filter	1 Ohm
C_{f}	Capacitor of filter	80 nF
C_{zk}	Capacitor of condenser in DC side	100 µF
$T_{\mathrm{I_C}}$	Time constant of PI controller for current loop	3.92 s
$K_{\mathrm{P_C}}$	Proportional of PI controller for current loop	0.033
$T_{\mathrm{I_U}}$	Time constant of PI controller for voltage loop	0.009 s
$K_{\mathrm{P_U}}$	Proportional of PI controller for voltage loop	0.1333
K_{f}	Proportional between DC and AC current	0.625
K_{SR}	Coefficient of amplifier in voltage loop	20.000

3.2 Parameter estimation of Digital Twin with proposed algorithms

In this section, the parameter estimation methods mentioned in chapter 2 are used in tuning the parameters of the DT, which is built in last section. The estimation process focuses on the two typical generation units: synchronous generator and VSI inverter- based renewable generation. Both are the essential components that impact the dynamic behaviour of power system. Accordingly, the accurate estimation of the parameter for both components decides the accuracy of DT in rebuilding the dynamic of physical power grid. On the basis of the DAE systems of the both components introduced in last section, the mathematic deduction of the parameter estimation algorithms with the variables in both models is described in this section.

3.2.1 Proposed estimation algorithms for parameterizing synchronous generator

In (3.5), the DAEs of synchronous generator model include six differential equations. The first two equations describe the rotor dynamics of the synchronous machine. The other equations depicts the electrical relation of stator in machine.

a) Least-square algorithm for estimating the parameter of synchronous generator

The state variables for 6$^{\mathrm{th}}$ order machine are $x = [\delta, \omega, e'_{\mathrm{q}}, e'_{\mathrm{d}}, e''_{\mathrm{q}}, e''_{\mathrm{d}}]^{\mathrm{T}}$. The input signals for DAEs are respectively from turbine with the mechanical torque T_{m}, the field voltage from exciter u_{fd} and the voltage at point of common coupling (PCC) with power grid on

d-and q-axis u_d and u_q. The observed variables are defined as $y = [n, i_\mathrm{d}, i_\mathrm{q}]^\mathrm{T}$. The relation between the observed variables (i_d and i_q) and the voltage at PCC is written in matrix form:

$$\begin{bmatrix} i_\mathrm{d} \\ i_\mathrm{q} \end{bmatrix} = \begin{bmatrix} -r_\mathrm{a} & x''_\mathrm{q} - x_\mathrm{l} \\ -x''_\mathrm{d} + x_\mathrm{l} & -r_\mathrm{a} \end{bmatrix}^{-1} \cdot \begin{bmatrix} u_\mathrm{d} - e''_\mathrm{d} \\ u_\mathrm{q} - e''_\mathrm{q} \end{bmatrix} \tag{3.28}$$

With the integration of the equation (3.28) into the LSQ objective function, the square of the current variables is:

$$\boldsymbol{\varphi}_\mathrm{c}^{\mathrm{LSQ}} = \sum_{i=1}^{N} (\boldsymbol{i}_{\mathrm{dq}i}^{m} - \boldsymbol{i}_{\mathrm{dq}i})^\mathrm{T} (\boldsymbol{i}_{\mathrm{dq}i}^{m} - \boldsymbol{i}_{\mathrm{dq}i}) \tag{3.29}$$

The minimization of the LSQ objective function in (3.29) is correlated with the coefficients in observed variables. Except for the parameters $r_\mathrm{a}, x''_\mathrm{q}, x''_\mathrm{d}$ in (3.28), the coefficients in the differential equations related to variables $\delta, \omega, e'_\mathrm{q}, e'_\mathrm{d}, e''_\mathrm{d}$ and e''_q influence the value of $\boldsymbol{\varphi}^{\mathrm{LSQ}}$.

Figure 3.15 shows the framework to implement the LSQ algorithm for parameter estimation. Initially, a setpoint change test is performed on the synchronous machine and the measured output are obtained. These data are used to make the initial estimation of parameters in synchronous machine. The LSQ factor in equation (3.29) is calculated to evaluate the error between this initial simulation and the measured output. With the iteration process, the new set parameters are estimated for minimizing the error until the optimal minimum φ^{LSQ}.

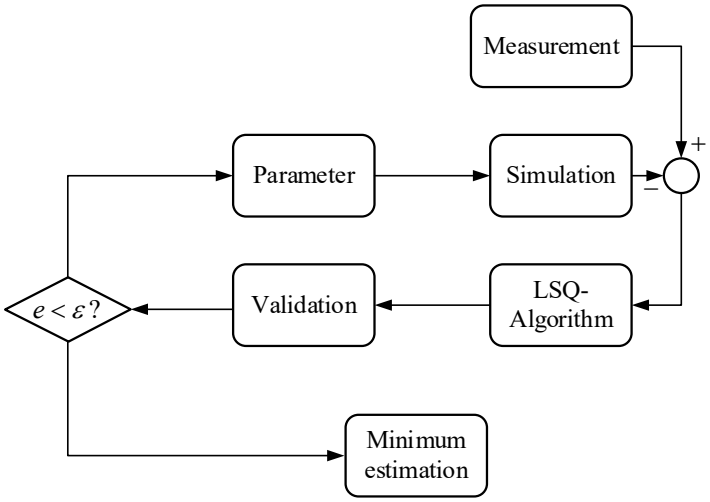

Figure 3.15: Parameter estimation framework by LSQ [190]

b) Recursive least square algorithm for estimating the parameter of synchronous generator

The implementation of the RLS based estimation utilizes the ARMAX model structure. The DAEs of synchronous generator are needed to transform to ARMAX structure in . Some assumptions are considered for simultaneous estimation of the 13 parameters in synchronous machine with RLS. The variables T_{m} and u_{fd}, which come from turbine and exciter, are assumed as the known measurement. The both are regarded as constant value. $\omega_{\mathrm{n}} = 1$ p.u. is set for simplification of the calculation. The input signal in DAEs of synchronous generator is the voltage u_{dq} at PCC. With z-transformation [68], the differential equations of synchronous generator are transformed as follows:

$$\begin{cases} \delta = \dfrac{z\cdot(\omega-1)}{z-1} \\ n = \dfrac{1}{2H}(T_{\mathrm{m}} - T_{\mathrm{e}} - D\cdot\Delta\omega)\cdot\dfrac{z}{z-1} \\ e_{\mathrm{q}}^{'} = \dfrac{1}{(\frac{z-1}{z}T_{\mathrm{d0}}^{'}+1)}\left(u_{\mathrm{fd}}^{*} - \left(x_{\mathrm{d}} - x_{\mathrm{d}}^{'} - \dfrac{T_{\mathrm{d0}}^{''}}{T_{\mathrm{d0}}^{'}}\dfrac{x_{\mathrm{d}}^{''}}{x_{\mathrm{d}}^{'}}\left(x_{\mathrm{d}} - x_{\mathrm{d}}^{'}\right)\right)i_{\mathrm{d}}\right) \\ e_{\mathrm{d}}^{'} = \dfrac{1}{(\frac{z-1}{z}T_{\mathrm{q0}}^{'}+1)}\left(x_{\mathrm{q}} - x_{\mathrm{q}}^{'} - \dfrac{T_{\mathrm{q0}}^{''}}{T_{\mathrm{q0}}^{'}}\dfrac{x_{\mathrm{q}}^{''}}{x_{\mathrm{q}}^{'}}\left(x_{\mathrm{q}} - x_{\mathrm{q}}^{'}\right)\right)i_{\mathrm{q}} \\ e_{\mathrm{q}}^{''} = \dfrac{1}{(\frac{z-1}{z}T_{\mathrm{d0}}^{''}+1)}\left(e_{\mathrm{q}}^{'} - \left(x_{\mathrm{d}} - x_{\mathrm{d}}^{'} - \dfrac{T_{\mathrm{d0}}^{''}}{T_{\mathrm{d0}}^{'}}\dfrac{x_{\mathrm{d}}^{''}}{x_{\mathrm{d}}^{'}}\left(x_{\mathrm{d}} - x_{\mathrm{d}}^{'}\right)\right)i_{\mathrm{d}}\right) \\ e_{\mathrm{d}}^{''} = \dfrac{1}{(\frac{z-1}{z}T_{\mathrm{q0}}^{''}+1)}\left(e_{\mathrm{d}}^{'} + \left(x_{\mathrm{q}} - x_{\mathrm{q}}^{'} - \dfrac{T_{\mathrm{q0}}^{''}}{T_{\mathrm{q0}}^{'}}\dfrac{x_{\mathrm{q}}^{''}}{x_{\mathrm{q}}^{'}}\left(x_{\mathrm{q}} - x_{\mathrm{q}}^{'}\right)\right)i_{\mathrm{q}}\right) \end{cases} \tag{3.30}$$

The observed variable y is rotation state n of the machine with the assumption that it exists no measurement noise $v(t) = 0$. The relation between the voltage u_{dq} and the rotation state ω is according to the ARMAX structure in (2.8) given by (3.31).

$$\left(\frac{r_{\mathrm{a}}x_{\mathrm{d}}^{'2}T_{\mathrm{d0}}^{'} + x_{\mathrm{d}}^{''}T_{\mathrm{q0}}^{'} + x_{\mathrm{d}}^{''}x_{\mathrm{q}}^{''}T_{\mathrm{d0}}^{'}T_{\mathrm{d0}}^{''} + x_{\mathrm{d}}^{''}x_{\mathrm{q}}^{''}T_{\mathrm{d0}}^{''}T_{\mathrm{q0}}^{''2}}{\sqrt{r_{\mathrm{a}}^{2} + x_{\mathrm{d}}^{''2}\cdot x_{\mathrm{q}}^{''2}}}z^{-6} + \cdots + \frac{x_{\mathrm{d}}^{''2} - x_{\mathrm{q}}^{''2}}{\sqrt{r_{\mathrm{a}}^{2} + x_{\mathrm{d}}^{''2}\cdot x_{\mathrm{d}}^{''2}}}z^{-1} + 1\right)y(t) = \left(2H\cdot z^{-1} - \frac{T_{\mathrm{m}}}{\sqrt{r_{\mathrm{a}}^{2} + x_{\mathrm{d}}^{''2}\cdot x_{\mathrm{q}}^{''2}}}\right)u(t) \tag{3.31}$$

The estimated parameter set in equation (3.31) is $\boldsymbol{\theta}^{\mathrm{T}} = [a_1, a_2, \cdots, a_6, b_1, b_2]$ and the states are $\boldsymbol{\varphi}^{\mathrm{T}}(t) = [-y(t-1), \cdots, -y(t-6), \cdots u(t-2)]$. The parameter set $\boldsymbol{\theta}^{\mathrm{T}}$ corresponds the coefficients in equation (3.31). The LS solution based on the synchronous generator observations $\boldsymbol{\varphi}(t)$ is given as solution according to equation (2.11):

$$\begin{bmatrix} -y(t-1) \\ -y(t-2) \\ \vdots \\ u(t-2) \end{bmatrix} \begin{bmatrix} -y(t-1) & -y(t-2) & \cdots & u(t-2) \end{bmatrix} \begin{bmatrix} \hat{a}_1 \\ \hat{a}_2 \\ \vdots \\ \hat{b}_2 \end{bmatrix} = y(t) \begin{bmatrix} -y(t-1) \\ -y(t-2) \\ \vdots \\ u(t-2) \end{bmatrix} \tag{3.32}$$

where $\widehat{\boldsymbol{\theta}}^{\mathrm{T}}$ is the initial coefficient set and it is assumed that the solution $\widehat{\boldsymbol{\theta}}$ is unique, i.e. the matrix $\boldsymbol{M} = \boldsymbol{\varphi}\boldsymbol{\varphi}^{\mathrm{T}}$ is inversible. Then, the initial solution is integrated into the recursive process according to equation (2.14):

$$\begin{aligned} \hat{\boldsymbol{\theta}}_1 &= \hat{\boldsymbol{\theta}}_0 + \boldsymbol{M}_1^{-1}\boldsymbol{\varphi}_1(y_1 - \hat{\boldsymbol{\theta}}_0^{\mathrm{T}}\boldsymbol{\varphi}_1) \\ \hat{\boldsymbol{\theta}}_2 &= \hat{\boldsymbol{\theta}}_1 + \boldsymbol{M}_2^{-1}\boldsymbol{\varphi}_2(y_2 - \hat{\boldsymbol{\theta}}_1^{\mathrm{T}}\boldsymbol{\varphi}_2) \\ &\vdots \\ \hat{\boldsymbol{\theta}}_t &= \hat{\boldsymbol{\theta}}_{t-1} + \boldsymbol{M}_t^{-1}\boldsymbol{\varphi}_t(y_t - \hat{\boldsymbol{\theta}}_{t-1}^{\mathrm{T}}\boldsymbol{\varphi}_t) \end{aligned} \tag{3.33}$$

The evaluation of the estimated parameter set $\widehat{\boldsymbol{\theta}}_t^{\mathrm{T}}$ depends on the indicator ε_t in equation (2.15). The indicator ε_t is the deviation of the measured rotation state ω^{m} and $\widehat{\boldsymbol{\theta}}_{\mathrm{t-1}}^{\mathrm{T}}\boldsymbol{\varphi}_{\mathrm{t}}$. If $\varepsilon_t < 0.001$ the estimation $\widehat{\boldsymbol{\theta}}_t$ is accurate and the recursive process can stop.

c) Neural network algorithm for estimating the parameter of synchronous generator

The application of NN identifier designed in previous section in synchronous generator is under the assumption that the stator current and voltage, the field current and the rotor speed are measurable. The DAEs of 6th order synchronous generator are rewritten in (3.34).

$$\begin{cases} \dot{x}_1 = \theta_1 \cdot (u_1 - \dfrac{1}{\cos\varphi} \cdot (i_{\mathrm{q}} \cdot \psi_{\mathrm{d}} - i_{\mathrm{d}} \cdot \psi_{\mathrm{q}}) - D \cdot \Delta\omega) \\ \dot{x}_2 = \theta_2 \cdot (u_2 - x_2 - \left(x_{\mathrm{d}} - x_{\mathrm{d}}^{'} - \dfrac{T_{\mathrm{d0}}^{''}}{T_{\mathrm{d0}}^{'}} \dfrac{x_{\mathrm{d}}^{''}}{x_{\mathrm{d}}^{'}} \left(x_{\mathrm{d}} - x_{\mathrm{d}}^{'} \right) \right) i_{\mathrm{d}}) \\ \dot{x}_3 = \theta_3 \cdot \left(-x_3 + \left(x_{\mathrm{q}} - x_{\mathrm{q}}^{'} - \dfrac{T_{\mathrm{q0}}^{''}}{T_{\mathrm{q0}}^{'}} \dfrac{x_{\mathrm{q}}^{''}}{x_{\mathrm{q}}^{'}} \left(x_{\mathrm{q}} - x_{\mathrm{q}}^{'} \right) \right) i_{\mathrm{q}} \right) \\ \dot{x}_4 = \theta_4 \cdot \left(-x_4 + x_2 - \left(x_{\mathrm{d}} - x_{\mathrm{d}}^{'} - \dfrac{T_{\mathrm{d0}}^{''}}{T_{\mathrm{d0}}^{'}} \dfrac{x_{\mathrm{d}}^{''}}{x_{\mathrm{d}}^{'}} \left(x_{\mathrm{d}} - x_{\mathrm{d}}^{'} \right) \right) i_{\mathrm{d}} \right) \right) \\ \dot{x}_5 = \theta_5 \cdot \left(-x_5 + x_3 + \left(x_{\mathrm{q}} - x_{\mathrm{q}}^{'} - \dfrac{T_{\mathrm{q0}}^{''}}{T_{\mathrm{q0}}^{'}} \dfrac{x_{\mathrm{q}}^{''}}{x_{\mathrm{q}}^{'}} \left(x_{\mathrm{q}} - x_{\mathrm{q}}^{'} \right) \right) i_{\mathrm{q}} \right) \end{cases} \tag{3.34}$$

where $x_1 = \omega$, $x_2 = e'_{\mathrm{q}}$, $x_3 = e'_{\mathrm{d}}$, $x_4 = e''_{\mathrm{q}}$ and $x_5 = e''_{\mathrm{d}}$ are the states of the system. $u_1 = T_{\mathrm{m}}$, $u_2 = u_{\mathrm{fd}}$, $u_3 = u_{\mathrm{d}}$ and $u_4 = u_{\mathrm{q}}$ are the measured input of the state space. The estimated parameter set $\widehat{\boldsymbol{\theta}} = [\theta_1, \theta_2, \theta_3, \theta_4, \theta_5]$ is respectively $\theta_1 = \frac{1}{2H}$, $\theta_2 = \frac{1}{T'_{\mathrm{d0}}}$, $\theta_3 = \frac{1}{T'_{\mathrm{q0}}}$, $\theta_4 = \frac{1}{T''_{\mathrm{d0}}}$ and $\theta_5 = \frac{1}{T''_{\mathrm{q0}}}$ .The NN-identifier can be applied with the following form:

$$\dot{\hat{x}}_i = b_i(x, \hat{x}, t) + \sum_j^N w_{ij} \Phi(\left\| X - C_j \right\|, v_j) = y_i \tag{3.35}$$

where $\boldsymbol{X} = [x_1, x_2, x_3, x_4, x_5, u_1, u_2, u_3, u_4]^{\mathrm{T}}$, $e_i = \hat{x}_i - x_i$, $b_i(x, \hat{x}, t) = -\alpha_i e_i - \frac{\hat{\lambda}^2 e_i}{|\hat{\lambda} e_i| + \epsilon}$ and $\dot{\hat{w}}_{ij} = e_i \exp\left(\frac{-\|\boldsymbol{X} - C_j\|^2}{2v_j^2}\right)$. Here the C_j and v_j are given by clustering method [191]. The parameter estimation is derived from the inversion of the DAEs formed in (3.36).

$$\begin{cases} \hat{\theta}_1 = \dfrac{y_1}{(u_1 - \dfrac{1}{\cos\varphi} \cdot (i_{\mathrm{q}} \cdot \psi_{\mathrm{d}} - i_{\mathrm{d}} \cdot \psi_{\mathrm{q}}) - D \cdot \Delta\omega)} \\ \hat{\theta}_2 = \dfrac{y_2}{(u_2 - x_2 - (x_{\mathrm{d}} - x'_{\mathrm{d}} - \dfrac{T''_{\mathrm{d0}}}{T'_{\mathrm{d0}}} \dfrac{x''_{\mathrm{d}}}{x'_{\mathrm{d}}} \left(x_{\mathrm{d}} - x'_{\mathrm{d}}\right)) i_{\mathrm{d}})} \\ \hat{\theta}_3 = \dfrac{y_3}{\left(-x_3 + \left(x_{\mathrm{q}} - x'_{\mathrm{q}} - \dfrac{T''_{\mathrm{q0}}}{T'_{\mathrm{q0}}} \dfrac{x''_{\mathrm{q}}}{x'_{\mathrm{q}}} \left(x_{\mathrm{q}} - x'_{\mathrm{q}}\right)\right) i_{\mathrm{q}}\right)} \\ \hat{\theta}_4 = \dfrac{y_4}{\left(-x_4 + x_2 - \left(x_{\mathrm{d}} - x'_{\mathrm{d}} - \dfrac{T''_{\mathrm{d0}}}{T'_{\mathrm{d0}}} \dfrac{x''_{\mathrm{d}}}{x'_{\mathrm{d}}} \left(x_{\mathrm{d}} - x'_{\mathrm{d}}\right)\right) i_{\mathrm{d}}\right)\right)} \\ \hat{\theta}_5 = \dfrac{y_5}{\left(-x_5 + x_3 + \left(x_{\mathrm{q}} - x'_{\mathrm{q}} - \dfrac{T''_{\mathrm{q0}}}{T'_{\mathrm{q0}}} \dfrac{x''_{\mathrm{q}}}{x'_{\mathrm{q}}} \left(x_{\mathrm{q}} - x'_{\mathrm{q}}\right)\right) i_{\mathrm{q}}\right)} \end{cases} \tag{3.36}$$

For $N(\hat{\theta}_i) \neq 0$ and $D(\hat{\theta}_i) \neq 0$, $i = 1,2,\cdots 5$, $N(\hat{\theta}_i)$ and $D(\hat{\theta}_i)$ are the numerators of $\hat{\theta}_i$ respectively. y_i is the output of the NN predictor (3.35). By (3.36), the parameters are estimated to accurately build the DAEs based DT of synchronous generator.

3.2.2 Proposed estimation algorithms for parameterizing VSI inverter

In this section, the deduction of the proposed parameter estimation algorithms for parameterizing the parameters in VSI inverter is demonstrated. In the DAE of VSI inverter, it is assumed that the loss of the switching operation is not considered by the inverter.

a) Least square algorithm for estimating the parameter of inverter

The state-space form of inverter model is written in equation (3.37). In this equation, the input and the output variables are defined with $u = [u_{\mathrm{Nd}}, u_{\mathrm{Nq}}, u_{\mathrm{SRd}}, u_{\mathrm{SRq}}]^{\mathrm{T}}$ and $y = [i_{\mathrm{Nd}}, i_{\mathrm{Nq}}]^{\mathrm{T}}$. The input signals are the measured network voltage on dq coordinate, the inverter voltage on dq coordinate and the control signal on dq axis. The output variables are respectively the voltage in DC side, the current feed-into network on dq axis. The states in the DAEs are defined as $x = [i_{\mathrm{fd}}, i_{\mathrm{fq}}, i_{\mathrm{Nd}}, i_{\mathrm{Nq}}, u_{\mathrm{C_f d}}, u_{\mathrm{C_f q}}]^{\mathrm{T}}$, where i_{fd} and i_{fq} are filter current, i_{Nd} and i_{Nq} are the current feed-into network and the $u_{\mathrm{C_f d}}$, $u_{\mathrm{C_f q}}$ are the capacitor voltage in LC filter.

$$
\begin{cases}
\dfrac{\mathrm{d}}{\mathrm{d}t}\begin{bmatrix} i_{\mathrm{fd}} \\ i_{\mathrm{fq}} \\ i_{\mathrm{Nd}} \\ i_{\mathrm{Nq}} \\ u_{\mathrm{C_f d}} \\ u_{\mathrm{C_f q}} \end{bmatrix} = \begin{bmatrix} -\dfrac{R_{\mathrm{f}}}{L_{\mathrm{f}}} & \omega & 0 & 0 & -\dfrac{1}{L_{\mathrm{f}}} & 0 \\ -\omega & -\dfrac{R_{\mathrm{f}}}{L_{\mathrm{f}}} & 0 & 0 & 0 & -\dfrac{1}{L_{\mathrm{f}}} \\ 0 & 0 & -\dfrac{R_{\mathrm{N}}}{L_{\mathrm{N}}} & \omega & \dfrac{1}{L_{\mathrm{N}}} & 0 \\ 0 & 0 & -\omega & \dfrac{R_{\mathrm{N}}}{L_{\mathrm{N}}} & 0 & \dfrac{1}{L_{\mathrm{N}}} \\ \dfrac{1}{C_{\mathrm{f}}} & 0 & -\dfrac{1}{C_{\mathrm{f}}} & 0 & 0 & -\omega \\ 0 & \dfrac{1}{C_{\mathrm{f}}} & 0 & -\dfrac{1}{C_{\mathrm{f}}} & \omega & 0 \end{bmatrix} \begin{bmatrix} i_{\mathrm{fd}} \\ i_{\mathrm{fq}} \\ i_{\mathrm{Nd}} \\ i_{\mathrm{Nq}} \\ u_{\mathrm{C_f d}} \\ u_{\mathrm{C_f q}} \end{bmatrix} + \begin{bmatrix} 0 & 0 & \dfrac{1}{L_{\mathrm{f}}} & 0 & 0 & 0 \\ 0 & 0 & 0 & \dfrac{1}{L_{\mathrm{f}}} & 0 & 0 \\ -\dfrac{1}{L_{\mathrm{N}}} & 0 & 0 & 0 & 0 & 0 \\ 0 & -\dfrac{1}{L_{\mathrm{N}}} & 0 & 0 & 0 & 0 \\ 0 & 0 & 0 & 0 & 0 & 0 \\ 0 & 0 & 0 & 0 & 0 & 0 \end{bmatrix} \begin{bmatrix} u_{\mathrm{Nd}} \\ u_{\mathrm{Nq}} \\ u_{\mathrm{SRd}} \\ u_{\mathrm{SRq}} \\ v_{\mathrm{d}} \\ v_{\mathrm{q}} \end{bmatrix} \\
\begin{bmatrix} i_{\mathrm{Nd}} \\ i_{\mathrm{Nq}} \end{bmatrix} = \begin{bmatrix} 0 & 0 & 1 & 0 & 0 & 0 \\ 0 & 0 & 0 & 1 & 0 & 0 \end{bmatrix}^{\mathrm{T}} \begin{bmatrix} i_{\mathrm{fd}} \\ i_{\mathrm{fq}} \\ i_{\mathrm{Nd}} \\ i_{\mathrm{Nq}} \\ u_{\mathrm{C_f d}} \\ u_{\mathrm{C_f q}} \end{bmatrix}
\end{cases}
\tag{3.37}
$$

The LSQ objective function of the output variables is:

$$
\boldsymbol{\varphi}_{\mathrm{c}}^{\mathrm{LSQ}} = \sum_{i=1}^{N} (\boldsymbol{i}_{\mathrm{Ndq}i}^{\mathrm{m}} - \boldsymbol{i}_{\mathrm{Ndq}i})^{\mathrm{T}} (\boldsymbol{i}_{\mathrm{Ndq}i}^{\mathrm{m}} - \boldsymbol{i}_{\mathrm{Ndq}i}) \tag{3.38}
$$

where $\boldsymbol{i}_{\mathrm{Ndq}}^{\mathrm{m}}$ is the measured current state in vector matrix form and $\boldsymbol{i}_{\mathrm{Ndq}}$ is the simulation states of current in vector form. $\boldsymbol{\varphi}_{\mathrm{c}}^{\mathrm{LSQ}}$ is the LSQ factor to evaluate the deviation between both states for parameter estimation. It is assumed that there is no noise signal to influence the value of LSQ factor. To determine the conditions that minimize the LSQ factor, the differential of the equation (3.38) with respect to the parameters equate the result to zero:

$$\frac{\partial \boldsymbol{\varphi}_{\mathrm{c}}^{\mathrm{LSQ}}}{\partial \boldsymbol{\theta}} = 0 \tag{3.39}$$

where $\boldsymbol{\theta}$ is the parameter vector. It refers to the parameters $L, R, L_{\mathrm{f}}, R_{\mathrm{f}}$ and C_{f}. Accordingly, the LS estimator of $\boldsymbol{\theta}$ is written as

$$\hat{\boldsymbol{\theta}} = (\boldsymbol{i}_{\mathrm{Ndq}i}^{\mathrm{T}} \cdot \boldsymbol{i}_{\mathrm{Ndq}i})^{-1} \boldsymbol{i}_{\mathrm{Ndq}i}^{\mathrm{T}} \cdot \boldsymbol{i}_{\mathrm{Ndq}i}^{\mathrm{m}} \tag{3.40}$$

The equation (3.40) is denoted as the least square estimator. The matrix $\boldsymbol{i}_{\mathrm{Ndq}}^{\mathrm{T}} \cdot \boldsymbol{i}_{\mathrm{Ndq}}$ is non-singular and has an inverse. The LSQ factor attains an absolute minimum if and only if $\boldsymbol{\theta} = \widehat{\boldsymbol{\theta}}$.

b) Recursive least square algorithm for estimating the parameter of inverter

As mentioned above, the implementation of the RLS based online estimation for inverter model utilizes the ARMAX model structure. The DAEs of inverter in equation (3.16) are transformed initially to ARMAX structure. Some assumptions are considered for simultaneous estimation of the parameters in inverter with RLS. u_{Nd} and u_{Nq} are the input variables i.e., the measurement voltage at PCC between inverter and network. u_{SRd} and u_{SRq} are the voltages of inverter in AC sides. By z-transformation, the equations(3.16) are transformed as

$$
\begin{aligned}
i_{\mathrm{fd}} &= \frac{z}{L_{\mathrm{f}}(z-1)} \cdot (-R_{\mathrm{f}} \cdot i_{\mathrm{fd}} + \omega L_{\mathrm{f}} \cdot i_{\mathrm{fq}} + u_{\mathrm{SRd}} - u_{\mathrm{C_f d}}) \\
i_{\mathrm{fq}} &= \frac{z}{L_{\mathrm{f}}(z-1)} \cdot (-R_{\mathrm{f}} \cdot i_{\mathrm{fq}} - \omega L_{\mathrm{f}} \cdot i_{\mathrm{fd}} + u_{\mathrm{SRq}} - u_{\mathrm{C_f q}}) \\
i_{\mathrm{Nd}} &= \frac{z}{L_{\mathrm{N}}(z-1)} \cdot (-R_{\mathrm{N}} \cdot i_{\mathrm{Nd}} + \omega L_{\mathrm{N}} \cdot i_{\mathrm{Nq}} + u_{\mathrm{C_f d}} - u_{\mathrm{Nd}}) \\
i_{\mathrm{Nq}} &= \frac{z}{L_{\mathrm{N}}(z-1)} \cdot (-R_{\mathrm{N}} \cdot i_{\mathrm{Nq}} - \omega L_{\mathrm{N}} \cdot i_{\mathrm{Nd}} + u_{\mathrm{C_f q}} - u_{\mathrm{Nq}}) \\
u_{\mathrm{C_f d}} &= \frac{z}{C_{\mathrm{f}}(z-1)} \cdot (-\omega C_{\mathrm{f}} \cdot u_{\mathrm{C_f q}} + i_{\mathrm{fd}} - i_{\mathrm{Nd}}) \\
u_{\mathrm{C_f q}} &= \frac{z}{C_{\mathrm{f}}(z-1)} \cdot (\omega C_{\mathrm{f}} \cdot u_{\mathrm{C_f d}} + i_{\mathrm{fq}} - i_{\mathrm{Nq}})
\end{aligned}
\tag{3.41}
$$

The observed variable $y = [i_{\mathrm{Nd}}\ i_{\mathrm{Nq}}]^{\mathrm{T}}$ is the currents feed into the network with the assumption that it exists no measurement noise $v(t) = 0$. The relation between the input variables u_{Nd} and u_{Nq} and currents is calculated based on the (3.41):

$$
\begin{bmatrix}
\frac{C_{\mathrm{f}}L_{\mathrm{f}}^2 \cdot z^{-3} + 2C_{\mathrm{f}}L_{\mathrm{f}}R_{\mathrm{f}} \cdot z^{-2} + (\omega^2 C_{\mathrm{f}}L_{\mathrm{f}}^2 + C_{\mathrm{f}}R_{\mathrm{f}}^2 + L_{\mathrm{N}} - L_{\mathrm{f}}) \cdot z^{-1} - R_{\mathrm{f}} + R_{\mathrm{N}}}{\sqrt{(C_{\mathrm{f}}L_{\mathrm{f}} + C_{\mathrm{f}}R_{\mathrm{f}} + \omega^2 C_{\mathrm{f}}L_{\mathrm{f}} - 1)^2 + \omega^2 C_{\mathrm{f}}^2 L_{\mathrm{f}}^2}} & \frac{\omega C_{\mathrm{f}}L_{\mathrm{f}}^2 \cdot z^{-2} + \omega^3 C_{\mathrm{f}}L_{\mathrm{f}}^2 + \omega C_{\mathrm{f}}R_{\mathrm{f}}^2 - \omega L_{\mathrm{N}} - 1}{\sqrt{(C_{\mathrm{f}}L_{\mathrm{f}} + C_{\mathrm{f}}R_{\mathrm{f}} + \omega^2 C_{\mathrm{f}}L_{\mathrm{f}} - 1)^2 + \omega^2 C_{\mathrm{f}}^2 L_{\mathrm{f}}^2}} \\
\frac{\omega C_{\mathrm{f}}L_{\mathrm{fl}}^2 \cdot z^{-2} + \omega^3 C_{\mathrm{f}}L_{\mathrm{f}}^2 + \omega C_{\mathrm{f}}R_{\mathrm{fl}}^2 + \omega L_{\mathrm{N}} - 1}{\sqrt{(C_{\mathrm{f}}L_{\mathrm{f}} + C_{\mathrm{f}}R_{\mathrm{f}} + \omega^2 C_{\mathrm{f}}L_{\mathrm{f}} - 1)^2 + \omega^2 C_{\mathrm{f}}^2 L_{\mathrm{f}}^2}} & \frac{C_{\mathrm{f}}L_{\mathrm{f}}^2 \cdot z^{-3} + 2C_{\mathrm{f}}L_{\mathrm{f}}R_{\mathrm{f}} \cdot z^{-2} + (\omega^2 C_{\mathrm{f}}L_{\mathrm{f}}^2 + C_{\mathrm{f}}R_{\mathrm{f}}^2 + L - L_{\mathrm{f}})z^{-1} - R_{\mathrm{f}} + R_{\mathrm{N}}}{\sqrt{(C_{\mathrm{f}}L_{\mathrm{f}} + C_{\mathrm{f}}R_{\mathrm{f}} + \omega^2 C_{\mathrm{f}}L_{\mathrm{f}} - 1)^2 + \omega^2 C_{\mathrm{f}}^2 L_{\mathrm{f}}^2}}
\end{bmatrix} \cdot \begin{bmatrix} i_{\mathrm{Nd}} \\ i_{\mathrm{Nq}} \end{bmatrix}
$$

$$
= \begin{bmatrix}
\frac{(C_{\mathrm{f}}L_{\mathrm{f}} \cdot z^{-2} + C_{\mathrm{f}}R_{\mathrm{f}} \cdot z^{-1} + \omega^2 C_{\mathrm{f}}L_{\mathrm{f}}) \cdot u_{\mathrm{SRd}} + \omega C_{\mathrm{f}}R_{\mathrm{f}} \cdot u_{\mathrm{SRq}}}{\sqrt{(C_{\mathrm{f}}L_{\mathrm{f}} + C_{\mathrm{f}}R_{\mathrm{f}} + \omega^2 C_{\mathrm{f}}L_{\mathrm{f}} - 1)^2 + \omega^2 C_{\mathrm{f}}^2 L_{\mathrm{fl}}^2}} - u_{\mathrm{Nd}} \\
\frac{(C_{\mathrm{f}}L_{\mathrm{f}} \cdot z^{-2} + C_{\mathrm{f}}R_{\mathrm{f}} \cdot z^{-1} + \omega^2 C_{\mathrm{f}}L_{\mathrm{f}}) \cdot u_{\mathrm{SRq}} + \omega C_{\mathrm{f}}R_{\mathrm{f}} \cdot u_{\mathrm{SRd}}}{\sqrt{(C_{\mathrm{f}}L_{\mathrm{f}} + C_{\mathrm{f}}R_{\mathrm{f}} + \omega^2 C_{\mathrm{f}}L_{\mathrm{f}} - 1)^2 + \omega^2 C_{\mathrm{f}}^2 L_{\mathrm{f}}^2}} - u_{\mathrm{Nq}}
\end{bmatrix}
\tag{3.42}
$$

The matrix in (3.42) is simplified as:

$$
\begin{bmatrix}
a_1 \cdot z^{-3} + a_2 \cdot z^{-2} + a_3 \cdot z^{-1} + 1 & b_1 \cdot z^{-2} + 1 \\
b_2 \cdot z^{-2} + 1 & a_1 \cdot z^{-3} + a_2 \cdot z^{-2} + a_3 \cdot z^{-1} + 1
\end{bmatrix} \cdot \begin{bmatrix} i_{\mathrm{Nd}} \\ i_{\mathrm{Nq}} \end{bmatrix} = \begin{bmatrix} (c_1 \cdot z^{-2} + c_2 \cdot z^{-1} + 1) \cdot u_{\mathrm{SRd}} + c_3 \cdot u_{\mathrm{SRq}} - u_{\mathrm{Nd}} \\ (d_1 \cdot z^{-2} + d_2 \cdot z^{-1} + 1) \cdot u_{\mathrm{SRd}} + d_3 \cdot u_{\mathrm{SRq}} - u_{\mathrm{Nq}} \end{bmatrix}
\tag{3.43}
$$

The estimated parameter set is $\boldsymbol{\theta}^{\mathrm{T}} = [a_1, a_2, a_3, b_1, b_2, c_1, c_2, c_3, d_1, d_2, d_3]$.The parameter set $\boldsymbol{\theta}^{\mathrm{T}}$ corresponds the coefficients in equation (3.42). The states refer to the $\boldsymbol{\varphi}(t) = [i_{\mathrm{Nd}}\ i_{\mathrm{Nq}}\ u_{\mathrm{Nd}}\ u_{\mathrm{Nq}}\ u_{\mathrm{SRd}}\ u_{\mathrm{SRq}}]^{\mathrm{T}}$. The LS solution based on inverter observations $\boldsymbol{\varphi}(t)$ is given as solution according to equation (2.11):

$$\boldsymbol{\varphi}(t)\boldsymbol{\varphi}^{\mathrm{T}}(t)\cdot\begin{bmatrix}\hat{a}_1\\ \hat{a}_2\\ \vdots\\ \hat{d}_3\end{bmatrix}=y(t)\cdot\boldsymbol{\varphi}^{\mathrm{T}}(t) \tag{3.44}$$

where $\widehat{\boldsymbol{\theta}}^{\mathrm{T}}=\left[\hat{a}_1,\hat{a}_2,\cdots,\hat{d}_3\right]$. is the initial coefficient set and it is assumed that the solution $\widehat{\boldsymbol{\theta}}$ is unique, i.e., the matrix $\boldsymbol{\varphi}(t)\boldsymbol{\varphi}^{\mathrm{T}}(t)$ is inversible. Then, the initial solution is integrated into the recursive process, which is the same as the parameter estimation of synchronous generator. The evaluation of the estimated parameter set $\widehat{\boldsymbol{\theta}}_t^{\mathrm{T}}$ depends on the indicator ε_t in equation (2.15).

c) Neural network algorithm for estimating the parameter of inverter

The implementation of NN identifier in estimating the parameters of inverter is the assumption that the input variables, i.e., the network voltage (u_{Nd} and u_{Nq}) and inverter voltage in AC side (u_{SRd} and u_{SRq}) are always measurable. Accordingly, the DAEs of inverter model are rewritten as:

$$\begin{cases}\dot{x}_1=\theta_1(u_1-\theta_2\cdot x_1+\omega\cdot\dfrac{1}{\theta_1}\cdot x_2-x_5)\\ \dot{x}_2=\theta_1\cdot(u_2-\theta_2\cdot x_2-\omega\cdot\dfrac{1}{\theta_1}\cdot x_1-x_6)\\ \dot{x}_3=\theta_3\cdot(-\theta_4\cdot x_3+\omega\cdot\dfrac{1}{\theta_3}\cdot x_4+x_5-u_3)\\ \dot{x}_4=\theta_3\cdot(-\theta_4\cdot x_4-\omega\cdot\dfrac{1}{\theta_3}\cdot x_3+x_6-u_4)\\ \dot{x}_5=\theta_5\cdot(-\omega\cdot\dfrac{1}{\theta_5}\cdot x_5+x_1-x_3)\\ \dot{x}_6=\theta_5\cdot(\omega\cdot\dfrac{1}{\theta_5}\cdot x_6+x_2-x_4)\end{cases} \tag{3.45}$$

where $x_1=i_{\mathrm{fd}}$, $x_2=i_{\mathrm{fq}}$, $x_3=i_{\mathrm{Nd}}$, $x_4=i_{\mathrm{Nq}}$, $x_5=u_{\mathrm{C_{fd}}}$ and $x_6=u_{\mathrm{C_{fq}}}$ are the states of the system. $u_1=u_{\mathrm{SRd}}$, $u_2=u_{\mathrm{SRq}}$, $u_3=u_{\mathrm{Nd}}$ and $u_4=u_{\mathrm{Nq}}$ are the measured input states. The estimated parameter set $\widehat{\boldsymbol{\theta}}=[\theta_1,\theta_2,\theta_3,\theta_4,\theta_5]$ is respectively $\theta_1=\frac{1}{L_{\mathrm{f}}}$, $\theta_2=R_{\mathrm{f}}$, $\theta_3=\frac{1}{L_{\mathrm{N}}}$, $\theta_4=R_{\mathrm{N}}$ and $\theta_5=\frac{1}{C_{\mathrm{f}}}$, .The NN-identifier can be directly applied:

$$\dot{\hat{x}}_i=b_i(x,\hat{x},t)+\sum_j^N w_{ij}\Phi(\left\|X-C_j\right\|,v_j)=y_i \tag{3.46}$$

where $\boldsymbol{X} = [x_1, x_2, x_3, x_4, x_5, x_6, u_1, u_2, u_3, u_4]^{\mathrm{T}}$, $e_i = \hat{x}_i - x_i$, $b_i(x, \hat{x}, t) = -\alpha_i e_i - \frac{\hat{\lambda}^2 e_i}{|\hat{\lambda} e_i| + \epsilon}$ and $\hat{w}_{ij} = e_i \exp\left(\frac{-\|\boldsymbol{x} - c_j\|^2}{2v_j^2}\right)$. The parameter estimation is derived from the inversion of the DAEs:

$$\begin{cases} \hat{\theta}_1 = \dfrac{y_1 - \omega \cdot x_2}{u_1 - \hat{\theta}_2 \cdot x_1 - x_5} \\ \hat{\theta}_2 = \dfrac{\hat{\theta}_1 \cdot u_2 - y_2 - \omega \cdot x_1 - \hat{\theta}_1 \cdot x_6}{\hat{\theta}_1 \cdot x_2} \\ \hat{\theta}_3 = \dfrac{y_3 - \omega \cdot x_4}{-u_3 - \hat{\theta}_4 \cdot x_3 + x_5} \\ \hat{\theta}_4 = \dfrac{-\hat{\theta}_3 \cdot u_4 - y_4 - \omega \cdot x_3 - \hat{\theta}_3 \cdot x_6}{\hat{\theta}_3 \cdot x_4} \\ \hat{\theta}_5 = \dfrac{y_5 + \omega \cdot x_5}{x_1 - x_3} \end{cases} \tag{3.47}$$

For $N(\hat{\theta}_i) \neq 0$ and $D(\hat{\theta}_i) \neq 0$, $i = 1,2,\cdots 5$, $N(\hat{\theta}_i)$ and $D(\hat{\theta}_i)$ are the numerators of $\hat{\theta}_i$ respectively. y_i is the output of the NN predictor. By (3.47), the parameters are estimated to build the DT of inverter. The proof of the convergence is achieved by Lyapunov equation (2.24).

3.3 Sensitivity analysis

In last section, three parameter estimation methods are introduced and have been implemented for tuning the parameters of synchronous generator and inverter model. This procedure is essential to build an accurate DT model. However, these models include the large number of tuneable parameters, which make the tasks of parameter estimation process challenging. Accordingly, a deeper understanding of parameter estimation is required for a more efficient estimation process. The sensitivity analysis provides an efficient insight into the estimation process for selecting the impacted parameters. Previously, the sensitivity analysis studies in [192, 193] has been proposed to study the impact of parameter uncertainties on simulation. The sensitivity concepts are generally related to the input-output relationship. Small changes in inputs map through the linearized relationship to small output changes [194]. It tracks the changes in the output resulting from perturbations in the underlying parameters and initial condition.

The classification of sensitivity analysis is introduced in [195]. The efficient form of sensitivity analysis is to vary one model parameter at a time by a given amount and examine on output results. The procedure of the sensitivity analysis is depicted in Figure 3.16.

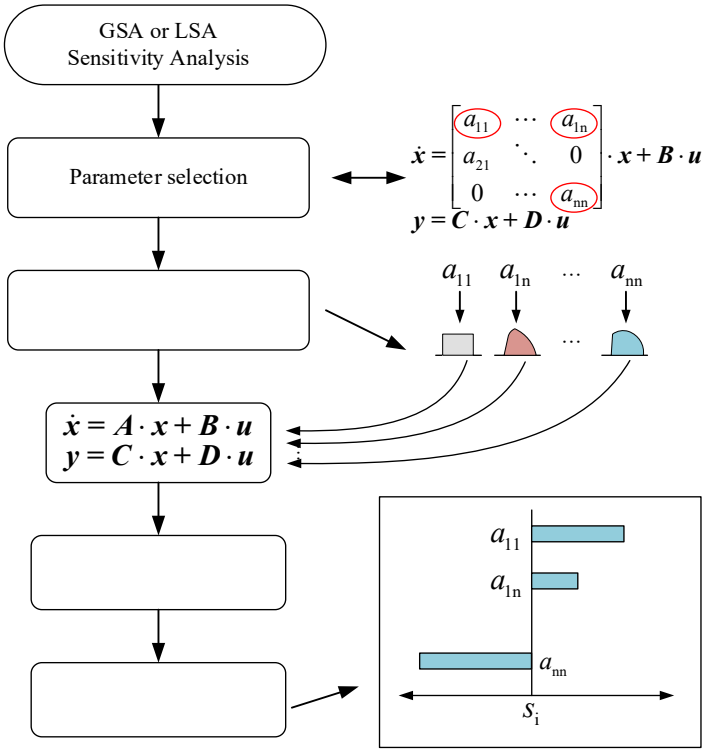

Figure 3.16: Flowchart of sensitivity analysis [196–198]

First of all, the parameters in DAE mentioned in last section, which need to be estimated, should be selected to assign probability distribution. With the assignment of probability distribution, the sensitivity index of the parameters is calculated with the variance decomposition of the model outputs. The analysis could be repeated for all model parameters independently at different times. The first method is known as local sensitivity analysis (LSA) or one-factor-at-a-time (OFAT) [199]. Although, LSA is easy to implement and computationally less burdensome. It does not explore the effect of entire parameter spaces on output variables as well as the interactions between the parameters. For the evaluation of the relative effect of the parameters on output variable in model, the normalized partial derivative provides a useful sensitivity index [200]. The normalized sensitivity index is calculated by multiplying the partial derivative with the ratio of nominal point estimates:

$$S_{ij} = \frac{\partial y_i}{\partial \theta_j} \times \frac{\theta_j}{y_i} \tag{3.48}$$

where y_i is the i-th output and θ_j is the j-th model parameter.

In application of LSA, the parameters are varied segment wise by some portion around a fixed value and the effects of individual perturbations on the observed parameters are studied in [195]. From the mathematic perspective, the normalized sensitivity coefficients are calculated with a first order finite differential method.

$$S_{ij} = \frac{\partial y_i}{\partial \theta_j} \times \frac{\theta_j}{y_i} = \lim_{\Delta\theta \to 0} \frac{y_i\left(\theta_j + \Delta\theta_j\right) - y_i\left(\theta_j\right)}{\Delta\theta_j} \times \frac{\theta_j}{y_i} \approx \frac{y_i\left(\theta_j + \Delta\theta_j\right) - y_i\left(\theta_j\right)}{\Delta\theta_j} \times \frac{\theta_j}{y_i} \tag{3.49}$$

The global sensitivity analysis (GSA) can perceive the drawbacks associated with LSA. The GSA quantifies the interactions effects among the parameters and also explores the impact of entire feasible parameter spaces on output variables [201, 202]. The OFAT presents the contribution of each input parameter on output uncertainty. The total effect of a parameter represents the first order effect plus higher-order effects on account of interactions with other parameters. This method is useful for non-linear and non-monotonic system, the only difficulty related to these methods is their computational cost [201]. The working scheme for GSA is summarized with four steps [201]:

- Definition of the quantities of interest of input and output
- Assignment of probability density function to each parameter
- Generation of the random numbers within the feasible regions of parameters from a known probability density function and evaluate the model outputs deterministically
- Quantification of the impact for parameters on output variables.

Two variance based-GSA methods are utilized on a lumped-parameter of the synchronous generator and inverter. In these methods, the total output variance (σ^2) of the model is apportioned into its parameters. The influential parameters contribute most on output uncertainty as compared to the less influential parameters [202]. These methods are available for the Investigation of the interaction effects of parameters on state variables. They provide the main effect (S_i) and total effect (S_{T_i}) of each parameter on state variables.

a) Sobol variance decomposition

The central idea of Sobol variance decomposition is to decompose the output of model into summands of elementary functions in terms of increasing dimensionality [202, 203]. Generally, the model can be formed as $Y = f(\boldsymbol{X}) = f(x_1, x_2, \ldots, x_k)$, where $\boldsymbol{X}$ is the vector of k uncertain parameters, which are independently generated within a unit hypercube. The output Y is decomposed as:

$$f\left(x_1, x_2, \ldots, x_K\right) = f_0 + \sum^{K} f_i\left(x_i\right) + \sum^{K} f_{ij}\left(x_i, x_j\right) + \ldots + f_{1,2,\ldots,K}\left(x_1, x_2, \ldots, x_K\right) \tag{3.50}$$

It is assumed that f is integrable and the total unconditional variance can be calculated as:

$$V = \int f^2(X)dX - f_0^2 \tag{3.51}$$

where is the f_0 constant function. With the form in equation (3.50), the total variance can be decomposed in a similar way as:

$$V(Y) = V = \sum_{i}^{k} V_i\left(x_i\right) + \sum_{i<j}^{n} V_{ij}\left(x_i, x_j\right) + \ldots + V_{1,2,\ldots,k}\left(x_1, x_2, \ldots, x_k\right) \tag{3.52}$$

where $V_i = V_{x_i}\left(E_{x_{\sim i}}(Y \mid x_i)\right)$ and

$$V_{ij} = V_{x_i x_j}\left(E_{x_{\sim ij}}\left(Y \mid (x_i, x_j)\right)\right) - V_{x_i}\left(E_{x_{\sim i}}(Y \mid x_i)\right) - V_{x_j}\left(E_{x_{\sim j}}(Y \mid x_j)\right)$$

V is the variance operator, E describes the mathematical expectation and $x_{\sim i}$ denotes all parameters except x_i. The main effect index for the *i*-th parameter is calculated:

$$S_i = \frac{V_i}{V} \tag{3.53}$$

The total effect is obtained :

$$S_{T_i} = \frac{E_{x\sim i}\left(V_{x_i}\left(Y \mid x_{\sim i}\right)\right)}{V} = 1 - \frac{V_{x_{\sim i}}\left(E_{x_i}\left(Y \mid x_{\sim i}\right)\right)}{V} \tag{3.54}$$

Generally, the main effect i.e. S_i is used for the identification of the key parameters and S_{T_i} is used for fixing factor. The total effect includes the first order effect index and higher-order with account into the interactions of the *i*-th parameter.

b) Fourier amplitude sensitivity test

The Fourier amplitude sensitivity test (FAST) method was initially presented in [204]. It also calculates the main effect and the total effect of the model parameters. The difference between FAST and the Sobol's method is in the procedure of calculating the indices. The FAST method uses Fourier decomposition to transform *K*-dimensional integrals in (3.51) into a one-dimensional integral [204]:

$$X_i(s) = G_i\left(\sin\left(\omega_i s\right)\right) = \frac{1}{2} + \frac{1}{\pi}\sin^{-1}\left(\sin\left(\omega_i s\right)\right) \tag{3.55}$$

where ω_i is a set of linearly independent integer frequencies assigned to each parameter. Then, the unconditional variance in Fourier form is:

$$V = \frac{1}{2\pi}\int_{-\pi}^{\pi} f^2(s)ds - E_0^2 = \frac{1}{2\pi}\int_{-\pi}^{\pi} f\left[\left(G_1\omega_1 s\right),\left(G_2\omega_2 s\right),\ldots,\left(G_K\omega_K s\right)\right]^2 ds - E_0^2 \tag{3.56}$$

where $E_0 = \frac{1}{2\pi}\int_{-\pi}^{\pi} f_0(s)\mathrm{d}s$. The expansion of Fourier series of equation (3.56) is:

$$V = \sum_{i=-\infty}^{\infty}\left((\frac{1}{2\pi}\int_{-\pi}^{\pi} f(s)\cdot\cos(is)\mathrm{d}s)^2 + (\frac{1}{2\pi}\int_{-\pi}^{\pi} f(s)\cdot\sin(is)\mathrm{d}s)^2\right) - \left((\frac{1}{2\pi}\int_{-\pi}^{\pi} f(s)\cdot\cos(0)\mathrm{d}s)^2 + (\frac{1}{2\pi}\int_{-\pi}^{\pi} f(s)\cdot\sin(0)\mathrm{d}s)^2\right) \tag{3.57}$$

Accordingly, the conditional variance for parameter x_i to calculate S_i can be calculated as,

$$V_i = 2\sum_{m=1}^{11}\left((\frac{1}{2\pi}\int_{-\pi}^{\pi} f(s)\cdot\cos(m\cdot\omega_i s)\mathrm{d}s)^2 + (\frac{1}{2\pi}\int_{-\pi}^{\pi} f(s)\cdot\sin(m\cdot\omega_i s)\mathrm{d}s)^2\right) \tag{3.58}$$

where m is the maximum harmonic. In this work, we consider the harmonic from 1-th to 11-th in power system. Finally, the main effect S_i is computed as:

$$S_i = \frac{V_i}{V} \tag{3.59}$$

The study case of sensitivity analysis in parameter estimation is shown in chapter 5. Except for selecting the important parameters to simplify the parameter estimation, it can be functional in factor fixing [205]. The parameters have negligible impact on state variables, which can be fixed at their nominal values without any loss of accuracy.

3.4 Conclusion

This chapter addresses the parameter estimation issue for creating the DT. The first research question related to this topic in this thesis is:

- *Which parameter estimation method is suitable for Digital Twin creation?*

To answer this question, it first addresses the DT modelling with the DAE systems. The 6th order synchronous generator and VSI inverter are used for the demonstration in this work. Both components are the typical dynamic elements in an electrical power system. The estimation of the correct parameters for both components and their related regulators decides the creation of an accurate DT. In Table 1, Table 3.2, and Table 3.3, the parameters used in synchronous generator, turbine and governor, AVR, and VSI inverter for emulating the real physical power grid are specified. The simulation with these parameters is demonstrated for the generation of measured PMU data. The measurement from benchmark simulation is used for the parameter estimation of DT.

DT modelling defines the structure of dynamic components. With the known structure of DT, the parameter estimation process of these elements fulfils the requirements of the grey-box model estimation. Three suitable algorithms for parameter estimation of grey-box model are investigated: LSQ, RLS and NN. LSQ algorithm utilizes the least square objective function to evaluate the deviation between the reference variable and DT's variable. The objective function of LSQ algorithm in the estimation of synchronous generator and VSI inverter is the square of the current variable. LSQ algorithm is an offline method. It has high performance in the estimation of the exact parameter, but it takes long computation time. Oppositely, RLS algorithm takes less computation in estimation procedure. However, the transformation of the DT DAEs to ARMAX equation for the estimation is necessarily. Because of its fast responds in the estimation, it can be used in online parameter estimation. NN algorithm for parameter estimation requires the specified precondition like the always measurable voltage variables (u_{Nd}, u_{Nq}, u_{SRd} and u_{SRq}). The evaluation and validation of these algorithms are addressed in chapter 5.

4 Proposed Machine Learning algorithms in event identification

The event identification framework developed by Machine Learning algorithm and Digital Twin is addressed in this chapter. Figure 4.1 depicts the schema of the event identification with Machine Learning algorithm and Digital Twin. The entire identification process is divided into two steps. Firstly, in the Machine Learning algorithm development phase, the corresponding DT model is firstly defined, and according to the exchanged data, the DT is correctly parameterized with the characteristic features from the physical power grid. Possible disturbance events are then examined using the DT instance to generate data patterns with which typical events in the real world can be identified. In section 4.1, it addresses the typical fault events in power system. The pattern data of these events are generated by DT simulation with different scenarios, see Figure 4.1.

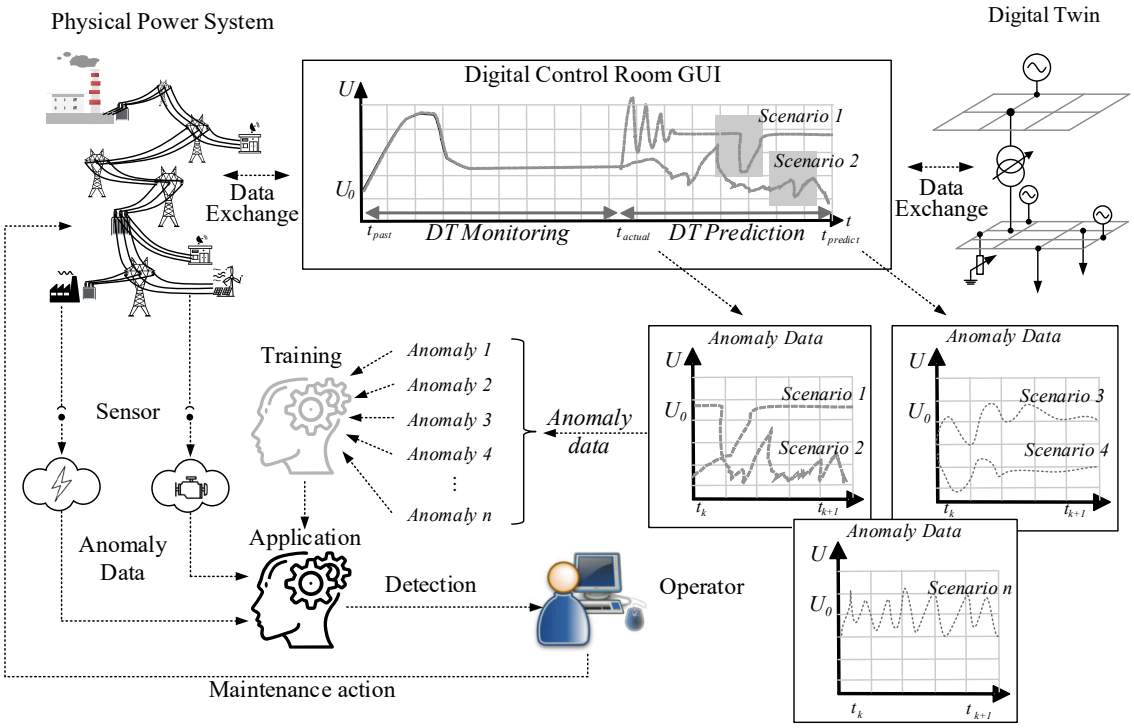

Figure 4.1: Schema of anomaly event identification with Machine Learning and Digital Twin

The second phase is the training process and validation. Machine learning is used as an assistant to form a detection model by learning the fault simulation data in the first phase. It should be noted that the training data must be sufficiently good in terms of quantity and quality to ensure that the event detection is as selective as possible. The objective is to combine the DT with the Machine Learning algorithm to perform this task. This procedure

can not only accurately predict and identify the anomaly in the early phase of the actual operating state in the power system, but also quickly prepare the appropriate reactions such as maintenance measures to prevent damage to the power system. The integration of the proposed Machine Learning algorithms namely *k*NN, decision tree, and SVM for event identification is addressed in chapter 4.2. The evaluation and validation of their performance in event identification are verified with the case studies in chapter 5.

4.1 Fault events in power system

Fault events are an unusual condition, brought on by climates conditions, human mistakes, smoke of flame, hardware let-downs like pivoting machines and transformers, and so on [206]. These events cause intrusion to electric streams, hardware damages and even cause passing of people and winged creatures [207], which are hazard to the congruity of power supply. Accordingly, an accurate and quick diagnosis of a fault in power system is essential to minimize the extent of damage occurred as the result of the fault [82, 83, 208]. The detection of the fault depends on the power system quantities i.e., voltage, current, phase angle etc., which exceeds its threshold values when the system faces the fault condition. In power system, the usual occurred fault events happen in transmission system [83]. The faults can be classified into two types, i.e. series faults (open conductor), and shunt (short circuit) faults [209]. The series faults can be identified by observing the voltage value in each phase, which is characterized by increase of voltage and frequency and fall in current in the faulted phases. Series faults take place when unbalanced series impedances conditions of the line are present. These faults disturb the symmetry in one or two phases and are therefore unbalanced faults, which are accordingly classified as one open conductor fault and two open conductor faults. Series faults can be identified by observing the voltage in each phase. If the voltage values increase, it indicates the open conductor faults occurred. These faults are rarely occurred faults compared with the shunt faults i.e., short circuit faults.

Generally, the shunt faults have two types: symmetrical faults and asymmetrical faults, see Figure 4.2. They are identified with the increased current value and decreased voltage when the faults occur. In symmetrical faults, all the three phases are short circuited to each other after the occurrence of the fault. These faults are balanced and symmetrical as the system remains balanced even after the occurrence of the fault. Although the symmetrical faults happen rarely, they generally lead to the most severe fault current flow. As shown in the following figure, the most faults occur in power system are unsymmetrical faults involving one or two phases. The most common type of unsymmetrical fault is the short circuit between a phase and earth i.e., Line-to-Ground (LG) fault. The next fault in severity and occurrence wise is Line-to-Line (LL) fault. It can be compared with diseases like fever

and Line-and-Line-to-Ground (LLG) fault with viral fever. The 3-phase (LLL and LLLG) faults can be compared with big diseases like heart attack, which means if they occur, the total system will be collapse. So protection schemes needs to detect the fault and classify feature of the fault and locate the fault within less time to avoid the major damages [207].

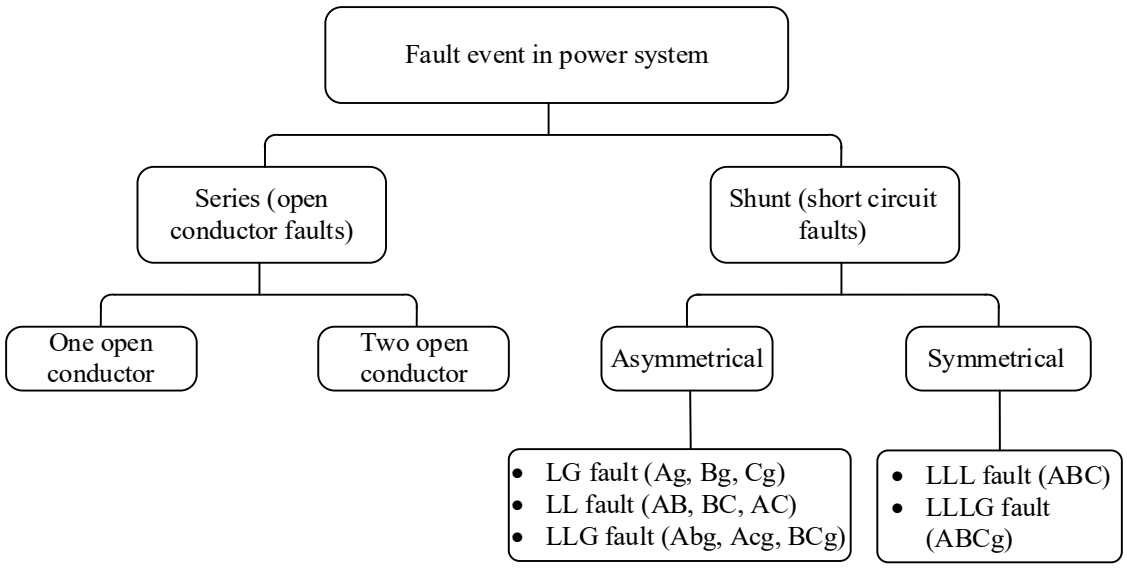

Figure 4.2: Fault classification in power system [207]

Although the measurements like current and voltage values contain the feature information for the classification of the events, it is still extremely difficult to fit the raw signals into sets of rules and criterions capable of intelligently interpreting the underlying messages brought in the measurements [73, 82]. The key information in the measured signals need the feature extraction techniques to dig out useful information and reduce the data dimension.

4.2 Proposed Machine Learning algorithm for event identification

Most of the available classification methods are based on classifiers and statistical learning theories [129]. PMU based approaches require synchronized phasor quantities from all the terminals of the transmission lines [210]. Genetic algorithms are the heuristic search and optimization methods which mimic the process of natural evolution. The deficiency of this method is that its slow computation process and the complexity in implementation for fault classification [210]. Figure 4.3 presents the fault classification and location identification method in transmission lines and distribution systems. To solve these problems, the methods used Machine Learning are applied for the improvement of event classification and location. In this section, the integration of the proposed Machine Learning algorithm in event classification is depicted.

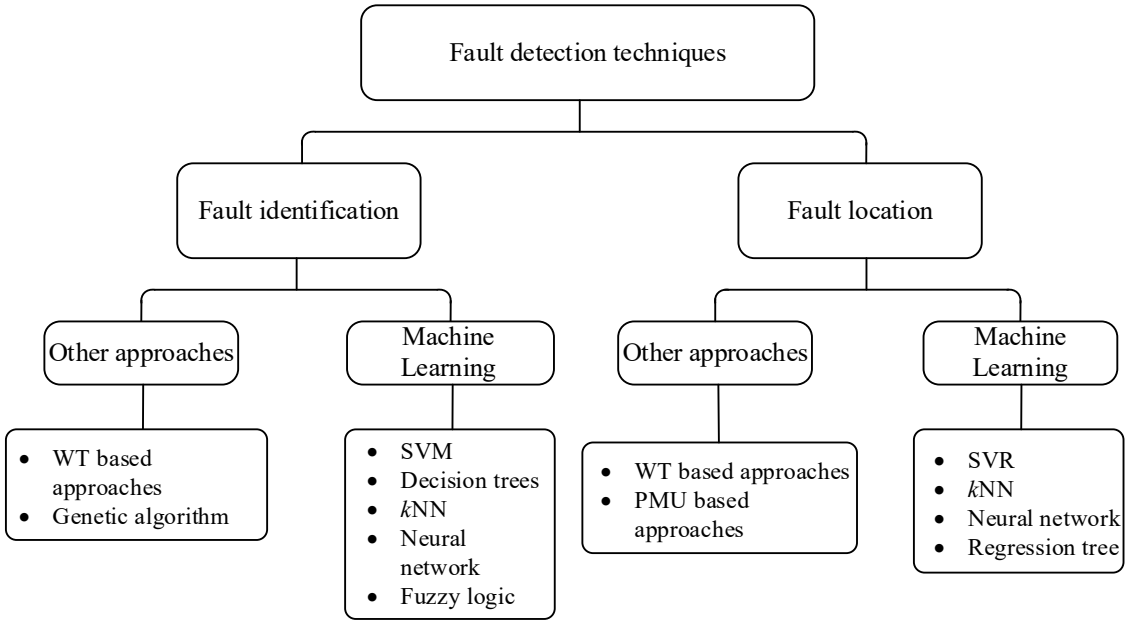

Figure 4.3: Fault classification and location methods in power system [129, 210]

4.2.1 *k*NN for event identification in power system

The basics of *k*NN have been introduced in previous chapter. This method is a widely applied time series analysis method for the anomalous window detection [74, 211]. It utilizes a specific distance measure to evaluate the similarity of two data sequence in time series. The data windows with similar sequence of samples are referred to as near neighbours. The fault data in anomalous windows are those distinct from the underlying trend of the time series [88]. By equation (2.33), the defined fault index (FI) is computed for detecting the distance of the measured data windows to its *k*th nearest neighbour. The FI value of a fault data window is much higher than that of any normal data windows, which is the central idea for application of *k*NN in fault detection and classification. The use of *k*NN in this work is combined with the PCA. The data vector $\boldsymbol{x}^{\mathrm{T}} = [x_1\ x_2\ \cdots\ x_n]$ refers to the measured variables e.g., voltage, current and frequency, where n denotes the dataset size. PCA is used to obtain eigenvector and covariance through decomposition of the data. The variables in the data vector are initially normalized with the sample means and variances to make the obtained data independent of its unit. The vector $\tilde{\boldsymbol{x}}^{\mathrm{T}}$ indicates the normalized data vector. The eigenvalue decomposition of $\boldsymbol{A}$ can be calculated as:

$$A = \frac{1}{N-1}\sum_{n=1}^{N} \tilde{\boldsymbol{x}}_n \tilde{\boldsymbol{x}}_n^{\mathrm{T}} = \boldsymbol{Q}\boldsymbol{\Lambda}\boldsymbol{Q}^{\mathrm{T}} = \sum_{i=1}^{m} \lambda_i^2 \boldsymbol{u}_i \boldsymbol{u}_i^{\mathrm{T}} \tag{4.1}$$

where $\boldsymbol{\Lambda} \in \mathbb{R}^{\boldsymbol{m}\times\boldsymbol{m}}$ is a diagonal matrix with the eigenvalues. $\boldsymbol{Q} \in \mathbb{R}^{\boldsymbol{m}\times\boldsymbol{m}}$ is the eigenvector matrix. $[\lambda_1\ \lambda_2\ \cdots\ \lambda_{\mathrm{m}}]$ is the eigenvalue and $[\boldsymbol{u}_1\ \boldsymbol{u}_2\ \cdots\ \boldsymbol{u}_{\mathrm{m}}]$ is the eigenvector. The PCs can be obtained by:

$$\boldsymbol{P} = \boldsymbol{Q}^{\mathrm{T}}\tilde{\boldsymbol{x}} \tag{4.2}$$

where the dimension of matrix PCs satisfies $\dim[\boldsymbol{P}] \leq \dim[\boldsymbol{A}]$. The vector of residual variables [212] is calculated by:

$$\boldsymbol{e} = \tilde{\boldsymbol{x}} - \boldsymbol{Q}\boldsymbol{Q}^{\mathrm{T}}\tilde{\boldsymbol{x}} \tag{4.3}$$

The variation of PCs within the PCA model can be detected by R^2 statistic:

$$R^2 = \boldsymbol{P}^{\mathrm{T}}\boldsymbol{\Sigma}\boldsymbol{P} = \sum_{j=1}^{K}\left(\frac{p_j}{\sqrt{\lambda_j}}\right)^2 \tag{4.4}$$

where $\boldsymbol{\Sigma}$ is the diagonal matrix with the value $[\lambda_1^{-1}\ \lambda_2^{-1}\ \cdots \lambda_k^{-1}]$. The residual variable is measured with E statistic:

$$E = \boldsymbol{e}^{\mathrm{T}}\boldsymbol{e} = \sum_{i}^{m} e_i^2 \tag{4.5}$$

The classification of fault data is dependent on the FI values by using kNN to analyze E and R^2. The detection threshold based on FI values is calculated for determining whether the faults occur or not. Based on the measured data $\{\boldsymbol{x}_n\}_{n=1}^{N}$, the value of E is calculated and the corresponding matrix $\boldsymbol{Z}$ is built:

$$\boldsymbol{Z} = \begin{bmatrix} \boldsymbol{z}_1^{\mathrm{T}} \\ \vdots \\ \boldsymbol{z}_{N-L+1}^{\mathrm{T}} \end{bmatrix} = \begin{bmatrix} E_1 & E_2 & \cdots & E_L \\ E_2 & E_3 & \cdots & E_{L+1} \\ \vdots & \vdots & \cdots & \vdots \\ E_{N-L+1} & E_{N-L+2} & \cdots & E_N \end{bmatrix} \tag{4.6}$$

where $\boldsymbol{Z}$ is the embedding matrix of E. The $\mathbf{z}_m$ indicate the m^{th} data window of $\{\boldsymbol{E}_n\}_{n=1}^{N}$, and L denotes the window length. The distance of the two rows can be calculated with ED:

$$D(\boldsymbol{z}_g, \boldsymbol{z}_m) \triangleq \left\|\boldsymbol{z}_g^{\mathrm{T}} - \boldsymbol{z}_m^{\mathrm{T}}\right\|_2 = \sqrt{\sum_{j=1}^{L}(E_{g-j+L} - E_{m-j+L})^2} \tag{4.7}$$

After getting all the distance values, the FI_Q is denoted as the kth smallest ED between it and all other rows except its near-in-time rows. The threshold is FI_Q^* defined as the highest the value in the sequence, which is the support vector for the classification. To classify the concrete the faults, i.e., LG, LL, LLL and LLLG, the thresholds of each phase need to be calculated in similar way, which are denoted as $FI_{Q,\mathrm{a}}^*$, $FI_{Q,\mathrm{b}}^*$ and $FI_{Q,\mathrm{c}}^*$.

Similar with FI_Q, another monitoring index FI_{R^2} can be calculated by applying kNN on the R^2 and the related detection threshold $FI_{R^2}^*$, $FI_{R^2,\mathrm{a}}^*$, $FI_{R^2,\mathrm{b}}^*$, $FI_{R^2,\mathrm{c}}^*$ can be determined. The framework of detection and classification of fault events with the FI values by using kNN is summarized in Figure 4.4.

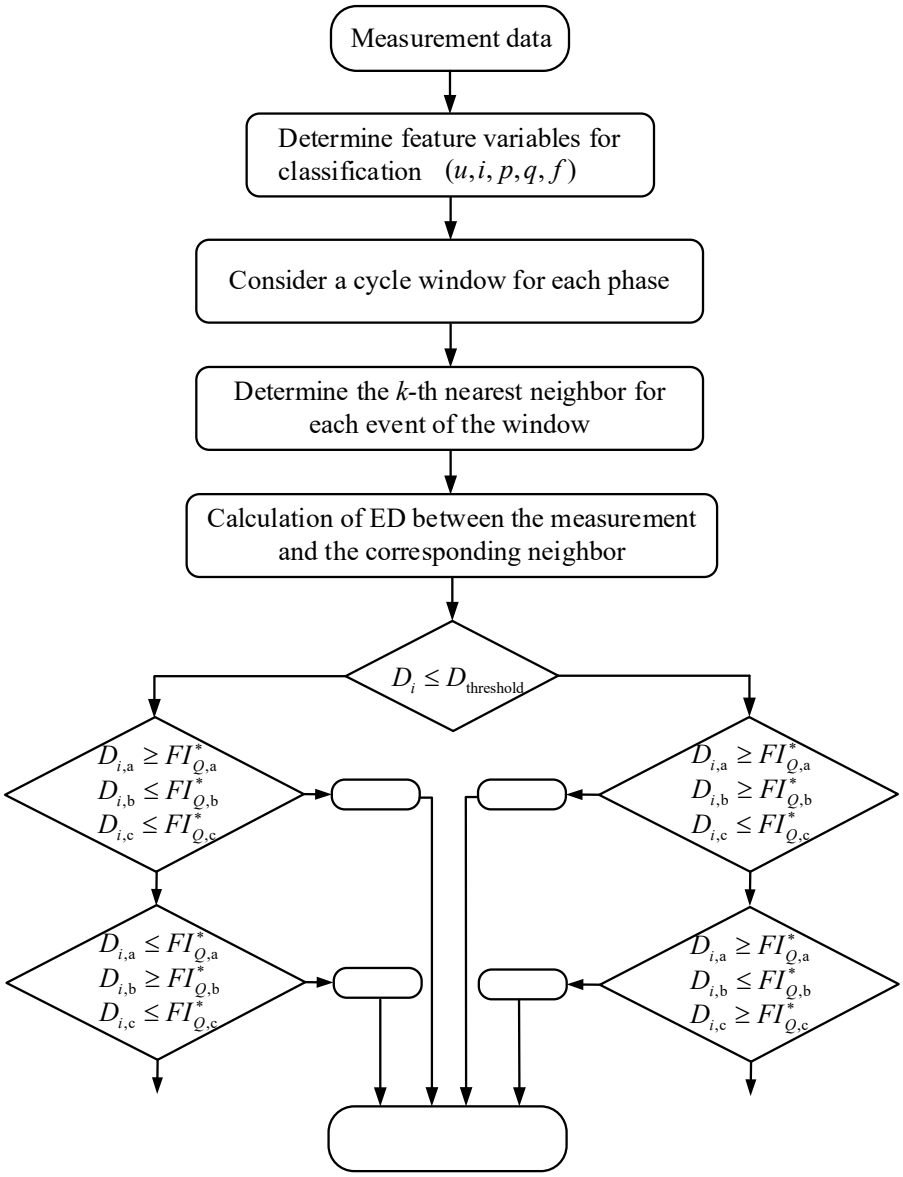

Figure 4.4: Framework of event identification by kNN

4.2.2 Decision tree for event identification

The second method used in this work for fault classification is the CART. The implementation of CART consists of three steps [213]: constructions of classification tree, choice of the right three size and classification. The classes of the learning principle are defined by the requirements of the task. As mentioned fault event type in chapter 2, ten classes are defined with AG, BG, CG, ABG, BCG, ACG, AB, AC, BC and ABC to construct the classification tree. In accordance with the splitting rules, the classification tree is built to perform the splitting of learning samples into smaller parts. The data needs to be divided into wo parts with maximum homogeneity at each time. Generally, the most effective feature is selected as the first node of the tree, which refers to the fault states or non-fault states. Its border value is used for building two branches. With the same criterion, the next key feature is defined to divide the next node of the three, which continues in all the branches. The Gini index denoted in equation (2.35) is used in calculation of key feature index. The impurity index of measurement in Gini splitting rule is denoted by:

$$P(n) = \sum_{k \neq l} p(k/n)\, p(l/n) \tag{4.8}$$

where $k, l = 1, \cdots, K$ is the index of the class. $p(k/n)$ is the conditional probability of class k. The change of impurity index is given by

$$\Delta P(n) = -\sum_{K}^{k=1} p^2\left(k/n_p\right) + P_L \sum_{K}^{k=1} p^2\left(k/n_L\right) + P_R \sum_{K}^{k=1} p^2\left(k/n_R\right) \tag{4.9}$$

Every time the entities are divided into two leaf nodes with maximum homogeneity which can be decided impurity function. Since the impurity of node n_p is constant for any of the possible split, the maximum homogeneity of left and right nodes is the maximization of the change of impurity index which is given by

$$\arg\max\left[-\sum_{K}^{k=1} p^2\left(k/n_p\right) + P_L \sum_{K}^{k=1} p^2\left(k/n_L\right) + P_R \sum_{K}^{k=1} p^2\left(k/n_R\right) \right] \tag{4.10}$$

With Gini algorithm, the largest class can be found in learning sample and isolate it from the rest of the data.

The next step of implementation of CART is to choose the right size of the three. The classification tree grows into sub-tree and the maximum number of nodes exceed hundreds of levels if the data is complex. Accordingly, the maximum number of tree nodes and leaf needs the optimization before implementation. There are usually two ways for the optimization: cutting-off insignificant nodes and sub-trees. The tree pruning methods like optimization of nodes and cross validation are utilized. The splitting rules define the condition of stopping the classification with the smaller number of observations in the nodes than

pre-defined number $N_{\min}$. Generally, the $N_{\min}$.is denoted as 10% of the total learning sample [130]. Another factor impacts the size of tree is the trade-off between the impurity and the complexity. In maximum tree, the impurity measurement is minimum, but the complexity of tree is maximum, which means the total number of nodes is maximum. The other optimization method is the cross-validation, which optimizes the proportion between the complexity of the tree and misclassification error. The increased size of tree can decrease the misclassification error. But for independent data, the complex decision tree show poor performance [213]. By cost complexity function, the optimal proportional between complexity and misclassification error can be found.

$$\min_{n}\{R_{\alpha}(n) = R(n) + \alpha(n)\} \tag{4.11}$$

where $R(n)$ is the misclassification error of the tree with n nodes. $\alpha(n)$ is the complexity measure.

4.2.3 Support Vector Machine for event identification

The third proposed algorithm in Machine Learning for fault classification is SVM. This learning method utilizes the vectors to classify the non-linear feature data [214]. The training algorithm of SVM with the sample set that belongs to one of the two categories with the target variables $[-1, 1]$ builds a classifier shown by space mapped features which are classified by a broad gap, see Figure 2.16. The gap called hyperplane is optimized by the Lagrange for maximization of the gap between the two categories [215]. With the kernel function, the non-linear SVM transformed in feature space based on optimal solution of (2.42) is denoted by:

$$f(\boldsymbol{x}) = \boldsymbol{w}^{\mathrm{T}}\phi(\boldsymbol{x}) + b = \sum_{i=1}^{N}\lambda_i y_i \phi(\boldsymbol{x}_i)^{\mathrm{T}}\phi(\boldsymbol{x}) + b = \sum_{i=1}^{N}\lambda_i y_i \kappa(\boldsymbol{x}, \boldsymbol{x}_i) + b \tag{4.12}$$

where $\kappa(\boldsymbol{x}_i, \boldsymbol{x}) = \phi(\boldsymbol{x}_i)^{\mathrm{T}}\phi(\boldsymbol{x})$ is the kernel function. It transforms the data from the input space to feature space with a high-dimensional capacity. The gauss kernel function is applied in this work.

$$\kappa(\boldsymbol{x}_i, \boldsymbol{x}_j) = \exp\left(-\frac{\left\|\boldsymbol{x}_i - \boldsymbol{x}_j\right\|^2}{2\sigma^2}\right) \tag{4.13}$$

Three SVMs are implemented to determine which phase is involved in the fault. The fourth SVM is used to determine the involvement of the ground in the fault. The SVM for each phase detects the current and voltage samples while the ground SVM receives the samples of zero sequence current (I_0). The output value of SVM ‘1’ and ‘-1’ indicate the presence

and absence of the fault. In Table 4.1, it shows the fault classification format in the proposed method.

Table 4.1: Fault classification format by SVMs

No.	Output of SVM for phase A	Output of SVM for phase B	Output of SVM for phase C	Output of SVM for phase ground	Result
1	1	-1	-1	1	Fault AG
2	-1	1	-1	1	Fault BG
3	-1	-1	1	1	Fault CG
4	1	1	-1	-1	Fault AB
5	1	-1	1	-1	Fault AC
6	-1	1	1	-1	Fault BC
7	1	1	-1	1	Fault ABG
8	1	-1	1	1	Fault ACG
9	-1	1	1	1	Fault BCG
10	1	1	1	1	Fault ABCG

After the event identification, the location information is also essential for protection relay. The ANN based location method has been studied in [86, 216–218]. It is integrated in protection system by identification of the symbols from current and voltage. The method based on ANNs were used for the development of reliable, accurate, and rapid algorithms for location. The process for anomaly location is based on the results of fault detection and classification. The classifier determines the fault type with LG, LL, LLL and LLLG. Four independent ANNs are applied for locating the four types of fault. The first fault locator (FL_1) uses the magnitudes of the three-phase currents. The second fault locator (FL_2) needs the input data with the magnitudes of the three-phase voltages. The third (FL_3) uses the magnitudes of both currents and voltages as the input data.

$$\begin{aligned} FL_1 &= [I_{a^*}(k), I_{b^*}(k), I_{c^*}(k)] \\ FL_2 &= [U_{a^*}(k), U_{b^*}(k), U_{c^*}(k)] \\ FL_3 &= [I_{a^*}(k), I_{b^*}(k), I_{c^*}(k), U_{a^*}(k), U_{b^*}(k), U_{c^*}(k)] \end{aligned} \tag{4.14}$$

where $I_{a*}(k), I_{b*}(k)$ and $I_{c*}(k)$ are magnitudes of three-phase current for four different type fault in p.u. U_{a*}, U_{b*} and U_{c*} are magnitudes of three-phase current. The output of the fault locator is the distance L_f km between fault location and measure location. The training data is generated by DT-based event simulation. The fault scenarios are taken different conditions such different fault locations, different fault inceptions angles and different fault

resistances into account. The simulated fault numbers for the ANN training are the multiplication of the number of fault types, fault location number, fault resistance number and fault inception angles. Except for the determination of input and output of ANN, the structure of ANN i.e. the number of hidden layers and the neurons impacts the accuracy and the time consumption of identifying location results [217]. The determination of the architecture for ANN can only be achieved according to a series of tests and modification of ANNs structure to find a best performance.

4.3 Conclusion

In this chapter, the proposed Machine Learning algorithms for fault event identification in the power system are elaborately addressed. At first, the classification typical fault events in power system and the feature of each event are discussed in chapter 4.1. Generally, two categories of fault events in the power system are classified: series fault and shunt fault. The series fault is referred to the open conductor fault, i.e., out-service of the line. This fault is represented with the increased voltage and frequency, and the decreased current in the fault phase. The other fault type, i.e., shunt fault is referred to as the short circuit fault. It is characterized by the obvious increased current value and decreased voltage amplitude when the fault occurs. These features are defined as the fingerprint of each event. The training data of these events for the Machine Learning algorithm is generated by DT-based event simulation. *k*NN algorithm utilizes the training data to calculate the reference value of the fault index. The classification process with *k*NN is to find the nearest neighbour data set. The data set corresponded event is the identified type of the event. In the decision tree, the Gini index is used to select the key feature for the identification. The decision of the leaf node in the decision tree utilizes the impurity function. The identification with SVM is to find the hyperplane between different events. The non-linear SVM is used in this work for event identification. The kernel function is integrated for the optimization of the hyperplane. These algorithms are further evaluated and validated with the case studies in chapter 5.

5 Numerical case studies

The parameter estimation methods for DT creation and the proposed Machine Learning algorithms to identify the event are addressed in chapter 3 and chapter 4. These algorithms will be evaluated and validated for their accuracy and efficiency in DT creation and event identification with numerical case studies with regard to research question Q1 and Q2. Regarding research Q1, three parameter estimation methods are specifically addressed with the DAE-based DT modelling. According to the proposed deduction in chapter 3.2.1 and 3.2.2, the estimation algorithm requires the measured data from physical system, simulated data from DT, and their deviation. This chapter firstly addresses the generation of the measured data with time series dynamic simulation in reference network. It emulates the dynamic feature of physical power grid. The topology of the reference network and the designed scenarios for the generation of measurements are presented in chapter 5.1. Afterward, the designed scenarios are simulated in DT and reference network to evaluate the deviation of the observed variables between both systems. According to the difference between DT and the reference network, the proposed parameter estimation methods are activated, and respectively calculates the new parameters for DT. Subsequently, the estimated parameters are updated in DT, and validated with the simulation of the designed scenarios. In chapter 5.3, the DT-based event simulation is carried out for the generation of the training data for Machine Learning algorithms. After training procedure, the algorithms are validated and evaluated with numerical case studies for the accuracy in event identification, which answers the proposed research question Q2. The conclusion of the chapter is in the last section.

5.1 Research objective

Regarding the focus of the study on DT creation with parameter estimation and its application in identification of event identification assisted with Machine Learning , the research objective in this work is initially to propose the appropriate algorithms for parameter estimation and the event identification with Machine Learning. To verify the performance of the proposed algorithms, the evaluation and validation with numerical case studies is necessitated. Accordingly, another objective of this work is to demonstrate the DT creation with the proposed parameter estimation methods and the application in event identification with Machine Learning algorithm with numerical case studies. Figure 5.1 depicts the first step of the numerical case study. The designed scenarios are simulated in reference network and DT to quantify the difference between both targets. The parameter estimation is activated with the condition that DT simulation results are deviated with the measurement.

The corresponding scenarios are described in section 5.1.2 and the comparison results are shown in section 5.2.1.

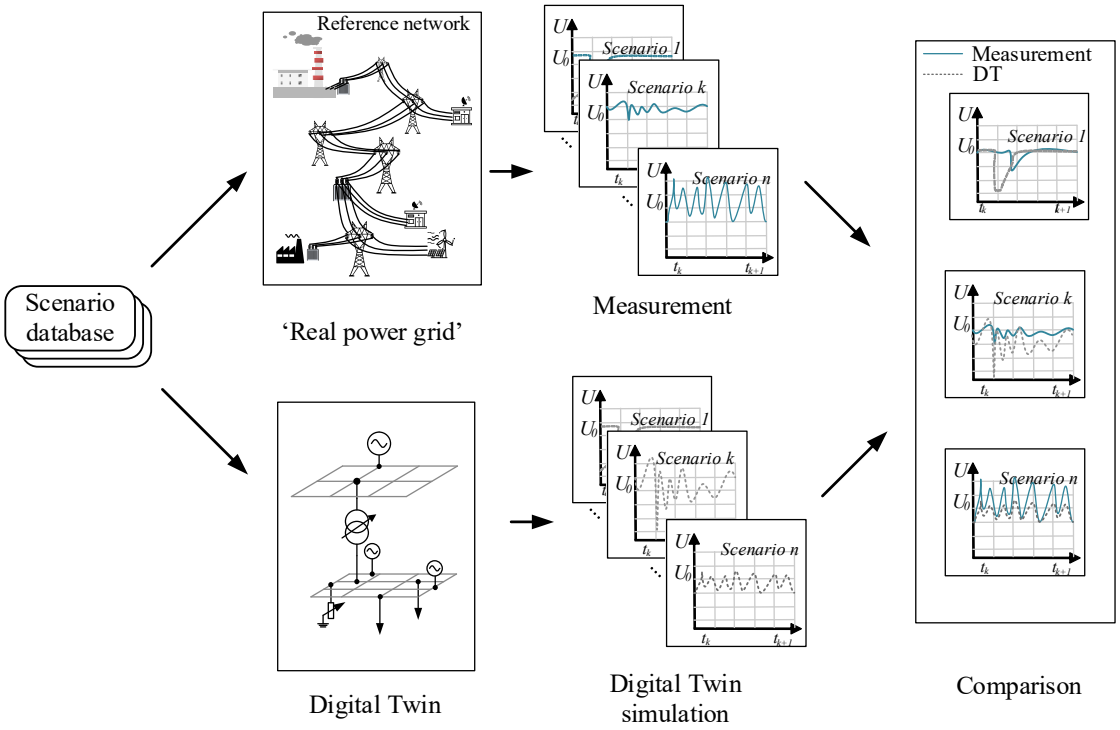

Figure 5.1: Procedure a): scenario simulation in DT and reference network

After detecting the difference between DT and measurement, the second step is to utilize the difference to estimate the new parameters for DT. LSQ, RLS, and NN-identifier are respectively used to estimate the new parameters for synchronous machine and VSI inverter. The results of the estimated parameters are shown in section 5.2.2. The new parameters are subsequently updated in DT. The evaluation of the parameter estimation is to compare the simulation results of DT with new parameters with the measurement. Except for it, the comparison of the new parameters with the parameters from reference network is also taken into account. The corresponding validation is presented in section 5.2.3. The whole process in the second step is described in Figure 5.2.

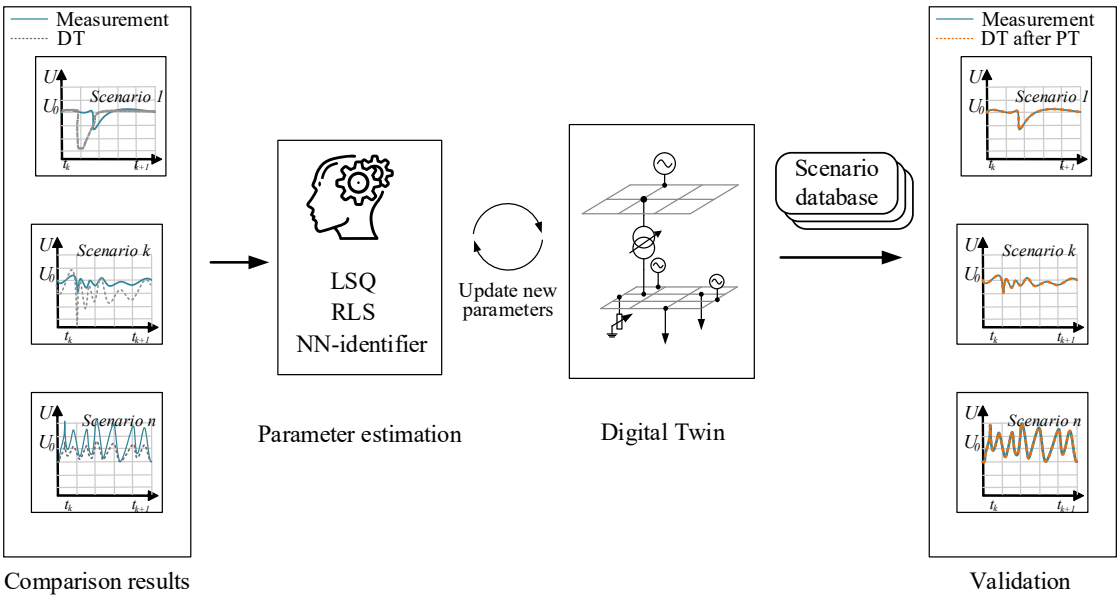

Figure 5.2: Procedure b): parameter estimation and validation in DT with new parameters

After the validation and evaluation of the parameter estimation algorithms, DT is able to accurately represent the dynamic behavior of the reference network. Under this condition, the event-based simulation with DT is used to generate the training data in the third step, see Figure 5.3. The main task in this procedure is to use DT to simulate all possible events including fault event and normal event. On account of it, the anomaly identification is transformed to the event identification problem. This is also the highlight in this work, which utilizes the DT to simplify the anomaly identification. With the generated database through DT simulation, each event has been fingerprinted. *k*NN, decision tree, and SVM take use of the database to print the characteristic in the algorithm. The evaluation process in the third step is to select the best performed algorithm for the event identification.

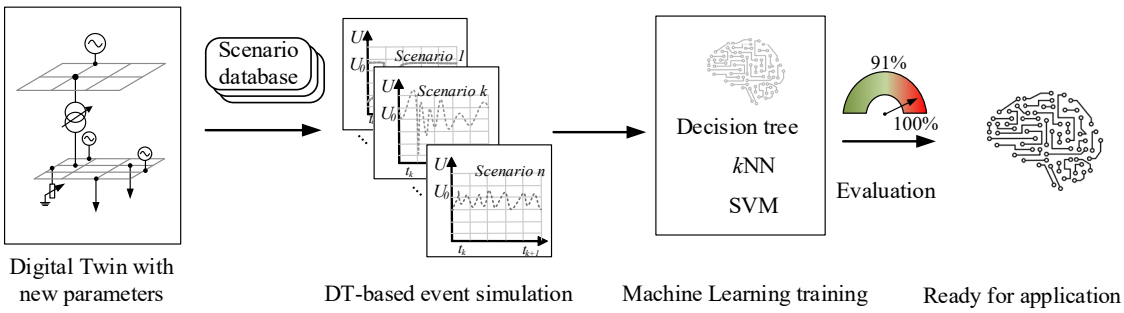

Figure 5.3: Procedure c): Machine Learning algorithm training with DT simulation

Figure 5.4 depicts the process of the application of the trained Machine Learning algorithm for the event identification. The measurement from the reference network presents the occurred event , and is then transferred to interface of Machine Learning algorithm. The

identification result shows the similarity degree of the occurred event with the training event in database. The high similarity illustrates that the occurred event in reference network is the corresponding event in the event list. The numerical case studies for the application is represented in chapter 5.3.

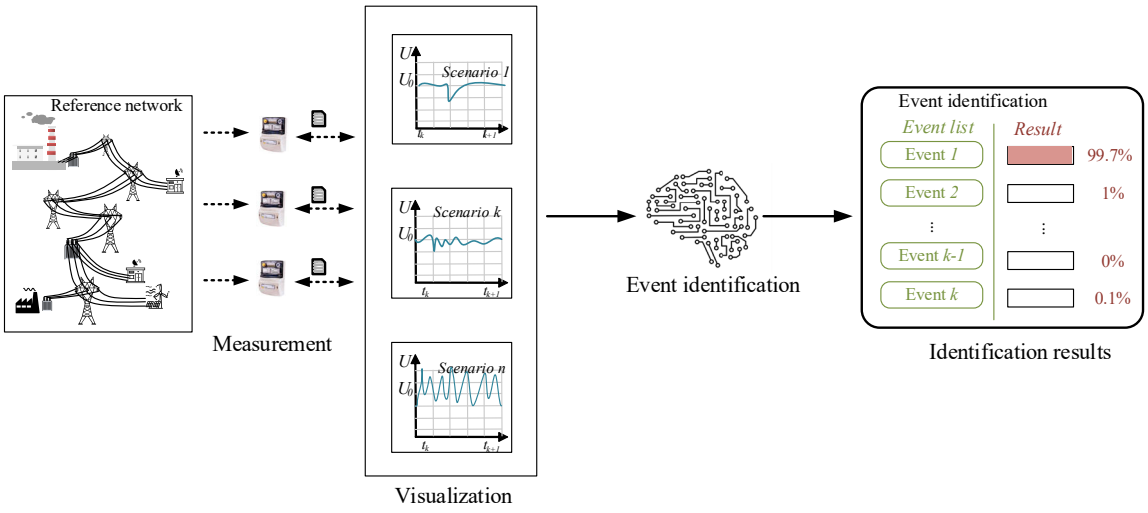

Figure 5.4: Procedure d): Event identification with Machine Learning algorithm

The above mentioned procedures address the research objective in this work to demonstrate the DT creation methods and the DT application in event identification. The following sections in this chapter describes firstly the topology of the reference network. The designed scenarios for the simulation in DT and reference network to generate the data for parameter estimation is presented in section 5.1.2. The scenario used for the validation of the DT after parameter is also presented in this section.

5.1.1 Reference network

The reference network is based on the CIGRÈ benchmark [38], which consists of a transmission network and two distribution networks. The network transmission voltages used in the benchmark are 220 kV and 380 kV, which are typical in European transmission systems [38]. It consists of 12 buses and 8 transmission lines. Four synchronous generators with regulators including turbine, governor, exciter and power system stabilizer (PSS) are respectively connected with Bus 9, Bus 10, Bus 11, and Bus 12. The underlaid networks in distribution grid depict the topology of the European medium voltage (MV) distribution feeders benchmark [38]. Two MV distribution networks are respectively connected with Bus 2 and Bus 4 in transmission power network through the 220kV/110kV transformer. The topology of the reference network is shown in Figure 5.5.

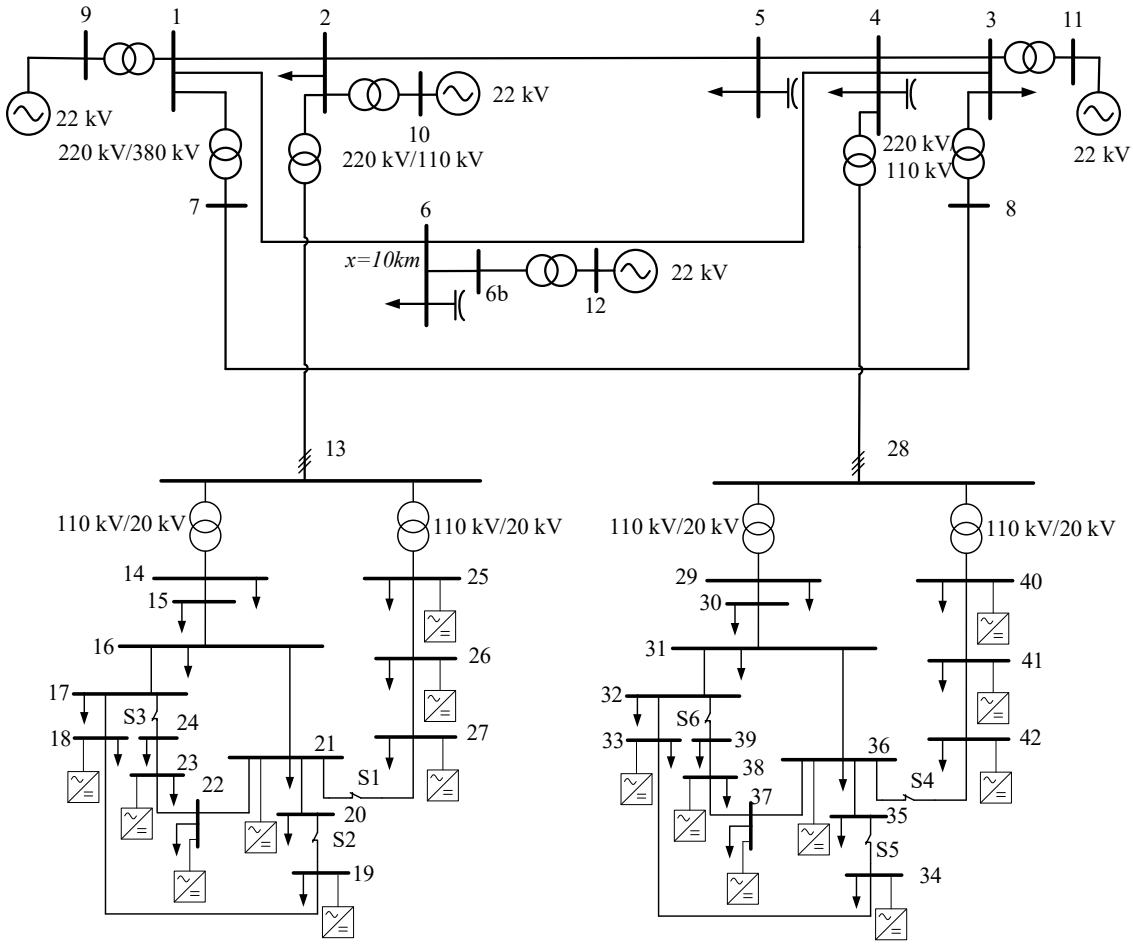

Figure 5.5: Topology of the reference network [38]

The model with synchronous generator and voltage source (VSC) inverter-based renewable feed-in generation are investigated. These components including the corresponding regulators influence the dynamic character of the power network. With the parameter estimation methods and its implementation in tuning the parameter of synchronous generator and VSC-inverter mentioned in chapter 3, the objective regarding the benchmark is to mirror the dynamic feature with DT after the parameter estimation. Eight inverters are connected with the buses in each MV network. The parameters of the benchmark network description is attached in appendix.

5.1.2 Scenario design

In this section, the scenarios are defined for the parameter estimation of DT and the validation of its performance for the representation of the dynamic behaviour in reference network. The base cases are considered as the measurement generation for the parameter estimation of DT based on the topology of the CIGRÈ benchmark power network described in section 5.1.1. In Table 5.1, it describes the scenarios for the simulation in reference

benchmark model. They include the small disturbance like the operation point of load and inverter-based generations, AC-lines failure, bus failure, and power plant failure. These events cause the operation state changes in power network, which are used to parameterize the inverter, synchronous generators, and the related regulators.

Table 5.1: Scenarios for parameter estimation of DT

No.	Scenario description	Result
1	Load increases with 20% at Bus 5	Operation state change
2	Load increases with 100% at Bus 31	Operation state change
3	Line failure between Bus 2 and Bus 5	Overload in line
4	Line out between Bus 33 and Bus 34	Overload in line
5	Setpoint change of inverters at Bus 40, 41 and 42	Operation state change
6	Setpoint change of inverters at Bus 25, 26 and 27	Operation state change
7	Short circuit at Bus 31	Overload in line
8	Short circuit at Bus 5	Overload in line

The parameter estimation is focused on the inverter-, synchronous machine-based generations, and their related regulators. They impact the dynamic feature for the power system. The validation of DT and the efficiency of parameter estimation utilizes the scenarios illustrated in Table 5.2. It includes the operation point changes with 20% of load at bus 4 in high voltage level and the change with 100% of load at bus 17 in medium voltage level of power network. Except it, the investigation of the influence from inverter is validated with DT. With the change of setpoint of inverters, the states of voltage and current at PCC are validated for testing the performance of DT. The contingency is included in the validation. The short circuit in line between bus 4 and bus 5 is simulated in benchmark model and DT. The evaluation of the deviation of the observed variables with time series simulation between DT and reference network uses the Root-Mean-Square-Error (RMSE) [219], which represents the difference of the observed states between DT and the reference objective. The equation to calculate the RMSE is given by:

$$e_{\mathrm{RMSE}} = \sqrt{\frac{1}{n}\sum_{i=1}^{n}(\hat{x}_i - x_i)} \tag{5.1}$$

where e_{RMSE} shows the deviation between the reference state $\hat{x}_i$ and DT state x_i.

Table 5.2: Scenarios for validation of DT

No.	Scenario description	Observed variables for validation
1	Operation point change of load at Bus 3 with 20%	Voltage, current and rotor speed
2	Operation point change of load at Bus 17 with 100%	Voltage and current
3	Line out between Bus 4 and Bus 5	Voltage, current and rotor speed
4	Setpoint change of inverters at Bus 25, 26, 27 and 40,41,42	Voltage and current at PCC
5	Line failure between Bus 4 and Bus 5	Voltage, current and rotor speed
6	Short circuit at Bus 4	Voltage, current and rotor speed

The following chapter addresses the demonstration of DT creation depicted in Figure 5.1 and Figure 5.2. According to the defined scenarios in Table 5.1, the comparison of simulation respectively in reference network and DT is addressed. With the detection of the deviation between DT and reference network, the parameter estimation process is activated. The validation of the DT after parameter estimation is presented with the scenarios described in Table 5.2.

5.2 Digital Twin creation and validation

The modelling of DT is realized in real-time simulator based on OPAL RT platform [31]. As depicted in Figure 5.1 and Figure 5.2, the parameter estimation of DT for the DT creation is divided into two steps. Firstly, the reference network is firstly constructed in simulator with phasor model, which is regarded as the real physical power network. The simulations regarded to the scenarios shown in Table 5.1 are carried out for the collecting of reference data. The comparison results between DT and reference network are shown in section 5.2.1. In section 5.2.2, the new parameters are estimated with the comparison results from section 5.2.1. DT with new parameters are validated in section 5.2.3 with scenarios depicted in Table 5.2.

5.2.1 Comparison of reference network and Digital Twin

According to the algorithms in chapter 3.2, the measurement required for the parameter estimation of the synchronous machine, AVR and turbine governor is the bus voltage u and the current i from SM feed-into the network. The angle speed of machine ω and the angle δ are also required to estimate the parameters in the rotor related equations. In Figure

5.6, it shows the voltage dynamics of the scenario 1 and 3 described in Table 5.1 at buses connected with SM in reference network. The simulation result of the other scenarios in reference network are shown in appendix A.3. The simulation results of scenario 1 and scenario 3 in DT with initial parameters are also presented in Figure 5.6.

The scenario 1 describes the operation point change of the load at bus 5. The change of load 5 (at t=10s) from P=103 MW, Q=62 MVar to P=123.6 MW, Q=74.4 MVar leads to the impulsive response of the voltage at generator buses in form of a damped oscillation of the frequency and partly also of the pole wheel angle, which is presented in the dynamics of the bus voltage amplitude and angle connected with the generators. The generator connected with bus 11 (Gen 11 in Figure 5.6 a)) is located in the nearest with bus 5, which has a stronger oscillation. The oscillation lasts for about 15s to reach the new operation point. The dashed lines present the simulation results with DT before parameter estimation. It can be obviously seen that the lines represented by DT are deviated with reference network.

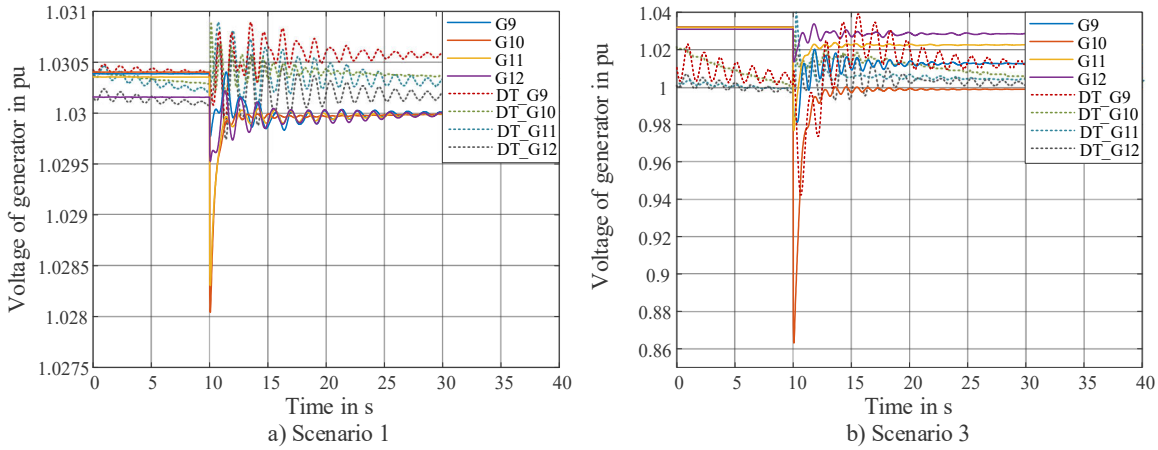

Figure 5.6: Comparison of voltage dynamics between measurement and DT simulation before parameter estimation with scenario 1 and 3

The scenario 3 present the bus failure (at t=10s) in high voltage level. The result in the stronger excitation of the power network. The dashed lines from DT in Figure 5.6 b) have different dynamic characteristic with reference network. The deviation of voltage dynamics between DT and reference network is evaluated by RMSE in Figure 5.7. The events in medium voltage level are depicted in scenario 2, 4, 5, and 6. They present the operation change of load in medium voltage level and the setpoint change of feed-in power by inverter-based renewable generations of benchmark model. The simulation results are shown in appendix A.3.

In Figure 5.7, it shows the RMSE of voltage dynamic on bus 9 to 11 with eight scenarios described in Table 5.1. From the result, it presents that the difference of voltage dynamic between DT and reference network is averagely over 60%. In scenario 1, the difference of

voltage dynamic in Gen 10 and Gen 12 is around 80%. It is indicated that the voltage dynamic of synchronous generator from reference network is totally different with DT simulation. According to the different deviation in scenario 1 to 8, the corresponding estimated parameter are displayed in section 5.2.2.

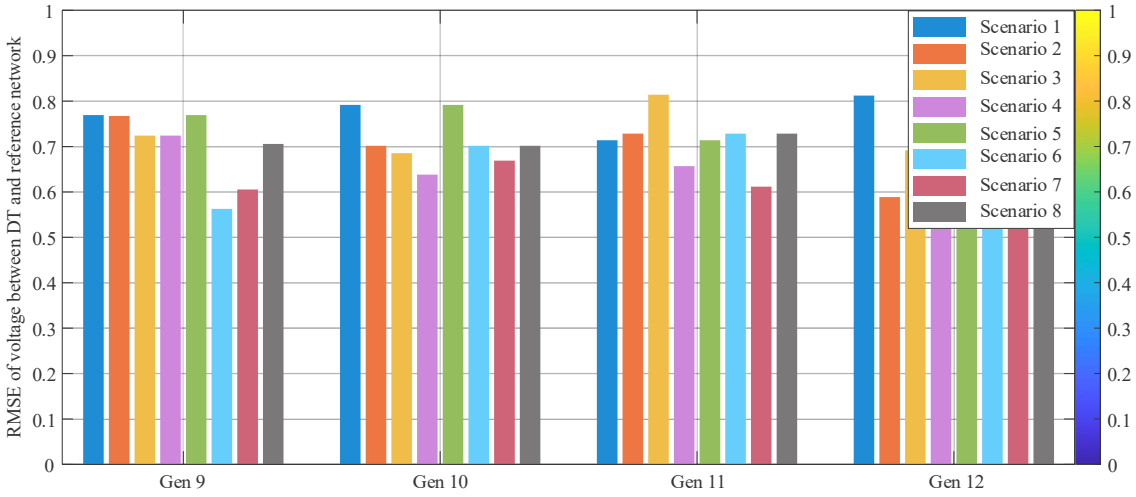

Figure 5.7: RMSE of voltage between DT and reference network in scenario 1-8

In Figure 5.8, it shows the rotor speed of generators of scenario 1 and 3 illustrated in Table 5.1 in reference network and DT. The other simulation results are attached in appendix A.3. The response of the rotor is similar with the voltage. The events occurred in high voltage level, which are geographic closer to the generator, lead to a stronger oscillation to the rotor speed. The oscillations last about 10s to 20s. The response of rotors in DT is different with reference network. The curves of rotor speed in DT are oscillated from the beginning of the simulation. They are obviously deviated with reference network in scenario 1 and 3. In (3.6), the DGLs describes the relations of electrical and magnetic transformations in synchronous generators. For parameter estimation of the coefficients in these DGL, the voltage is regarded as the input signal, and the rotor speed, and the current $i_\mathrm{d}, i_\mathrm{q}$ that feed-into power network are regarded as the target variables.

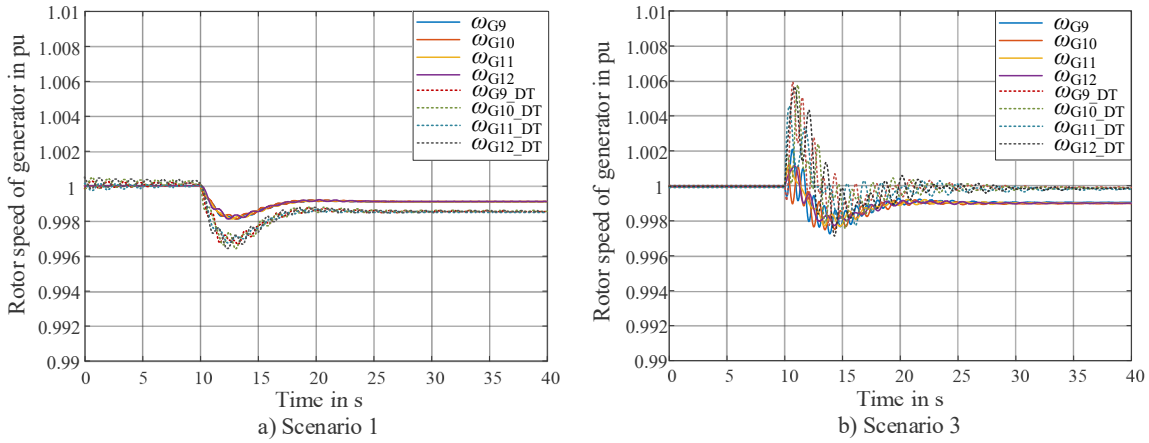

Figure 5.8: Comparison of rotor dynamics between measurement and DT simulation before parameter estimation with scenario 1 and 3

Figure 5.9 shows us the RMSE of rotor speed between DT and reference network in scenario 1 to 8. An overview of the difference between DT and reference in scenario 1 and 3 has been presented in Figure 5.8. The dynamics of the rotor speed between both system are obviously different. According to the evaluation result from Figure 5.9, the deviations are averagely around 45% among four synchronous machines with these scenarios.

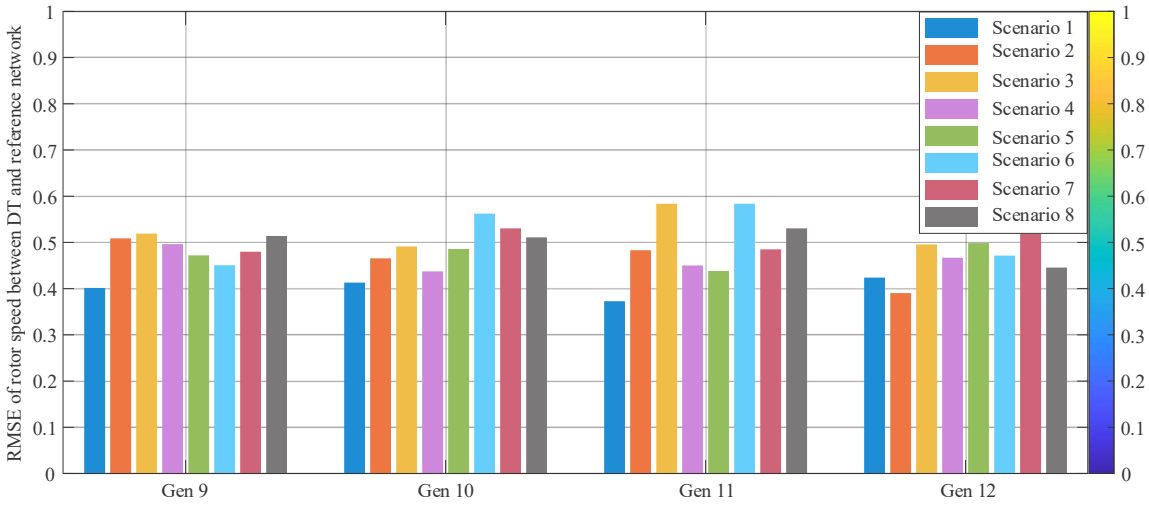

Figure 5.9: RMSE of rotor speed between DT and reference network in scenario 1-8

The scenarios in Table 5.1 are designed for the parameter estimation. From the comparison results in this section, the difference between DT simulation and measurement from reference network exists. The parameter estimation for DT is required to reduce the deviation between them. The next section is focused on this perspective. Three above mentioned methods are used respectively to calculate the new parameters according to the deviation in these scenarios.

5.2.2 Parameter estimation of Digital Twin

According to the results in the last section, the initial parameters used in DT are not identical with the reference network, which result in the difference of the dynamics in DT with reference network. DT is characterized with accurate representation of the reference system. On this account, this section is proposed to use the LSQ, RLS and NN algorithm to estimate the appropriate parameters for the reduction of the difference between DT and reference network. In chapter 3.2, the integration of these algorithms for the parameter estimation of synchronous generator and VSI inverter is described. The input data of these algorithms for the corresponding components is different. Figure 5.10 shows the required input data of LSQ for the estimation of synchronous generator and VSI inverter. It requires the data of voltage and the feed-in current from reference network and DT. The objective function is to minimize the deviation between current dynamic with the new parameters.

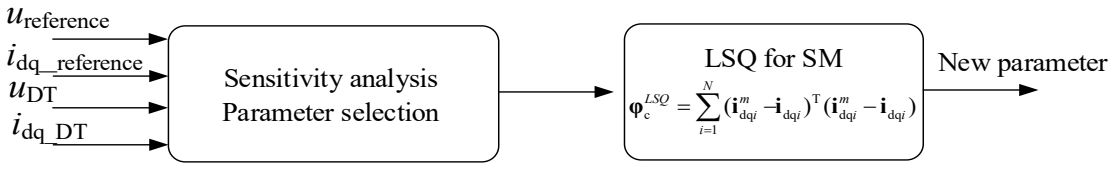

Figure 5.10: Procedure of parameter estimation with LSQ algorithm

According to the explanation in chapter 3.3, the sensitivity analysis (SA) is used to select the parameters, which have the key impact on the target output. With this process, the complexity of parameter estimation process can be reduced with the reduced number of to be estimated parameters. The SA factor is accordingly used to evaluate the correlation between parameter and the observed variables is described by (3.49) in section 3.3. It presents the contribution of i-th parameter on observed variable.

The SA factor S_i describes the impact of the i-th parameter in the synchronous generator. In Figure 5.11, the correlation index S_i ranges from -1 to 1. The value from -1 to 0 presents the reverse effect of the parameters on the dynamic of machine, which means that the increment of the parameters leads to the decrement of the variable. While $S_i \in [0,1]$ indicates the positive impact of the parameters on rotor speed, the definition of the key parameters depend on the absolute value of S_i, which satisfies the $|S_i| \geq |S_{\min}|$ [201, 204]. The red lines in Figure 5.11 label the boundary value. Accordingly, the K_ω, x_d, R_a, x_l and $T''_{\text{q}0}$ are the key parameters that accounts for a significant impact on the dynamics of the machine. These parameters are estimated with LSQ algorithm.

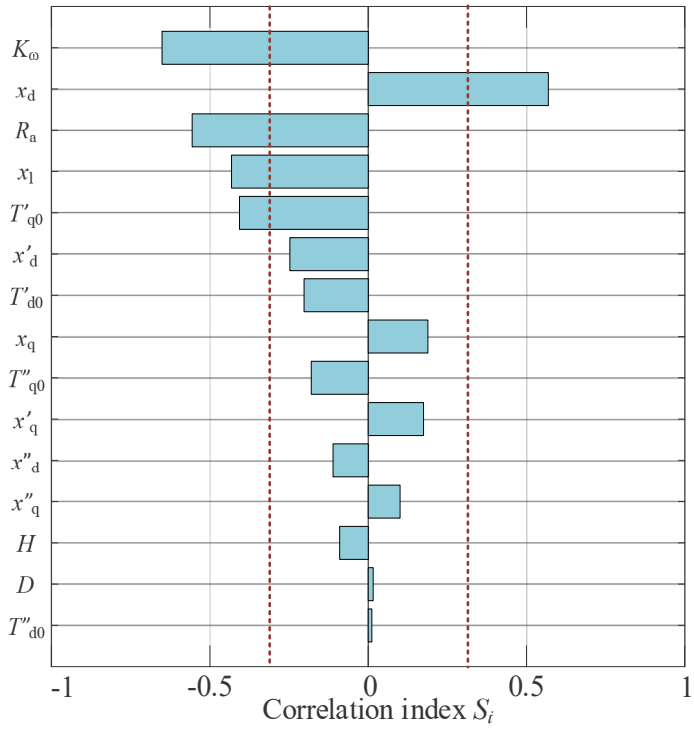

Figure 5.11: Result of SA for the parameters correlated with the rotor speed

Except for the rotor speed as the target output, the feed-in current is also an essential output variable for the DT. It represents the dynamic of power that is fed into the power network. Figure 5.12 presents the result of SA with considering the current of synchronous generator as the target output. It shows different correlated parameters that have impact on the current and on the rotor speed. The armature resistance R_a has the highest effect on the dynamic of current. The other key parameters are T'_{q0}, x''_d, and x''_q. The absolute values of the correlation index S_i for these parameters are over the boundary condition (see red lines in Figure 5.12).

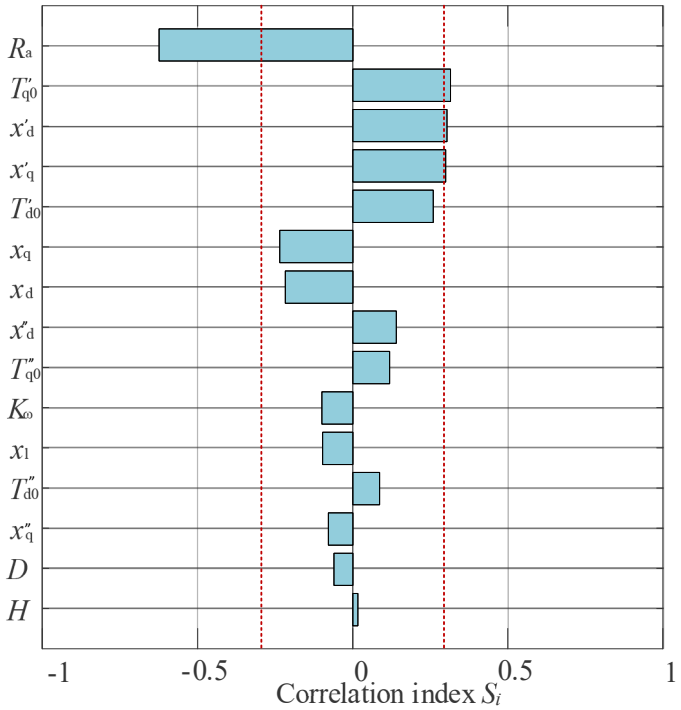

Figure 5.12: Result of SA for the parameters correlated with the current

The parameters of the inverter are correlated with the dynamics of the current i.e., the output signals in inverter DT. The results of SA for the inverter model are shown in Figure 5.13. The parameters related to filter L_f, C_f and R_f have an influence on the dynamic of current. The impact of the current controller $K_{\mathrm{I\_current}}$ and $K_{\mathrm{p\_current}}$ is also necessary to take into account. The low-pass filter is used for the elimination of the high-frequency harmonic in back-loop of current and voltage. The related parameters are referred to as the constant value according to [184], which are not considered in parameter estimation. Consequently, the parameters to be estimated are totally eight for VSI.

According to the SA result mentioned, the key parameters of SM have been selected, and these parameters are taken more attention in the estimation procedure. The integration of these methods for parameterization of 6$^{\mathrm{th}}$ order generator and VSC-inverter have been introduced in section 3.2 The SA is used to reduce the consumption of the parameter estimation. In the parameterization process, the results of considering SA and without SA are compared to evaluate the improvement of the efficient in parameter estimation.

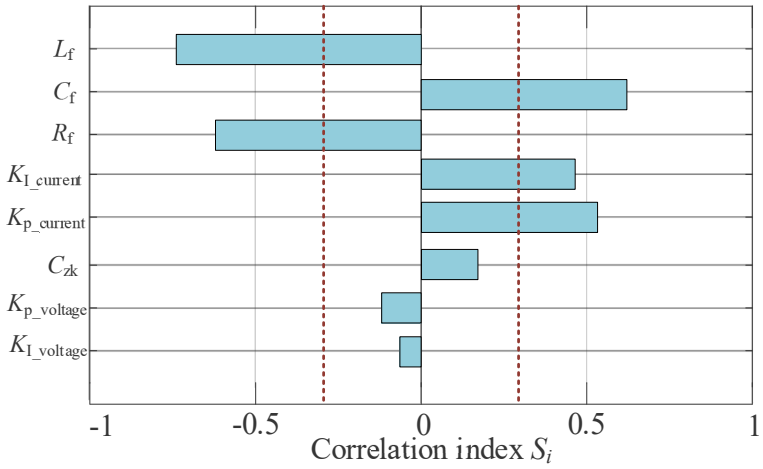

Figure 5.13: Result of SA for the parameters correlated with VSC-inverter

a. LSQ algorithm for parameter estimation of SM and VSI

The first method is based on the LSQ algorithm. The parameters are iteratively calculated based on the objective function described in (3.15). As mentioned above, two target output variables, i.e., rotor speed and current in DT are selected for synchronous generator in LSQ objective function. It means that the dynamic of rotor speed and current in DT after parameter estimation should be theoretical identical with reference network. On the basis of the deviation between the measurement and the results of the DT simulation in last section, the parameters related to observed variables are calculated with setting in (3.39). The minimum objective function $\boldsymbol{\varphi}_c^{LSQ}$ is the sign of the end of literation, which indicates that the simulation results are identical or similar with the measured data from the benchmark model.

In Table 5.2, it shows the time consumption of the parameter estimation of 6th order synchronous generator with LSQ. Without the SA, all the parameters related to SM are considered in estimation. The generators connected with bus 10,11 and 12, which include 45 parameters, are taken for the parameter estimation into account. This number is reduced to 15 with consideration of SA. The time consumption of the parameter estimation with SA can be reduced with over 65% in comparison to the estimation without SA.

Table 5.2: Comparison of time consumption for parameter estimation with and without SA

Method	Model	Time consumption in s (with SA)	Time consumption in s (without SA)
LSQ	6th synchronous generator	782s	3789s
LSQ	VSC-Inverter	367s	478s

Figure 5.14 shows the iteration process of the parameter estimation by LSQ algorithm for 6th order SM model. The initial values of the parameter are adopted according to Table A. 4. With these initial values, the rotor speed of the SM model is deviated with the measurement from benchmark. The parameters are corrected with the LSQ objective function. After 5th iteration, the most parameters have been revised, and some of them are fine-tuned until 10th iteration. The ten times iterations last about 3790s for one SM model included 15 parameters. The final estimated values are shown in appendix Table A. 4.

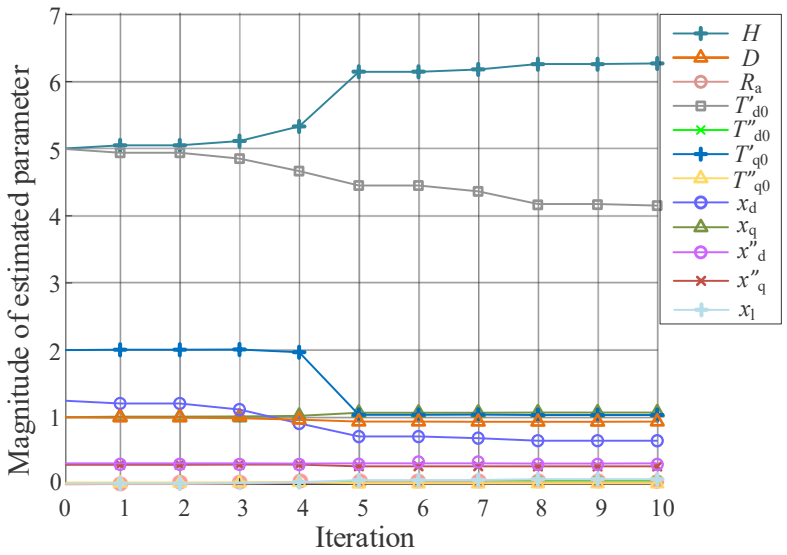

Figure 5.14: Iteration of parameter estimation for SM by LSQ without SA

With the SA, the key parameters are selected for optimization of the time consumption for the parameter estimation by LSQ. From Table 5.2, it is illustrated that the time cost for parameter estimation with SA is reduced four times than without SA. The estimation process for parameter estimation with LSQ algorithm by considering SA is shown in Figure 5.15. The estimation is finished with 10 times iterations. According to the results of the SA illustrated in Figure 5.11 and Figure 5.12, the parameters defined as correlated parameters are estimated with the LSQ method. The estimation process shows different feature with the Figure 5.14. The transient time constant T'_{d0} is tuned from the 5s to 0.2s after 10 times iterations. The sub-transient reactance x''_d and x''_q increase from 0.292 p.u. to 1.73 p.u. and 0.9 p.u. respectively. The not estimated parameters keep the initial value. The rest parameters with estimation are accessible in Table A. 5.

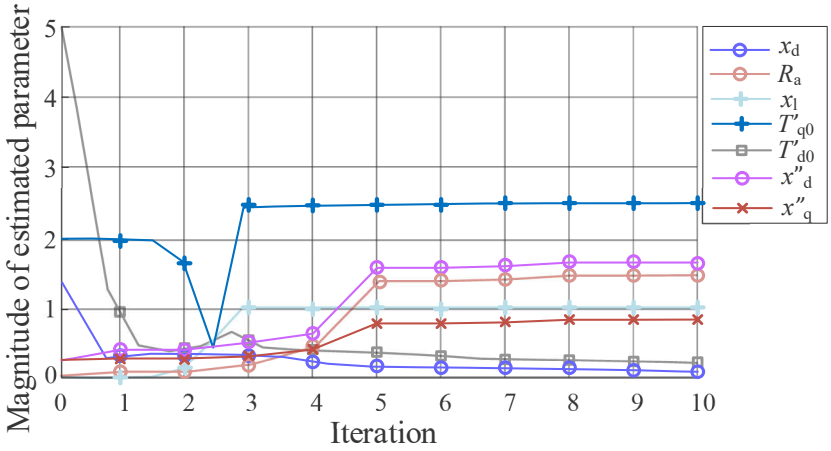

Figure 5.15: Iteration of parameter estimation for SM by LSQ with SA

The simulation results before and after the parameter estimation by LSQ are shown in Figure 5.16. In a), it shows the dynamic of rotor speed of the benchmark objective and the DT prototype of SM on bus 10. The orange curve presents the results of the scenario 2 in reference network. The blue curve shows the dynamic of rotor speed of DT before parameter estimation by simulating of scenario 2. Both curves show the different features with the simulating the same scenario. After the parameter estimation with LSQ algorithm, the deviation between both curves is reduced. The upper figure shows the results of generator DT with parameter estimation by LSQ without SA. The blue curve is more identical with the orange curve compared with the figure a). The index RMSE is used to evaluate the deviation between them, which is R_1=0.86% in upper figure, and R_2=3.74% in the result of the parameter estimation with SA.

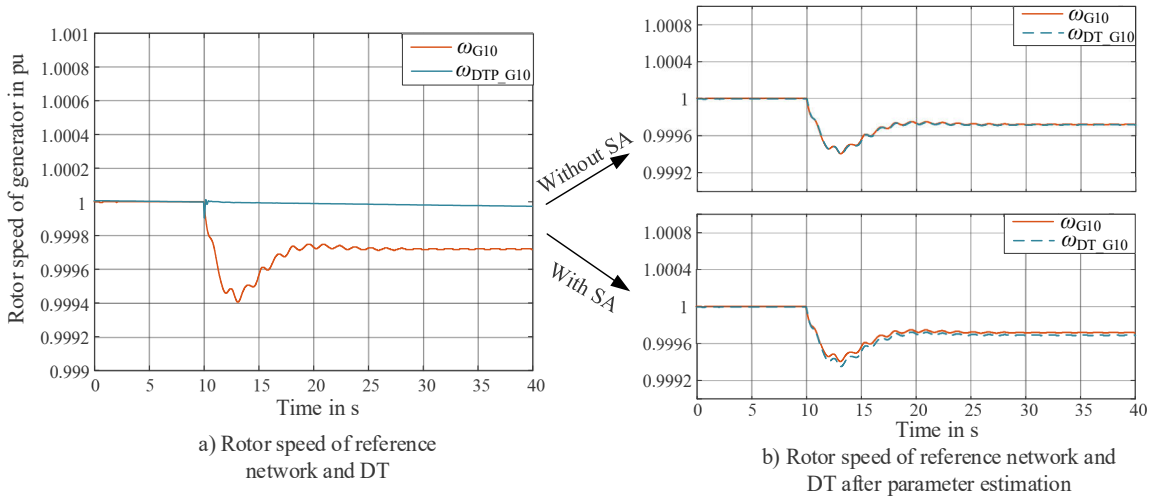

a) Rotor speed of reference network and DT

b) Rotor speed of reference network and DT after parameter estimation

Figure 5.16: Rotor speed of DT SM model before and after the parameter estimation with scenario 2

The scenario 8 describes the bus fault event close to the generator bus. The estimated parameters with this scenario are shown in Table A. 4 and Table A. 5. From a) in Figure 5.17, the deviation between DT and reference is obvious from 10 s after the fault event starts. The rotor speed in DT has different oscillation character with the reference network. The oscillation in DT lasts about 5 seconds until to the stationary condition, while the SM in benchmark objective needs about more than 30 seconds. In Figure 5.17 b), it shows the comparison result of the rotor speed between DT and reference network after parameter estimation. The upper figure has not considered SA. All the parameters related to SM are taken into account for the parameter estimation. The result with the consideration of SA is shown in the figure below. It can be seen that the rotor dynamic of DT (see blue curve in b)) is more similar with the feature of SM in reference network presented by orange curve. The parameter estimation without SA shows a better performance in twinning process but a higher time consumption in parameter estimation process. The RSME between both curves in upper figure in b) is around 1%, while the index is about 4% in figure with SA.

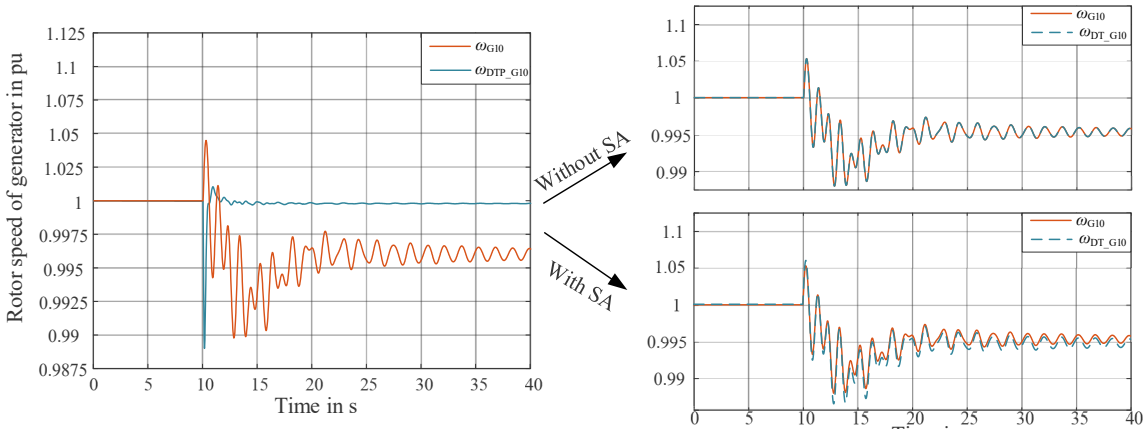

a) Rotor speed of benchmark model and Digital Twin prototype

b) Rotor speed of benchmark model and Digital Twin after parameter estimation

Figure 5.17: Rotor speed of DT SM model before and after the parameter estimation with scenario 8

After parameter estimation with LSQ, the results in scenario 2 and scenario 8 from DT present that DT has a more similar dynamic with reference network. Figure 5.18 shows the comparison of difference of rotor speed dynamic between DT and reference network.

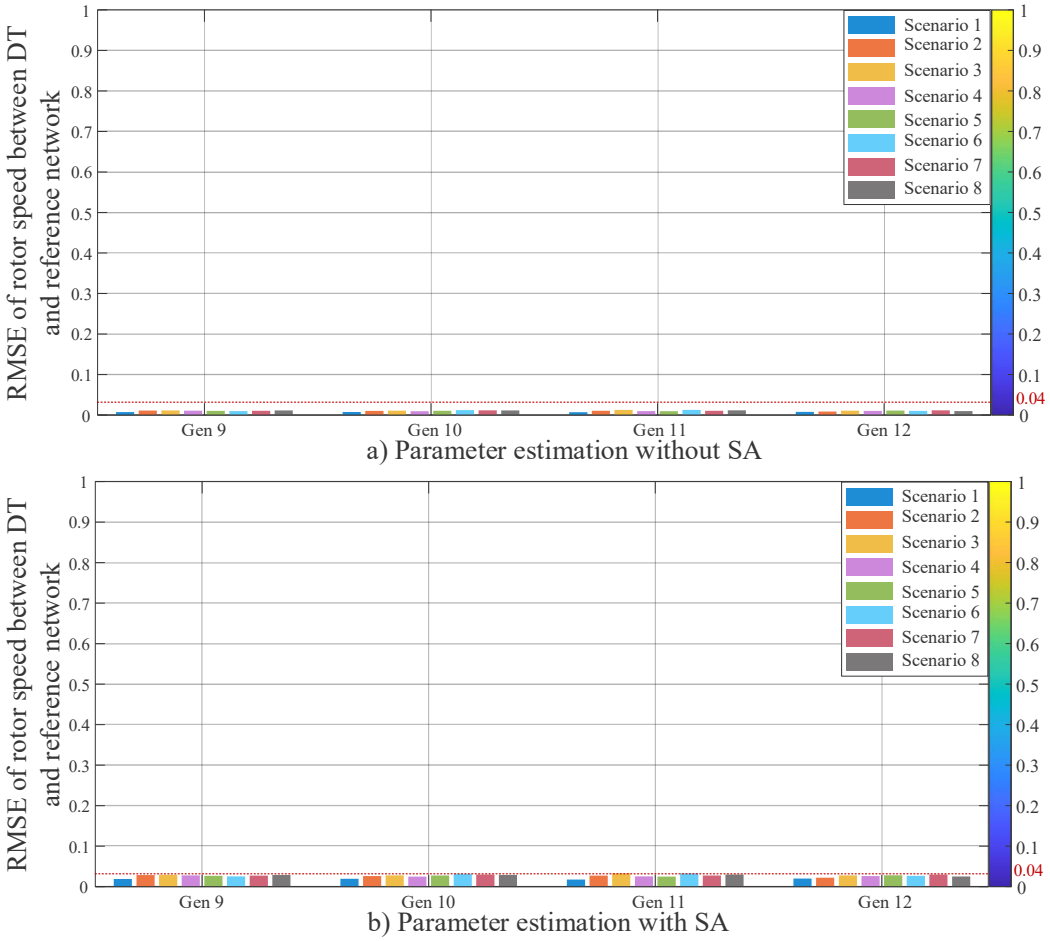

Figure 5.18: RMSE of rotor speed between DT and reference network after parameter estimation with and without SA

In Figure 5.18 a), it is the result without SA process. It illustrates that the deviation between DT and reference network is around 1%, which means that the rotor speed character of DT is around 99% identical with reference network in simulating scenarios 1 to 8. In comparison with the results in Figure 5.9, the difference between DT and reference network has reduced averagely over 45% after parameter estimation. The result after parameter estimation with SA is shown in Figure 5.18 b). It presents the slight difference between DT and reference network, which is around 3% to 4%. According to the result, it illustrates that the parameter estimation with LSQ has improved the accuracy of DT. The validation of the accuracy with scenarios in Table 5.2 is carried out in next section.

There are eight parameters in VSI model for the estimation. As shown in Table 5.2, the estimation of the parameters in VSI takes less consumption than in SM model. The iteration process without SA is shown in Figure 5.19. The parameters are finalized after 8th iteration. The time constant T_{I_C} of PI controller in current loop is estimated to 4.23s. The

resistance of filter R_f increases from 1 Ohm to 2.32 Ohm. The estimated parameters with LSQ method are shown in appendix.

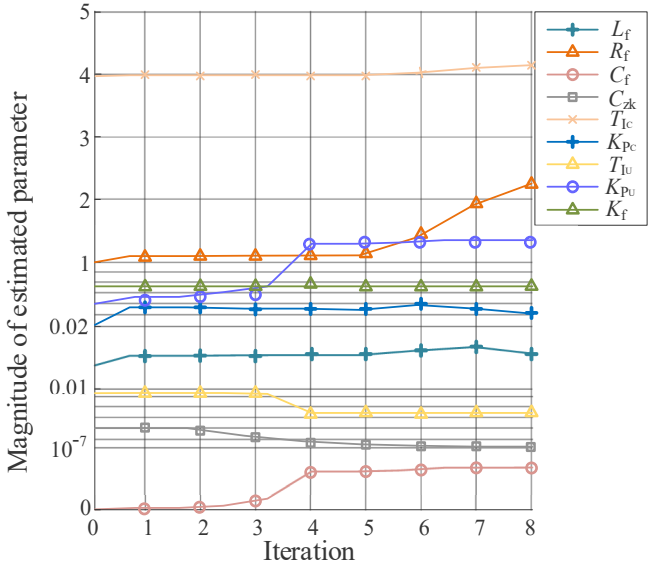

Figure 5.19: Iteration of parameter estimation for VSI by LSQ without SA

The results of SA referred to VSI in Figure 5.13 show the correlated parameters in parameter estimation by LSQ. The correlation index over 0.35 defines the key parameters in this work, which include the parameters related to filter of VSI R_f, C_f, and L_f. The controller related parameters in current loop i.e., T_{I_C} and K_{P_C} also have an essential impact on the dynamic of the current. Accordingly, the parameter estimation with SA reduces the calculation consumption with considering less parameters. The estimation results are shown in Figure 5.20. The estimated values like K_{P_C} and C_f are obviously deviated with the parameters estimated without SA. The final values after estimation with SA for inverters are illustrated in appendix.

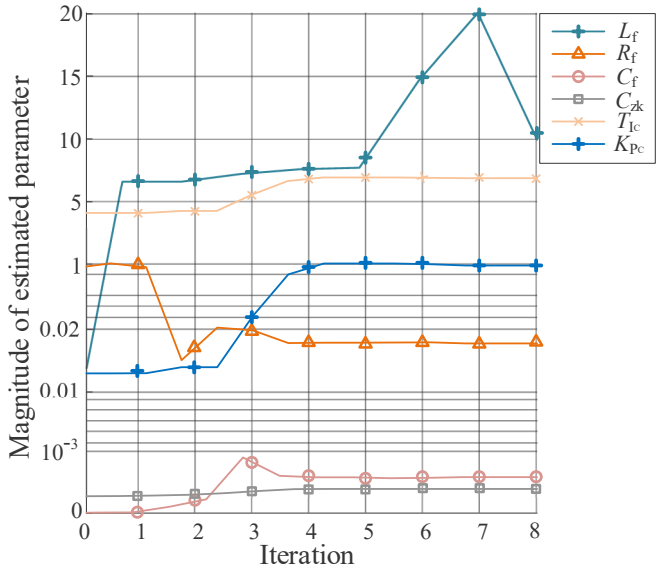

Figure 5.20: Iteration of parameter estimation for VSI by LSQ with SA

The simulation results by LSQ parameter estimation are shown in Figure 5.21. With the initial parameters, the current dynamic of inverter DT prototype is oscillated in the stationary state before and after 10s. The setpoint of active power increases from 4.75 MW to 10 MW at 10s. The orange curve in a) shows the measurement of the reference network. The DT before parameter estimation is deviated for over 70% with the measured feature. With the LSQ parameter estimation, the deviation is reduced to 3.34% without SA, and 3.98% with SA.

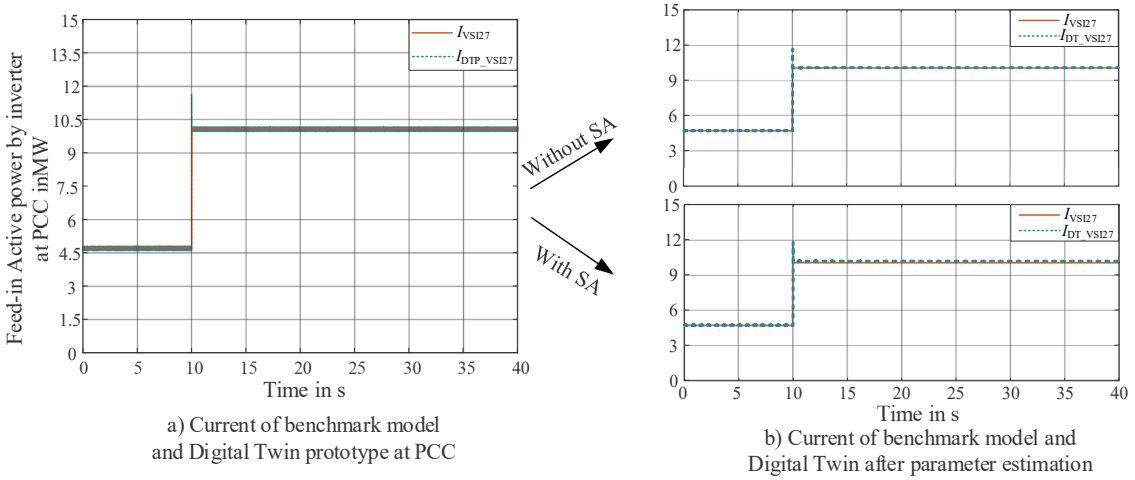

a) Current of benchmark model and Digital Twin prototype at PCC

b) Current of benchmark model and Digital Twin after parameter estimation

Figure 5.21: Current of VSI model in DT at bus 40 before and after the parameter estimation with scenario 5

b. RLS algorithm for parameter estimation of SM and VSI

The implementation process of RLS algorithm in parameter estimation of SM is explained in section 3.2. The transformation of the DAEs to equation with ARMAX structure has been accomplished with the (3.32)-(3.33). The RLS method is used to calculate the proper coefficients of ARMAX equation. Afterwards, the coefficients are retransformed to the parameters related to the SM. The measurements of scenario 1, scenario 3 and scenario 8 are utilized for the parameter estimation. In Table 5.3, it shows the estimated coefficients in the ARMAX structure-based equation. The coefficients a_1-a_6 are related to the parameters of reactance and resistance in SM. The coefficients estimated by RLS method with measurement data from scenario 1, 3 and 8 presents small difference. The b_1 and b_2 are the coefficients of the polynomial related with $u(t)$, which are referred to the parameters in the mechanical equation for SM.

Table 5.3: Estimated coefficients of ARMAX equation for SM with scenario 1, 3 and 8

Scenario	a_1	a_2	a_3	a_4	a_5	a_6	b_1	b_2
Scenario 1	0.0765	0.0919	0.1122	0.1439	0.2007	0.3317	0.0867	-0.00867
Scenario 3	0.0764	0.09215	0.1124	0.1442	0.2009	0.3312	0.1079	-0.01138
Scenario 8	0.0764	0.09215	0.1124	0.1442	0.2009	0.3312	0.0992	-0.01226

Table 5.4 shows the parameters of SM estimated by RLS method. These parameters are calculated by retransformation with the estimated coefficients in Table 5.3. The parameters related to mechanical relation in SM i.e., H and D are correlated with the coefficients b_1 and b_2. With the different scenarios, the coefficients b_1 and b_2 are estimated with different values, which lead to the different values of H and D. The estimated values of the parameters related to electrical and magnetic equations have not obvious gap with the estimated parameters by LSQ methods.

Table 5.4: Parameters of SM retransformed by the coefficients of ARMAX equation

Parameter	Before parameter estimation	Scenario 1	Scenario 3	Scenario 8
H	8.0 MWs/MVA	5.767 MWs/MVA	4.634 MWs/MVA	5.04 MWs/MVA
D	5.0	1.123	1.012	1.044
x_d	2.5 p.u.	1.03 p.u.	0.99 p.u.	0.99 p.u.
x_q	2.5 p.u.	0.97 p.u.	1.01 p.u.	1.01 p.u.
x'_d	1.5 p.u.	0.3132 p.u.	0.3387 p.u.	0.3387 p.u.

x'_q	1.5 p.u.	0.298 p.u.	0.302 p.u.	0.302 p.u.
x''_d	1 p.u.	0.299 p.u.	0.31 p.u.	0.31 p.u.
x''_q	1 p.u.	0.299 p.u.	0.29 p.u.	0.29 p.u.
T'_{d0}	10.0 s	4.876 s	4.223 s	4.223 s
T'_{q0}	10.0 s	2.076 s	1.875 s	1.875 s
T''_{d0}	1 s	0.0367 s	0.0212 s	0.0212 s
T''_{q0}	1 s	0.0367 s	0.0212 s	0.0212 s
r_a	0.2 p.u.	0.0017 p.u.	0.0087 p.u.	0.0087 p.u.
x_l	0.1 p.u.	0.028 p.u.	0.032 p.u.	0.032 p.u.

The parameter estimation by RLS is not necessary to consider the SA. All the parameters related to the DAE of SM are converted into the coefficients of equation with ARMAX structure. However, this method utilizes the linearization to build the ARMAX equation, which results in the slight deviation of the estimated value. Figure 5.22 shows the dynamics of the rotor speed before and after the parameter estimation by RLS. The dynamic of rotor speed after parameter estimation by RLS is presented by the equation with ARMAX structure (see black curves in Figure 5.22). After the estimation process, the deviation between the DT prototype (blue curve) and measurement (orange curve) is decreased. RMSE between benchmark model and the DT after parameter estimation with RLS is 0.92% in a), and 0.88% in b). The RMSE of scenario 3, which is not shown in figure, is 0.88%. The indexes present the similarity over 99% between the DT and objective model. It indicates that the parameter estimation by RLS is effective to build DT to replicate the dynamic feature of the benchmark objective.

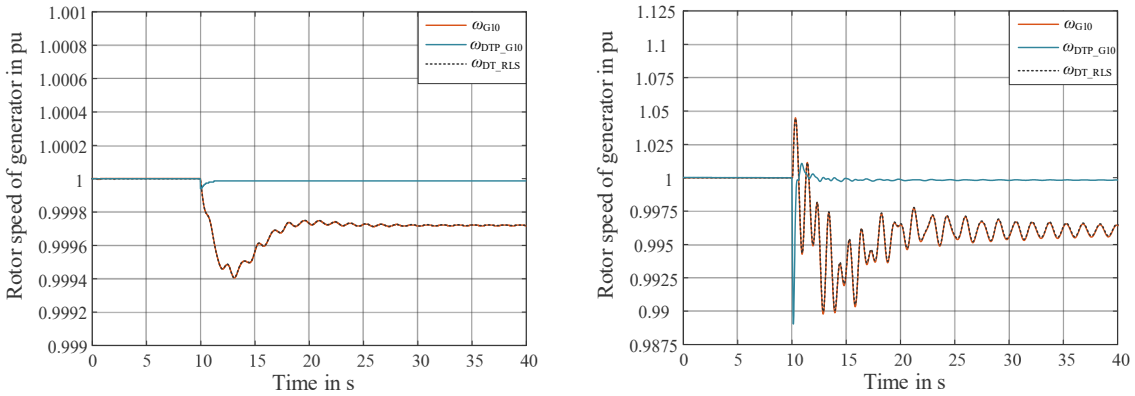

a) Rotor speed of benchmark model and Digital Twin with scenario 1

b) Rotor speed of benchmark model and Digital Twin with scenario 8

Figure 5.22: Rotor speed of DT before and after the parameter estimation by RLS with scenario 1 and 8

Figure 5.23 presents the deviation of rotor speed between DT and reference network in scenarios 1 to 8. After parameter estimation with RLS, the dynamic of rotor speed of DT is averagely under 2% different with reference network. It indicates that the RLS algorithm accurately estimates the parameters of DT. The result shows that DT after parameter estimation with RLS can represent the dynamic of reference network over 98%. In some scenarios, the similarity of DT is over 99% with reference network. The validation of the DT with the estimated parameters is presented in next section.

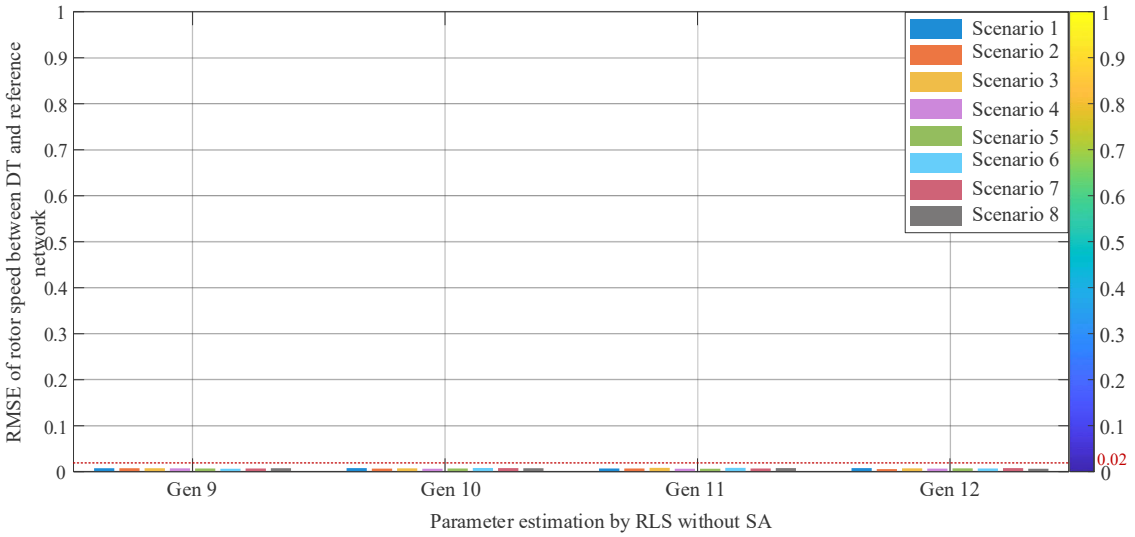

Figure 5.23: RMSE of rotor speed between DT and reference network after parameter estimation with RLS in scenarios 1 to 8

The use of RLS for identification of parameters in VSI has been described in section 3.2. The (3.42) is the ARMAX equation based on DAE of VSI. The matrices in the equation present the coefficients and polynomial of the current and the voltage on d- and q- axis. The coefficients of the equation after estimation are shown in Table 5.5. The coefficients a_1-a_3 and b_1, b_2 are related to the polynomial for current variable on d-and q-axis. Otherwise, the coefficients c_1-c_3 and d_1-d_3 belongs to the polynomial of voltage variable in ARMAX equation.

Table 5.5: Estimated coefficients of ARMAX equation for VSI with scenario 5

Scenario	a_1	a_2	a_3	b_1	b_2	c_1	c_2	c_3	d_1	d_2	d_3
Scenario 5	0.274	0.427	0.203	0.129	0.159	0.013	0.007	0.008	0.011	0.017	0.028

Table 5.6 shows the parameters of VSI estimated by RLS. These parameters are related with the coefficients in Table 5.5, which are calculated with the equation (3.43). The parameters referred to filter i.e., L_f, R_f and C_f are estimated to the different values with the

initial value. The parameters of controllers and the DC link capacitor are differently estimated with the ARMAX equation. The mainly reason leads to the different value estimated by RLS and LSQ is because of the transformation of DAE to ARMAX equation and then retransformation of the parameters, which include the linearization procedure.

Table 5.6: Parameters of VSI retransformed by the coefficients of ARMAX equation

Parameter	Description	Before parameter estimation	Scenario 5
L_{f}	Induction of filter	13 mH	100.13 mH
R_{f}	Resistance of filter	1 Ohm	0.01 Ohm
C_{f}	Capacitor of filter	80 nF	102.3 nF
C_{zk}	Capacitor of condenser in DC side	100 µF	117.89 µF
$T_{\mathrm{I_C}}$	Time constant of PI controller for current loop	3.92s	1.73s
$K_{\mathrm{P_C}}$	Proportional of PI controller for current loop	0.033	0.0234
$T_{\mathrm{I_U}}$	Time constant of PI controller for voltage loop	0.009 s	0.0076s
$K_{\mathrm{P_U}}$	Proportional of PI controller for voltage loop	0.1333	0.246
K_{f}	Proportional between DC and AC current	0.625	1.233

The simulation result before and after estimation by RLS are shown in Figure 5.24. It is obvious that after the estimation with RLS, the DT has replicated the feature of the reference VSI. The deviation of both dynamics is reduced from over 70% to 0.75%.

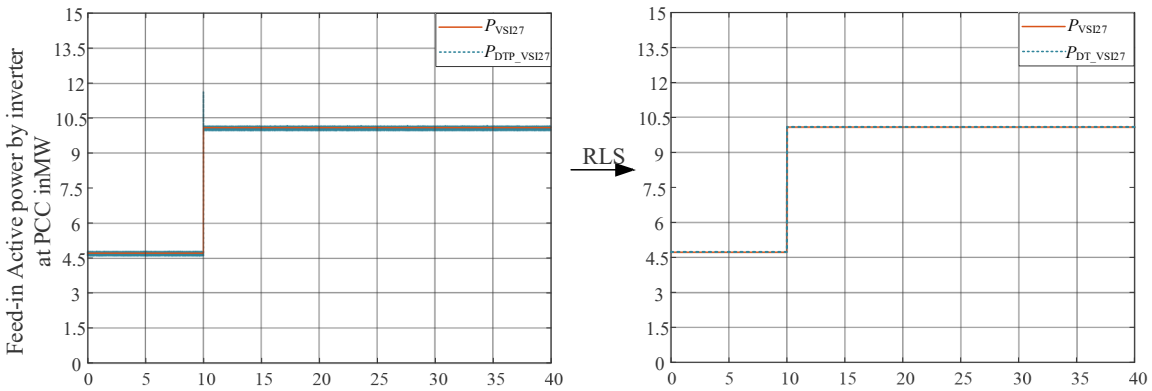

a) Active power of benchmark model and Digital Twin prototype at PCC

b) Active power of benchmark model and Digital Twin with RLS method

Figure 5.24: Feed-in power of DT VSI model before and after the parameter estimation by RLS with scenario 5

c. NN-identifier for parameter estimation of SM and VSI

According to the NN-identifier in section 3.2, the used radial basis function is an adaptive algorithm for parameter estimation, which requires no training process, but the initial setting of the parameters in neural network. The initial values of $\hat{w}_{ij}$ are random numbers while the initial values of $\hat{\lambda}_i$ is zero. The learning rates used for $b_i(x, \hat{x}, t) = -\alpha e_i - \frac{\hat{\lambda}^2 e_i}{|\hat{\lambda} e_i| + \epsilon}$ in (3.46) are: $\alpha = 12000$ and $\epsilon = 0.01$. This method is applied without consideration of SA. Not all the parameters related to SM are estimated with NN-identifier. As illustrated in (3.46), the parameter set $\boldsymbol{\theta}$ includes $\theta_1 = \frac{1}{2H}$, $\theta_2 = \frac{1}{T'_{\mathrm{d0}}}$, $\theta_3 = \frac{1}{T'_{\mathrm{q0}}}$, $\theta_4 = \frac{1}{T''_{\mathrm{d0}}}$, $\theta_5 = \frac{1}{T''_{\mathrm{q0}}}$ and $\theta_6 = R_{\mathrm{a}}$, which are defined as the unknown parameters for parameter estimation. The other parameters are defined as the known parameters, which are equal to the initial values explained in Table 5.4. Except for the voltage u_{d} and u_{q}, the output of exciter u_{fd} and turbine governor T_{m} are the other input signals for the NN-identifier. The structure of the identifier is depicted in Figure 5.25. Like most feedforward NN, the structure has the input layer, hidden layer, and output layer. The weights in the output layers are continuously adjusted by the learning rules with evaluation the error between measured outputs and estimated outputs.

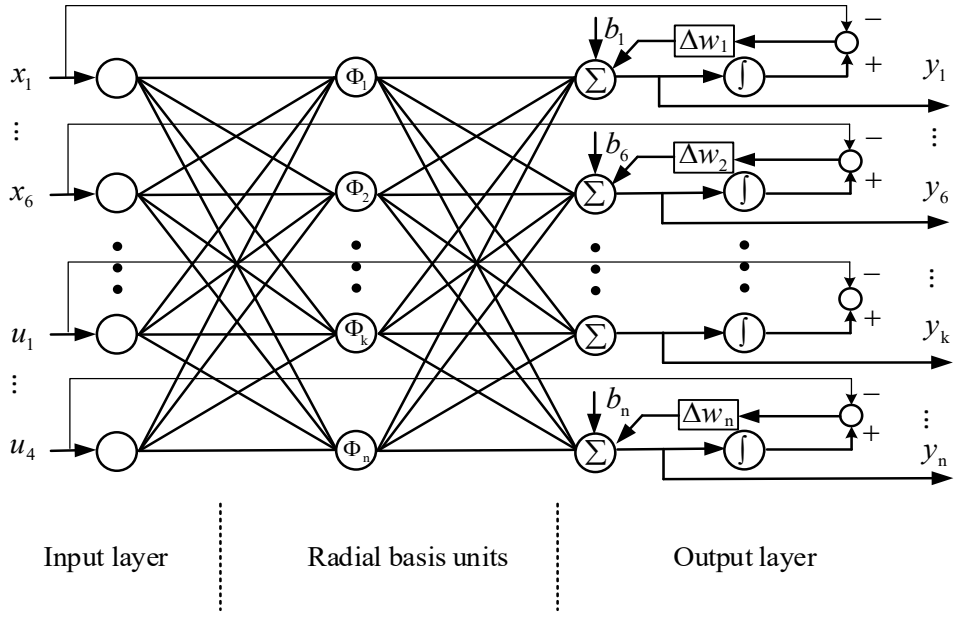

Figure 5.25: Structure of the proposed NN-identifier

The result of parameter identification by NN-identifier based on RBFN is shown in Figure 5.26. The parameter set H, T'_{d0}, T'_{q0}, T''_{d0}, T''_{q0} and R_{a} are estimated with the equation (3.38). The weights of bias in NN are changed according to the error between the measured field

states in (3.39) and the computed using the sliding mode observer algorithm. The estimated parameters are varied with the change of bias within first 15s. H is increased from 5 MWs/MVA to about 5.04 MWs/MVA after 3s. After 10s, the value is stable around 5.015 MWs/MVA. The oscillation of the estimated value lasts about 10s till to the stable state. T''_{d0} and T''_{q0} are comparatively less changed than other parameters.

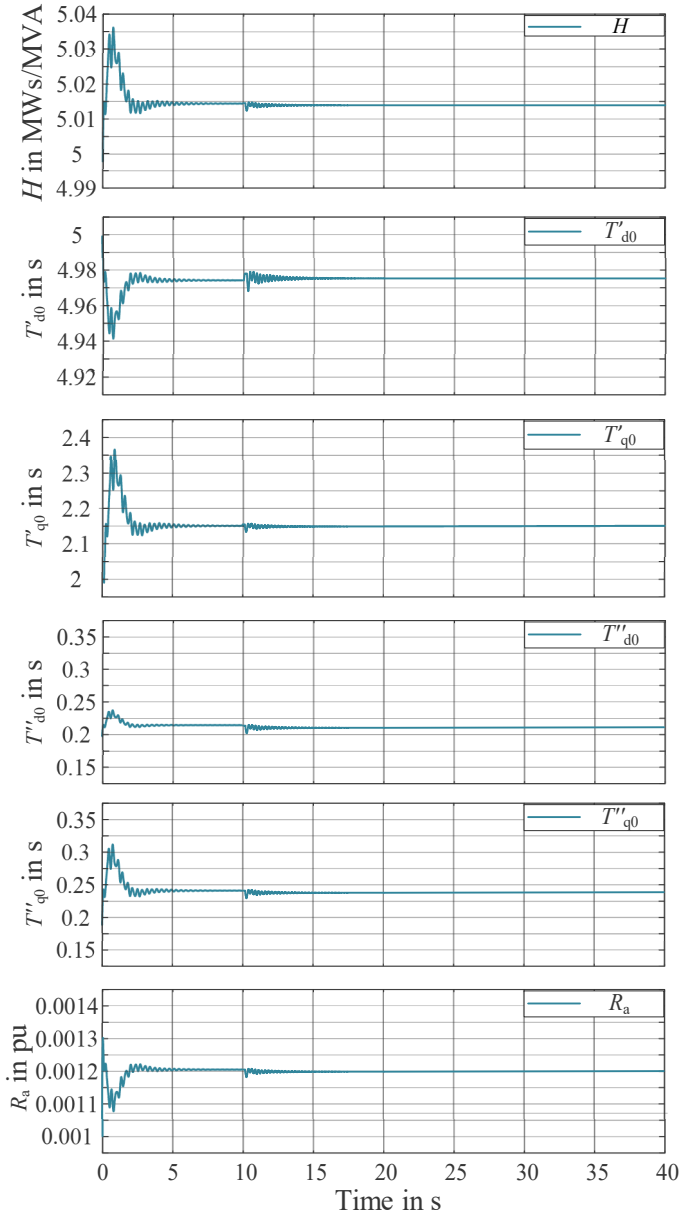

Figure 5.26: Estimated parameters related to SM by NN-identifier

Figure 5.27 depicts the simulation results of the scenario 1 and scenario 8 by estimation with NN-identifier. The result shows the comparison of the rotor speed dynamics in both scenarios between the measurement from reference objective, DT prototype, and the term

y_1 represents the simulated rotor speed with NN-identifier for G10. In a), the increased setpoint of load at Bus 5 leads to the oscillation reaction of the rotor speed. There is an obvious difference between black curve and orange curve from 0s to 8s. The RBFN detects the deviation between x_i and the NN-observer y_i. The new weights are updated in NN-identifier with the aim of decreasing the error $e_i = \frac{1}{2}(x_i - y_i)^2$. From 10s to 14s, the parameters are converged into the stable state. Accordingly, the error is reduced to lower than 2%. To evaluate the error between DT built by NN-identifier and the measurement, two RMSEs are constructed by fitting the simulation in scenario 1 and scenario 8. The focus is concentrated on the simulations between 10s and 40s. The deviation rates are presented with values $R_1 = 1.24\%$ and $R_8 = 1.97\%$.

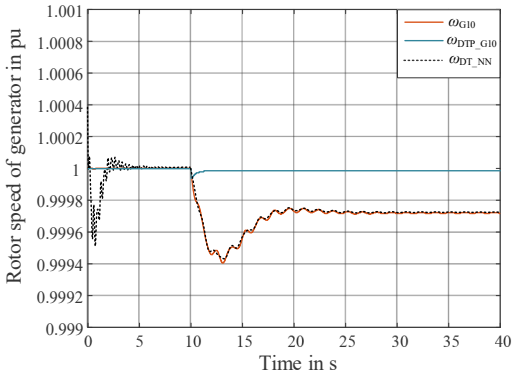

a) Rotor speed of benchmark model and Digital Twin with scenario 1

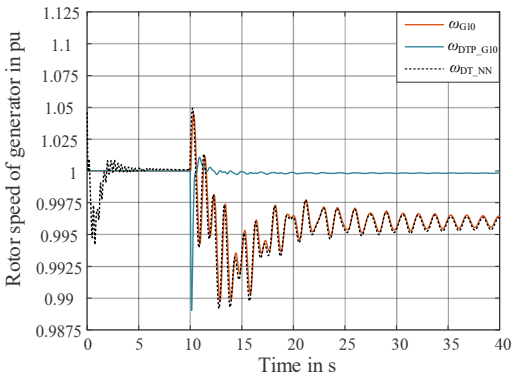

b) Rotor speed of benchmark model and Digital Twin with scenario 8

Figure 5.27: Comparison with dynamic of rotor speed simulated by NN-identifier with scenario 1 and scenario 8

The parameter estimation laws of VSI by NN-identifier are derived from the equation (3.45). The parameter set $\boldsymbol{\theta}$ in VSI includes $\theta_1 = \frac{1}{L_\mathrm{f}}$, $\theta_2 = R_\mathrm{f}$, $\theta_3 = \frac{1}{L_\mathrm{N}}$, $\theta_4 = R_\mathrm{N}$, and $\theta_5 = \frac{1}{C_\mathrm{f}}$. The initial values of weights in NN layers are uniform random numbers while the $\hat{\lambda}_i$ is chosen with zero. The parameter tuning values used in estimation schema for VSI are: $\alpha = 10000$ and $\epsilon = 0.02$. The inputs of NN-identifier are the measured inverter voltage (u_{SRd} and u_{SRq}), network voltage at PCC point (u_{Nd} and u_{Nq}). The state variables for NN-identifier are currents (i_{fd} ,i_{fq},i_{Nd}, i_{Nq}), and the filter voltages ($u_{\mathrm{C_{fd}}}$ and $u_{\mathrm{C_{fq}}}$). It is assumed that these inputs and the state variables are measurable. As is shown in Figure 5.28, the estimated parameters are oscillated during the initial states for finding the parameter solution. Since the maximum observed error is 0.0001 for VSI estimator, based on this work, the estimation process is stopped with the deviation between the observer and the measured states less than 0.0001. The first convergence of the parameter estimation is after 8s. The estimation has found the optimized solution. At 10s, the setpoint of VSI changes from 4.75 MW to 10 MW. The estimation is slightly oscillated and converged after 4s.

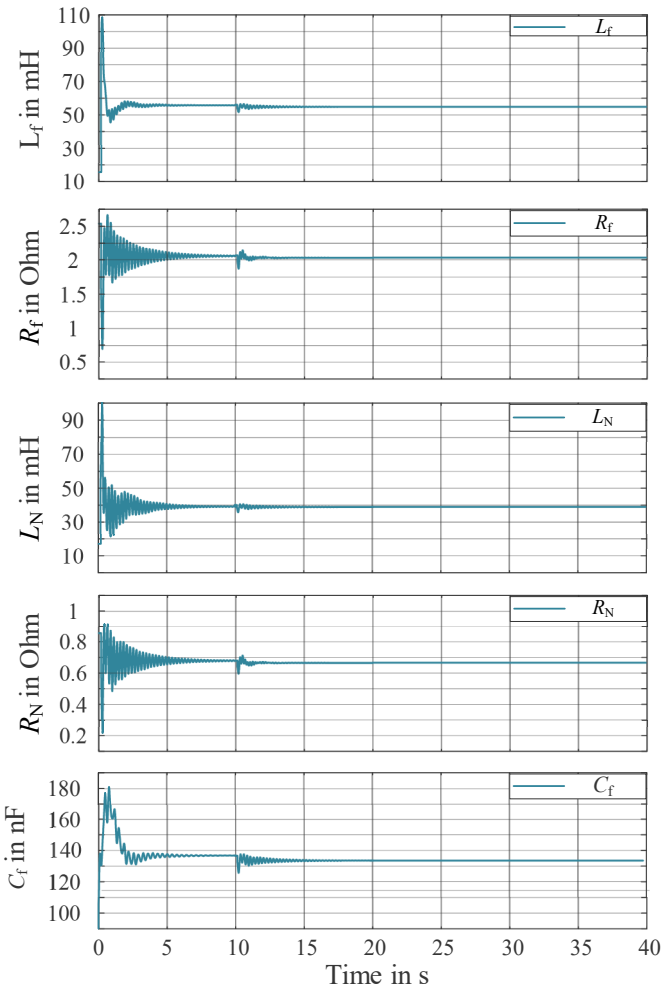

Figure 5.28: Estimated parameters related to VSI by NN-identifier

The observed variable of NN-identifier is the dynamic of feed-in current, which is represented with the variables i_{fd} ,i_{fq},i_{Nd}, and i_{Nq}. The simulation results for scenario 5 by NN-identifier is illustrated in Figure 5.29 by plotting the measurement of objective, result before and after parameter estimation together, indicating that the parameter estimation by NN-identifier is effective to improve the performance of the DT. In Figure 5.29 b), the green dashed line shows that the simulated dynamic of current by NN-identifier is not converged with the orange line initially. The maximum RMSE between them is about 150% at 2.3s. With the computation of the proper weights in NN by supervised learning algorithm, this error is reduced to 0 after 17s, i.e., the dynamics of the current simulated by NN-identifier is fitted with the reference objective.

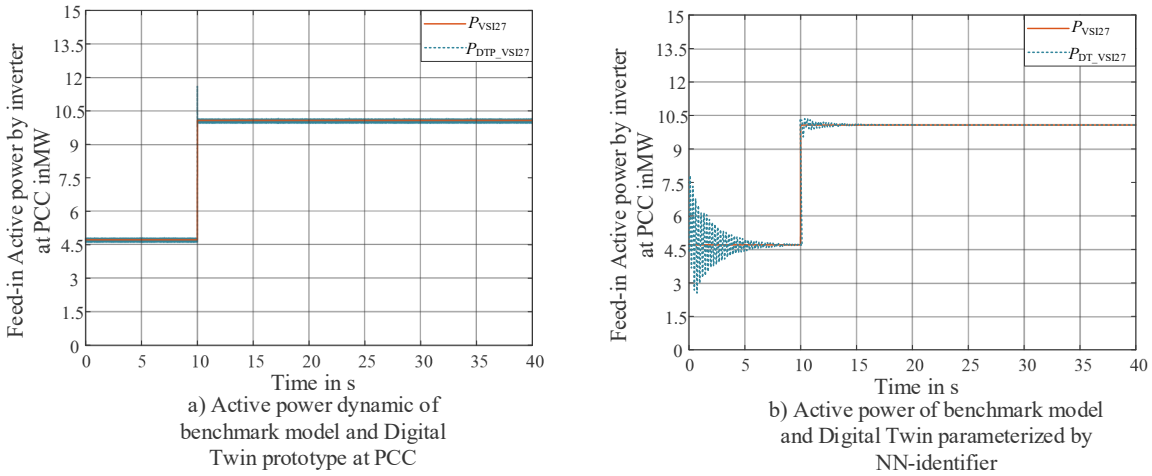

a) Active power dynamic of benchmark model and Digital Twin prototype at PCC

b) Active power of benchmark model and Digital Twin parameterized by NN-identifier

Figure 5.29: Dynamics of active power simulated by NN-identifier

5.2.3 Validation of Digital Twin

To verify the efficiency of the proposed approach and validate the accuracy in replication of the dynamic feature by DT, numerical cases are carried out according to Table 5.2. In the beginning of this chapter, Figure 5.2 depicts the second procedure of the case studies namely validation of the DT. With the estimated parameters in the last section, the DT simulates the scenarios in Table 5.2 firstly, and then these scenarios are carried out in reference network to validate the similarity degree of the dynamics between DT and reference system. Figure 5.30 shows the procedure of verifying the accuracy of DT for the representation of the reference network by DT.

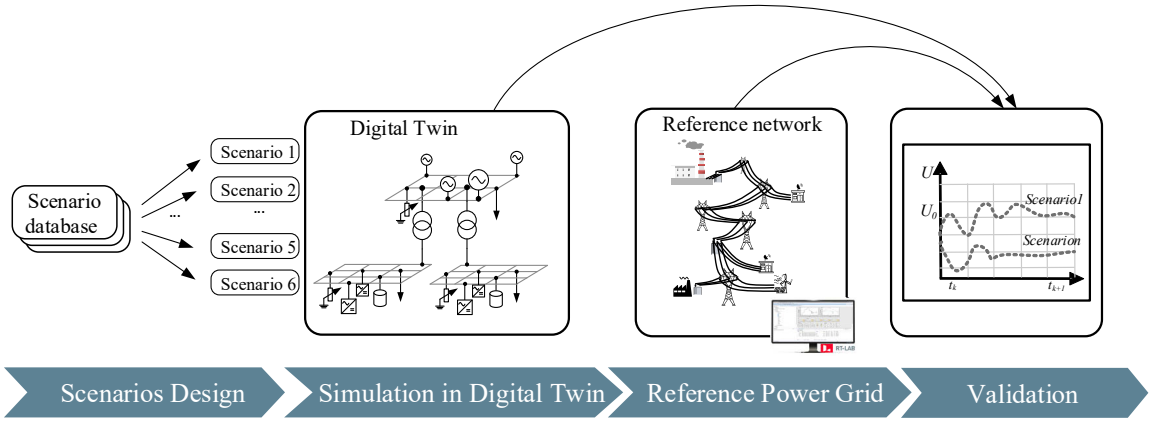

Figure 5.30: Scheme of validation procedure for DT

The nominal values of the dynamic states are observed for the validation. The variables of SM and VSI at PCC for observation are rotor speed of SM ω_i $(i = 1,2,3,4)$, feed-in current of SM i_{gi} $(i = 1,2,3,4)$ and feed-in current of VSI $i_{\mathrm{VSI}i}(i = 1,2,\ldots,16)$. In the transmission network, the SM and the corresponding regulators connected with bus 10,11, and 12 are

modelled with DAEs and implemented in OPAL-RT system [31]. The parameters are applied with the estimation results in section 5.2.2. In distribution grid level, two medium voltage grids based on the CIGRÈ benchmark are connected with transmission network. With the co-simulation theory in [41, 220], the DT is established with hybrid model form. Figure 5.31 shows the topology of the DT, which is divided into two parts: the dynamic components (marker with pink area) are simulated in EMT depth with the estimated parameter. The network including the slack SM at bus 9, transformers, loads and the compensation station are simulated with the phasor model [31, 220].

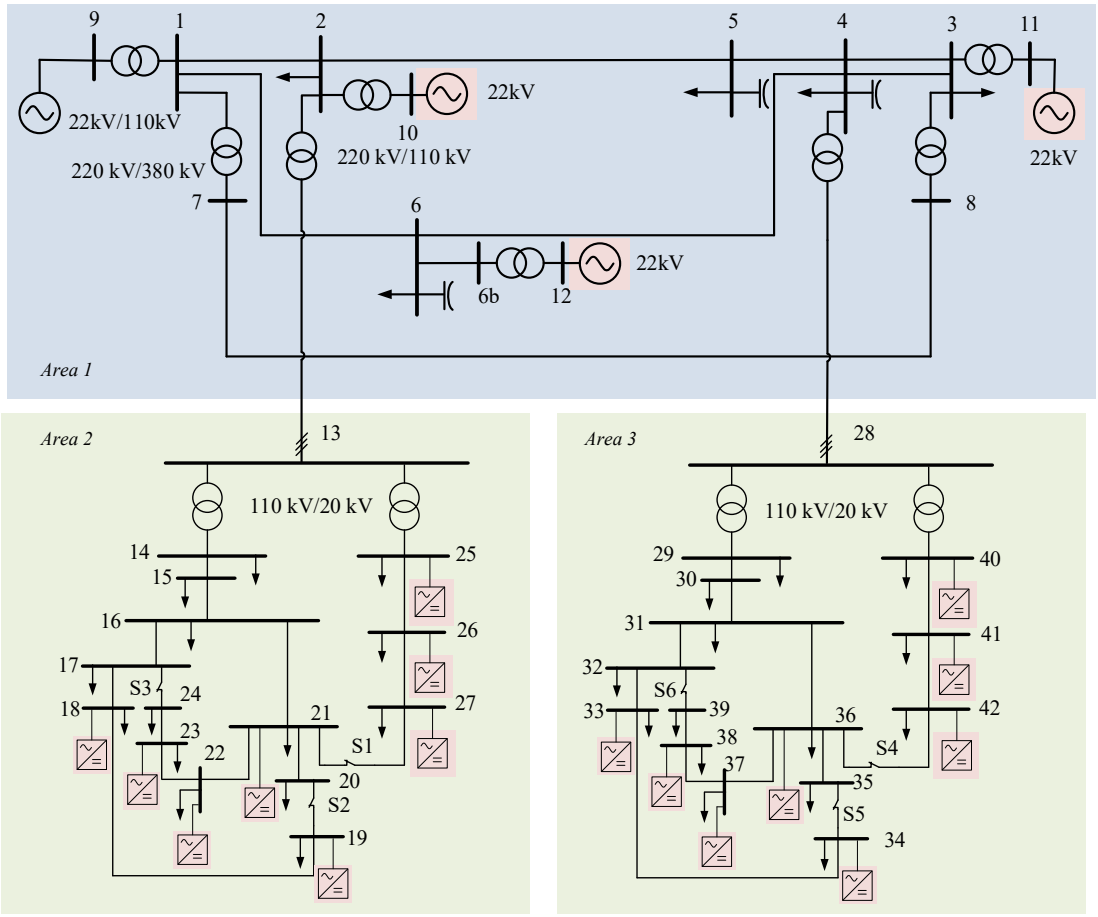

Figure 5.31: Topology of DT

The scenario 1, 3, 5, and 6 in Table 5.2 depicts the events in area 1. The simulation of these events is used to validate the DT, i.e., the transmission network and the SMs in *Area 1*. The scenario 2 and 4 describe the events of setpoint change in load and the feed-in power by VSI. It is designed for validation of the DT in *Area 2* and *Area 3*. Figure 5.32 presents the dynamics of voltage at generator buses with simulation of scenarios 1, 3, 5, and 6. The solid lines in the figure show the measurement of the voltages from the reference system at generator buses (bus 9, bus 10, bus 11, and bus 12). The corresponding dash lines present

the simulated results of the same scenarios by DT. It is seen that the dash line coincides with the solid line, which means that DT is able to replicate the voltage dynamic feature of reference objective in *Area 1* for simulating these scenarios. The 1- RMSEs of the voltage between DT and reference network shown in the figure are presented in Table 5.7.

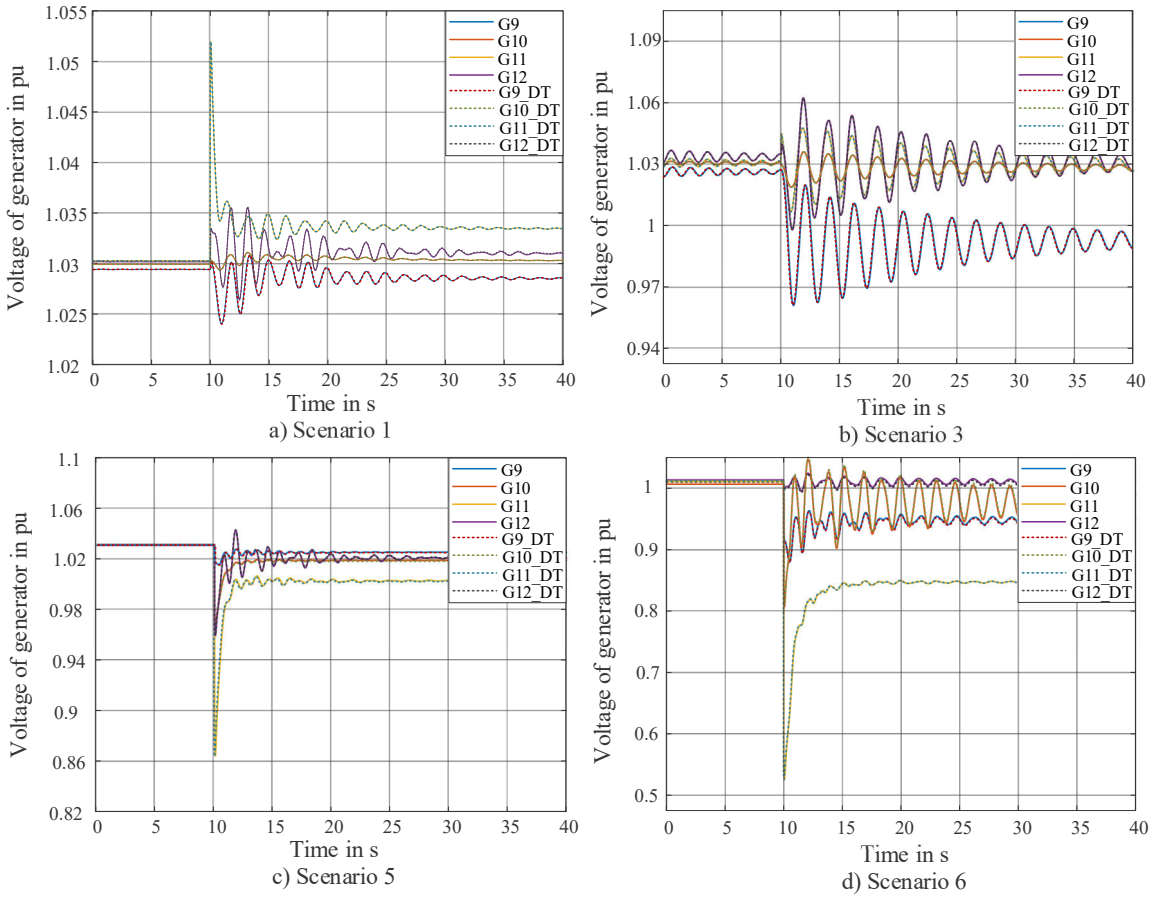

Figure 5.32: Voltage dynamics of DT and reference objective in *Area 1* for validation scenarios

To validate the accuracy of the DT in replication of the dynamics in the reference objective, the fitting rate between the solid lines and dash lines in Figure 5.32 is calculated in Table 5.7. The results show the 1-RMSE values of voltage data at bus 9, 10, 11, and 12 between DT and the reference objective. It is presented that the accuracy of the DT in these scenarios is over 99% similar to the reference network, which means that the DT is precise in replication of the reference network after parameter estimation.

Table 5.7: 1-RMSE of the voltages and rotor speed for scenario 1, 3, 5, and 6

No.		1-RMSE (Voltage)	1-RMSE (Rotor Speed)
Scenario 1	G9 and G9 DT	99.94%	99.98%
	G10 and G10 DT	99.76%	99.87%

	G11 and G11 DT	99.87%	99.88%
	G12 and G12 DT	99.18%	99.65%
Scenario 3	G9 and G9 DT	99.65%	99.98%
	G10 and G10 DT	99.77%	99.87%
	G11 and G11 DT	99.82%	99.88%
	G12 and G12 DT	99.12%	99.65%
Scenario 5	G9 and G9 DT	99.75%	99.98%
	G10 and G10 DT	99.77%	99.87%
	G11 and G11 DT	99.86%	99.88%
	G12 and G12 DT	99.14%	99.65%
Scenario 6	G9 and G9 DT	99.63%	99.98%
	G10 and G10 DT	99.72%	99.87%
	G11 and G11 DT	99.83%	99.88%
	G12 and G12 DT	99.16%	99.65%

Except for the voltage dynamics, the dynamics of rotor speed for the SMs in DT and reference objective are shown in Figure 5.33. It can be seen that the dash lines are overlaid with the solid lines, which means the DT (dash lines) is precise in replication of the dynamics of SMs in reference objective. According to Figure 5.33 b), the DT can be also accurate in triggering dynamics of SMs for outage events. The accuracy is evaluated by RMSE values shown in Table 5.7. The values of 1-RMSE are over 99%. It means that the similarity of the rotor speed dynamics between DT SM and SM in reference network is over 99%, which could be validated that the parameter estimation methods explained in the last section are effective in building DT.

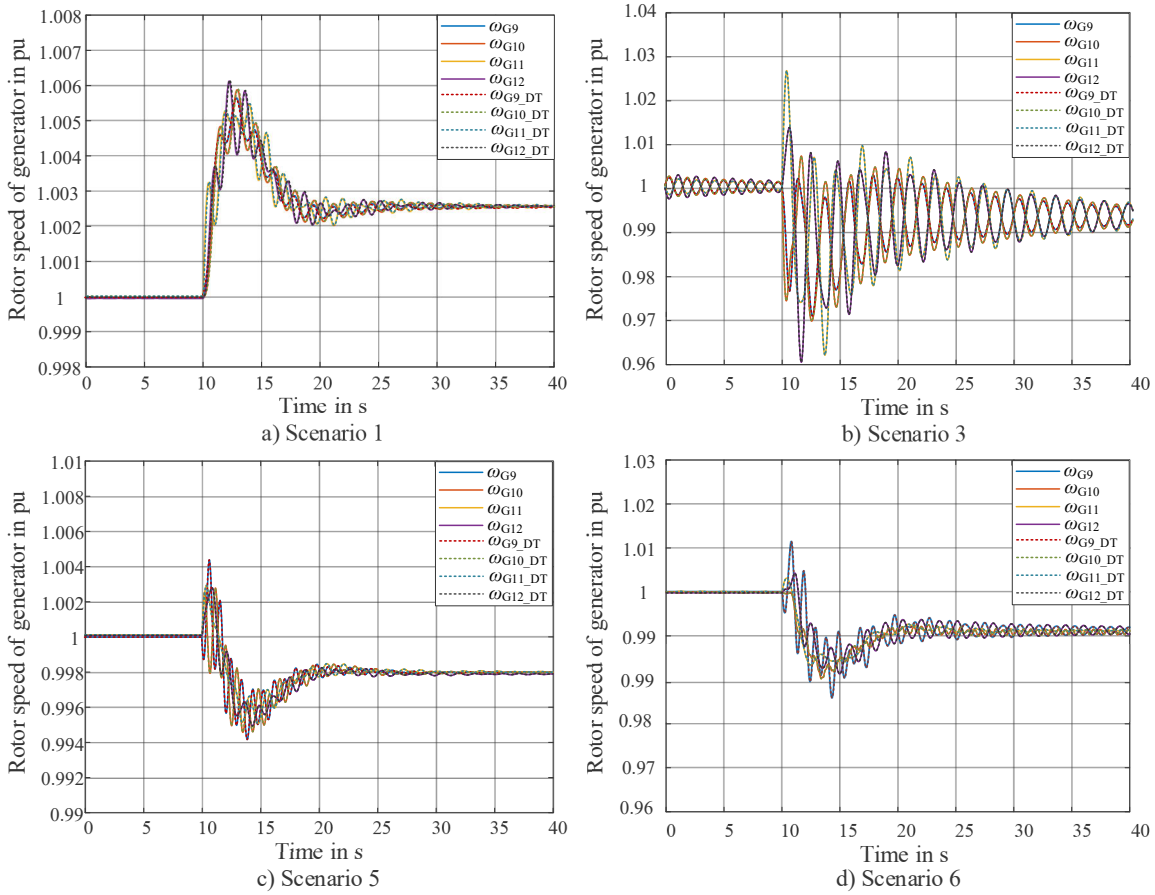

Figure 5.33: Rotor dynamics of DT and reference objectives for validation scenarios

Scenario 2 and 4 are designed for validation of the DT in *Area 2* and *Area 3*. The validation results of both scenarios for the voltage dynamics are shown in Figure 5.34. In Figure 5.34 a), the drop of load on bus 17 (in *Area 2*) leads to the increasing of the operation point for voltage in this area. The voltage is oscillated without changing the operation point in *Area 3*. It can be seen that the dash lines (DT) are overlaid with the solid lines (reference network) with a high similarity degree.

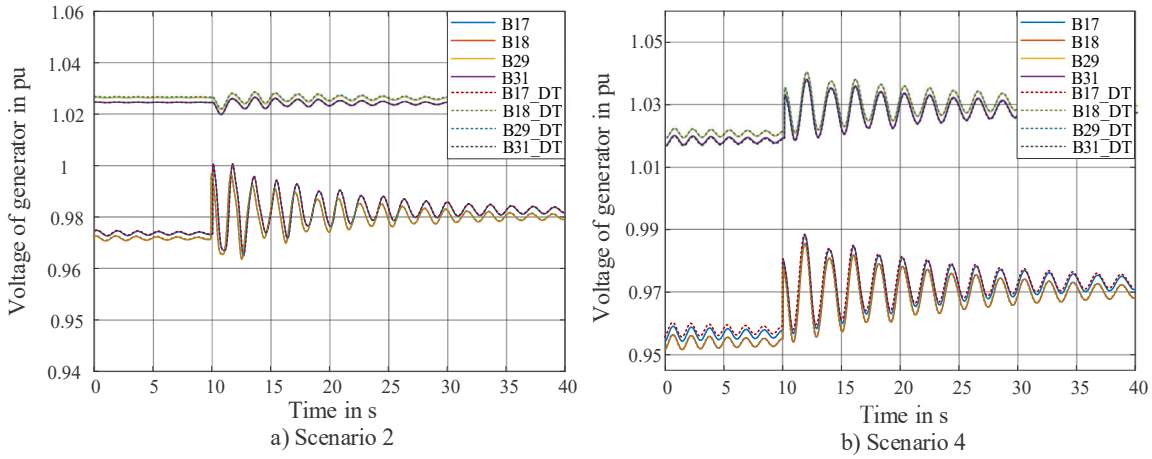

Figure 5.34: Validation of voltage dynamics between DT and reference network

Figure 5.34 b) depicts the voltage dynamics of scenario 4 with changing the setpoint of feed-in power of inverters on bus 25-27 and bus 40-42 in both areas. The setpoint of these inverters is increased from 4.75 MW to 10 MW at 10s. This results in the voltage rise and the oscillation before the stationary state of the new operation pinot. DT shows also high accuracy for replicating reference systems in scenario 4.

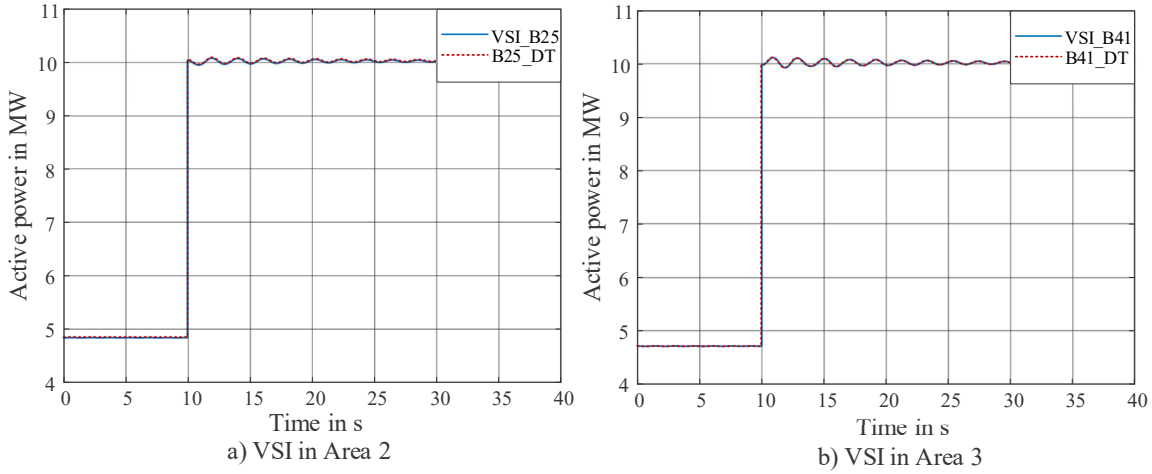

Figure 5.35: Validation of active power dynamics between DT and reference network

Except for the validation of the voltage dynamics in distribution grids, the dynamic of inverter, i.e., the dynamics of feed-in power of inverters in DT is validated to evaluate the parameter estimation for inverter. Figure 5.35 shows the results of dynamic feature for VSI in scenario 4. The setpoint of inverters on buses 25-27 and 40-42 rise to 10 MW. It can be seen that the operation state is oscillated at the first 15s by reaching to new stationary state. The inverter DTs at bus 25 and 41 are not only identical with the reference system in stationary state, but also they are accurate in the oscillation state.

Table 5.8: 1- RMSE of the voltages and active power of VSI for scenario 2 and 4

No.		1-RMSE (Voltage)	1-RMSE (Active power)
Scenario 2	B17 and B17 DT	99.78%	-
	B18 and B18 DT	99.69%	-
	B29 and B29 DT	99.97%	-
	B31 and B31 DT	99.88%	-
Scenario 4	B17 and B17 DT	99.78%	-
	B18 and B18 DT	99.89%	-
	B29 and B29 DT	99.84%	-
	B31 and B31 DT	99.88%	-
	VSI 25 and VSI 25 DT	99.96%	99.96%
	VSI 41 and VSI 41 DT	99.91%	99.93%

The similarity degree of the voltage and active power in *Area 2* and *Area 3* is calculated in Table 5.8. In scenario 2, DT is over 99% identical with reference objective for voltage dynamics. Because of no feed-in power with VSI in this scenario, the dynamics of active power are not considered. The dynamics of active power on bus 25 and bus 41 are observed, and the VSI DT of both buses is over 99.9% similar to the VSIs in reference system. According to it, these values verify that the parameter estimation methods mentioned in the last section are effective in building VSI DT.

5.3 Digital Twin application for anomaly event identification

The results in the previous section demonstrate a DT with the accurate performance for the replication of the dynamic feature for reference power grid. Except for applying the DT in monitoring the states of physical system, the anomaly event identification by Machine Learning assisted with DT is validated with case studies in this section. Figure 5.36 depicts the schema of the anomaly identification by Machine Learning assisted by DT. The events are initially simulated offline randomly in DT for generation of the training data. Each event is fingerprinted with the simulation result represented by vector signal with voltage ($\boldsymbol{u}$), current ($\boldsymbol{i}$), active- and reactive power ($\boldsymbol{p}, \boldsymbol{q}$), or the frequency ($\boldsymbol{f}$). The labeled vector data is applied in training of Machine Learning. Afterward, the trained algorithm is applied for the identification of the measurement from the physical system.

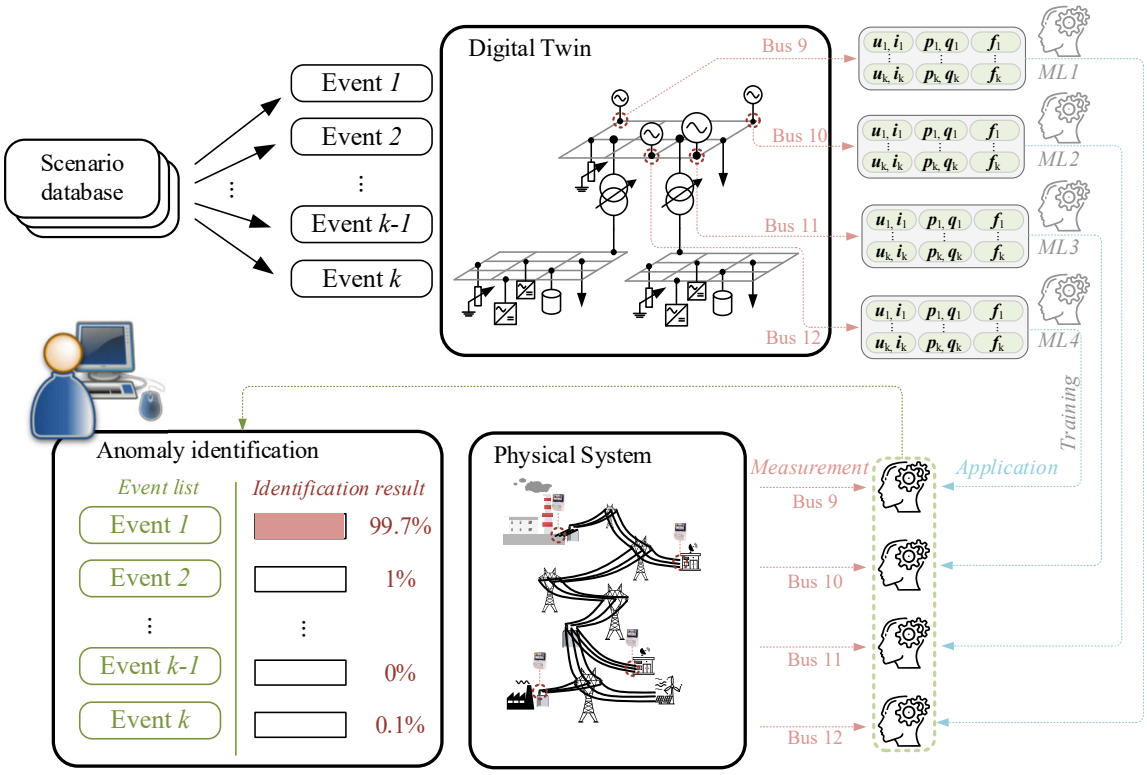

Figure 5.36: Schema of anomaly event identification with DT and Machine Learning

To evaluate the accuracy of the algorithms in Machine Learning for the anomaly identification illustrated in chapter 4, the dataset for training the Machine Learning is initially generated with simulation of events in the DT. DT-based event simulation in this work provides four types of events for the simulation: three-phase-to-ground fault on the line, three-phase-to-ground fault on the bus, line out-of-service, setpoint change of the load and the inverter. Due to the single-phase simulation in DT, the one-phase and two-phase related fault events are not taken into account for the identification in this work. This thesis is focused on the validation of the identification of these four event.

Table 5.9: Trial experiments to generate data for training process

Event type	Scenario description	Measured variable
Bus contingency (Anomaly 1)	3-phase short circuit on the buses in DT	Voltage and current on B9, B10, B11, B12, B16, B21, B26, B28, B31, B36, and B41
Line out (Anomaly 2)	Line out of service in DT	Voltage and current on B9, B10, B11, B12, B16, B21, B26, B28, B31, B36, and B41

Line contingency (Anomaly 3)	Line short circuit in DT (10 km, 20km, ⋯, 100km)	Voltage and current on B9, B10, B11, B12, B16, B21, B26, B28, B31, B36, and B41
Setpoint change (Anomaly 4)	Setpoint change of feed-in power of inverter and load	Voltage and current on B9, B10, B11, B12, B16, B21, B26, B28, B31, B36, and B41

It is assumed that four measurements are available in three areas of the reference objective respectively. As is shown in Figure 5.36, four generator buses are installed with the measurement units. In distribution grid level, the bus 13, 16, 21 and 26 are assumed in *Area 2* to set up with the measurement point. In *Area 3*, the bus 28, 31, 36 and 41 are installed with the measurements. The random trial experiments for generation of data in training process are operated according to Table 5.9. Each type of the event is simulated in all the buses and lines for generating the complete database. The line contingency, i.e., three phase short circuit is simulated on the line with different distance to train the Machine Learning for location detection. The feature data of voltage and current in DT are collected, and then applied to calculate the threshold value for CART, *k*NN, and SVM.

The normalized value of voltage and current are generated with 251 cases, which include 42 bus outage cases, 39 line-out cases, 90 cases for line outage with different locations, 39 cases for line outage in distribution grid, and 41 setpoint changes of inverter and load. The objective is to train the Machine Learning with the data of the above mentioned events, and then implement the trained algorithms into reference system for anomaly identification. The evaluation of the accuracy for anomaly identification by Machine Learning utilizes the confusion matrix [221]. The possible outcomes of the identification results are summarized in Table 5.11.

Table 5.10: Confusion matrix for the possible outcomes of the anomaly identification

		Identified	
		Normal	Anomaly 1-4
Actual	Normal	True Negative (TN)	False Positive (FP)
	Anomaly 1-4	False Negative (FN)	True Positive (TP)

The accuracy rate depicts the correct identified fraction (anomaly and normal state). In multiclass classification, the accuracy is equal to the Jaccard index, which describes the size of the intersection divided by the size of the union label sets [221, 222].

$$Accuracy = \frac{TP + TN}{TP + TN + FN + TP} \tag{5.2}$$

The idea of utilization of *k*NN is to calculate the *FI* for each anomaly by simulation in DT. Figure 5.37 shows the simulation results of four different scenarios depicted in Table 5.9 on buses (B9, B10, B11, B12). It is presented that four anomalies happened in 320s. These events result in individual dynamic behaviour for voltage. The classification by *k*NN depends on the value of FI on each buses. Because the distance between each bus and the anomaly location, the amplitude of voltage dynamics on these buses has different feature, which leads to the different FI values for the identification. The anomaly 2 represents the voltage dynamics of line open circuit between B3 and B4. The values of FI for anomaly on B9, 10, 11 and 12 are 1.008, 1.036, 1.051 and 1.061. The dynamic between 160s and 240s shows the voltage feature of anomaly 3 i.e. three-phase-to-ground short circuit on the line between B2 and B5 on B9, 10, 11 and 12. It is illustrated that this line outage has a worse impact on B10. The FI value to identify this anomaly on B10 after calculation is 1.12. The other values on B9, 11 and 12 are 1.005, 1.08 and 1.09 separately.

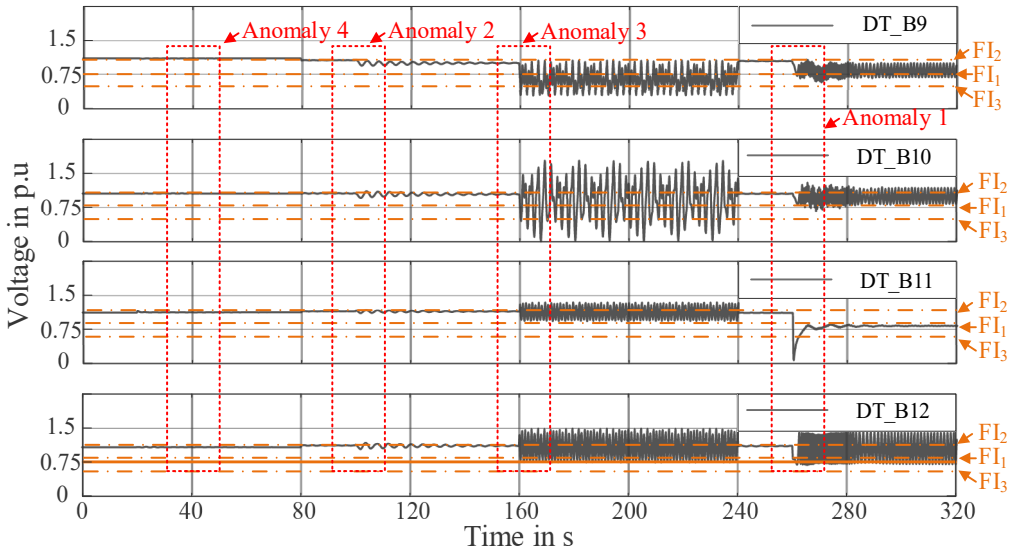

Figure 5.37: Classification of anomaly with voltage fault indicator

The validation of the accuracy for the identification of anomaly with *k*NN index FI mentioned above is illustrated with the confusion matrix in Figure 5.38. There are 260 events mixed up with anomalies 1 to 4 and normal events simulated in DT for the identification. The identification of anomaly 1 and 3 has the highest accuracy with 99.8% and 98%. The anomaly 2 and anomaly 4 have the similar FI values, which lead to low accuracy for the identification. It can be seen from Figure 5.37 that the voltage dynamics of anomaly 2 and

4 are not as apparent as the others, which are like the normal states. There are 3.5% (misidentified as anomaly 2) and 1.5% (misidentified as normal states) misidentification rate separately for anomaly 4.

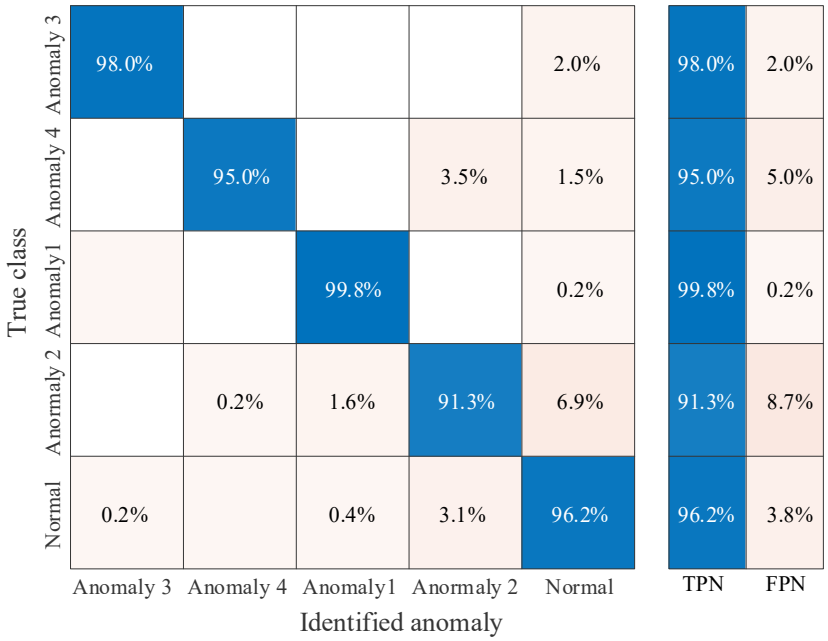

Figure 5.38: Confusion matrix of anomaly identification with *k*NN

Except for the confusion matrix, the Receiver Operating Characteristic (ROC) curve [223] is used as the evaluation for the identification's performance. It is a cross-validated estimate of the identification accuracy i.e., the probability of a correct response. The plotted values of the probability of true positive rate and the false positive rate are called the ROC curve. The curve is mainly of use when visualizing the performance of the identification as the decision threshold is varied. Any point on the curve is a possible operation point for the identification and so can be evaluated in the same manner as accuracy. Figure 5.39 shows the ROC curve and the corresponding area under the curve (AUC) of the identification performance for anomaly 1-4. The orange marker on the ROC curve presents the current TPN and FPN of the identification for different anomalies. The ROC curves and AUCs of four anomalies show high accuracy in the identification process.

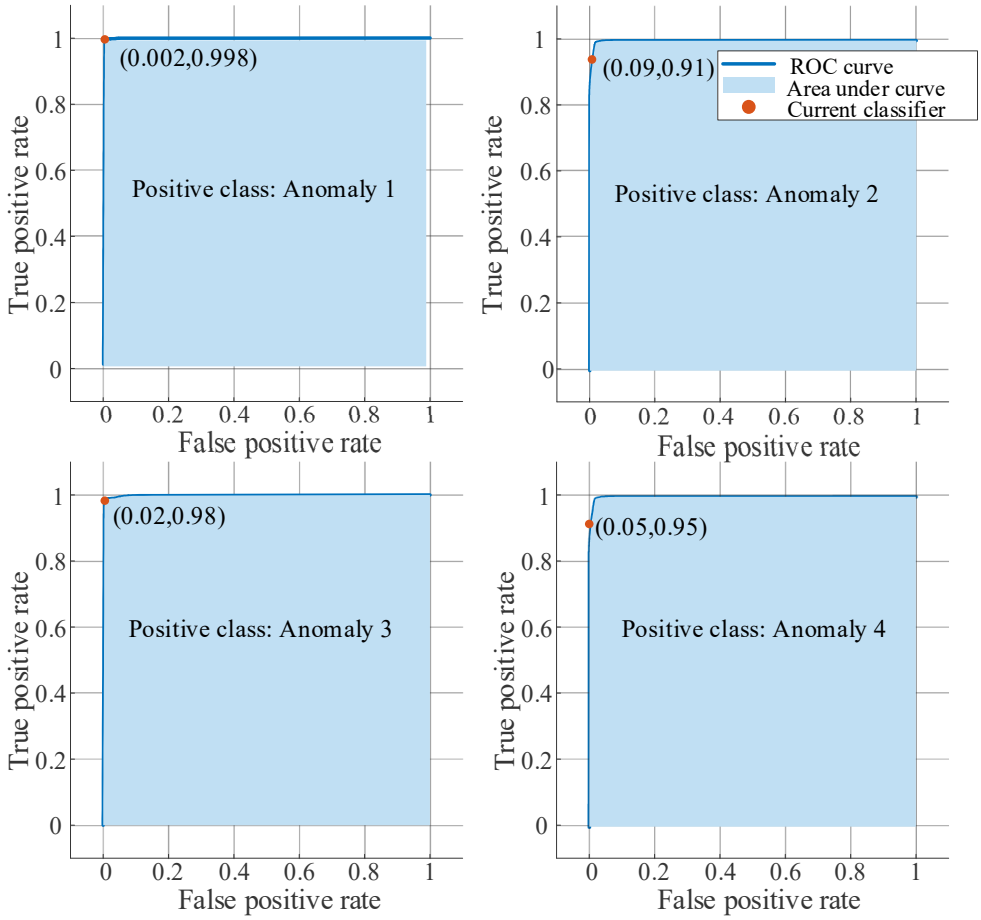

Figure 5.39: ROC curve for *k*NN in anomaly identification

The structure of the decision tree used in this work is shown in Figure 5.40. The simulation results in DT are utilized to calculate the threshold values in vector $\boldsymbol{x}_1, \boldsymbol{x}_2, \cdots, \boldsymbol{x}_5$. They are the key features in decision tree for the identification. The Gini index of voltage and current variable are 0.89 and 0.88. It means that both variables can be used for anomaly identification. The condition for the classification of first two leaf nodes is $\boldsymbol{x}_1$=[Δu=0.2 p.u., Δi=0.15 p.u.,0.95 p.u.<u<1.05 p.u.,0.9 p.u.<i<1.1 p.u.]. These feature values in $\boldsymbol{x}_1$ are decided with the simulations in DT and then applied into identification. With conditions in $\boldsymbol{x}_1$, two leaf nodes are divided: small signal events and outages events. The conditions in $\boldsymbol{x}_2$ =[Δu=0.05 p.u.,Δi=0.02 p.u.,0.98 p.u.<u<1.02 p.u.,0.95 p.u.<i<1.03 p.u.] and $\boldsymbol{x}_3$ = [Δu=0.01 p.u.,Δi=0.01 p.u.,0.98 p.u.<u<1.01 p.u.,0.98 p.u.<i<1.01 p.u.] are used to classify normal and anomaly 4. The anomaly 1-3 are identified in decision tree with threshold vector $\boldsymbol{x}_4$ =[$\Delta u_{\min}$=0.25 p.u.,$\Delta i_{\min}$=0.25 p.u.,0.8 p.u.<u<0.95 p.u.or 1.05 p.u.<u<1.15 p.u.,0.8 p.u.<i<0.95 p.u. or 1.06 p.u.<i<1.18 p.u.] and $\boldsymbol{x}_5$ = [$\Delta u_{\min}$ =0.28 p.u.,$\Delta i_{\min}$ =0.3 p.u., 0.1 p.u.<u<0.6 p.u.or u>1.2 p.u.,i>1.3 p.u.].

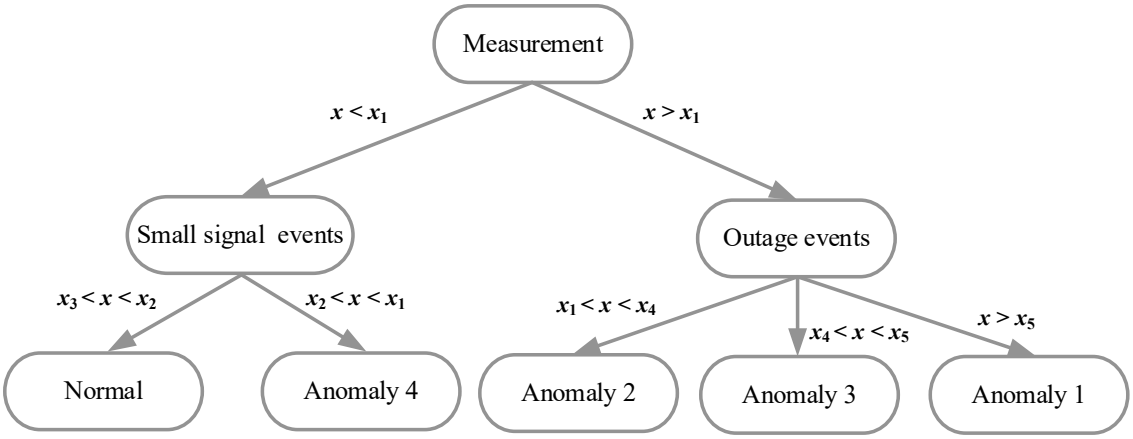

Figure 5.40: Schema of decision tree for anomaly identification

The results with decision tree in anomaly identification are illustrated with the confusion matrix in Figure 5.41. It can be seen that the accuracy of identification for anomaly 1 by decision tree is the highest, which has a 100% identification rate. The second identification rate is anomaly 3, which has 97.7% accuracy for the anomaly identification. There is a 2.3% misidentification rate to anomaly 1. Because of the line-outage event on the essential lines (e.g. line between B2 and B5), it results in significant voltage and current changes on the measurement point, which leads to the misidentification of the anomaly 3 as the anomaly 1.

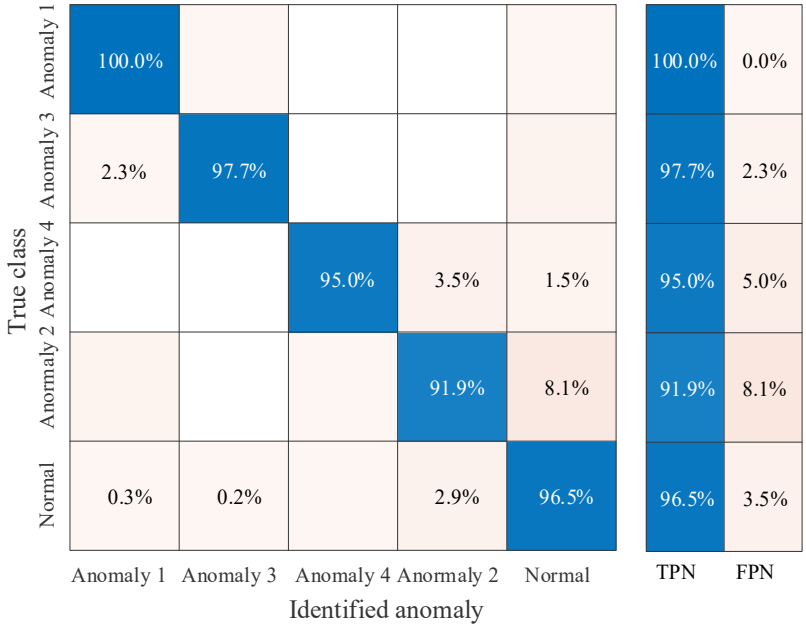

Figure 5.41: Confusion matrix of anomaly identification with decision tree

The anomaly 4 has the lowest accuracy because of the 8.1% misidentification the anomaly 4 as normal operation states in power grid. The changes of load and VSI in the distribution

network have a tiny influence on the transmission network, which leads to minor fluctuation of the measured states on B9, B10, B11 and B12. Accordingly, these events are identified as the 'Normal' with the Machine Learnings in transmission network. The ROC curve of the identification for anomaly 1-4 is shown in Figure 5.42. Except for anomaly 2, the false positive rate of the identification for anomaly 1, 3 and 4 is zero, which means an high performance of the identification. The AUC of the ROC curve in anomaly 2 is 0.98, which is presented that the predictive error rate in identifying this anomaly is 2%. The false positive rate of anomaly 2 identifier is also 2%. The other AUCs of the ROC curves are all equal to 1, which means that the anomaly identification is 100% correct.

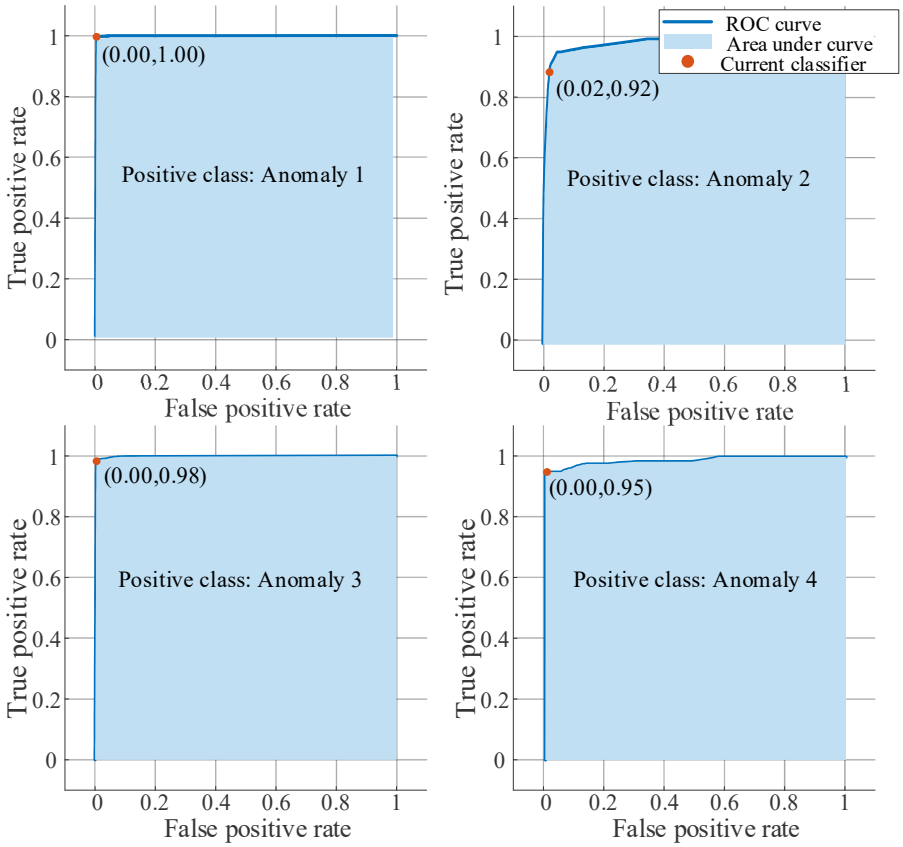

Figure 5.42: ROC curve for decision tree in anomaly identification

The anomaly identification with SVM is to find the appropriate support vectors as the key feature for the identification. Figure 5.43 depicts the identification results of anomaly 1-4 with SVM by voltage measurement on B10 and B12. The two dimension axis in the figure depicts the label data of voltage with different anomalies and the normal states. Each type is classified by a hyperplane. Its margin is decided with the support vector (see SV1 and SV2). With the training process, four hyperplanes are found for the classification of the five types. The normal type represents that there are no changes of the voltage variables. It can be seen in the figure that some of the labelled data (anomaly 1 with blue label and

anomaly 3 with orange label) are mixed up and overlaid, which means the misidentification. The identification accuracy and the misidentification rate are shown with confusion matrix in Figure 5.44.

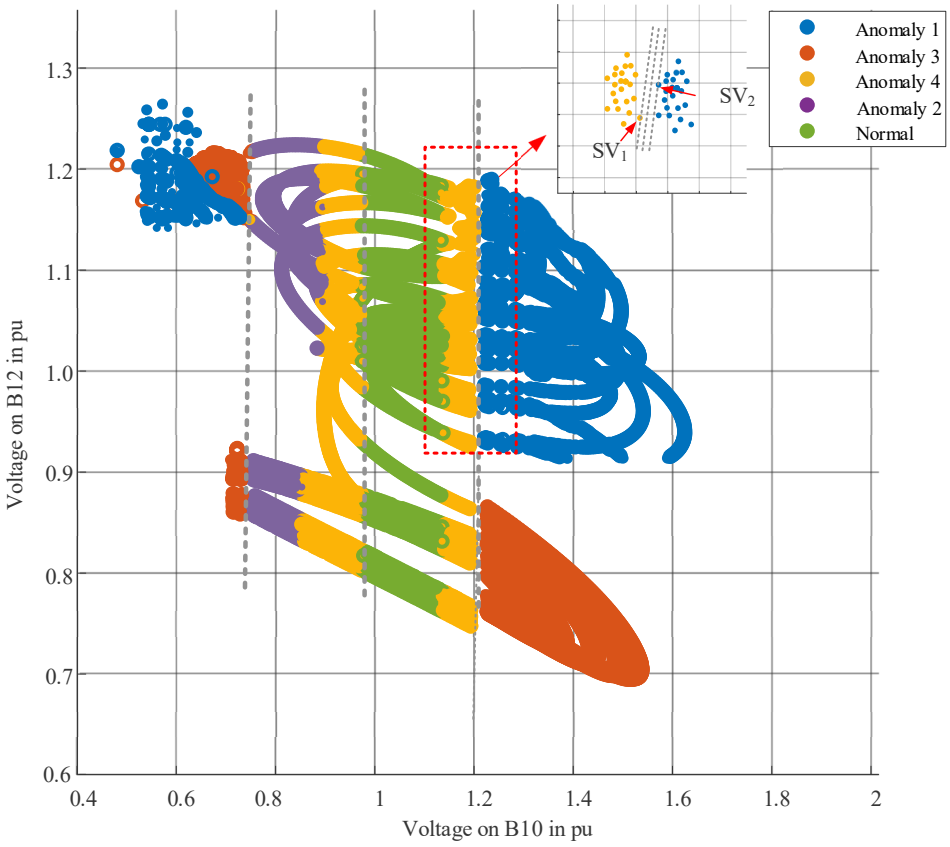

Figure 5.43: Result of anomaly identification with SVM

The confusion matrix of the SVM for anomaly identification is shown in Figure 5.44. It is illustrated that the anomaly 1 in numerical cases can be 100% identified by SVM. The anomaly 4 has over 20% misidentification rate including 17.5% misidentification of the anomaly 4 as the normal states.

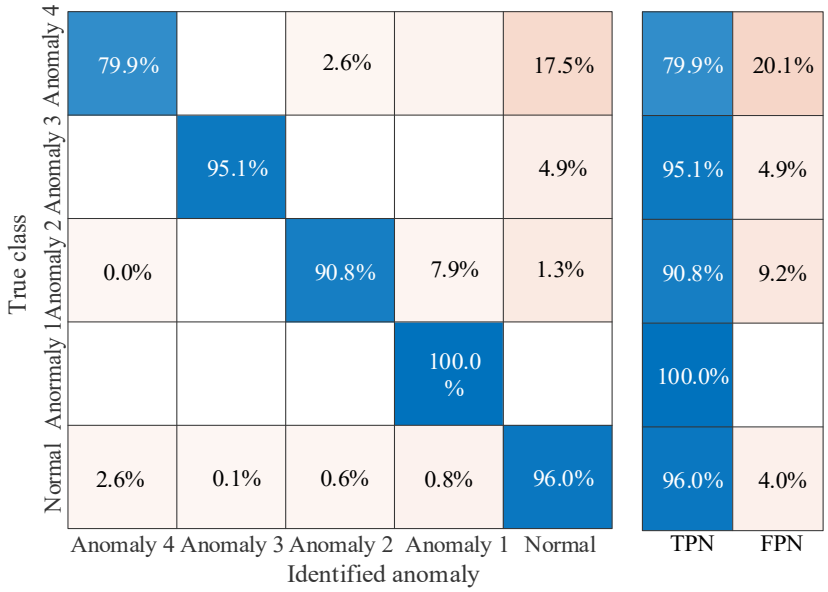

Figure 5.44: Confusion matrix of anomaly identification with SVM

There are about 3% misidentification of anomaly 4 as anomaly 2, which could be also presented in Figure 5.43 (see yellow and purple label data). The total accuracy in the numerical test cases with SVM is over 92%, which is lower than the last two methods but still in high performance in the anomaly identification. Except for it, the training process of SVM takes longer time than decision tree and *k*NN. Consequently, the identification results of three methods illustrate that the decision tree and *k*NN shows better performance and less consumption for the anomaly identification in this work.

5.4 Conclusion

The research questions addressed in this dissertation are "*Which parameter estimation method is suitable for Digital Twin creation?* (see Q1)" and "*How Digital Twin can be used for event identification?*" (see Q2). The parameter estimation methods presented in chapter 3 provide approaches for the DT creation to estimate correct parameters for the synchronous generator and the VSI inverter. Both components play an essential issue in the dynamics of the power system and decide the performance of the DT creation. The Machine Learning algorithm mentioned in chapter 4 presents a solution combined with DT for event identification. This work specifies the anomaly identification, which is simplified with DT as the event identification. The validation of the proposed parameter estimation method and the Machine Learning algorithm for the research questions is carried out with the numerical case studies in this chapter.

Based on the results of the investigated scenarios for the parameter estimation of DT with LSQ, RLS, and NN-identifier, it can be demonstrated that the presented approaches enable

the accurate estimation of the parameters with the measurement from the reference system. The square objective function is used to evaluate the deviation of the observed variables between DT and the reference network. The aim of the parameter estimation is to minimize the objective function by adopting the correct parameters in DT. LSQ is a non-linear algorithm and takes the longest time for the estimation process. SA is an option in parameter estimation with LSQ used to select the parameters correlated with the observed output. It can be used to simplify the complexity and time consumption in parameter estimation with LSQ. RLS is a linearization algorithm and can be used as an online estimation method. It is labelled with fast estimation speed but limited with the ARMAX equation of the DT. NN-identifier is an adaptive parameter estimation method. It uses a radial basis function for the estimation process, which requires no training process. Before the use of it, one restriction is that more measurable variables are required than the other two methods. The result of the case study for the event identification by Machine Learning demonstrates that *k*NN, DT, and SVM have high accuracy for the identification of anomaly events in the power system. Assisted with DT-based event simulation, all the potential happened events are simulated in DT to generate the training data. After the training process, the algorithms provide an averagely of over 96% accurate identification of the event type, which not only saves the manpower cost but also enables automatic identification in the power system.

6 Conclusion and outlook

6.1 Conclusion

To study the impacts caused by the decentralized RES and ensure reliable operation, an accurate simulation model referred to the physical, real power system is accordingly required. The concept of DT proposes a highly accurate digital model for the representation of the physical power system. The methods for building a DT of power system referred to as accurately replication of physical system are investigated in this work. The essential method for DT creation is parameter estimation. It is used to estimate the correct parameters of the dynamic components in the power system with the measurement from the reference network. Based on the created DT, one of the most important functions for the application is anomaly event identification. A quick and accurate anomaly event identification is essential for the stable operation and maintenance of the power system.

In this thesis, three parameter estimation methods, i.e., LSQ, RLS, and NN-identifier, are proposed to calculate the proper parameters for the DT with the measured variable from the physical power system. LSQ algorithm utilizes the square of the error to evaluate the deviation between DT and the reference network. The objective of the LSQ algorithm is to reach the minimized square error of the observed variable with the appropriate parameters. RLS is a linearized parameter estimation method, which uses recursive iteration to minimize the square error of the deviation between DT and reference network with the appropriate parameters. NN-identifier is the parameter estimation method on the basis of the radial basis function network. The radial basis function network checks the deviation between DT and reference network to match the proper weight parameters for the network to minimize the deviation. The numerical case studies are used to evaluate how accurate the proposed methods are to estimate parameters for DT and in which condition it can be used for the estimation. The investigation is carried out structured on the basis of the first research question Q1. The application of the DT in anomaly identification assisted by Machine Learning is addressed in Q2. The answer to both research questions is summarized in the following.

Q1 *Which parameter estimation method is suitable for Digital Twin creation?*

In this thesis, DT is referred to as a dynamic digital model that can accurately mirror the phenomena of the physical power system to replicate the operation states for monitoring. Besides, it can precisely predict the dynamic behaviour of the power system to generate

the training data for the identification of the type of the occurred event. The parameter estimation is used to adapt the real parameters in DT timely according to the actual states of the physical system. According to the results, the proposed LSQ algorithm is suitable for offline parameter estimation with available history measurement from the reference network, which, however, is not appropriate for the estimation of the numerous parameters because of its burden computation and long-time cost. RLS can be used as the online parameter estimation method, which requires the transformation of DT into ARMAX structure and retransformation of the estimated coefficients of the equations into the corresponding parameters. NN-identifier is suitable for the online adaptive parameter estimation for DT creation, which uses its learning character to adaptively modulate the proper parameters in DT for the reduction of the error between DT and the reference network.

Q2 How Digital Twin can be used for event identification?

Within the framework of this thesis, the application of DT assisted with Machine Learning for event identification is proposed. Under the condition of the created DT, it can be utilized to simulate all the potential events to generate the training data. The event data is like a fingerprint printed in the Machine Learning algorithm with the training process. The supervised learning algorithms *k*NN, decision tree, and SVM are proposed in this work to identify the anomaly. *k*NN utilizes the distance between the reference data windows in a time series and the identified data segments from measurement to evaluate similar properties for the identification. The decision tree makes use of the divide-and-conquer method to classify the data by sorting them down the tree from the root node to the leaf node. The key process is to determine the proper classification threshold in each node according to the training data. SVM aims to find the optimal hyperplane as the classification margin. The support vector is referred to the data points closest to the hyperplane, which decides the position and size of the margin. From the results of the case studies, the algorithms trained with plenty of data have excellent performance in accurate identification of the occurred event.

The following new scientific contributions were developed, and new findings were obtained to answer the above-mentioned research questions:

- Investigation and evaluation of the suitable parameter estimation algorithms for the DT creation
- LSQ algorithm suitable for non-linear system and offline parameter estimation; RLS and NN-identifier appropriate for online parameter estimation.

- Design of event identification framework with Machine Learning assisted DT, which is developed for the automatic identification and improvement of the accuracy in the identification.
- Demonstrate the feasibility of the parameter estimation for DT creation and the application in event identification with Machine Learning algorithm.

6.2 Outlook

The application of DT in power systems is not limited to anomaly event identification, as explicated in this work. This work is focused on the investigation of methods to build the DT and the demonstration of the anomaly identification framework with DT. The results in this work provide opportunities for further research of the DT in power system.

Because of the dynamic and varietal feature of the power grid, the DT could not be permanently identified with the physical system after one parameter estimation. Significantly, the topology changes in the physical power grid have a crucial impact on the estimation process. Accordingly, the investigation of how to update the topology and the corresponding new parameters of DT in time has to be considered.

In this work, the DAE of 6th order SM and voltage source inverter with standard overlaid voltage and current control, including the passive LC filter, are utilized for modelling of reference objective. There are still many other standard SM like 8th and VSI in the library. The selection of the appropriate digital model decides the accuracy of the DT and the consumption of the parameter estimation process. It should be noted that the more complexity of the dynamic component built in the digital model leads to more estimation consumption of parameters.

In the physical power grid, the measurement of voltage and current includes harmonics, leading to inaccuracy for parameter estimation. It should be considered that the harmonic needs to be taken into account for the modelling of DT. With it, the dynamics in DT is closer to the actual physical behaviour. The DT should be validated with the measurements and could then be applied for monitoring of physical power grid.

The DT is more intelligent with the assistance of Machine Learning. Due to its powerful data processing ability, the future power system can utilize it for automatic dealing with enormous data streams with the purpose of quick and exact analysis and optimization. By training the Machine Learning algorithm with the history data, it can study the inherent feature in the past time and give the potential prediction in the future. It plays an important role in the protection system of the power grid to set up the protective device in advance. There are still many application fields for DT in the power system to be investigated as proposed in section 2.2, such as cyber-physical surveillance as well as security assessment.

It is essential to support the operator to make the decision for keeping the stable operation in the power system.

7 Reference

[1] Deutsche Bundesregierung, *Energiekonzept für eine umweltschonende, zuverlässige und bezahlbare Energieversorgung*, 2010.

[2] Europäische Kommission, *Ein sauberer Planet für alle Eine Europäische strategische, langfristige Vision für eine wohlhabende, moderne,wettbewerbsfähige und klimaneutrale Wirtschaft.* [Online]. Verfügbar unter: https://eur-lex.europa.eu/legal-content/DE/TXT/PDF/?uri=CELEX:52018DC0773&from=EN.

[3] Publications Office of the European Union, *Energy roadmap 2050*. Luxembourg, 2012.

[4] Umwelt Bundesamt, *Erneuerbare Energien in Deutschland Daten zur Entwicklung im Jahr 2020.* [Online]. Verfügbar unter: https://www.umweltbundesamt.de/sites/default/files/medien/5750/publikationen/2021_hgp_erneuerbareenergien_deutsch_bf.pdf (Zugriff am: März 2021).

[5] S. Rahmstorf und A. Ganopolski, „Long-term global warming scenarios computed with an efficient coupled climate model“, *Climatic Change*, Jg. 43, Nr. 2, S. 353–367, 1999, doi: 10.1023/A:1005474526406.

[6] A. J. Schwab, *Elektroenergiesysteme*. Berlin, Heidelberg: Springer Berlin Heidelberg, 2009.

[7] European Energy Agency, *Renewable energy in Europe – 2017 Update: Recent growth and knock-on effects*. Luxembourg, 2017.

[8] Bundesverband der Energie- und Wasserwirtschaft, *Bruttostromverbrauch in Deutschland bis 2020.* [Online]. Verfügbar unter: https://de.statista.com/statistik/daten/studie/256942/umfrage/bruttostromverbrauch-in-deutschland/ (Zugriff am: Dezember 2020).

[9] Prof. Dr. Bruno Burger, *Stromerzeugung in Deutschland im Jahr 2020.* [Online]. Verfügbar unter: https://www.ise.fraunhofer.de/de/presse-und-medien/news/2020/nettostromerzeugung-in-deutschland-2021-erneuerbare-energien-erstmals-ueber-50-prozent.html (Zugriff am: 4. Januar 2021).

[10] Bundesnetzagentur, *Monitoringbericht 2020.* [Online]. Verfügbar unter: https://www.bundesnetzagentur.de/SharedDocs/Mediathek/Berichte/2020/Monitoringbericht_Energie2020.pdf?__blob=publicationFile&v=7.

[11] F. Blaabjerg, A. Consoli, J. A. Ferreira und J. D. vanWyk, „The Future of Electronic Power Processing and Conversion“, *IEEE Trans. Power Electron.*, Jg. 20, Nr. 3, S. 715–720, 2005, doi: 10.1109/TPEL.2005.846516.

[12] Deutsche Energie-Agentur, *Ausbau- und Innovationsbedarf der Stromverteilnetze in Deutschland bis 2030.* [Online]. Verfügbar unter: https://www.dena.de/fileadmin/dena/Dokumente/Pdf/9100_dena-Verteilnetzstudie_Abschlussbericht.pdf (Zugriff am: Dezember 2012).

[13] Francisco Gonzalez-Longatt, „Section 1. Introduction to Power System Simulation“, 2020.

[14] D. Jakominich, R. Krebs, D. Retzmann und A. Kumar, „Real time digital power system simulator design considerations and relay performance evaluation“, *IEEE Trans. Power Delivery*, Jg. 14, Nr. 3, S. 773–781, 1999, doi: 10.1109/61.772314.

[15] S. Weyer, T. Meyer, M. Ohmer, D. Gorecky und D. Zühlke, „Future Modeling and Simulation of CPS-based Factories: an Example from the Automotive Industry“, *IFAC-PapersOnLine*, Jg. 49, Nr. 31, S. 97–102, 2016, doi: 10.1016/j.ifacol.2016.12.168.

[16] B. M. Buchholz, D. Povh und D. Retzmann, „Stability analysis for large power system interconnections in Europe“ in *2005 IEEE Russia Power Tech*, St. Petersburg, Russia, 062005, S. 1–7, doi: 10.1109/PTC.2005.4524416.

[17] M. Grieves, „Digital Twin: Manufacturing Excellence through Virtual Factory Replication“ in . [Online]. Verfügbar unter: https://www.researchgate.net/publication/275211047

[18] Q. Qi und F. Tao, „Digital Twin and Big Data Towards Smart Manufacturing and Industry 4.0: 360 Degree Comparison“, *IEEE Access*, Jg. 6, S. 3585–3593, 2018, doi: 10.1109/ACCESS.2018.2793265.

[19] F. Tao, H. Zhang, A. Liu und A. Y. C. Nee, „Digital Twin in Industry: State-of-the-Art“, *IEEE Trans. Ind. Inf.*, Jg. 15, Nr. 4, S. 2405–2415, 2019, doi: 10.1109/TII.2018.2873186.

[20] E. Glaessgen und D. Stargel, „The Digital Twin Paradigm for Future NASA and U.S. Air Force Vehicles“ in *53rd AIAA/ASME/ASCE/AHS/ASC Structures, Structural Dynamics and Materials Conference
20th AIAA/ASME/AHS Adaptive Structures Conference
14th AIAA*, Honolulu, Hawaii, 04232012, doi: 10.2514/6.2012-1818.

[21] W. Qiong, L. Wenyin, Y. Yihan, Z. Chuan und L. Yong, „Intelligent Decision Support System for Power Grid Dispatching Based on Multi-Agent System“ in *2006 International Conference on Power System Technology*, Chongqing, China, 102006, S. 1–5, doi: 10.1109/ICPST.2006.321468.

[22] X. Song, H. Cai, J. Kircheis, T. Jiang, S. Schlegel und D. Westermann, „Application of Digital Twin Assistant-System in State Estimation for Inverter Dominated Grid“ in *2020 55th International Universities Power Engineering Conference (UPEC)*, Torino, Italy, 92020, S. 1–6, doi: 10.1109/UPEC49904.2020.9209876.

[23] X. Song, T. Jiang, S. Schlegel und D. Westermann, „Parameter tuning for dynamic digital twins in inverter-dominated distribution grid“, *IET Renewable Power Generation*, Jg. 14, Nr. 5, S. 811–821, 2020, doi: 10.1049/iet-rpg.2019.0163.

[24] L. Cai, N. F. Thornhill, S. Kuenzel und B. C. Pal, „Real-Time Detection of Power System Disturbances Based on k -Nearest Neighbor Analysis“, *IEEE Access*, Jg. 5, S. 5631–5639, 2017, doi: 10.1109/ACCESS.2017.2679006.

[25] P.-N. Tan, M. Steinbach, A. Karpatne und V. Kumar, *Introduction to data mining*. NY, NY: Pearson, 2020.

[26] Andreas Janecek, „Efficient Feature Reduction and Classification Methods: Application in Drug Discovery and Email Categorization“. DISSERTATION, Wien, Dezember/2009. [Online]. Verfügbar unter: https://homepage.univie.ac.at/andreas.janecek/stuff/dissertation-andreasjanecek.pdf

[27] E. E. Bernabeu, J. S. Thorp und V. Centeno, „Methodology for a Security/Dependability Adaptive Protection Scheme Based on Data Mining“, *IEEE Trans. Power Delivery*, Jg. 27, Nr. 1, S. 104–111, 2012, doi: 10.1109/TPWRD.2011.2168831.

[28] *IEEE Standard for Synchrophasor Data Transfer for Power Systems*, Piscataway, NJ, USA.

[29] J.-N. Paquin *et al.,* „Real-time simulation applications for future power systems and smart grids“ in *Artificial Intelligence for Smarter Power Systems: Fuzzy logic and neural networks*, M. G. Simões, Hg., Institution of Engineering and Technology, 2021, S. 9–64, doi: 10.1049/PBPO161E_ch2.

[30] H. Pan, Z. Dou, Y. Cai, W. Li, X. Lei und D. Han, „Digital Twin and Its Application in Power System“ in *2020 5th International Conference on Power and Renewable Energy (ICPRE)*, Shanghai, China, 9122020, S. 21–26, doi: 10.1109/ICPRE51194.2020.9233278.

[31] OPAL-RT TECHNOLOGIES, *Software toolboxes & Software bundles.* [Online]. Verfügbar unter: https://www.opal-rt.com/.

[32] Y. Himeur, K. Ghanem, A. Alsalemi, F. Bensaali und A. Amira, „Artificial intelligence based anomaly detection of energy consumption in buildings: A review, current trends and new perspectives“, *Applied Energy*, Jg. 287, S. 116601, 2021, doi: 10.1016/j.apenergy.2021.116601.

[33] J. Huang, L. Zhao, F. Wei und B. Cao, „The Application of Digital Twin on Power Industry“, *IOP Conf. Ser.: Earth Environ. Sci.*, Jg. 647, S. 12015, 2021, doi: 10.1088/1755-1315/647/1/012015.

[34] Z. Hasani und S. Krrabaj, „Survey and Proposal of an Adaptive Anomaly Detection Algorithm for Periodic Data Streams“, *JCC*, Jg. 07, Nr. 08, S. 33–55, 2019, doi: 10.4236/jcc.2019.78004.

[35] T. Ahmed-Ali, G. Kenné und F. Lamnabhi-Lagarrigue, „Nonlinear systems parameter estimation using neural networks: Application to synchronous machines“, *Mathematical and Computer Modelling of Dynamical Systems*, Jg. 13, Nr. 4, S. 365–382, 2007, doi: 10.1080/13873950600913787.

[36] S. CHEN und S. A. BILLINGS, „Neural networks for nonlinear dynamic system modelling and identification“, *International Journal of Control*, Jg. 56, Nr. 2, S. 319–346, 1992, doi: 10.1080/00207179208934317.

[37] R. Isermann und M. Münchhof, „State and Parameter Estimation by Kalman Filtering“ in *Identification of dynamic systems: An introduction with applications / Rolf Isermann, Marco Münchhof*, R. Isermann und M. Münchhof, Hg., Berlin: Springer, 2011, S. 539–551, doi: 10.1007/978-3-540-78879-9_21.

[38] C. i. g. r. Des électriques, *Benchmark systems for network integration of renewable and distributed energy resources*. [Paris] (21 rue d'Artois, 75008): CIGRÉ, 2014.

[39] X. Song, H.Cai T. Jiang, S. Schlegel and Dirk Westermann (Ed.), *Parameter Tuning for dynamic Digital Twin of Generation Unit in Power Grid*. ISGT-Europe, 2021..

[40] X. Song, H.Cai T. Jiang, S. Schlegel and Dirk Westermann (Ed.) (): *Surveillance of Operation States for Distributed Renewable Generations by Digital Twin*. CIGRE Symposium. Ljubljana, 2021.

[41] X. Song *et al.,* „Research on Performance of Real-Time Simulation Based on Inverter-Dominated Power Grid“, *IEEE Access*, Jg. 9, S. 1137–1153, 2021, doi: 10.1109/ACCESS.2020.3016177.

[42] J. Autiosalo, J. Vepsalainen, R. Viitala und K. Tammi, „A Feature-Based Framework for Structuring Industrial Digital Twins“, *IEEE Access*, Jg. 8, S. 1193–1208, 2020, doi: 10.1109/ACCESS.2019.2950507.

[43] OPAL-RT TECHNOLOGIES, *The 'Digital Twin' in Hardware in the Loop (HiL) Simulation: A Conceptual Primer.* [Online]. Verfügbar unter: https://www.opal-rt.com/the-digital-twin-in-hardware-in-the-loop-hil-simulation-a-conceptual-primer/.

[44] S. M. Miraftabzadeh, F. Foiadelli, M. Longo und M. Pasetti, „A Survey of Machine Learning Applications for Power System Analytics" in *2019 IEEE International Conference on Environment and Electrical Engineering and 2019 IEEE Industrial and Commercial Power Systems Europe (EEEIC / I&CPS Europe)*, Genova, Italy, 62019, S. 1–5, doi: 10.1109/EEEIC.2019.8783340.

[45] B. R. Barricelli, E. Casiraghi und D. Fogli, „A Survey on Digital Twin: Definitions, Characteristics, Applications, and Design Implications", *IEEE Access*, Jg. 7, S. 167653–167671, 2019, doi: 10.1109/ACCESS.2019.2953499.

[46] NASA, *The Ill-Fated Space Odyssey of Apollo 13.* [Online]. Verfügbar unter: https://er.jsc.nasa.gov/seh/pg13.htm (Zugriff am: 16. Oktober 2019.).

[47] M. Grieves, „Origins of the Digital Twin Concept", 2016.

[48] Kary Främling, Jan Holmström, Timo Ala-Risku, Mikko Kärkkäinen, „Product Agents for Handling Information about Physical Objects", Helsinki University of Technology, Laboratory of Information Processing Science, Espoo, Finland TKO-B 153/03, 28. Nov. 2003.

[49] E. J. Tuegel, A. R. Ingraffea, T. G. Eason und S. M. Spottswood, „Reengineering Aircraft Structural Life Prediction Using a Digital Twin", 2011, doi: 10.1155/2011/154798.

[50] *The Airframe Digital Twin: Some Challenges to Realization | Structures, Structural Dynamics, and Materials and Co-located Conferences* (Zugriff am: 18. September 2020).

[51] U.S. Air Force., *Global Horizons Final Report: United States Air Force Global Science and Technology Vision.* [Online]. Verfügbar unter: https://www.hsdl.org/?view&did=741377 (Zugriff am: 16. Oktober 2019.).

[52] J. Vachalek, L. Bartalsky, O. Rovny, D. Sismisova, M. Morhac und M. Loksik, „The digital twin of an industrial production line within the industry 4.0 concept" in *2017 21st International Conference on Process Control (PC)*, Strbske Pleso, Slovakia, 06.06.2017 - 09.06.2017, S. 258–262, doi: 10.1109/PC.2017.7976223.

[53] J. Ríos, J. Hernández, M. Oliva, and F. Mas, Hg., *Product avatar as digital counterpart of a physical individual product: Literature review and implications in an aircraft*, 2015.

[54] M. G. Simões, *Artificial Intelligence for Smarter Power Systems: Fuzzy logic and neural networks*. Institution of Engineering and Technology, 2021.

[55] K. Y. H. Lim, P. Zheng und C.-H. Chen, „A state-of-the-art survey of Digital Twin: techniques, engineering product lifecycle management and business innovation perspectives“, *J Intell Manuf*, Jg. 31, Nr. 6, S. 1313–1337, 2020, doi: 10.1007/s10845-019-01512-w.

[56] S. Yun, J.-H. Park und W.-T. Kim, „Data-centric middleware based digital twin platform for dependable cyber-physical systems“ in *2017 Ninth International Conference on Ubiquitous and Future Networks (ICUFN)*, Milan, 72017, S. 922–926, doi: 10.1109/ICUFN.2017.7993933.

[57] C. Brosinsky, X. Song, and D. Westermann, Hg., *Digital Twin - Concept of a Continuously Adaptive Power System Mirror*, 2019.

[58] F. Schweppe und J. Wildes, „Power System Static-State Estimation, Part I: Exact Model“, *IEEE Trans. on Power Apparatus and Syst.*, PAS-89, Nr. 1, S. 120–125, 1970, doi: 10.1109/TPAS.1970.292678.

[59] B. Xie *et al.,* „A Performance Comparison Study of Quasi-Dynamic State Estimation and Static State Estimation“ in *2020 IEEE Power & Energy Society General Meeting (PESGM)*, Montreal, QC, Canada, 822020, S. 1–5, doi: 10.1109/PESGM41954.2020.9282017.

[60] J. Zhao *et al.,* „Power System Dynamic State Estimation: Motivations, Definitions, Methodologies, and Future Work“, 2019, doi: 10.1109/TPWRS.2019.2894769.

[61] C. Bualek, W. Khunpeng, N. Eua-Anant und T. Paukatong, „Protocol modification between substation and control center with IEC 60870-5-104“ in *2011 IEEE International Conference on Advanced Power System Automation and Protection (APAP)*, Beijing, China, 102011, S. 766–769, doi: 10.1109/APAP.2011.6180502.

[62] Quoc Dong Vu, „Parameter Estimation in Complex Nonlinear Dynamical Systems“. Dissertation, Technischen Universit¨at Ilmenau, 2015.

[63] J. Sjöberg *et al.,* „Nonlinear black-box modeling in system identification: a unified overview“, *Automatica*, Jg. 31, Nr. 12, S. 1691–1724, 1995, doi: 10.1016/0005-1098(95)00120-8.

[64] Y. Bard, *Nonlinear parameter estimation*. London: Academic Press, New York.

[65] W. R. Esposito und C. A. Floudas, „Global Optimization for the Parameter Estimation of Differential-Algebraic Systems“, *Ind. Eng. Chem. Res.*, Jg. 39, Nr. 5, S. 1291–1310, 2000, doi: 10.1021/ie990486w.

[66] I. D. Landau, B. Anderson und F. Bruyne, „Recursive identification algorithms for continuous-time nonlinear plants operating in closed loop“, *Automatica*, Jg. 37, Nr. 3, S. 469–475, 2001, doi: 10.1016/S0005-1098(00)00171-0.

[67] I. D. Landau und A. Karimi, „A recursive algorithm for ARMAX model identification in closed loop“, *IEEE Trans. Automat. Contr.*, Jg. 44, Nr. 4, S. 840–843, 1999, doi: 10.1109/9.754830.

[68] S. CHEN, S. A. BILLINGS, C. F. N. COWAN und P. M. GRANT, „Practical identification of NARMAX models using radial basis functions“, *International Journal of Control*, Jg. 52, Nr. 6, S. 1327–1350, 1990, doi: 10.1080/00207179008953599.

[69] S. Mohagheghi, Jung-Wook Park, R. G. Harley, G. K. Venayagamoorthy und M. L. Crow, „An adaptive neural network identifier for effective control of a static compensator connected to a power system“ in *Proceedings of the International Joint Conference on Neural Networks, 2003*, 2003, 2964-2969 vol.4, doi: 10.1109/IJCNN.2003.1224042.

[70] G. Kenné, T. Ahmed-Ali, F. Lamnabhi-Lagarrigue und H. Nkwawo, „Nonlinear systems parameters estimation using radial basis function network“, *Control Engineering Practice*, Jg. 14, Nr. 7, S. 819–832, 2006, doi: 10.1016/j.conengprac.2005.04.002.

[71] R. Gelli und G. Manimaran, „Anomaly Detection and Mitigation for Wide-Area Damping Control using Machine Learning“ in *2020 IEEE Power & Energy Society General Meeting (PESGM)*, Montreal, QC, Canada, 822020, S. 1, doi: 10.1109/PESGM41954.2020.9281615.

[72] Xiaodong Zhang, M. M. Polycarpou und T. Parisini, „A robust detection and isolation scheme for abrupt and incipient faults in nonlinear systems“, *IEEE Transactions on Automatic Control*, Jg. 47, Nr. 4, S. 576–593, 2002, doi: 10.1109/9.995036.

[73] R. A. Sowah *et al.,* „Design of Power Distribution Network Fault Data Collector for Fault Detection, Location and Classification using Machine Learning“ in *2018 IEEE 7th International Conference on Adaptive Science & Technology (ICAST)*, 2018, doi: 10.1109/icastech.2018.8506774.

[74] V. Chandola, A. Banerjee und V. Kumar, „Anomaly detection“, *ACM Comput. Surv.*, Jg. 41, Nr. 3, S. 1–58, 2009, doi: 10.1145/1541880.1541882.

[75] E. M. Voumvoulakis, A. E. Gavoyiannis und N. D. Hatziargyriou, „Application of Machine Learning on Power System Dynamic Security Assessment“ in *2007 International Conference on Intelligent Systems Applications to Power Systems*,

Kaohsiung, Taiwan, 11/5/2007 - 11/8/2007, S. 1–6, doi: 10.1109/ISAP.2007.4441604.

[76] A. E. Gavoyiannis, D. G. Vogiatzis, D. R. Georgiadis und N. D. Hatziargyriou, „Combined support vector classifiers using fuzzy clustering for dynamic security assessment“ in *Proceedings of Power Engineering Society Summer Meeting*, Vancouver, BC, Canada, 2001, 1281-1286 vol.2, doi: 10.1109/PESS.2001.970257.

[77] B. P. Soni, A. Saxena und V. Gupta, „Online identification of coherent generators in power system by using SVM“ in *2017 4th International Conference on Power, Control & Embedded Systems (ICPCES)*, Allahabad, India, März 2017, S. 1–5, doi: 10.1109/ICPCES.2017.8117615.

[78] S. Brahma, R. Kavasseri, H. Cao, N. R. Chaudhuri, T. Alexopoulos und Y. Cui, „Real-Time Identification of Dynamic Events in Power Systems Using PMU Data, and Potential Applications—Models, Promises, and Challenges“, *IEEE Trans. Power Delivery*, Jg. 32, Nr. 1, S. 294–301, 2017, doi: 10.1109/TPWRD.2016.2590961.

[79] Le Xie, Y. Chen und P. R. Kumar, „Dimensionality Reduction of Synchrophasor Data for Early Event Detection: Linearized Analysis“, *IEEE Trans. Power Syst.*, Jg. 29, Nr. 6, S. 2784–2794, 2014, doi: 10.1109/TPWRS.2014.2316476.

[80] Y Singh, PK Bhatia, O Sangwan, Hg., *A review of studies on machine learning techniques*, 2007.

[81] R. Sun, „Research on Machine Learning Natural Feature Matching Method Based on Statistical Classification“ in *2019 International Conference on Information Technology and Computer Application (ITCA)*, Guangzhou, China, 2019, S. 35–38, doi: 10.1109/ITCA49981.2019.00015.

[82] K. Chen, C. Huang und J. He, „Fault detection, classification and location for transmission lines and distribution systems: a review on the methods“, *High Voltage*, Jg. 1, Nr. 1, S. 25–33, 2016, doi: 10.1049/hve.2016.0005.

[83] V. Venkatesh und M. Cristea, „Fault Classification and Location Identification on Electrical Transmission Network Based on Machine Learning Methods“, *undefined*, 2019. [Online]. Verfügbar unter: https://www.semanticscholar.org/paper/Advanced-techniques-for-fault-detection-and-in-An-Tirnovan-Cristea/82a1f416cd278699f9c358910766055481a6f95c

[84] A. H. Al-Mohammed und M. A. Abido, „Fault Location Based on Synchronized Measurements: A Comprehensive Survey“, *The Scientific World Journal*, Jg. 2014, S. 1–10, 2014, doi: 10.1155/2014/845307.

[85] B. Bhalja und R. P. Maheshwari, „Wavelet-based Fault Classification Scheme for a Transmission Line Using a Support Vector Machine“, *Electric Power Components and Systems*, Jg. 36, Nr. 10, S. 1017–1030, 2008, doi: 10.1080/15325000802046496.

[86] M. Ben Hessine und S. Ben Saber, „Accurate Fault Classifier and Locator for EHV Transmission Lines Based on Artificial Neural Networks“, *Mathematical Problems in Engineering*, Jg. 2014, S. 1–19, 2014, doi: 10.1155/2014/240565.

[87] A. Çapar und A. Basa Arsoy, „A performance oriented impedance based fault location algorithm for series compensated transmission lines“, *International Journal of Electrical Power & Energy Systems*, Jg. 71, S. 209–214, 2015, doi: 10.1016/j.ijepes.2015.02.020.

[88] L. Cai, N. F. Thornhill, S. Kuenzel und B. C. Pal, „Wide-Area Monitoring of Power Systems Using Principal Component Analysis and k-Nearest Neighbor Analysis“, *IEEE Trans. Power Syst.*, Jg. 33, Nr. 5, S. 4913–4923, 2018, doi: 10.1109/TPWRS.2017.2783242.

[89] S. Cherry, „Some Comments on Singular Value Decomposition Analysis“, *J. Climate*, Jg. 10, Nr. 7, S. 1759–1761, 1997, doi: 10.1175/1520-0442(1997)010<1759:SCOSVD>2.0.CO;2.

[90] H. Okumus und F. M. Nuroglu, „Power System Event Classification Based on Machine Learning“ in *2018 3rd International Conference on Computer Science and Engineering (UBMK)*, Sarajevo, 2018, S. 402–405, doi: 10.1109/UBMK.2018.8566324.

[91] YongchangWang und L. Zhu, „Research and implementation of SVD in machine learning“ in *2017 IEEE/ACIS 16th International Conference on Computer and Information Science (ICIS)*, Wuhan, Mai 2017, S. 471–475, doi: 10.1109/ICIS.2017.7960038.

[92] K. Fukunaga, *Introduction to Statistical Pattern Recognition*. San Diego: Academic press, 1990.

[93] G. M. Jackson, I. M. Mason und S. A. Greenhalgh, „Principal component transforms of triaxial recordings by singular value decomposition“, *GEOPHYSICS*, Jg. 56, Nr. 4, S. 528–533, 1991, doi: 10.1190/1.1443068.

[94] T. Celik, „Unsupervised Change Detection in Satellite Images Using Principal Component Analysis and k-Means Clustering“, *IEEE Geosci. Remote Sensing Lett.*, Jg. 6, Nr. 4, S. 772–776, 2009, doi: 10.1109/LGRS.2009.2025059.

[95] M. W. Berry, Z. Drmac und E. R. Jessup, „Matrices, Vector Spaces, and Information Retrieval“, *SIAM Rev.*, Jg. 41, Nr. 2, S. 335–362, 1999, doi: 10.1137/S0036144598347035.

[96] J. W. Demmel, *Applied numerical linear algebra*. Philadelphia: Society for Industrial and Applied Mathematics, 1997.

[97] S. R. Samantaray und P. K. Dash, „Transmission line distance relaying using a variable window short-time Fourier transform“, *Electric Power Systems Research*, Jg. 78, Nr. 4, S. 595–604, 2008, doi: 10.1016/j.epsr.2007.05.005.

[98] Sun-Li Yu und Jyh-Cherng Gu, „Removal of decaying DC in current and voltage signals using a modified Fourier filter algorithm“, *IEEE Transactions on Power Delivery*, Jg. 16, Nr. 3, S. 372–379, 2001, doi: 10.1109/61.924813.

[99] D. Chanda, N. K. Kishore und A. K. Sinha, „Application of wavelet multiresolution analysis for identification and classification of faults on transmission lines“, *Electric Power Systems Research*, Jg. 73, Nr. 3, S. 323–333, 2005, doi: 10.1016/j.epsr.2004.07.006.

[100] Gawali N.U., „A comparison of different mother wavelet for fault detection & classification of series compensated transmission line“, *Int. J. Innov. Res. Sci. Technol.*, Jg. 1, S. 57, 2015.

[101] A. G. Shaik und R. R. V. Pulipaka, „A new wavelet based fault detection, classification and location in transmission lines“, *International Journal of Electrical Power & Energy Systems*, Jg. 64, S. 35–40, 2015, doi: 10.1016/j.ijepes.2014.06.065.

[102] P. K. Dash, S. R. Samantaray und G. Panda, „Fault Classification and Section Identification of an Advanced Series-Compensated Transmission Line Using Support Vector Machine“, *IEEE Transactions on Power Delivery*, Jg. 22, Nr. 1, S. 67–73, 2007, doi: 10.1109/tpwrd.2006.876695.

[103] D. Chanda, N. K. Kishore und A. K. Sinha, „A wavelet multiresolution analysis for location of faults on transmission lines“, *International Journal of Electrical Power & Energy Systems*, Jg. 25, Nr. 1, S. 59–69, 2003, doi: 10.1016/s0142-0615(02)00021-2.

[104] U. B. Parikh, Biswarup Das und R. P. Prakash Maheshwari, „Combined Wavelet-SVM Technique for Fault Zone Detection in a Series Compensated Transmission Line“, *IEEE Transactions on Power Delivery*, Jg. 23, Nr. 4, S. 1789–1794, 2008, doi: 10.1109/tpwrd.2008.919395.

[105] A. K. Pradhan, A. Routray, S. Pati und D. K. Pradhan, „Wavelet Fuzzy Combined Approach for Fault Classification of a Series-Compensated Transmission Line“,

IEEE Transactions on Power Delivery, Jg. 19, Nr. 4, S. 1612–1618, 2004, doi: 10.1109/tpwrd.2003.822535.

[106] Alves da Silva, Alexandre P., A. C. Lima und S. M. Souza, „Fault location on transmission lines using complex-domain neural networks“, *International Journal of Electrical Power & Energy Systems*, Jg. 43, Nr. 1, S. 720–727, 2012, doi: 10.1016/j.ijepes.2012.05.046.

[107] C. K. Chui und J. Lian, „A study of orthonormal multi-wavelets“, *Applied Numerical Mathematics*, Jg. 20, Nr. 3, S. 273–298, 1996, doi: 10.1016/0168-9274(95)00111-5.

[108] M. Jayabharata Reddy und D. K. Mohanta, „A wavelet-fuzzy combined approach for classification and location of transmission line faults“, *International Journal of Electrical Power & Energy Systems*, Jg. 29, Nr. 9, S. 669–678, 2007, doi: 10.1016/j.ijepes.2007.05.001.

[109] P. K. Dash, B. K. Panigrahi und G. Panda, „Power quality analysis using s-transform“, *IEEE Transactions on Power Delivery*, Jg. 18, Nr. 2, S. 406–411, 2003, doi: 10.1109/tpwrd.2003.809616.

[110] R. G. Stockwell, L. Mansinha und R. P. Lowe, „Localization of the complex spectrum: the S transform“, *IEEE Transactions on Signal Processing*, Jg. 44, Nr. 4, S. 998–1001, 1996, doi: 10.1109/78.492555.

[111] P. K. Dash, S. Das und J. Moirangthem, „Distance protection of shunt compensated transmission line using a sparse S-transform“, *IET Generation, Transmission & Distribution*, Jg. 9, Nr. 12, S. 1264–1274, 2015, doi: 10.1049/iet-gtd.2014.1002.

[112] K. K. R. und P. K. Dash, „A New Real-Time Fast Discrete S-Transform for Cross-Differential Protection of Shunt-Compensated Power Systems“, *IEEE Transactions on Power Delivery*, Jg. 28, Nr. 1, S. 402–410, 2013, doi: 10.1109/tpwrd.2012.2221749.

[113] S. R. Samantaray und P. K. Dash, „Pattern recognition based digital relaying for advanced series compensated line“, *International Journal of Electrical Power & Energy Systems*, Jg. 30, Nr. 2, S. 102–112, 2008, doi: 10.1016/j.ijepes.2007.06.018.

[114] S. R. Samantaray, P. K. Dash und G. Panda, „Fault classification and location using HS-transform and radial basis function neural network“, *Electric Power Systems Research*, Jg. 76, 9-10, S. 897–905, 2006, doi: 10.1016/j.epsr.2005.11.003.

[115] Z. Moravej, M. Khederzadeh und M. Pazoki, „New Combined Method for Fault Detection, Classification, and Location in Series-compensated Transmission Line“,

Electric Power Components and Systems, Jg. 40, Nr. 9, S. 1050–1071, 2012, doi: 10.1080/15325008.2012.675409.

[116] A. M. Martinez und A. C. Kak, „PCA versus LDA“, *IEEE Transactions on Pattern Analysis and Machine Intelligence*, Jg. 23, Nr. 2, S. 228–233, 2001, doi: 10.1109/34.908974.

[117] A. Dasgupta, S. Nath und A. Das, „Transmission Line Fault Classification and Location Using Wavelet Entropy and Neural Network“, *Electric Power Components and Systems*, Jg. 40, Nr. 15, S. 1676–1689, 2012, doi: 10.1080/15325008.2012.716495.

[118] J.-A. Jiang *et al.,* „A Hybrid Framework for Fault Detection, Classification, and Location—Part I: Concept, Structure, and Methodology“, *IEEE Transactions on Power Delivery*, Jg. 26, Nr. 3, S. 1988–1998, 2011, doi: 10.1109/tpwrd.2011.2141157.

[119] F. B. Costa, „Fault-Induced Transient Detection Based on Real-Time Analysis of the Wavelet Coefficient Energy“, *IEEE Transactions on Power Delivery*, Jg. 29, Nr. 1, S. 140–153, 2014, doi: 10.1109/tpwrd.2013.2278272.

[120] T. M. Lai, L. A. Snider, E. Lo und D. Sutanto, „High-Impedance Fault Detection Using Discrete Wavelet Transform and Frequency Range and RMS Conversion“, *IEEE Transactions on Power Delivery*, Jg. 20, Nr. 1, S. 397–407, 2005, doi: 10.1109/tpwrd.2004.837836.

[121] David Chan Tat Wai und Xia Yibin, „A novel technique for high impedance fault identification“, *IEEE Transactions on Power Delivery*, Jg. 13, Nr. 3, S. 738–744, 1998, doi: 10.1109/61.686968.

[122] A.-R. Sedighi, M.-R. Haghifam, O. P. Malik und M.-H. Ghassemian, „High Impedance Fault Detection Based on Wavelet Transform and Statistical Pattern Recognition“, *IEEE Transactions on Power Delivery*, Jg. 20, Nr. 4, S. 2414–2421, 2005, doi: 10.1109/tpwrd.2005.852367.

[123] A. Raza, A. Benrabah, T. Alquthami und M. Akmal, „A Review of Fault Diagnosing Methods in Power Transmission Systems“, *Applied Sciences*, Jg. 10, Nr. 4, S. 1312, 2020, doi: 10.3390/app10041312.

[124] S. M. Yeo *et al.,* „A novel algorithm for fault classification in transmission lines using a combined adaptive network and fuzzy inference system“, *International Journal of Electrical Power & Energy Systems*, Jg. 25, Nr. 9, S. 747–758, 2003, doi: 10.1016/s0142-0615(03)00029-2.

[125] K. M. Silva, B. A. Souza und N. Brito, „Fault Detection and Classification in Transmission Lines Based on Wavelet Transform and ANN“, *IEEE Transactions on Power Delivery*, Jg. 21, Nr. 4, S. 2058–2063, 2006, doi: 10.1109/tpwrd.2006.876659.

[126] U. B. Parikh, B. Das und R. Maheshwari, „Fault classification technique for series compensated transmission line using support vector machine“, *International Journal of Electrical Power & Energy Systems*, Jg. 32, Nr. 6, S. 629–636, 2010, doi: 10.1016/j.ijepes.2009.11.020.

[127] T. Dalstein und B. Kulicke, „Neural network approach to fault classification for high speed protective relaying“, *IEEE Transactions on Power Delivery*, Jg. 10, Nr. 2, S. 1002–1011, 1995, doi: 10.1109/61.400828.

[128] Huisheng Wang und W. Keerthipala, „Fuzzy-neuro approach to fault classification for transmission line protection“, *IEEE Transactions on Power Delivery*, Jg. 13, Nr. 4, S. 1093–1104, 1998, doi: 10.1109/61.714467.

[129] A. Prasad, J. Belwin Edward und K. Ravi, „A review on fault classification methodologies in power transmission systems: Part-II“, *Journal of Electrical Systems and Information Technology*, Jg. 5, Nr. 1, S. 61–67, 2018, doi: 10.1016/j.jesit.2016.10.003.

[130] A. Jamehbozorg und S. M. Shahrtash, „A Decision Tree-Based Method for Fault Classification in Double-Circuit Transmission Lines“, *IEEE Transactions on Power Delivery*, Jg. 25, Nr. 4, S. 2184–2189, 2010, doi: 10.1109/tpwrd.2010.2050911.

[131] R. Diao *et al.,* „Decision Tree-Based Online Voltage Security Assessment Using PMU Measurements“, *IEEE Trans. Power Syst.*, Jg. 24, Nr. 2, S. 832–839, 2009, doi: 10.1109/TPWRS.2009.2016528.

[132] I. M. Cecilio, J. R. Ottewill, H. Fretheim und N. F. Thornhill, „Multivariate Detection of Transient Disturbances for Uni- and Multirate Systems“, *IEEE Trans. Contr. Syst. Technol.*, Jg. 23, Nr. 4, S. 1477–1493, 2015, doi: 10.1109/TCST.2014.2377182.

[133] N. F. Thornhill, H. Melbø und J. Wiik, „Multidimensional Visualization and Clustering of Historical Process Data“, *Ind. Eng. Chem. Res.*, Jg. 45, Nr. 17, S. 5971–5985, 2006, doi: 10.1021/ie051054q.

[134] B. Zhou, M. Chioua und J.-C. Schlake, „Practical methods for detecting and removing transient changes in univariate oscillatory time series“, *IFAC-PapersOnLine*, Jg. 50, Nr. 1, S. 7987–7992, 2017, doi: 10.1016/j.ifacol.2017.08.997.

[135] D. Fabozzi und T. van Cutsem, „Assessing the proximity of time evolutions through dynamic time warping“, *IET Gener. Transm. Distrib.*, Jg. 5, Nr. 12, S. 1268, 2011, doi: 10.1049/iet-gtd.2011.0415.

[136] C. E. Shannon, „Prediction and Entropy of Printed English“, *Bell System Technical Journal*, Jg. 30, Nr. 1, S. 50–64, 1951, doi: 10.1002/j.1538-7305.1951.tb01366.x.

[137] S. L. Salzberg, „C4.5: Programs for Machine Learning by J. Ross Quinlan. Morgan Kaufmann Publishers, Inc., 1993“, *Mach Learn*, Jg. 16, Nr. 3, S. 235–240, 1994, doi: 10.1007/BF00993309.

[138] J. R. Quinlan, *C4.5: Programs for machine learning / J. Ross Quinlan*. San Mateo, Calif.: Morgan Kaufmann, 1993.

[139] T. Wang, T. Bi, H. Wang und J. Liu, „Decision tree based online stability assessment scheme for power systems with renewable generations“, *CSEE Power and Energy Syst.*, Jg. 1, Nr. 2, S. 53–61, 2015, doi: 10.17775/CSEEJPES.2015.00019.

[140] A. Pal, J. S. Thorp, T. Khan und S. S. Young, „Classification Trees for Complex Synchrophasor Data“, *Electric Power Components and Systems*, Jg. 41, Nr. 14, S. 1381–1396, 2013, doi: 10.1080/15325008.2013.824048.

[141] Z. Li und W. Wu, „Phasor Measurements-Aided Decision Trees for Power System Security Assessment“ in *2009 Second International Conference on Information and Computing Science*, 2009, S. 358–361, doi: 10.1109/ICIC.2009.98.

[142] S. Rovnyak und Y. Sheng, „Using measurements and decision tree processing for response-based discrete-event control“ in *1999 IEEE Power Engineering Society Summer Meeting. Conference Proceedings (Cat. No.99CH36364)*, 1999, 10-15 vol.1, doi: 10.1109/PESS.1999.784315.

[143] J. N. Barlin *et al.,* „Classification and regression tree (CART) analysis of endometrial carcinoma: Seeing the forest for the trees“ (eng), *Gynecologic oncology*, Jg. 130, Nr. 3, S. 452–456, 2013, doi: 10.1016/j.ygyno.2013.06.009.

[144] V. N. Vapnik, *The Nature of Statistical Learning Theory*. New York, NY: Springer, 2000.

[145] M. Tobita, T. Nishikawa und R. Nagashima, „A discriminant model constructed by the support vector machine method for HERG potassium channel inhibitors“ (eng), *Bioorganic & medicinal chemistry letters*, Jg. 15, Nr. 11, S. 2886–2890, 2005, doi: 10.1016/j.bmcl.2005.03.080.

[146] N. Takahashi und T. Nishi, „Global Convergence of Decomposition Learning Methods for Support Vector Machines“, *IEEE Transactions on Neural Networks*, Jg. 17, Nr. 6, S. 1362–1369, 2006, doi: 10.1109/TNN.2006.880584.

[147] V. Malathi und N. S. Marimuthu, „Multi-class Support Vector Machine approach for fault classification in power transmission line“ in *2008 IEEE International Conference on Sustainable Energy Technologies (ICSET)*, Singapore, Singapore, 2008, S. 67–71, doi: 10.1109/ICSET.2008.4746974.

[148] R. Salat und S. Osowski, „Accurate fault location in the power transmission line using support vector machine approach“, *IEEE Transactions on Power Systems*, Jg. 19, Nr. 2, S. 979–986, 2004, doi: 10.1109/TPWRS.2004.825883.

[149] O. A. Youssef, „An optimised fault classification technique based on Support-Vector-Machines“ in *2009 IEEE/PES Power Systems Conference and Exposition (PSCE)*, Seattle, WA, USA, 2009, S. 1–8, doi: 10.1109/PSCE.2009.4839949.

[150] S. Amornsamankul, B. Pimpunchat, W. Triampo, J. Charoenpong und N. Nuttavut, „A Comparison of Machine Learning Algorithms and Their Applications“, *International journal of simulation: systems, science & technology*, 2019, doi: 10.5013/IJSSST.a.20.04.08.

[151] Q. Gao und S. M. Rovnyak, „Decision Trees Using Synchronized Phasor Measurements for Wide-Area Response-Based Control“, *IEEE Trans. Power Syst.*, Jg. 26, Nr. 2, S. 855–861, 2011, doi: 10.1109/TPWRS.2010.2067229.

[152] C. Li *et al.,* „Research and Application of Power System Data Anomaly Identification Based on Time Series and Deep Learning“, *J. Phys.: Conf. Ser.*, Jg. 2095, Nr. 1, S. 12021, 2021, doi: 10.1088/1742-6596/2095/1/012021.

[153] A. J. Allen, S.-W. Sohn, S. Santoso und W. M. Grady, „Algorithm for screening PMU data for power system events“ in *2012 3rd IEEE PES Innovative Smart Grid Technologies Europe (ISGT Europe)*, Berlin, Germany, 14.10.2012 - 17.10.2012, S. 1–6, doi: 10.1109/ISGTEurope.2012.6465867.

[154] D.-I. Kim, T. Y. Chun, S.-H. Yoon, G. Lee und Y.-J. Shin, „Wavelet-based event detection method using PMU data“ in *2017 IEEE Power & Energy Society General Meeting (PESGM)*, Chicago, IL, 16.07.2017 - 20.07.2017, S. 1, doi: 10.1109/PESGM.2017.8274161.

[155] A. Allen, M. Singh, E. Muljadi, and S. Santoso, „PMU Data Event Detection: A User Guide for Power Engineers“, National Renewable Energy Labortory, 2014. [Online]. Verfügbar unter: www.nrel.gov/publications. Zugriff am: 1. Oktober 2016.

[156] M. Biswal, Y. Hao, P. Chen, S. Brahma, H. Cao und P. de Leon, „Signal features for classification of power system disturbances using PMU data“ in *2016 Power Systems Computation Conference (PSCC)*, Genoa, Italy, 20.06.2016 - 24.06.2016, S. 1–7, doi: 10.1109/PSCC.2016.7540867.

[157] O. P. Dahal, H. Cao, S. Brahma und R. Kavasseri, „Evaluating performance of classifiers for supervisory protection using disturbance data from phasor measurement units“ in *2014 IEEE PES Innovative Smart Grid Technologies Conference Europe (ISGT-Europe)*, Istanbul, Turkey, 12.10.2014 - 15.10.2014, S. 1–6, doi: 10.1109/ISGTEurope.2014.7028892.

[158] J. Ma, Y. V. Makarov, C. H. Miller und T. B. Nguyen, „Use multi-dimensional ellipsoid to monitor dynamic behavior of power systems based on PMU measurement“ in *Energy Society General Meeting*, Pittsburgh, PA, USA, 20.07.2008 - 24.07.2008, S. 1–8, doi: 10.1109/PES.2008.4596578.

[159] H. Mori, „State-of-the-art overview on data mining in power systems“ in *2006 IEEE Power Engineering Society General Meeting*, 2006, 5 pp, doi: 10.1109/PES.2006.1709104.

[160] J. C. Bezdek, *Pattern Recognition with Fuzzy Objective Function Algorithms*. Springer US. Verfügbar unter: http://dx.doi.org/10.1007/978-1-4757-0450-1.

[161] M. Biswal, S. M. Brahma und H. Cao, „Supervisory Protection and Automated Event Diagnosis Using PMU Data“, *IEEE Transactions on Power Delivery*, Jg. 31, Nr. 4, S. 1855–1863, 2016, doi: 10.1109/TPWRD.2016.2520958.

[162] J. Hazra und A. K. Sinha, „Identification of Catastrophic Failures in Power System Using Pattern Recognition and Fuzzy Estimation“, *IEEE Transactions on Power Systems*, Jg. 24, Nr. 1, S. 378–387, 2009, doi: 10.1109/TPWRS.2008.2009475.

[163] M. Panteli und D. S. Kirschen, „Situation awareness in power systems: Theory, challenges and applications“, *Electric Power Systems Research*, Jg. 122, S. 140–151, 2015, doi: 10.1016/j.epsr.2015.01.008.

[164] G. N. Ericsson, „Cyber Security and Power System Communication—Essential Parts of a Smart Grid Infrastructure“, *IEEE Trans. Power Delivery*, Jg. 25, Nr. 3, S. 1501–1507, 2010, doi: 10.1109/TPWRD.2010.2046654.

[165] D.-J. Kang, J.-J. Lee, S.-J. Kim und J.-H. Park, „Analysis on cyber threats to SCADA systems“ in *2009 Transmission & Distribution Conference & Exposition: Asia and Pacific*, Seoul, South Korea, 2009, S. 1–4, doi: 10.1109/TD-ASIA.2009.5357008.

[166] *e-TWIN- Ganzheitliche digitale Zwillingstechnologie für das Energiesystem.* [Online]. Verfügbar unter: https://www.enargus.de/pub/bscw.cgi/?op=enargus.eps2&q=Digitaler%20Zwilling&v=10&id=1324962.

[167] *TwinERGY-Intelligent interconnection of prosumers in positive energy communities with twins of things for digital energy markets.* [Online]. Verfügbar unter: https://cordis.europa.eu/project/id/957736.

[168] *Stimulating scientific excellence through twinning in the quest for sustainable energy (TwinPV).* [Online]. Verfügbar unter: http://www.twinpv.eu/.

[169] *EPC4SES - Energieausweis-basierte digitale Zwillinge für intelligente Energiesysteme.* [Online]. Verfügbar unter: https://www.enargus.de/pub/bscw.cgi/?op=enargus.eps2&q=%2201196452/1%22&v=10&id=1303521.

[170] *Digital-Twin-Solar - Nachweis der Machbarkeit und Demonstration des Nutzens eines 'Digitalen Zwillings' im Bereich der Batterie- und PV-Systemtechnik.* [Online]. Verfügbar unter: https://www.energiesystem-forschung.de/news/digitalisierung-projektstart-digital-twin-solar.

[171] *DiMoWind-Inspect - Digitale Modellierungsprozesse in der wiederkehrenden Prüfung von Windenergieanlagen.* [Online]. Verfügbar unter: https://www.enargus.de/pub/bscw.cgi/?op=enargus.eps2&q=%2201222216/1%22&v=10&id=1935869.

[172] *HyLITE - Digital-Twin-zentrische Dienste und Applikationen für den dynamischen Betrieb und den Schutz des zukünftigen Energieversorgungssystems.* [Online]. Verfügbar unter: https://www.enargus.de/pub/bscw.cgi/?op=enargus.eps2&q=HyLITE&v=10&id=937886.

[173] N. Mohan, W. P. Robbins, T. M. Undeland und R. Nilssen, „Simulation of power electronic and motion control systems-an overview“, *Proc. IEEE*, Jg. 82, Nr. 8, S. 1287–1302, 1994, doi: 10.1109/5.301689.

[174] P. Kundur, N. J. Balu und M. G. Lauby, *Power system stability and control*. New York, London: McGraw-Hill, 1994.

[175] F. Milano, *Power System Modelling and Scripting*. Berlin, Heidelberg: Springer-Verlag Berlin Heidelberg, 2010. [Online]. Verfügbar unter: http://site.ebrary.com/lib/alltitles/docDetail.action?docID=10415318

[176] B. Lehman und R. M. Bass, „Switching frequency dependent averaged models for PWM DC-DC converters“ in *PESC '95 - Power Electronics Specialist Conference*, Atlanta, GA, USA, 1995, S. 636–642, doi: 10.1109/PESC.1995.474878.

[177] J. Sun, „Unified averaged switch models for stability analysis of large distributed power systems“ in *APEC 2000 - Applied Power Electronics Conference*, New Orleans, LA, USA, 2000, S. 249–255, doi: 10.1109/APEC.2000.826112.

[178] P.-K. Budig, *Stromrichtergespeiste Drehstromantriebe: Theorie und Betriebsverhalten von Asynchronantrieben*. Berlin: VDE Verl., 2001.

[179] I. Report, „Excitation System Models for Power System Stability Studies“, *IEEE Trans. on Power Apparatus and Syst.*, PAS-100, Nr. 2, S. 494–509, 1981, doi: 10.1109/TPAS.1981.316906.

[180] *IEEE Recommended Practice for Excitation System Models for Power System Stability Studies*, Piscataway, NJ, USA.

[181] E. Larsen und D. Swann, „Applying Power System Stabilizers Part I: General Concepts“, *IEEE Trans. on Power Apparatus and Syst.*, PAS-100, Nr. 6, S. 3017–3024, 1981, doi: 10.1109/TPAS.1981.316355.

[182] F. Demello und C. Concordia, „Concepts of Synchronous Machine Stability as Affected by Excitation Control“, *IEEE Trans. on Power Apparatus and Syst.*, PAS-88, Nr. 4, S. 316–329, 1969, doi: 10.1109/TPAS.1969.292452.

[183] S. Chiniforoosh *et al.,* „Definitions and Applications of Dynamic Average Models for Analysis of Power Systems“, *IEEE Trans. Power Delivery*, Jg. 25, Nr. 4, S. 2655–2669, 2010, doi: 10.1109/TPWRD.2010.2043859.

[184] Z. Wang, Y. Wang und S. Wu, „Enhanced Single Phase Locked Loop for Grid-Connected Converter in Distribution Network“ in *2010 International Conference on Electrical and Control Engineering (ICECE)*, Wuhan, China, 2010, S. 3705–3709, doi: 10.1109/iCECE.2010.904.

[185] K. Reinisch, *Analyse und Synthese kontinuierlicher Steuerungs- und Regelungssysteme,* 3. Aufl. Berlin: Verl. Technik, 1996.

[186] K. G. Papadopoulos und N. I. Margaris, „Extending the Symmetrical Optimum criterion to the design of PID type-p control loops“, *Journal of Process Control*, Jg. 22, Nr. 1, S. 11–25, 2012, doi: 10.1016/j.jprocont.2011.10.014.

[187] S. Preitl und R.-E. Precup, „An extension of tuning relations after symmetrical optimum method for PI and PID controllers“, *Automatica*, Jg. 35, Nr. 10, S. 1731–1736, 1999, doi: 10.1016/S0005-1098(99)00091-6.

[188] P. K. Dash, P. Nayak, P. Satapathy und L. Tripathy, „Optimal control of PV–WS battery-based microgrid using an adaptive water cycle technique“, *Electr Eng*, Jg. 102, Nr. 4, S. 2193–2210, 2020, doi: 10.1007/s00202-020-01027-1.

[189] M. A. Attia, „Optimized controllers for enhancing dynamic performance of PV interface system“, *Journal of Electrical Systems and Information Technology*, Jg. 5, Nr. 1, S. 1–10, 2018, doi: 10.1016/j.jesit.2018.01.003.

[190] R. Isermann und M. Münchhof, Hg., *Identification of dynamic systems: An introduction with applications / Rolf Isermann, Marco Münchhof*. Berlin: Springer, 2011.

[191] A. K. Jain und R. C. Dubes, *Algorithms for clustering data*, 1988.

[192] P. Mitra, V. Vittal, P. Pourbeik und A. Gaikwad, „Load Sensitivity Studies in Power Systems With Non-Smooth Load Behavior“, *IEEE Trans. Power Syst.*, Jg. 32, Nr. 1, S. 705–714, 2017, doi: 10.1109/TPWRS.2016.2554398.

[193] I. A. Hiskens und J. Alseddiqui, „Sensitivity, Approximation, and Uncertainty in Power System Dynamic Simulation“, *IEEE Trans. Power Syst.*, Jg. 21, Nr. 4, S. 1808–1820, 2006, doi: 10.1109/TPWRS.2006.882460.

[194] A. Wang, Z. Zheng und J. Zheng, „Parameter identification of synchronous condenser based on sensitivity analysis of parameters“ in *2017 China International Electrical and Energy Conference (CIEEC)*, 2017, S. 725–730, doi: 10.1109/CIEEC.2017.8388539.

[195] J. Chureemart und P. Churueang, „Sensitivity analysis and its applications in power system improvements“ in *2008 5th International Conference on Electrical Engineering/Electronics, Computer, Telecommunications and Information Technology (ECTI-CON)*, Krabi, Thailand, 2008, S. 945–948, doi: 10.1109/ECTICON.2008.4600587.

[196] *Implementation of SoboŒs Method of Global Sensitivity Analysis to a Compressor Simulation Model*, 2014.

[197] C. Hübler, „Global sensitivity analysis for medium-dimensional structural engineering problems using stochastic collocation“, *Reliability Engineering & System Safety*, Jg. 195, S. 106749, 2020, doi: 10.1016/j.ress.2019.106749.

[198] I. N. Moghaddam, Z. Salami und L. Easter, „Sensitivity Analysis of an Excitation System in Order to Simplify and Validate Dynamic Model Utilizing Plant Test Data“, *IEEE Trans. on Ind. Applicat.*, Jg. 51, Nr. 4, S. 3435–3441, 2015, doi: 10.1109/TIA.2015.2406658.

[199] T. Latunde und O. M. Bamigbola, „Parameter Estimation and Sensitivity Analysis of an Optimal Control Model for Capital Asset Management“ (en), *Advances in Fuzzy Systems*, Jg. 2018, 2018, doi: 10.1155/2018/4756520.

[200] X. S. Zhou, X. Q. Shi und Y. J. Ma, „A Review of Application of Sensitivity in Power System“, *AMM*, 494-495, S. 1670–1673, 2014, doi: 10.4028/www.scientific.net/AMM.494-495.1670.

[201] A. Saltelli, *Global sensitivity analysis: The primer / Andrea Saltelli … [et al.]*. Chichester: John Wiley & Sons, 2008. [Online]. Verfügbar unter: http://www.loc.gov/catdir/enhancements/fy0805/2007045551-d.html

[202] I. Sobol′, „Global sensitivity indices for nonlinear mathematical models and their Monte Carlo estimates“, *Mathematics and Computers in Simulation*, Jg. 55, Nr. 1, S. 271–280, 2001, doi: 10.1016/S0378-4754(00)00270-6.

[203] A. Saltelli, S. Tarantola und K. P.-S. Chan, „A Quantitative Model-Independent Method for Global Sensitivity Analysis of Model Output“, *Technometrics*, Jg. 41, Nr. 1, S. 39–56, 1999, doi: 10.1080/00401706.1999.10485594.

[204] R. I. Cukier, C. M. Fortuin, K. E. Shuler, A. G. Petschek und J. H. Schaibly, „Study of the sensitivity of coupled reaction systems to uncertainties in rate coefficients. I Theory“ (en), *The Journal of Chemical Physics*, Jg. 59, Nr. 8, S. 3873, 2003, doi: 10.1063/1.1680571.

[205] H. Azarkish und M. Rashki, „Reliability and reliability-based sensitivity analysis of shell and tube heat exchangers using Monte Carlo Simulation“, *Applied Thermal Engineering*, Jg. 159, S. 113842, 2019, doi: 10.1016/j.applthermaleng.2019.113842.

[206] M. U. Usman, J. Ospina und M. O. Faruque, „Fault Classification and Location Identification in a Smart Distribution Network Using ANN“ in *2018 IEEE Power & Energy Society General Meeting (PESGM)*, 2018, doi: 10.1109/pesgm.2018.8586471.

[207] A. Prasad, J. Belwin Edward und K. Ravi, „A review on fault classification methodologies in power transmission systems: Part—I“, *Journal of Electrical Systems and Information Technology*, Jg. 5, Nr. 1, S. 48–60, 2018, doi: 10.1016/j.jesit.2017.01.004.

[208] V. Venkatesh und M. Cristea, „Fault Classification and Location Identification on Electrical Transmission Network Based on Machine Learning Methods“, *undefined*, 2019. [Online]. Verfügbar unter: https://www.semanticscholar.org/paper/Advanced-techniques-for-fault-detection-and-in-An-Tirnovan-Cristea/82a1f416cd278699f9c358910766055481a6f95c

[209] P. Ray und D. P. Mishra, „Support vector machine based fault classification and location of a long transmission line“, *Engineering Science and Technology, an International Journal*, Jg. 19, Nr. 3, S. 1368–1380, 2016, doi: 10.1016/j.jestch.2016.04.001.

[210] Quanyuan Jiang, Xingpeng Li, Bo Wang und Haijiao Wang, „PMU-Based Fault Location Using Voltage Measurements in Large Transmission Networks“, *IEEE Transactions on Power Delivery*, Jg. 27, Nr. 3, S. 1644–1652, 2012, doi: 10.1109/tpwrd.2012.2199525.

[211] R. Mukherjee und A. De, „Real-time dynamic security analysis of power systems using strategic PMU measurements and decision tree classification“, *Electr Eng*, 2020, doi: 10.1007/s00202-020-01118-z.

[212] Y. Zhang, Z. Wang und Jinfang Zhang, „PCA fault location based on wide area measurement systems“ in *2010 5th International Conference on Critical Infrastructure (CRIS)*, 2010, S. 1–4, doi: 10.1109/CRIS.2010.5617572.

[213] J. Upendar, C. P. Gupta und G. K. Singh, „Statistical decision-tree based fault classification scheme for protection of power transmission lines“, *International Journal of Electrical Power & Energy Systems*, Jg. 36, Nr. 1, S. 1–12, 2012, doi: 10.1016/j.ijepes.2011.08.005.

[214] K. Hosseini, „Short Circuit Fault Classification and Lo cation in Transmission Lines Using A Combination of Wavelet Transform and Support Vector Machines“, *ijeei*, Jg. 7, Nr. 2, S. 353–365, 2015, doi: 10.15676/ijeei.2015.7.2.14.

[215] S. R. Samantaray, P. K. Dash und G. Panda, „Distance relaying for transmission line using support vector machine and radial basis function neural network“, *International Journal of Electrical Power & Energy Systems*, Jg. 29, Nr. 7, S. 551–556, 2007, doi: 10.1016/j.ijepes.2007.01.007.

[216] Whei-Min Lin, Chin-Der Yang, Jia-Hong Lin und Ming-Tong Tsay, „A fault classification method by RBF neural network with OLS learning procedure“, *IEEE Transactions on Power Delivery*, Jg. 16, Nr. 4, S. 473–477, 2001, doi: 10.1109/61.956723.

[217] Z. Chen und J.-C. Maun, „Artificial neural network approach to single-ended fault locator for transmission lines“, *IEEE Trans. Power Syst.*, Jg. 15, Nr. 1, S. 370–375, 2000, doi: 10.1109/59.852146.

[218] M. Joorabian, S. Taleghani Asl und R. K. Aggarwal, „Accurate fault locator for EHV transmission lines based on radial basis function neural networks“, *Electric*

Power Systems Research, Jg. 71, Nr. 3, S. 195–202, 2004, doi: 10.1016/j.epsr.2004.02.002.

[219] L. M. Surhone, M. T. Timpledon und S. F. Marseken, *Root Mean Square Deviation*. Betascript Publishing, 2010. [Online]. Verfügbar unter: https://books.google.de/books?id=T43ucQAACAAJ

[220] T. J. Member, S. Xinya, J. Willkomm, S. Schlegel und D. Westermann, „Hybrids-Simulation using EMT - And Phasor-Based Model for Converter Dominated Distribution Grid“ in *2018 IEEE PES Innovative Smart Grid Technologies Conference Europe (ISGT-Europe)*, Sarajevo, Bosnia and Herzegovina, 102018, S. 1–6, doi: 10.1109/ISGTEurope.2018.8571555.

[221] K. K. Al-jabery, T. Obafemi-Ajayi, G. R. Olbricht und D. C. Wunsch II, „Data analysis and machine learning tools in MATLAB and Python“ in *Computational Learning Approaches to Data Analytics in Biomedical Applications*, Elsevier, 2020, S. 231–290, doi: 10.1016/B978-0-12-814482-4.00009-7.

[222] J. M. Hancock, „Jaccard Distance (Jaccard Index, Jaccard Similarity Coefficient)“ in *Dictionary of Bioinformatics and Computational Biology*, J. M. Hancock und M. J. Zvelebil, Hg., Chichester, UK: John Wiley & Sons, Ltd, 2004, doi: 10.1002/9780471650126.dob0956.

[223] A. P. Bradley, „The use of the area under the ROC curve in the evaluation of machine learning algorithms“, *Pattern Recognition*, Jg. 30, Nr. 7, S. 1145–1159, 1997, doi: 10.1016/S0031-3203(96)00142-2.

A. Appendix

A.1 Reference network based on CIGRÉ Benchmark System [38]

The network model consists of 13 nodes, four power plants, three compensation devices and five loads, see Figure A.1. It covers three geographical areas called Area 1, 2 and 3. Area 1 is predominantly a generator area. Area 2, about 500 km away from Area 1, is a load area with one generator available. Area 3 is located between the generator area Area 1 and the load area Area 2. In the high voltage grid model there are two voltage levels: generation bus voltage of 22 kV, primary transmission voltage of 110 kV.

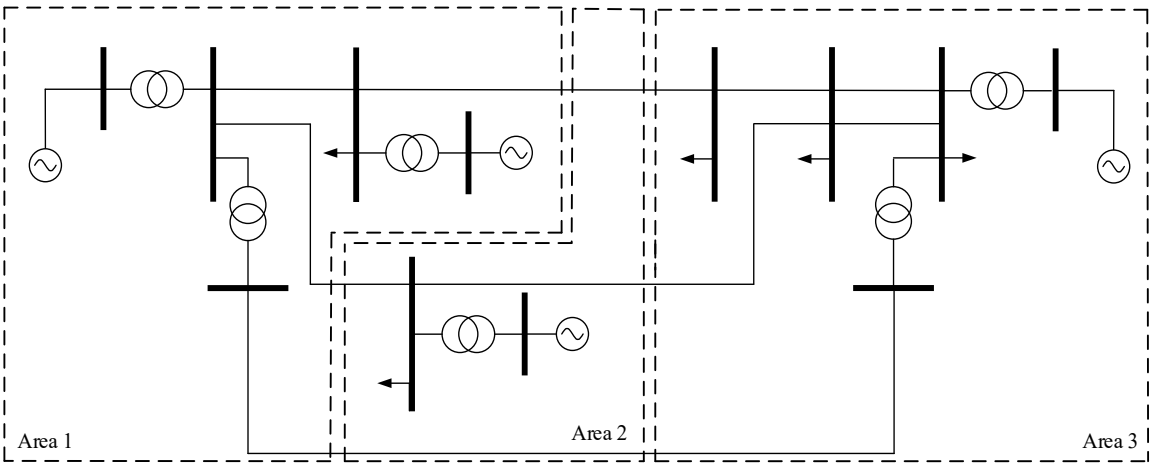

Figure A. 1: Topology of high-voltage network based on Cigré benchmark [38]

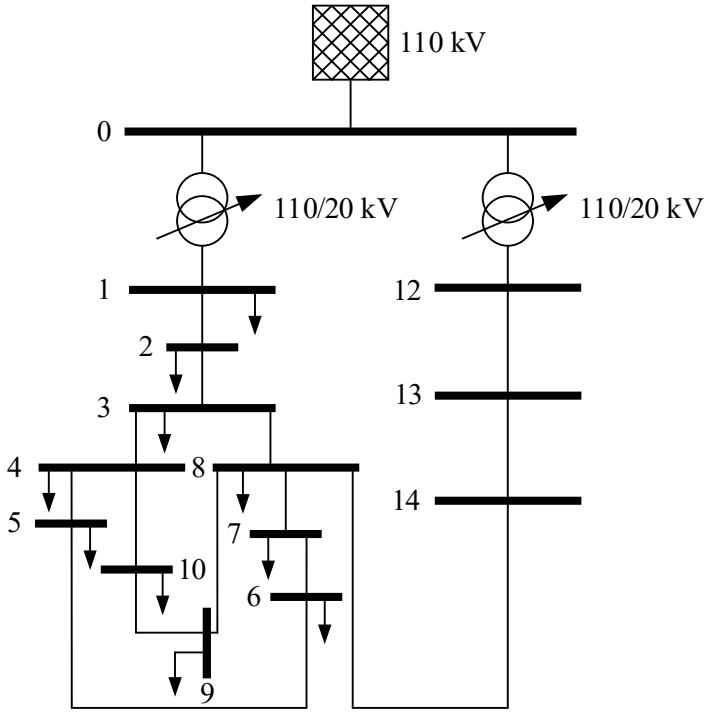

Figure A. 2: Topology of medium-voltage network based on Cigré benchmark [38]

The Cigré reference grid at the medium-voltage level of 20 kV forms a ring structure that is connected to the high-voltage grid via two transformers, see Figure A.2. In addition to synchronous generators in conventional power plants, distributed generation plants in the form of renewable energy sources, such as wind and PV plants, and decentralized generation plants are increasingly used as generators. The latter are also partly operated with asynchronous motors and connected to the energy grid with converters, just like renewable energy sources, for their better control.

A.2 Network data

The reference objective plays the role as the physical power grid, which is simulated in ePHASORSIM based on OPAL RT platform. ePHASORSIM is an data-driven software for the simulation, which provides three input formats at present: EXECEL-based, PSSe and CYME format [31]. In this work, the EXCEL format is utilized to build the reference model and simulate it in ePHASORSIM platform. The data for the SM, controllers and line used in ePHASORSIM is illustrated in the following tables.

Table A. 1: Connection and line parameter in reference network

From node	To node	*R* in p.u.	*X* in p.u.	*B* in p.u.
1	2	1.35×10^{-2}	8.22×10^{-2}	4.394×10^{-5}
1	6	4.05×10^{-2}	2.47×10^{-1}	1.318×10^{-4}
2	5	4.05×10^{-2}	2.47×10^{-1}	1.318×10^{-4}
3	4	1.35×10^{-2}	8.22×10^{-2}	4.394×10^{-5}
3	4	1.35×10^{-2}	8.22×10^{-2}	4.394×10^{-5}
4	5	4.05×10^{-2}	2.47×10^{-1}	1.318×10^{-4}
4	6	4.05×10^{-2}	2.47×10^{-1}	1.318×10^{-4}
8	9	4.07×10^{-2}	3.87×10^{-1}	3.339×10^{-4}
6	6b	1.35×10^{-5}	8.22×10^{-5}	4.394×10^{-8}
14	15	2.92×10^{-3}	4.17×10^{-3}	2.063×10^{-5}
15	16	4.58×10^{-3}	6.54×10^{-3}	3.234×10^{-5}
16	17	6.31×10^{-4}	9.02×10^{-4}	4.463×10^{-6}
17	18	5.80×10^{-4}	8.28×10^{-4}	4.097×10^{-6}
18	19	1.59×10^{-3}	2.28×10^{-3}	1.126×10^{-5}
20	21	1.73×10^{-3}	2.47×10^{-3}	1.221×10^{-5}
21	22	3.31×10^{-4}	4.73×10^{-4}	2.341×10^{-6}
22	23	7.97×10^{-4}	1.14×10^{-3}	5.633×10^{-6}
23	24	3.42×10^{-4}	4.88×10^{-4}	2.414×10^{-6}
16	21	1.35×10^{-3}	1.92×10^{-3}	9.511×10^{-6}
25	26	5.15×10^{-3}	3.70×10^{-3}	2.389×10^{-6}
26	27	3.15×10^{-3}	2.26×10^{-3}	1.461×10^{-6}
19	20	2.48×10^{-4}	3.55×10^{-4}	1.756×10^{-6}
24	17	5.07×10^{-4}	7.25×10^{-4}	3.585×10^{-6}
27	21	2.11×10^{-3}	1.51×10^{-3}	9.773×10^{-7}
29	30	2.92×10^{-3}	4.17×10^{-3}	2.063×10^{-5}
30	31	4.58×10^{-3}	6.54×10^{-3}	3.234×10^{-5}
31	32	6.31×10^{-4}	9.02×10^{-4}	4.463×10^{-6}
32	33	5.80×10^{-4}	8.28×10^{-4}	4.097×10^{-6}
33	34	1.59×10^{-3}	2.28×10^{-3}	1.126×10^{-5}
35	36	1.73×10^{-3}	2.47×10^{-3}	1.221×10^{-5}
36	37	3.31×10^{-4}	4.73×10^{-4}	2.341×10^{-6}
37	38	7.97×10^{-4}	1.14×10^{-3}	5.633×10^{-6}
38	39	3.42×10^{-4}	4.88×10^{-4}	2.414×10^{-6}
31	36	1.35×10^{-3}	1.92×10^{-3}	9.511×10^{-6}
40	41	5.15×10^{-3}	3.70×10^{-3}	2.389×10^{-6}
41	42	3.15×10^{-3}	2.26×10^{-3}	1.461×10^{-6}
34	35	2.48×10^{-4}	3.55×10^{-4}	1.756×10^{-6}
39	32	5.07×10^{-4}	7.25×10^{-4}	3.585×10^{-6}
42	36	2.11×10^{-3}	1.51×10^{-3}	9.773×10^{-7}

Table A. 2: Parameter of SM in reference network

Parameter	Description	SM on bus 9-12
H	Inertia constant	5.0 MWs/MVA
D	Damping coefficient	1.0
x_{d}	Synchronous reactance d-axis	1.25 p.u.
x_{q}	Synchronous reactance q-axis	1.0 p.u.
x'_{d}	Transient reactance d-axis	0.333 p.u.
x'_{q}	Transient reactance q-axis	0.3 p.u.
x''_{d}	Subtransient reactance d-axis	0.292 p.u.
x''_{q}	Subtransient reactance q-axis	0.292 p.u.
T'_{d0}	Transient time constant d-axis	5.0 s
T'_{q0}	Transient time constant q-axis	2.0 s
T''_{d0}	Subtransient time constant d-axis	0.02 s
T''_{q0}	Subtransient time constant q-axis	0.02 s
r_{a}	Armature resistance	0.002 p.u.
x_{l}	Leakage reactance	0.03 p.u.

Table A. 3: Parameter of controllers for SM in reference network

Parameter	Description	Value
T_{G}	Governor time constant	0.4 s
T_{S1}	Servo motor time constant	1.8 s
T_{S2}	Servo motor time constant	6.0 s
R	Proportional of primary frequency regulation	0.05 p.u.
K_{a}	Exciter field proportional constant	46 p.u.
T_{a}	Exciter field time constant	0.06 s
K_{f}	Rate feedback gain	0.05 p.u.
T_{f}	Rate feedback time constant	1 s
T_{b}	Time constant	0.05 s
T_{c}	Time constant	0.003 s
K_{PSS}	PSS gain	3.15 p.u.
T_{w}	PSS washout time constant	10 s
T_1	PSS lead compensating time constant	0.05 s
T_2	PSS lag compensating time constant	0.02 s
T_3	PSS lead compensating time constant	3 s
T_4	PSS lag compensating time constant	5.4 s
u_{PSSmax}	Maximum PSS output	0.2 p.u.
u_{PSSmin}	Minimum PSS output	-0.2 p.u.

A.3 Reference network simulation results

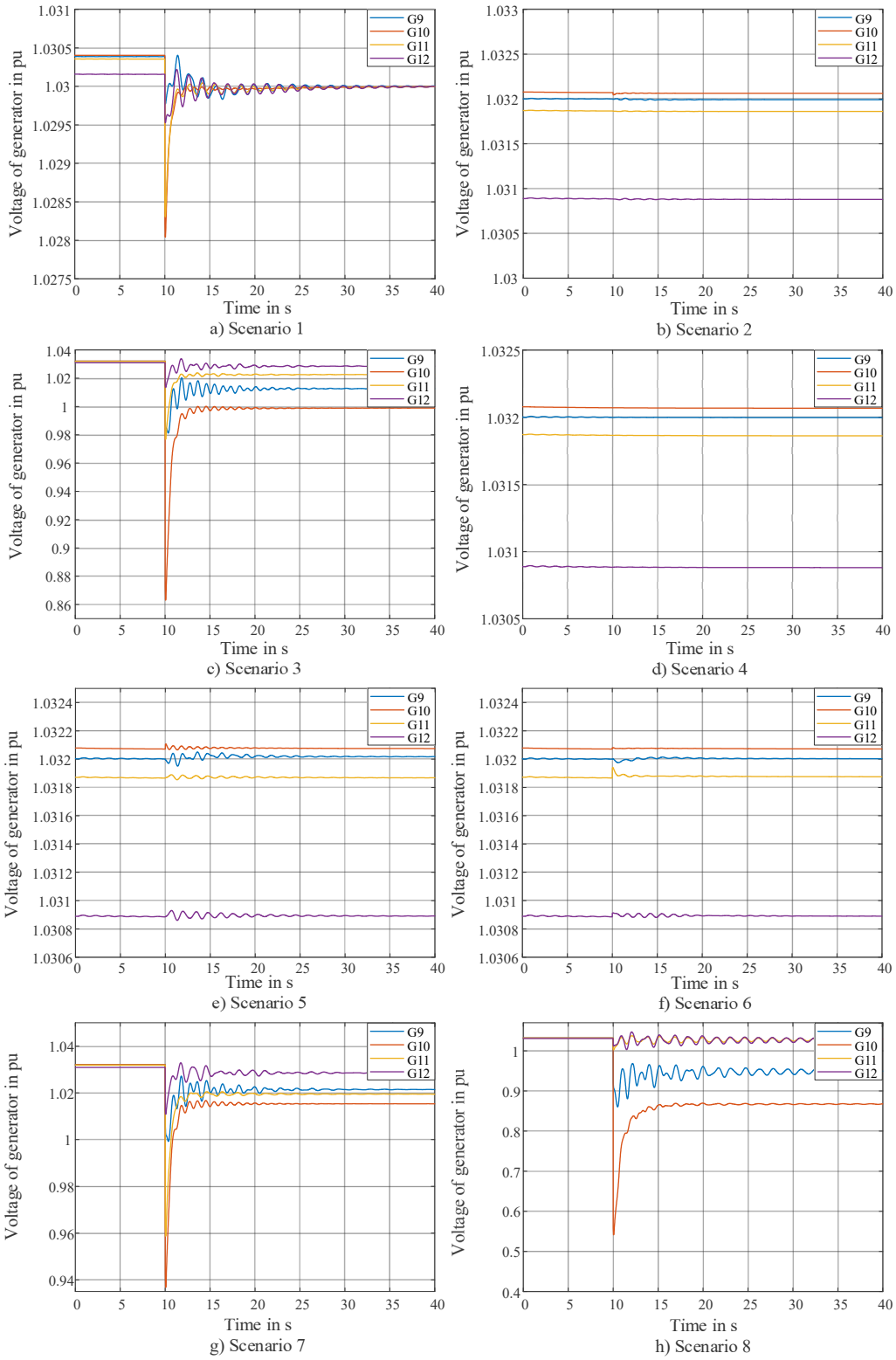

Figure A. 3: Voltages at SM buses of scenario 1-8 in Table 5.1

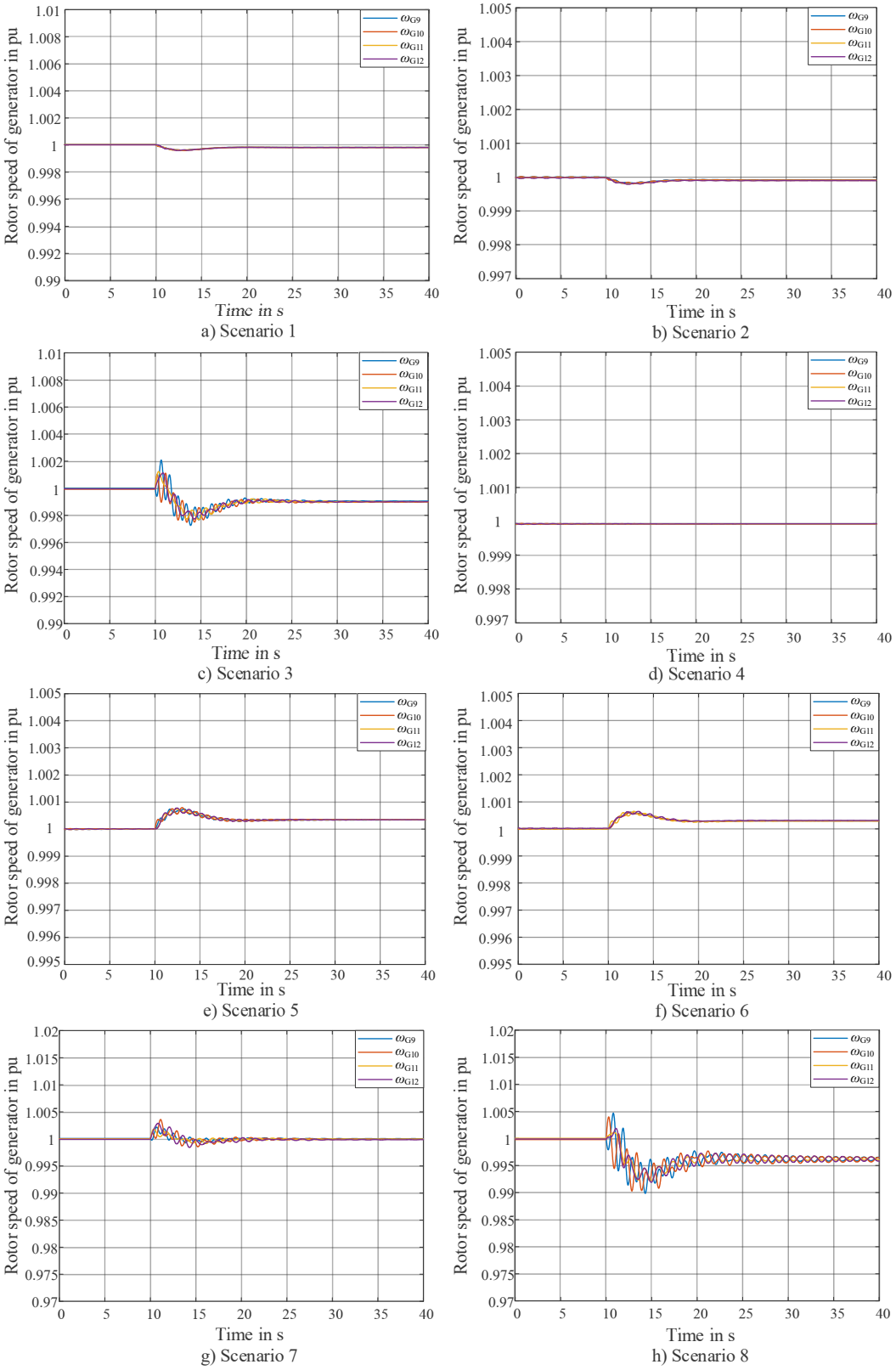

Figure A. 4: Rotor speed of generators with scenario1-8 in Table 5.1

A.4 Parameters before and after estimation

Table A. 4: Estimated values of parameters from SM by LSQ without SA

Parameter	Description	Before parameter estimation	Reference nework	Estimated by LSQ
H	Inertia constant	8.0 MWs/MVA	5.0 MWs/MVA	6.2 MWs/MVA
D	Damping coefficient	5.0	1.0	1.03
x_{d}	Synchronous reactance d-axis	2.5 p.u.	1.25 p.u.	0.99 p.u.
x_{q}	Synchronous reactance q-axis	2.5 p.u.	1.0 p.u.	1.07 p.u.
x'_{d}	Transient reactance d-axis	1.5 p.u.	0.333 p.u.	0.34 p.u.
x'_{q}	Transient reactance q-axis	1.5 p.u.	0.3 p.u.	0.302 p.u.
x''_{d}	Subtransient reactance d-axis	1 p.u.	0.292 p.u.	0.31 p.u.
x''_{q}	Subtransient reactance q-axis	1 p.u.	0.292 p.u.	0.292 p.u.
T'_{d0}	Transient time constant d-axis	10.0 s	5.0 s	4.2 s
T'_{q0}	Transient time constant q-axis	10.0 s	2.0 s	1.1 s
T''_{d0}	Subtransient time constant d-axis	1 s	0.02 s	0.02 s
T''_{q0}	Subtransient time constant q-axis	1 s	0.02 s	0.02
r_{a}	Armature resistance	0.2 p.u.	0.002 p.u.	0.009 p.u.
x_{l}	Leakage reactance	0.1 p.u.	0.03 p.u.	0.03 p.u.

Table A. 5: Estimated values of parameters from SM by LSQ with SA

Parameter	Description	Before parameter estimation	Reference network	Estimated value by LSQ
H	Inertia constant	8.0 MWs/MVA	5.0 MWs/MVA	Not estimated
D	Damping coefficient	5.0	1.0	Not estimated
x_{d}	Synchronous reactance d-axis	2.5 p.u.	1.25 p.u.	0.15 p.u.
x_{q}	Synchronous reactance q-axis	2.5 p.u.	1.0 p.u.	Not estimated
x'_{d}	Transient reactance d-axis	1.5 p.u.	0.333 p.u.	Not estimated
x'_{q}	Transient reactance q-axis	1.5 p.u.	0.3 p.u.	Not estimated
x''_{d}	Subtransient reactance d-axis	1 p.u.	0.292 p.u.	1.73 p.u.
x''_{q}	Subtransient reactance q-axis	1 p.u.	0.292 p.u.	0.9 p.u.
T'_{d0}	Transient time constant d-axis	10.0 s	5.0 s	0.2 s
T'_{q0}	Transient time constant q-axis	10.0 s	2.0 s	2.63 s
T''_{d0}	Subtransient time constant d-axis	1 s	0.02 s	Not estimated
T''_{q0}	Subtransient time constant q-axis	1 s	0.02 s	Not estimated
r_{a}	Armature resistance	0.2 p.u.	0.002 p.u.	1.63 p.u.
x_{l}	Leakage reactance	0.1 p.u.	0.03 p.u.	1 p.u.

Table A. 6: Estimated values of parameters for VSI by LSQ without SA

Parameter	Description	Initial value	Estimated value by LSQ
L_{f}	Induction of filter	13 mH	56.9 mH
R_{f}	Resistance of filter	1 Ohm	2.32 Ohm
C_{f}	Capacitor of filter	80 nF	140 nF
C_{zk}	Capacitor of condenser in DC side	100 µF	56 µF
$T_{\mathrm{I_C}}$	Time constant of PI controller for current loop	3.92s	4.23s
$K_{\mathrm{P_C}}$	Proportional of PI controller for current loop	0.033	0.234
$T_{\mathrm{I_U}}$	Time constant of PI controller for voltage loop	0.009 s	0.00498s
$K_{\mathrm{P_U}}$	Proportional of PI controller for voltage loop	0.1333	1.381
K_{f}	Proportional between DC and AC current	0.625	1.215

Table A. 7: Estimated values of parameters for VSI by LSQ without SA

Parameter	Description	Initial value	Estimated value by LSQ
L_{f}	Induction of filter	13 mH	11.76 mH
R_{f}	Resistance of filter	1 Ohm	0.012 Ohm
C_{f}	Capacitor of filter	80 nF	37.8 µF
C_{zk}	Capacitor of condenser in DC side	100 µF	210 µF
$T_{\mathrm{I_C}}$	Time constant of PI controller for current loop	3.92s	7.83s
$K_{\mathrm{P_C}}$	Proportional of PI controller for current loop	0.033	1

B. Abbreviation

ADT Airframe Digital Twin

AI Artificial Intelligence

ANN	Artificial neural network
ARMAX	Auto-Regressive Moving Average Exogenous
AUC	Area under curve
AVM	Average value model
AVR	Automatic Voltage Regulator
CART	Classification and regression tree
DAE	Differential algebraic equation
DFT	Discrete Fourier Transformation
DSA	Dynamic security assessment
DSE	Dynamic state estimation
DTA	Digital Twin Aggregate
DTI	Digital Twin Instance
DTP	Digital Twin Prototype
ED	Euclidean distance
EMS	Energy Management System
EMT	Electromagnetic transient
FACTS	Flexible AC transmission system
FAST	Fourier amplitude sensitivity test
FFT	Fast Fourier Transformation
FI	Fault index
FN	False Negative
FP	False Positive
FT	Fourier Transformation
GSA	Global sensitivity analysis IoT
HIF	High impedance faults
IoT	Internet of Things
*k*NN	*k*-nearest neighbour
LDA	Linear discriminant analysis

LG	Line-to-Ground
LL	Line-to-Line
LLG	Line-and-Line-to-Ground
LSA	Local sensitivity analysis
LSQ	Least square
ML	Maximal likelihood
MV	Medium voltage
OFAT	One-factor-at-a-time
PC	Principal component
PCA	Principal component analysis
PCC	Point of common coupling
PDC	Phasor Data Concentrator
PLL	Phase-locked-loop
PLM	Product Lifecycle Management
PMU	Phasor Measurement Unit
PSS	Power System stabilizer
QoI	Quantities of interest
RES	Renewable energy sources
RLS	Recursive least square
RMS	Root-mean-square
ROC	Receiver Operating Characteristic
RTU	Remote Terminal Unit
ST	S-Transformation
SVC	Support vector classifier
SVD	Singular value decomposition
SVM	Support vector machine
TN	True Negative
TP	True Positive

VSI	Voltage source inverter
WLS	Weighted least square
WT	Wavelet transformation

C. Notation

Notation

The notation used in this work is described below using the letter "a" as an example. All variables are represented by italic letters with serif (a). A matrix is marked with a bold capital letter ($\boldsymbol{A}$). Vectors are represented by a bold lower case letter ($\boldsymbol{a}$). Scalar variables are represented in physical quantities as upper case (A) and in related quantities as lower case (a).

List of Symbol

U	Voltage
I	Current
P	Active power
Q	Reactive power
δ	Angle
Λ	Diagonal matrix in PCA
Σ	Diagonal matrix in SVD
$D(\boldsymbol{m}, \boldsymbol{n})$	Euclidean distance between measured data vectors $\boldsymbol{m}$ and $\boldsymbol{n}$
Gini	Gini index
L_{P}	Primary Lagrange
$\boldsymbol{e}_i$	Vectors of difference between measurement and observed output
φ^{LSQ}	Objective function of LSQ
φ^{WLS}	Objective function of WLS
φ^{ML}	Objective function of ML
Φ	Radial basis function
ω	Angular speed of rotor
T_{m}	Mechanical torque
T_{d}	Damping torque
p_{t}	Turbine power
T_{e}	Electrical torque
H	Inertia constant
D	Damping coefficient
x_{d}	Synchronous reactance d-axis
x_{q}	Synchronous reactance q-axis

x'_{d}	Transient reactance d-axis
x'_{q}	Transient reactance q-axis
x''_{d}	Sub-transient reactance d-axis
x''_{q}	Sub-transient reactance q-axis
T'_{d0}	Transient time constant d-axis
T'_{q0}	Transient time constant q-axis
T''_{d0}	Sub-transient time constant d-axis
T''_{q0}	Sub-transient time constant q-axis
r_a	Armature resistance
x_l	Leakage reactance
e''_{d} and e''_{q}	d- and q-axis subtransient voltage
f	Frequency
p_{ac}	AC voltage
p_{dc}	DC voltage
$i_{\alpha\beta}$	AC current in vector coordinate
i_{dq}	AC current in dq coordinate
u_{SR}	Inverter voltage
U_{zk}	DC-capacitor voltage
u_{N}	Network voltage
$u_{\mathrm{C_f}}$	AC-filter capacitor voltage
i_{zk}	Current feed from DC-link into AC-side
i_c	DC-capacitor current
i_f	AC-filter current
i_{C_f}	AC-filter capacitor current
L_f	Induction of filter
R_f	Resistance of filter
C_f	Capacitor of filter
C_{zk}	Capacitor of condenser in DC side
T_{I_C}	Time constant of PI controller for current loop
K_{P_C}	Proportional of PI controller for current loop
T_{I_U}	Time constant of PI controller for voltage loop
K_{P_U}	Proportional of PI controller for voltage loop

K_f	Proportional between DC and AC current
K_{SR}	Coefficient of amplifier in voltage loop
i_{N}	Network current
$\vec{\boldsymbol{v}}$	Control signal of switch in inverter
S_{ij}	Sensitivity index between i-th output and j-th parameter
FI_{Q}	Value of kth smallest distance
FI_{Q}^{*}	Highest value in the sequence of FI_Q
κ	Kernel function
G(s)	Transfer function in frequency dominan

Unit

A	Ampere, [I] = A
D	Tag, [t] = D
h	Hour, [t] = h
Hz	Hertz, [f] = Hz
p.u.	per unit
V	Volt, [U] = V
VA	Volt-ampere, [S] = VA
VAr	Volt-ampere reactive, [Q] = VAr
MVA	Mega volt-ampere
MVAr	Mega volt-ampere reactive
W	Watt, [P] = W
MW	Mega watt
Wh	Watt-hour, [E] = Wh
TWh	Terawatt-hours

D. List of Figures and Tables